Université de Paris

Ecole doctorale Cerveau, cognition, comportement (3C) – ED 158

INCC - Integrative Neuroscience & Cognition Center, Equipe orientation spatiale
CNRS UMR 8002, Université de Paris

Modèles murins de pathologies cochléo-vestibulaires : une approche fonctionnelle du système vestibulaire

Par François SIMON

Thèse de doctorat de neurosciences

Dirigée par Mathieu BERANECK
Et par Françoise DENOYELLE

Présentée et soutenue publiquement le 2 novembre 2020

JURY

Pr Cécile PARIETTI-WINKLER, PU-PH, Université de Lorraine	Rapporteur
Dr Christophe LOPEZ, CR, CNRS & Aix Marseille Université	Rapporteur
Pr Natacha TEISSIER, PU-PH, Université de Paris	Examinatrice
Dr Saaid SAFIEDDINE, DR, Institut Pasteur & Sorbonne Université	Examinateur
Pr Françoise DENOYELLE, PU-PH, Université de Paris	Directrice de thèse
Dr Mathieu BERANECK, CR, CNRS & Université de Paris	Directeur de thèse

Dans la perception nous ne pensons pas l'objet et nous ne nous pensons pas le pensant,
nous sommes à l'objet et nous nous confondons avec ce corps
qui en sait plus que nous sur le monde,
sur les motifs et les moyens qu'on a d'en faire la synthèse.

Maurice Merleau-Ponty,

Phénoménologie de la Perception, 1945

Remerciements

Mes premiers remerciements vont à ma famille. Jeanne, merci pour ton soutien indéfectible. C'est un bonheur de partager ma vie avec toi, nous formons une véritable équipe pour relever les défis de la vie ! A Gaspard, merci pour tes cours instructifs sur l'acquisition de la posture et de l'équilibre du jeune enfant. Tu seras toujours une inspiration pour moi ! A mes parents, merci de m'avoir porté, vous êtes la source de ma motivation.

A Mathieu, merci de m'avoir accueilli dans ton équipe, et d'avoir été si conciliant entre mes travaux de recherche et mes activités à l'hôpital. Tu as été un directeur toujours avec le parfait équilibre ente autonomie et écoute. J'espère pouvoir poursuivre encore de nombreux projets avec toi !

Je souhaiterais remercier Madame le Professeur Denoyelle, pour sa confiance et pour l'opportunité de poursuivre ce projet de recherche en même temps que mon clinicat dans son service. Je me rends bien compte de la rareté de ce type d'organisation qui permet une véritable approche translationnelle.

Je souhaite également remercier Madame le Professeur Parietti-Winkler et Monsieur le Docteur Christophe Lopez d'avoir accepté d'être mes rapporteurs, en espérant pouvoir poursuivre de longues discussions éthiques ou phénoménologiques par la suite.

Je souhaite enfin remercier Madame le Professeur Natacha Teissier et Monsieur le Docteur Saaid Safieddine d'avoir accepté de siéger à mon jury mais surtout de m'avoir conseillé tout au long de ma thèse lors des comités de suivi de thèse.

Je tiens à remercier les membres du laboratoire « Orientation Spatiale ». J'ai pris beaucoup de plaisir à faire partie de ce groupe depuis trois ans. Je salue plus particulièrement Desdemona et Michele avec qui nous allons poursuivre des projets passionnants !

Je souhaiterais aussi remercier mes collègues co-thésards, Louis, Louise, Jules et Filipa. Une mention particulière pour Filipa qui m'a accueillie dans le monde du doctorant et m'a montré les ficelles de la vidéonystagmographie et de la manipulation des souris. A Cassandre, ma première étudiante en M2,

merci d’avoir tenu bon malgré le COVID-19. Je te suis très reconnaissant pour ta rigueur et ta perspicacité, ces derniers mois auront été un joli mélange de Matlab et de Merleau-Ponty.

A l’équipe de Necker, merci beaucoup de m’avoir aidé à poursuivre la thèse en même temps que mon clinicat, ce n’aurait pas été possible sans adapter mon emploi du temps, je tiens à remercier très sincèrement toute l’équipe pour sa flexibilité. Je souhaiterais remercier plus particulièrement Messieurs les Professeurs Garabédian, Couloigner et Leboulanger pour leurs nombreux enseignements et conseils.

A Marine, Natalie, Sophie et Isabelle, dans l’attente de la prise en charge des vestibulopathies chez l’enfant ! Votre dynamisme est admirable.

A mes cochefs, anciens et actuels : Marie-Cécile, Sinasi, Bénédicte, Romain, Amine, Fiona, Emilie, Auriane, Sophie, merci pour votre flexibilité et votre soutien moral quotidien surtout dans la dernière ligne droite !

A Charlotte Hautefort, avec de bons souvenirs de ce semestre d’explorations à Lariboisière, merci d’avoir mis la fibre de la vestibulo en moi !

A mes internes passant leur thèse d’exercice de médecine cette année, Françoise, Julia, Léa, Diane et Yohan, ces heures à passer du côté de l’encadrant m’auront beaucoup aidé pour la rédaction. Merci pour vos encouragements.

Résumé

Les déficits vestibulaires chez l'enfant sont retrouvés dans environ un tiers des consultations pour troubles de l'équilibre et dans la moitié des consultations pré-implant cochléaire. Les complications peuvent être importantes avec au premier plan des troubles de l'équilibre et un retard à l'acquisition de la verticalité (position assise, marche), mais aussi un déficit de la stabilisation du regard, de l'orientation spatiale et de la construction du soi. Les modèles murins peuvent aider à mieux comprendre la physiologie vestibulaire, à identifier les acteurs moléculaires ou cellulaires de la physiopathologie vestibulaires, et aider à mettre en place des thérapeutiques innovantes telles que la thérapie génique. L'exploration fonctionnelle chez la souris permet grâce à la vidéonystagmographie, d'explorer différents réflexes vestibulo-oculaires canalaires et otolithiques. Nous avons dans ce travail exploré différents modèles murins, soit des modèles mutants (inactivation des gènes de la *clarine*, *snap-25* ou *celsr1*), soit des souris normales en induisant une lésion vestibulaire chirurgicale ou chimique par kaïnate (TTK) ou 3-3'-iminodipropanenitrile (IDPN). Les mutations du gène *CLARINE-1* sont responsables du syndrome cochléo-vestibulaire de Usher type III. Des modèles murins avec invalidation des gènes *clarine-1* et/ou *clarine-2* ont été développés pour mieux comprendre le rôle de ces molécules et étudier l'efficacité de la thérapie génique. Nous avons montré que la clarine-1 semble indispensable au bon fonctionnement vestibulaire (dysfonction en son absence malgré une présence de clarine-2), à l'inverse de la clarine-2. La molécule SNAP-25 est une protéine impliquée dans le mécanisme d'exocytose synaptique des cellules ciliées. Les souris *snap-25-KO* sans thérapie génique étaient incapable de nager et leurs explorations vestibulaires ont montré des déficits canalaire et otolithique complets. La fonction vestibulaire était entièrement restaurée après thérapie génique, ce qui semble montrer le caractère essentiel de la protéine snap25 dans le fonctionnement de la cellule ciliée vestibulaire mature. Enfin, la molécule CELSR1 est une protéine qui participe à la polarité cellulaire planaire et le modèle de souris *celsr1-KO* présente une désorganisation de la polarité des cellules ciliées vestibulaires chez la souris, surtout au niveau de la cupule. L'étude fonctionnelle a montré chez les souris mutantes une hypo-fonction canalaire d'environ 50% surtout sur les basses fréquences et otolithique d'environ 70%. La polarité ciliaire semble particulièrement critique pour le bon fonctionnement otolithique, ainsi que le recrutement d'un nombre suffisant de cellules ciliées avec des informations concordantes pour les mouvements rotatoires, surtout lors des mouvements lents. Le modèle de lésion vestibulaire le plus ancien pour étudier la compensation vestibulaire chez le rongeur est chirurgical. Une labyrinthectomie unilatérale (UL) est plus simple à réaliser avec moins de comorbidités qu'une neurectomie unilatérale du VIII (UVN), même si cette dernière technique est utile si une destruction du premier neurone vestibulaire est recherchée. La fonction vestibulaire résiduelle et la récupération fonctionnelle sont cependant comparables pendant le 1er mois de compensation. Un autre modèle de lésion chimique a été développé par injection trans-tympanique de TTK, qui permet de déclencher une désafférentation des cellules ciliées, avec un déficit fonctionnel transitoire et partiel par rapport à la neurectomie. Enfin une lésion chimique par injection péritonéale d'IDPN permet de détruire préférentiellement les cellules de type I. L'analyse fonctionnelle a montré une relation dose-dépendante, avec un déficit canalaire surtout sur les fréquences rapides et un déficit otolithique peu prononcé lors d'inclinaisons statiques de la tête. L'exploration des troubles fonctionnels vestibulaires de modèles murins de pathologies cochléo-vestibulaires est une étape décisive pour permettre d'une part une meilleure compréhension de la physiopathologie et d'autre part le développement de thérapies ciblées comme la thérapie génique.

Summary

Vestibular deficits in children are found in about a third of consultations for balance disorders and in half of pre-cochlear implant consultations. Complications can be significant with, more importantly balance disorders and a delay in posture acquisitions (sitting position, walking), but also impaired of gaze stabilisation, spatial orientation or self-construction. Murine models can help better understand vestibular physiology, identify molecular or cellular mechanisms in vestibular pathophysiology, and help set up innovative treatments such as gene therapy. Functional exploration in mice enables, using videonystagmography, exploration of different vestibulo-ocular canal and otolith reflexes. In this work, we explored different murine models, either mutant models (inactivation of *clarin*, *snap-25* or *celsr1* genes), or normal mice inducing a surgical vestibular lesion or a chemical one by kainate (TTK) or 3-3'-iminodipropanenitrile (IDPN) injections. Mutations of the *CLARINE-1* gene are responsible for the cochleo-vestibular syndrome of Usher type III. Murine models with inactivation of the *clarin-1* and / or *clarin-2* genes have been developed to better understand the role of these molecules and to study the effectiveness of gene therapy. A total of 51 mice were explored. We have shown that clarin-1 seems essential for proper vestibular function (impairment in its absence despite the presence of clarin-2), unlike clarin-2. The SNAP-25 molecule is a protein involved in the mechanism of synaptic exocytosis in hair cells. A total of 29 mice were studied including 8 *snap-25-KO* mice treated by gene therapy. *Snap-25-KO* mice without injection were unable to swim and their vestibular explorations showed complete canalar and otolithic deficits. Vestibular function was fully restored after gene therapy, which seems to show the importance of the snap25 protein in the mature vestibular hair cell function. Finally, the CELSR1 molecule is a protein which participates in planar cell polarity and a *celsr1-KO* mouse model induced a disorganization of the polarity of vestibular hair cells, especially in the crista ampullaris. The functional study of 10 *celsr1-KO* mice and 10 control mice showed in mutant mice a 50% canalar hypofunction especially at low frequencies and a 70% otolithic residual function. Ciliary polarity appears to be particularly critical for correct otolithic function. Also, recruiting a sufficient numbers of hair cells with coherent directional information for rotational movements, especially during slow movements, seems important. The most radical vestibular lesion model to study vestibular compensation in rodents is surgery. A unilateral labyrinthectomy (UL) is simpler to perform with fewer comorbidities than a unilateral VIII neurectomy (UVN), although the latter technique is useful if destruction of the first vestibular neuron is required. The residual vestibular function and functional recovery are however similar during the 1st month of vestibular compensation. Another model is a chemical lesion by trans-tympanic injection of TTK, which triggers deafferentation of hair cells, and induces a transient and partial functional deficit compared to neurectomy. Finally, a chemical lesion by peritoneal injection of IDPN makes it possible to preferentially destroy type I hair cells. Functional analysis of 43 mice showed a dose-dependent relationship, with a canalar deficit, especially at fast frequencies and a moderate otolithic deficit during static inclinations of the head. Functional exploration of vestibular disorders in murine models of cochleo-vestibular pathologies is of paramount importance to, on the one hand, better understand of the pathophysiology of the vestibular organs and, on the other hand, enable the development of targeted treatment such as gene therapy.

Sommaire

Liste des illustrations

Liste des Tableaux

Liste des abréviations et acronymes

3,3' IDPN : 3,3'-iminodipropanenitrile
AAV : adeno-associated virus
aVOR : angular vestibulo-ocular reflex (réflexe vestibulo-oculaire angulaire)
CA^{2+} : ion calcium
CCW et **CW :** counter-clockwise et clockwise (rotation anti-horaire et horaire)
CSC : canal semi-circulaire
cVEMP: cervical vestibular evoked myogenic potential (=PEOMs)
DAV : dilatation de l'aqueduc du vestibule
DFNB4 : surdité récessive autosomale 4, avec élargissement de l'aqueduc du vestibule, lié à une mutation du gène *SLC26A4*
DSM-5 : diagnostic and statistical manual of mental disorders, 5^{th} edition (manuel diagnostique et statistique des troubles mentaux)
hsteps : horizontal steps (rotation à vitesse continue dans le plan horizontal, à début et arrêt brutal)
K^+ : ion potassium
IRM : imagerie par résonance magnétique
MOR : maculo-ocular reflex (réflexe maculo-oculaire)
Na^+ : ion sodium
OCR : ocular counter-roll (contre-rotation oculaire)
OKR : opto-kinetic reflex (réflexe optocinétique)
OTR : ocular tilt reaction
OVAR: Off-Vertical Axis Rotation (rotation autour d'un axe incliné par rapport à la verticale)
$_{OVAR}$MOR : maculo-ocular reflex bias during OVAR (réflexe maculo-oculaire pendant l'OVAR)
oVEMP : ocular vestibular evoked myogenic potential (= POEMu)
PEOMs : potentiel évoqué otolithique musculaire sacculaire (=cVEMP)
PEOMu : potentiel évoqué otolithique musculaire utriculaire (=oVEMP)
pitch : rotation antéro-postérieure autour de l'axe de tangage
roll : rotation latérale autour de l'axe de roulis
SHA : sinusoidal harmonic acceleration test (rotation sinusoïdale à fréquence constante au fauteuil, autour de l'axe yaw)
snap 25 : synaptosomal-associated protein 25
SNARE : soluble N-éthylmaleimide-sensitive-factor Attachment protein REceptor
TDM : tomodensitométrie
$_{tilt}$MOR : réflexe maculo-oculaire lié à une inclinaison de la tête (avec une composante torsionnelle et de mouvement vertical de la pupille)
tVOR : translational vestibulo-ocular reflex (réflexe vestibulo-oculaire translationnel)
VCR : vestibulocollic reflex (réflexe vestibulo-colique)
VOR : vestibulo-ocular reflex (réflexe vestibulo-oculaire)
VSR : vestibulospinal reflex (réflexe vestibulo-spinal)
yaw: rotation dans la plan horizontal autour d'un axe de lacet

Préambule

Le système vestibulaire est fréquemment appelé le « sixième sens » pour insister sur son importance par rapport aux cinq sens classiques que sont la vue, l'ouïe, l'odorat, le goût et le toucher. Il est cependant mal connu et est souvent réduit à une fonction annexe de l'audition, faisant partie anatomiquement de l'oreille interne. Son rôle est cependant fondamental et va bien au-delà du maintien de l'équilibre et de la posture, participant à notre orientation dans l'espace, la coordination motrice et la corporéité au sens phénoménologique du terme.

Organe difficilement accessible, non visible ni manipulable, son exploration chez l'Homme se fait soit de façon indirecte, par exploration du réflexe vestibulo-oculaire ou par électromyographie, soit par IRM. Malgré l'amélioration importante de la performance de ces examens ces dernières années, les modèles animaux et plus particulièrement murins permettent de progresser en étudiant les mécanismes cellulaires et moléculaires dans la pathologie et la physiologie du vestibule. Il est possible de faire des corrélations entre fonction vestibulaire et fonction cellulaire et d'étudier des modèles modifiés génétiquement.

Dans ce travail nous analyserons plusieurs modèles murins, à la fois pour mieux comprendre la physiologie vestibulaire, et pour mieux appréhender dans quelle mesure des maladies génétiques qui affectent ce système perturbent la fonction.

Partie 1 : Introduction

1. Le système vestibulaire

1.1. Anatomie du labyrinthe

Le labyrinthe (ensemble qui comprend la cochlée, le vestibule et les canaux semi-circulaires) est une structure anatomiquement complexe creusée dans l'os temporal, médialement à l'oreille moyenne (***Figure 1***). Il contient deux compartiments liquidiens : le liquide périlymphatique riche en sodium dans le labyrinthe osseux, et le liquide endolymphatique, riche en potassium, dans le labyrinthe membraneux où se trouvent les organes vestibulaires.

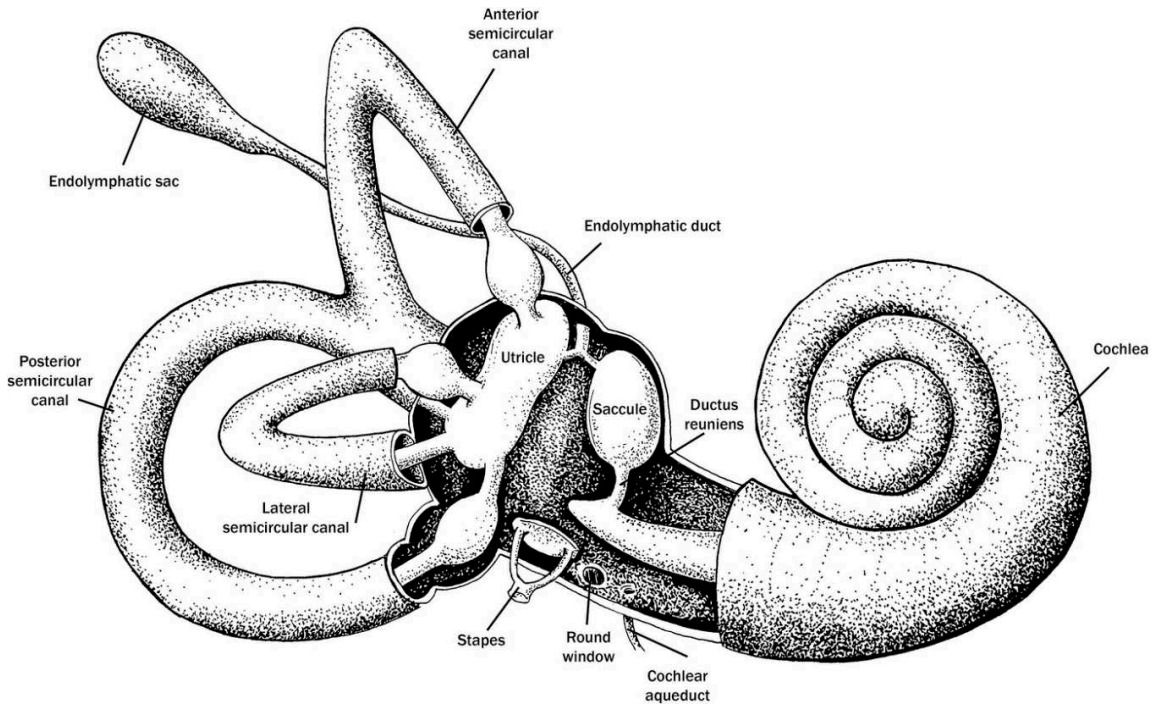

Figure 1: Anatomie du labyrinthe osseux et membraneux chez l'Homme

Le labyrinthe osseux comprend les trois canaux semi-circulaires, le vestibule et la cochlée. Il est rempli de liquide périlymphatique, proche du LCR (riche en sodium) et peut communiquer par l'aqueduc cochléaire. Le labyrinthe membraneux comprend les cinq organes vestibulaires : les trois ampoules des canaux semi-circulaires, l'utricule et le saccule. Le liquide endolymphatique est très riche en potassium (Practical Otology, Pender, 1992).

Les structures du labyrinthe sont conservées parmi les mammifères (Ekdale, 2013), même si la morphologie peut changer. L'anatomie est notamment très similaire entre l'homme et la souris (***Figure 2***), le labyrinthe est plus petit et plus allongé suivant la forme du crâne chez la souris.

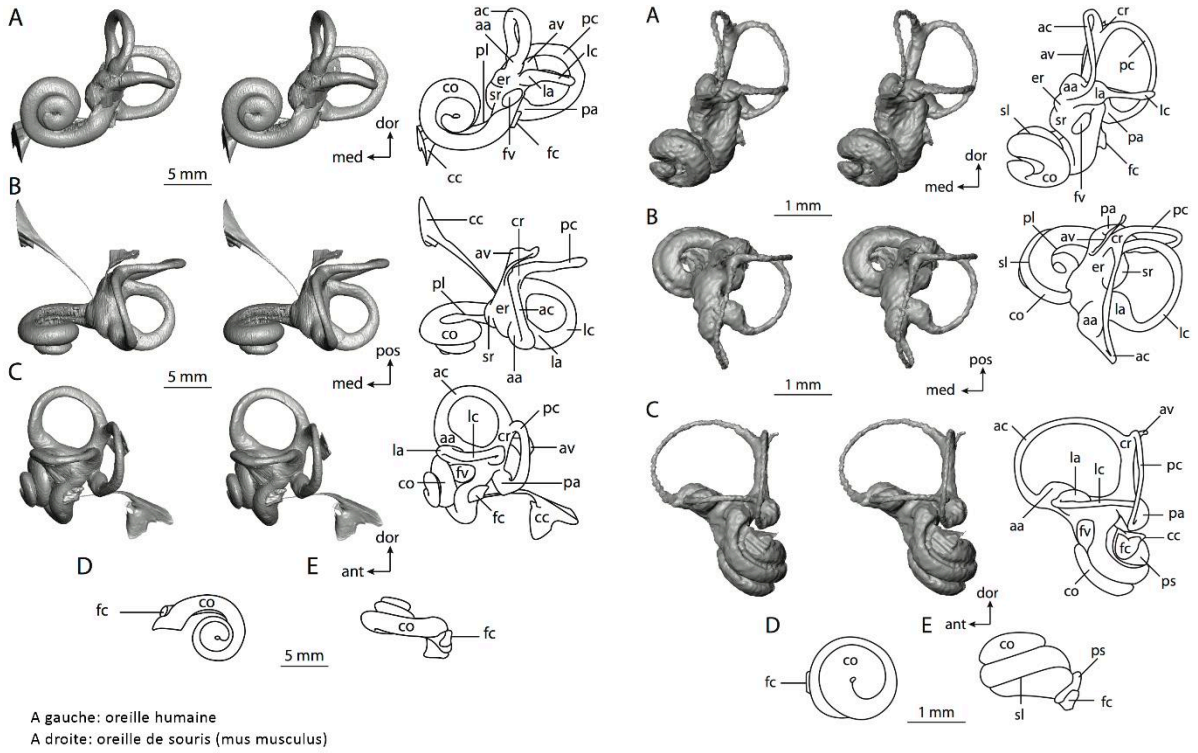

Figure 2: Anatomie comparative du labyrinthe osseux de l'Homme et de la souris

Segmentation TDM puis reconstruction 3D, en vue antérieure (A), dorsale (B) et latérale (C). Dessin montrant l'enroulement de la cochlée (D) et de la cochlée de profil (E). Légendes: aa, anterior ampulla; ac, anterior semicircular canal; ant, anterior direction; av, bony channel for vestibular aqueduct; cc, canaliculus cochleae for cochlear aqueduct; co, cochlea; cr, common crus; dor, dorsal direction; er, elliptical recess of vestibule; fc, fenestra cochleae; fv, fenestra vestibuli; la, lateral ampulla; lc, lateral semicircular canal; med, medial direction; pa, posterior ampulla; pc, posterior semicircular canal; pos, posterior direction; ps, outpocketing for perilymphatic sac; sl, secondary bony lamina; sr, spherical recess of vestibule (Ekdale, 2013).

La vascularisation du labyrinthe se fait par le tronc basilaire puis l'artère cérébelleuse moyenne. Le vestibule est vascularisé par deux troncs, l'artère vestibulaire antérieure et postérieure (***Figure 3***). Le vestibule est innervé par le nerf vestibulaire, une branche du nerf cochléo-vestibulaire. Le nerf vestibulaire se divise lui-même en deux branches, inférieure et supérieure, innervant les différents organes vestibulaires (***Figure 4***). L'atteinte d'une partie de ces deux systèmes peut entrainer des

dysfonctions spécifiques, qui peuvent orienter le diagnostic (névrite vestibulaire inférieure, accident ischémique de l'artère cochléo-vestibulaire, etc.).

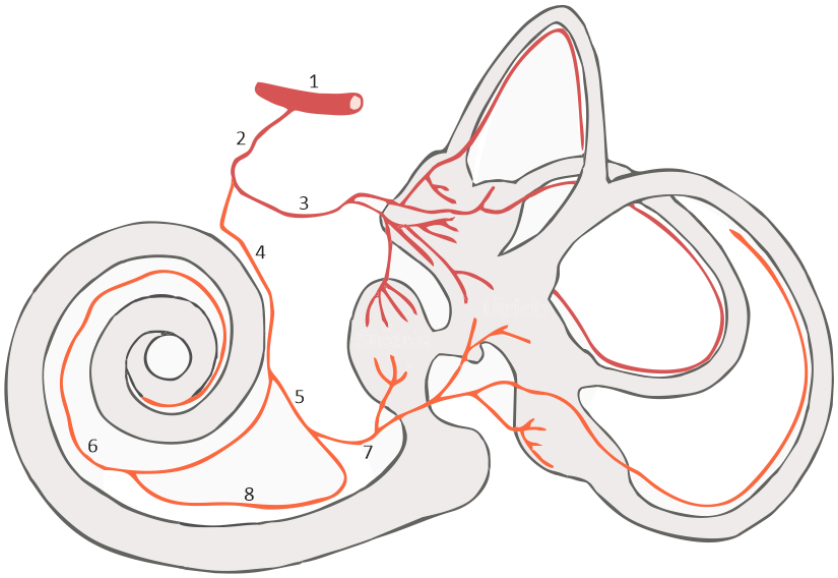

Figure 3: Vascularisation labyrinthique chez l'Homme

Schéma de la vascularisation du labyrinthe. 1 : artère cérébelleuse moyenne ; 2 : artère auditive interne ; 3 : artère vestibulaire antérieure ; 4 : artère cochléaire ; 5 : artère cochléo-vestibulaire ; 6 : artère cochléaire propre ; 7 : branche vestibulaire de l'artère cochléo-vestibulaire (artère vestibulaire postérieure) ; 8 : branche cochléaire de l'artère cochléo-vestibulaire.

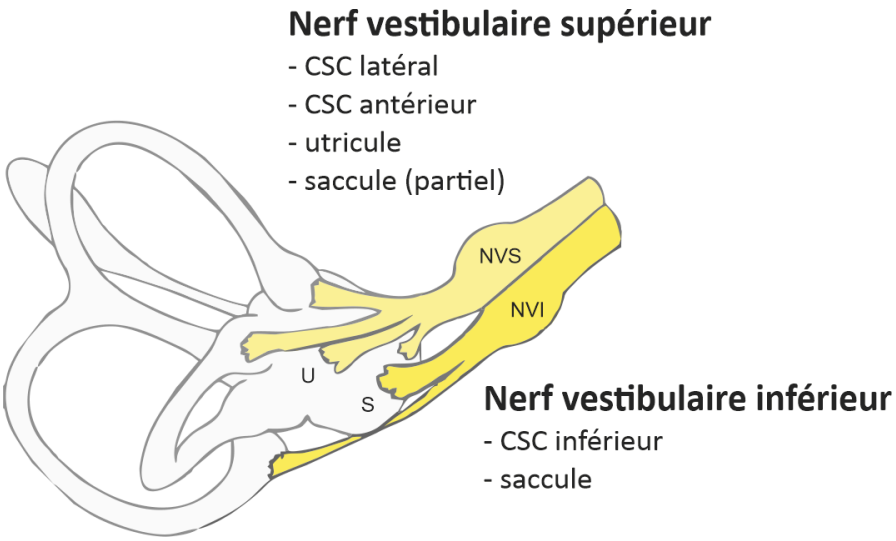

Figure 4: Innervation vestibulaire chez l'Homme

Le nerf vestibulaire se divise en nerf vestibulaire supérieur et inférieur dans le conduit auditif interne. Seul le saccule a une innervation double (principalement inférieure). CSC canal semi-circulaire.

1.2. Embryologie du système vestibulaire

Le développement de l'oreille interne est complexe et débute chez l'Homme vers la 4ème semaine de vie fœtale jusqu'à la 25ème semaine, date à laquelle le vestibule et la cochlée sont fonctionnels et de taille adulte. Les étapes principales sont représentées dans la ***Figure 5***.

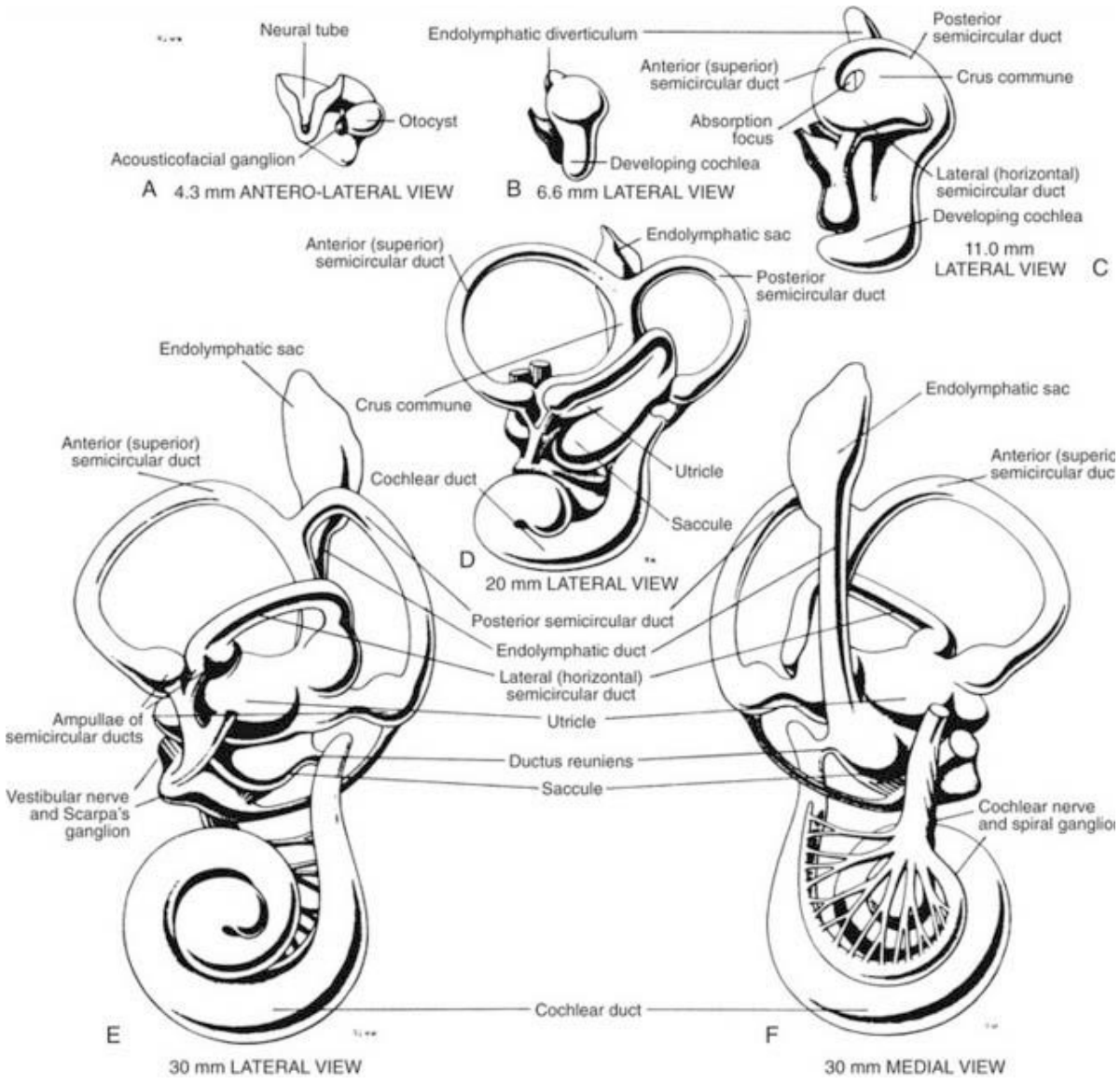

Figure 5: Embryologie du vestibule chez l'Homme

A. *Chez un embryon de 3 semaines.* ***B.*** *Embryon de 4 semaines****. C.*** *Embryon de 6 semaines.* ***D.*** *Embryon de 7 semaines.* ***E*** *et* ***F.*** *Embryon de 8 semaines, avec une morphologie ressemblant à l'adulte. Adapté de* (Gray's anatomy. 36th Edition, Williams and Warwick, 1980)

Chez l'embryon humain, un épaississement de l'ectoderme forme au 22ème jour la placode otique qui s'invagine pour former la vésicule otique au 30ème jour. Le sac endolymphatique s'individualise 1 à 2 jours plus tard, puis l'utricule et le saccule primordiaux. Les canaux semi-circulaires et l'utricule se développent à partir de l'utricule primordial ; la cochlée et le saccule à partir du saccule primordial. Les canaux semi-circulaires apparaissent à partir du 35ème jour embryonnaire et s'individualisent nettement à partir du 45ème jour, d'abord l'antérieur puis le postérieur et enfin le latéral. L'ampoule est visible à la 7ème semaine de développement et l'aspect du labyrinthe membraneux est quasiment celui de l'adulte à la 8ème semaine (Catala, 2014). Au niveau des organes vestibulaires, les macules utriculaires auraient un aspect définitif vers la 11-14ème semaine et les crêtes ampullaires une semaine plus tard bien qu'elles continuent à croitre pour se rapprocher de la taille adulte vers 20 semaines (Dechesne and Sans, 1985).

La configuration orthogonale adulte des canaux semi-circulaires est constatée chez l'Homme dès 22 semaines de grossesse (Mejdoubi et al., 2015) et la fonction électrophysiologique des cellules ciliées vestibulaires à 18 semaines de grossesse (Lim et al., 2014), tout comme la fonction cochléaire vers 18-20 semaines (Pujol and Lavigne-Rebillard, 1995).

Chez la souris, le développement de l'oreille interne débute également pendant la vie fœtale mais se termine après la naissance, de E9 (9ème jour de développement fœtal) à P20 (20ème jour après la naissance). L'ouverture de la lumière du sac endolymphatique a lieu à E10,5 et celle de la lumière cochléaire à E14,5; l'utricule et le saccule sont formés à E17; l'endolymphe mature est produite à partir de P3 et un fonctionnement auditif est mesurable à partir de P12. Une poursuite de la maturation du potentiel endolymphatique a lieu de P7 à P15 ainsi que la maturation fonctionnelle du réflexe vestibulo-oculaire à partir de l'ouverture des yeux à P12 (Gorlin et al., 1995). Cette différence est bien sûr fondamentale, notamment concernant la date d'injection de la thérapie génique chez la souris (qui se fait habituellement en période péri-natale), qui correspondrait en termes de développement de l'oreille interne, à une injection pendant la vie fœtale chez l'Homme.

1.3. Les organes vestibulaires

1.3.1. Les cellules ciliées et leurs synapses

Les organes vestibulaires sont constitués de cellules de soutien et de cellules ciliées qui permettent la mécano-transduction. Le pôle apical des cellules ciliées baigne dans le liquide endolymphatique et est constitué d'une rangée de cils de taille croissante (appelée la touffe ciliaire), jusqu'au kinocil. Un mouvement de la tête entraine un mouvement des cils dans l'endolymphe, qui est excitateur si celui-ci est en direction du kinocil (ouvrant les canaux potassiques) ou inhibiteur dans le sens inverse (fermant les canaux), comme indiqué dans la ***Figure 6***.

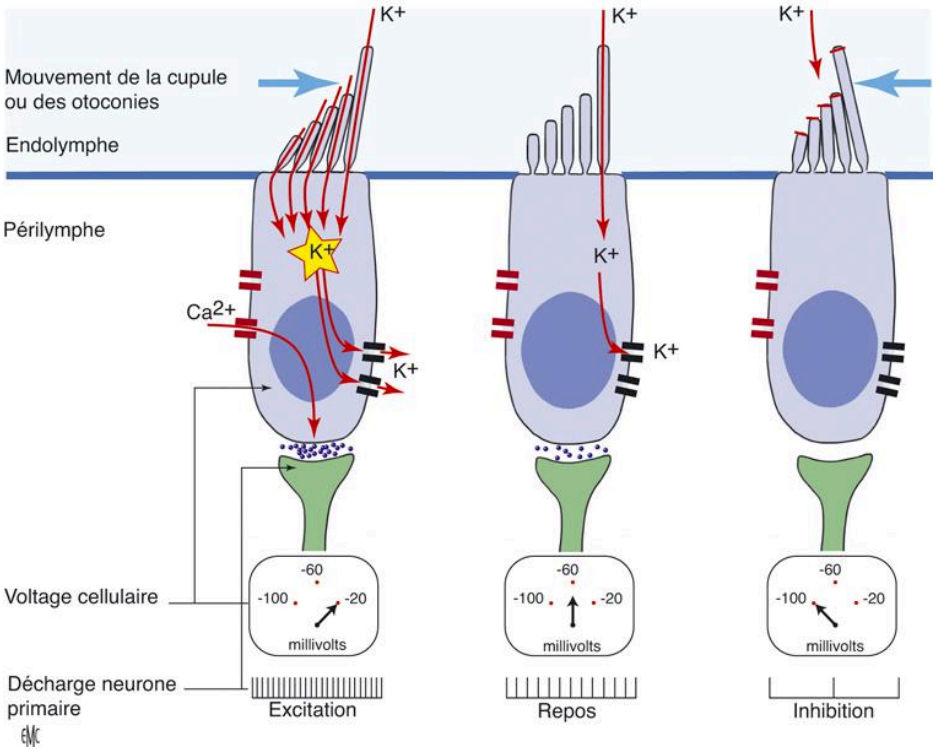

Figure 6: Schéma illustrant le principe de transduction mécano-électrique

Les canaux de transductions apicaux sont partiellement ouverts au repos assurant une activité de décharge de repos dans les neurones primaires. Un mouvement mécanique inhibiteur (dessin à droite) va fermer ces canaux, et un mouvement excitateur (dessin à gauche) va ouvrir les canaux apicaux permettant une entrée massive de K^+ puis de Ca^{2+} (par des canaux voltages-dépendants baso-latéraux) dans la cellule, augmentant le voltage, libérant un neurotransmetteur excitateur dans la fente synaptique (le glutamate) et activant la décharge des neurones primaires. (Chabbert, 2015).

Ainsi une stimulation mécanique de la cellule entraine soit une excitation soit une inhibition du neurone afférent, lequel transmet l'information aux noyaux vestibulaires. Les neurones vestibulaires primaires qui se chargent de cette étape sont des neurones bipolaires dont les corps sont localisés dans le ganglion vestibulaire inférieur ou supérieur (renflement du nerf vestibulaire inférieur ou supérieur), ou ganglion de Scarpa, dans le canal auditif interne.

Morphologiquement, les cellules ciliées sont soit de type I en calice soit de type II en bouton, les cellules de type I n'existant que chez les oiseaux et les mammifères. La forme de la synapse du neurone afférent est différente (***Figure 7***), englobant l'ensemble du pôle basal et latéral de la cellule de type I.

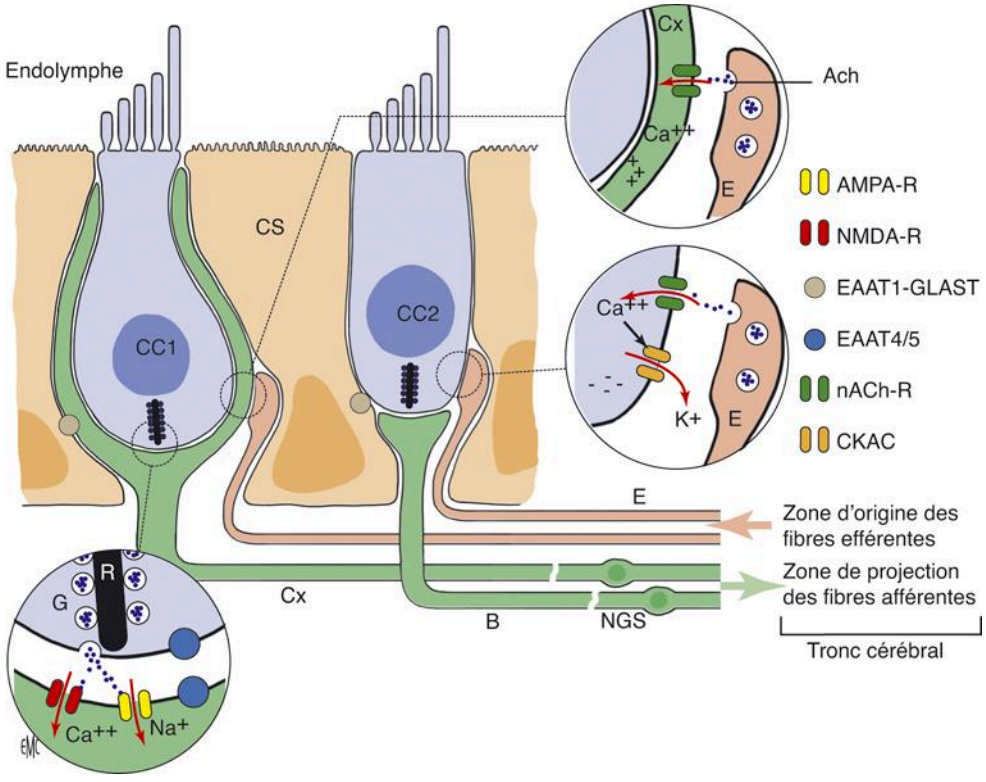

Figure 7: Synapses vestibulaires, cellules de Type I et de Type II

CC1 : cellule ciliée de type I ; CC2 : cellule ciliée de type II. CS : cellule de soutien. Cx : neurone afférent en calice. B : neurone afférent en bouton. E : neurone efférent. NGS : ganglion de Scarpa (neurone primaire). R : ruban présynaptique. G : glutamate. AMPA-R et NMDA-R : récepteurs glutamatergiques. EAAT1-GLAST et EAAT4/5 : transporteurs de glutamate (sur CC1 et CS respectivement). ACh : acéthylcholine. nACh-R : récepteur cholinergique de type nicotinique. CKAC : canal potassique activé par le calcium (Chabbert, 2015).

Il existe une régionalisation morphologique et fonctionnelle des fibres nerveuses afférentes, qui peuvent être classées d'après des critères électrophysiologiques en neurones phasiques et toniques. Les neurones phasiques innervent préférentiellement la région centrale des macules otolithiques et crêtes ampullaires, alors que les neurones toniques sont retrouvés essentiellement en périphérie. Chaque groupe neuronal permettrait de coder différentes composantes des informations vestibulaires (Beraneck and Straka, 2011) : les neurones toniques déchargent régulièrement et codent préférentiellement les mouvements à basses fréquences; les neurones phasiques fonctionnent irrégulièrement et codent préférentiellement les mouvements de haute fréquence (Straka et al., 2009). La majorité des neurones phasiques sont associés aux cellules de type I et la majorité des cellules toniques aux cellules de type II (***Figure 8***).

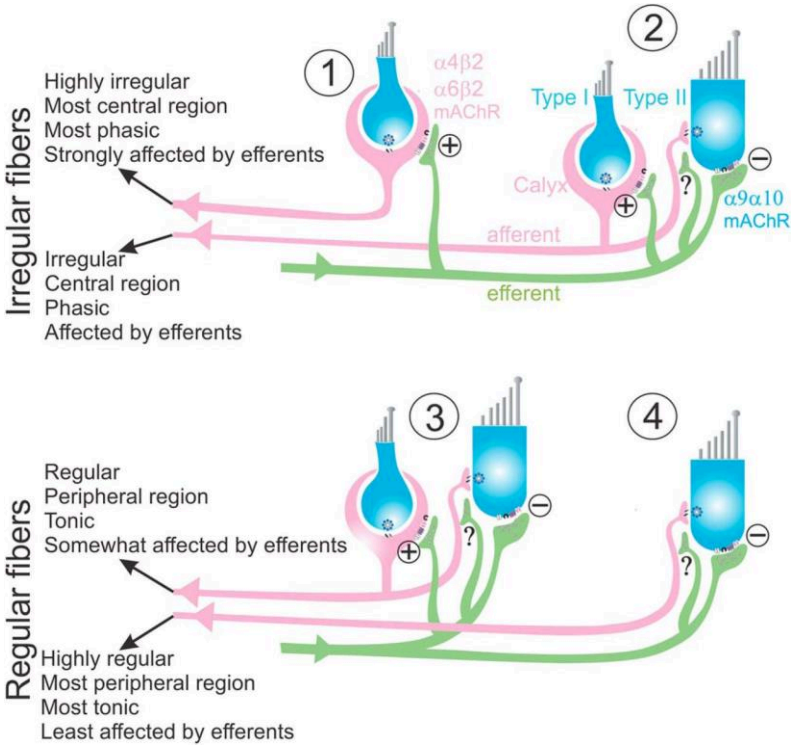

Figure 8: Synapses afférentes et efférentes

Représentation schématique des connexions efférentes sur les différents types de neurones afférents réguliers et irréguliers. Les neurones afférents irréguliers proviennent soit de cellules en calice uniquement (1), soit dimorphiques (2). Les afférents réguliers proviennent de cellules soit dimorphiques (3) soit de cellules en bouton uniquement (4). Les synapses efférentes sont excitatrices sur les cellules en calice et inhibitrices sur les cellules en bouton. L'effet des neurones efférents sur les afférents des cellules en bouton n'a pas encore été étudié directement (Raghu et al., 2019).

Les cellules ciliées sont contactées par des neurones efférents provenant du tronc cérébral (proche du noyau abducens), dont les axones remontent dans le nerf vestibulaire et les synapses se fixent sur les calices des cellules de type I et directement sur le pôle basal des cellules de type II. Cette différence est importante car les synapses efférentes cholinergiques pourraient exciter le neurone afférent en calice, mais directement inhiber les cellules en bouton en favorisant la fuite de K^+ (Chabbert, 2015).

Le rôle de ces connexions efférentes pourrait être principalement de réguler l'activité des cellules de type I et donc d'ajuster la perception des mouvements rapides de la tête (Raghu et al., 2019).

Le ***Tableau 1*** résume les différentes caractéristiques des cellules ciliées vestibulaires.

Tableau 1: Types de cellules ciliées vestibulaires (tableau simplifié)

Cellule	Synapse	Répartition dans les organes vestibulaires	Décharge des neurones afférents	Rétrocontrôle des neurones efférents	Codage
Type I	Calice	Centrale	Phasique (Irrégulière)	Important (Excitation)	Hautes fréquences
Type II	Bouton	Périphérique	Tonique (Régulière)	Faible (Inhibition)	Basses fréquences

1.3.2. Les canaux semi-circulaires

Les canaux semi-circulaires permettent de capter les accélérations angulaires de la tête allant de 0,1 à 20Hz (Schneider et al., 2015). La cupule, masse inertielle surmontant les cellules ciliées de la crête ampullaire, est déformée lors d'un mouvement de la tête dans son axe de rotation. Les cellules ciliées ampullaires sont toutes orientées dans l'axe du canal. Un mouvement de la cupule en direction de l'ampoule (ampullipète) est excitateur pour les canaux horizontaux alors qu'un mouvement dans le sens opposé à l'ampoule (ampullifuge) est excitateur pour les canaux verticaux (dans les deux cas, un mouvement dans le sens opposé est inhibiteur). Les trois CSC de chaque côté sont orientés dans les trois plans de l'espace, le canal horizontal est dans un plan incliné de 30° par rapport au plan transversal et les deux canaux verticaux (antérieurs et postérieurs), à 90° environ avec lui et entre eux. Chaque CSC forme ainsi un plan de rotation dans l'espace avec l'un des CSC contralatéraux : les deux

CSC horizontaux entre eux, le canal antérieur gauche avec le postérieur droit et le canal antérieur droit avec le postérieur gauche. Ces trois paires coplanaires fonctionnent de façon symétrique à une même stimulation, l'un étant excité et l'autre inhibé : c'est le phénomène *push-pull* (***Figure 9***).

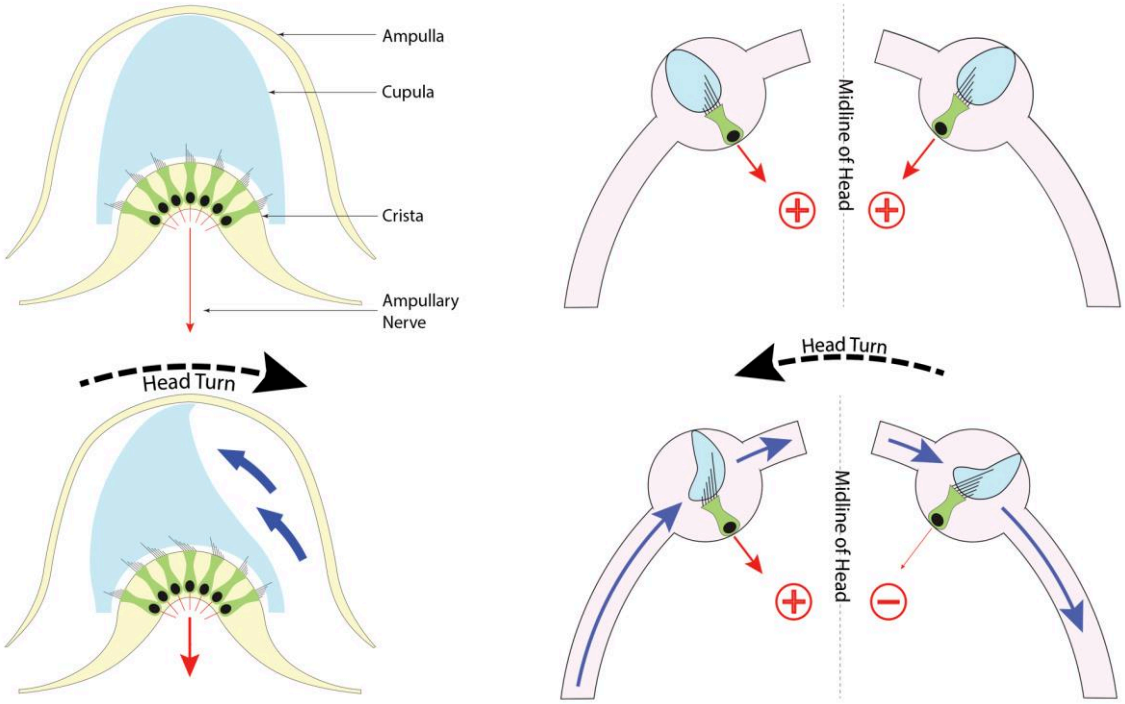

Figure 9: Ampoule des canaux semi-circulaires horizontaux

A gauche : La crête ampullaire (cristа) surmontée par la cupule dans l'ampoule du canal semi-circulaire. La rotation de la tête dans un sens entraine un mouvement de la cupule dans le sens contraire excitant les cellules ciliées. A droite : Lors d'une stimulation dans le plan horizontal, le canal ipsilatéral au sens de la stimulation va être excité et le contralatéral inhibé, c'est l'effet push-pull. (enteducationswansea.org)

Cette redondance permet au système vestibulaire de percevoir un mouvement de rotation même en cas de perte unilatérale. Le système push-pull a un seuil limite d'action (environ 180°/s) puisque l'inhibition du côté contralatéral atteint 0 potentiels d'action (*inhibitory cut-off*) par seconde alors que le côté ipsilatéral continue à être stimulé intensément. Ceci explique dans un déficit vestibulaire unilatéral compensé, la persistance d'oscillopsies aux rotations très rapides de la tête vers le côté lésé, le côté contralatéral inhibé ne permettant pas de coder seul ces stimulations.

1.3.3. Le système otolithique

Le système otolithique est composé du saccule et de l'utricule, qui codent pour les accélérations linéaires et les inclinaisons statiques de la tête par rapport au vecteur de la gravité. Les cellules ciliées sont surmontées par une grande masse inertielle, les otoconies, qui bougent en fonction de l'accélération ou de la gravité et stimulent les cellules ciliées (***Figure 10***).

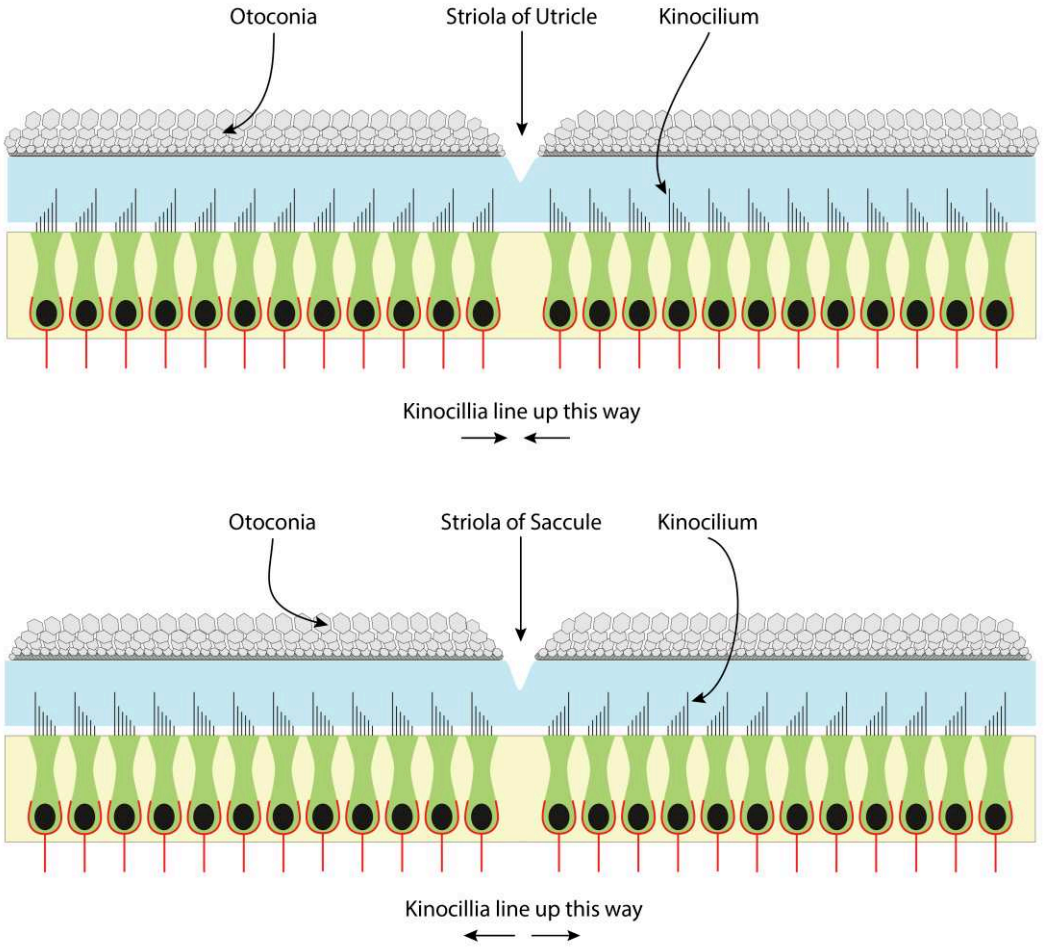

Figure 10: Organisation des cellules ciliées otolithiques

En haut : utricle avec les kinocils des cellules ciliées en direction de la striole. En bas : saccule avec les kinocils des cellules ciliées à l'opposé de la striole. (enteducationswansea.org)

Les cellules ciliées sont organisées de façon symétrique autour d'une striole, de sorte qu'un mouvement des otoconies stimule les cellules dans l'axe du mouvement avec une excitation des

cellules d'un côté de la striole (dont la touffe ciliaire penche vers le kinocil) et une inhibition de l'autre côté (touffe ciliaire qui s'éloigne du kinocil). Ce fonctionnement binaire couplé aux organes otolithiques contralatéraux rend le système très robuste. Le saccule est orienté dans un plan vertical para-sagittal et l'utricule dans un plan horizontal (***Figure 11***). Ainsi le saccule est stimulé lors des mouvements dans l'axe vertical (par exemple un ascenseur) et dans l'axe antéro-postérieur. L'utricule est stimulé lors des mouvements latéraux et également dans l'axe antéro-postérieur. Les inclinaisons statiques en roulis sont essentiellement codées par l'utricule.

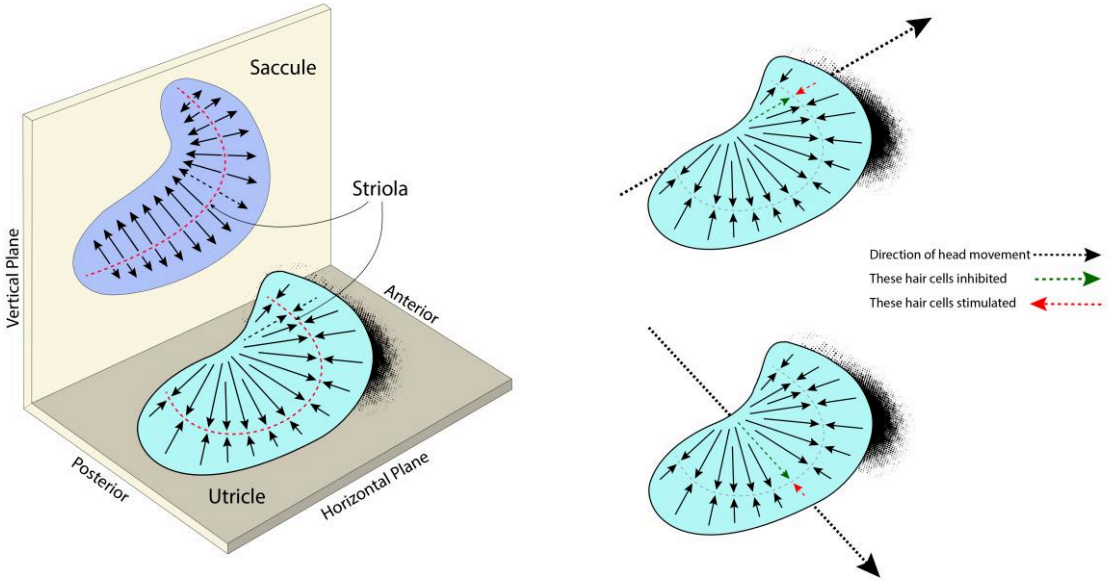

Figure 11: Orientation des cellules ciliées otolithiques

A gauche : L'utricule est dans un plan horizontal et le saccule est dans un plan vertical (même si le saccule est en réalité en dessous de l'utricule). A droite : axe de mouvement et stimulation de l'utricule, qui inhibe et stimule les cellules ciliées du même axe en fonction de leur organisation. (enteducationswansea.org)

1.4. Voies de projection des neurones vestibulaires secondaires

1.4.1. Les noyaux vestibulaires

Les noyaux vestibulaires se situent dans le plancher du 4ème ventricule, à la jonction bulbo-protubérantielle et comprennent les neurones vestibulaires secondaires. Il y a quatre noyaux principaux qui reçoivent les afférents des neurones vestibulaires primaires (***Figure 12***) : le supérieur, le latéral, le médian et l'inférieur.

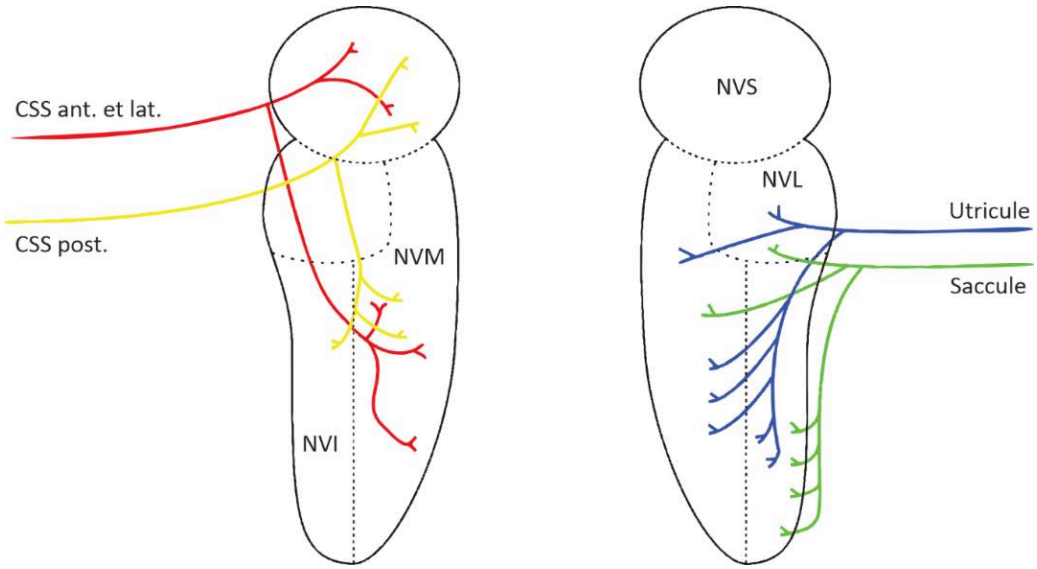

Figure 12 : Projection des organes vestibulaires sur les noyaux vestibulaires

CCS : Canal semi-circulaire ; NVS : Noyau vestibulaire supérieur ; NVL : Noyau vestibulaire latéral ; NVM : Noyau vestibulaire médian ; NVI : Noyau vestibulaire inférieur. (Modifié de enteducationswansea.org)

En simplifiant, les canaux semi-circulaires se projettent essentiellement dans les noyaux supérieurs et médians, qui à leur tour se projettent sur les noyaux oculo-moteurs. Le système otolithique se projette principalement sur les noyaux latéraux et inférieurs, qui à leur tour sont à l'origine des voies vestibulo-spinales. De nombreuses autres voies vestibulaires centrales existent et sont représentées dans la ***Figure 13***. Les neurones vestibulaires secondaires se projettent dans des zones d'intégrations multisensorielles ou participent aux réflexes vestibulo-oculaires ou vestibulo-spinaux.

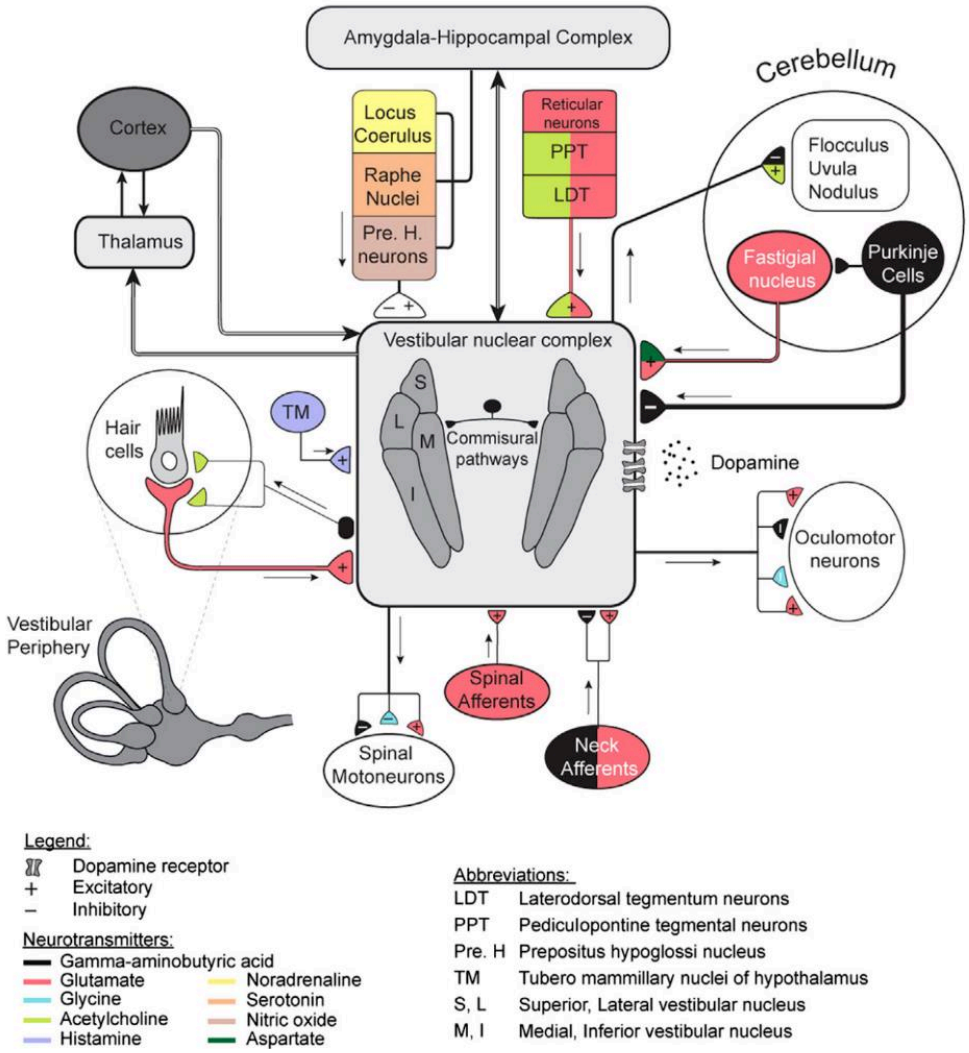

Figure 13 : Projections des neurones vestibulaires secondaires

Les neurones vestibulaires secondaires se projettent dans de nombreuses zones en utilisant divers neurotransmetteurs. Les projections sur les neurones oculomoteurs et voies spinales participent à la stabilité du regard et au maintien de la posture lors des mouvements. Une intégration multisensorielle est également réalisée dans le cervelet et le cortex vestibulaire (Gurvich et al., 2013).

Les noyaux vestibulaires communiquent entre eux, à la fois avec les autres noyaux ipsilatéraux mais aussi avec les noyaux contralatéraux grâce à un réseau commissural (***Figure 14***). Les connexions entre les noyaux ipsilatéraux sont majoritairement réciproques entre les noyaux supérieurs et inférieurs et supérieurs et médiaux, mais une zone centrale à cheval sur les noyaux inférieurs, latéraux et médians reçoivent des projections sans réciprocité (Ito et al., 1985). Chacun des noyaux (sauf le noyau latéral) est connecté à chacun des trois noyaux contralatéraux (Epema et al., 1988).

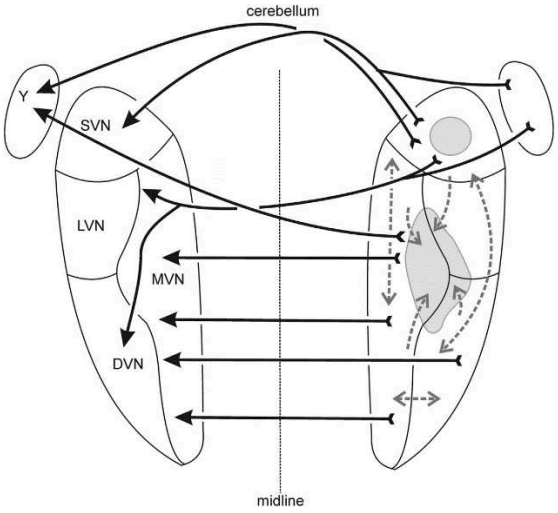

Figure 14 : Communication entre les noyaux vestibulaires

CCS : Canal semi-circulaire ; SVN : Noyau vestibulaire supérieur ; LVN : Noyau vestibulaire latéral ; MVN : Noyau vestibulaire médian ; DVN : Noyau vestibulaire inférieur (descending en anglais). Le groupe Y est un groupe de neurones vestibulaires secondaires accessoires. Les connexions entre les noyaux ipsilatéraux sont représentées en gris et pointillés, les connexions commissurales en trait noir et plein (Horn, 2020).

1.4.2. Voies vestibulo-oculaires

La fonction principale des voies vestibulo-oculaires est de stabiliser le regard compensant des mouvements de rotation la tête, grâce à différents réflexes (décrits ci-après), en fonction de mouvements de rotation, translation ou de changement d'axes de la tête et du corps (Baker et al., 1981). La voie vestibulo-oculaire des canaux semi-circulaires est un circuit court et rapide à trois neurones et une latence de 5 à 7ms (Angelaki and Hess, 2005; Huterer and Cullen, 2002), très bien conservé chez les vertébrés (Dieringer et al., 1996). Elle comprend le neurone vestibulaire primaire (ganglion de Scarpa), qui transmets l'information des cellules ciliées en calice, le neurone vestibulaire secondaire qui se trouve majoritairement dans le noyau vestibulaire supérieur ou médian et intègre les informations sensorielles et en fin le motoneurone oculaire qui transmet l'ordre moteur au muscle oculaire. Chacune des trois paires de noyaux oculomoteurs est innervée : les noyaux oculomoteurs, abducens et trochléaires. Les neurones vestibulaires secondaires envoient des informations à plusieurs motoneurones à la fois pour générer un mouvement oculaire cohérent (***Figure 15***).

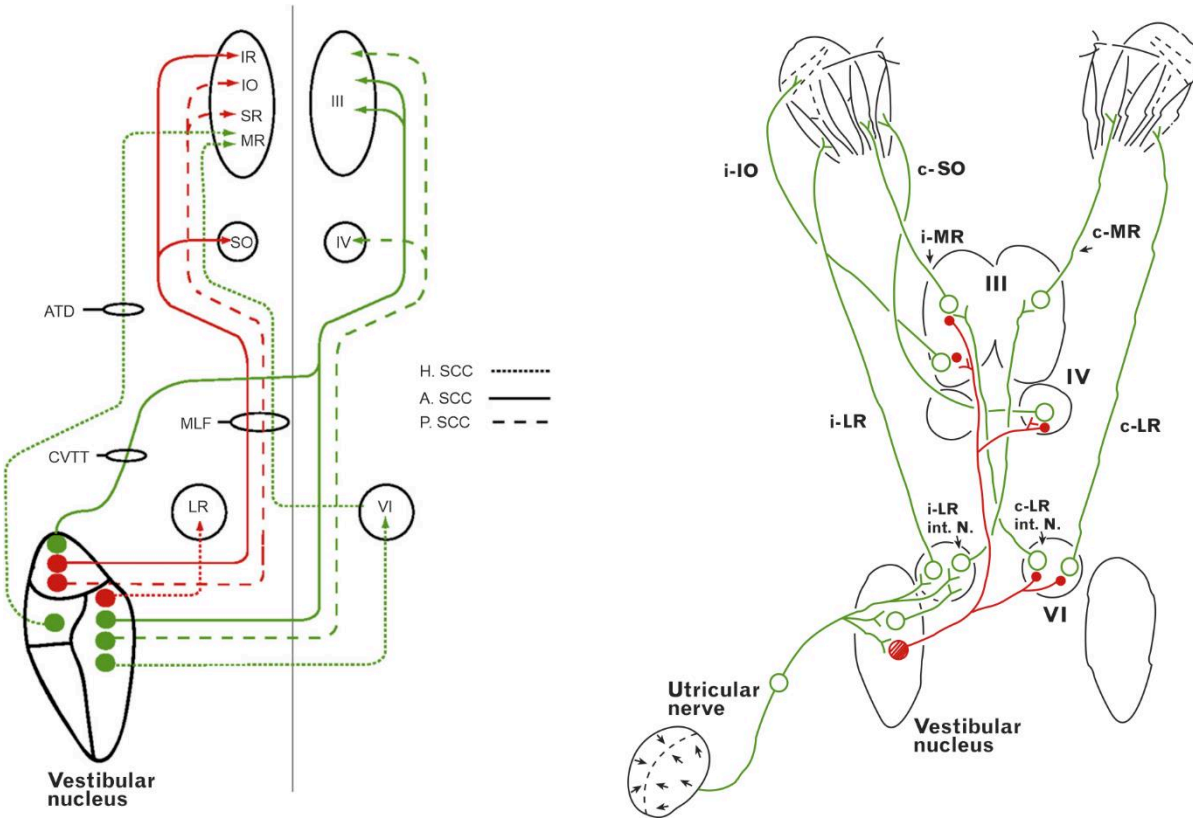

Figure 15 : Voies vestibulo-oculaires

Sur les deux schémas : en vert : voies excitatrices ; en rouge : voies inhibitrices. Noyaux oculomoteurs (III, IV et VI) et muscles correspondants (LR : lateral rectus *; MR :* medial rectus *; IR :* inferior rectus *; SR :* superior rectus *; IO :* inferior oblique *; SO :* superior oblique*). Les courbes pleins à pointillés correspondent aux canaux horizontaux, antérieurs ou postérieurs. A gauche : Stimulation canalaire gauche. Les trois voies principales sont la voie* medial longitudinal fasciculus *(MLF),* ascending tract of Deiters *(ATD) et* crossing ventral tegmental tract *(CVTT). A droite : Stimulation utriculaire gauche. Schémas modifiés de* (Holstein, 2012) *et* (Uchino et al., 1996)*, provenant d'études chez le chat.*

La voie vestibulo-oculaire utriculaire comprend une connexion monosynaptique vers le noyaux abducens ipsilatéral (Imagawa et al., 1995) et polysynaptique vers l'abducens contralatéral et vers les autres noyaux pairs oculomoteurs et trochléaires.

1.4.3. Voies vestibulo-spinales

Les voies vestibulo-spinales (représentées dans la ***Figure 16)*** sont organisées en trois faisceaux, le latéral, médian et caudal, et proviennent principalement des noyaux latéraux (pour le faisceau latéral), médian et inférieur. Le faisceau latéral se projette ipsilatéralement sur l'ensemble de la hauteur de la

moelle épinière, stimulant les muscles extenseurs. Le faisceau médian se projettent ipsilatéralement et contralatéralement sur les muscles du cou et du tronc (Shinoda et al., 2006). Le faisceau caudal se projette surtout en région cervicale (Peterson et al., 1978). Les noyaux vestibulaires secondaires reçoivent également des afférents cervicaux et spinaux rapportant des informations sur la position du corps et de la tête.

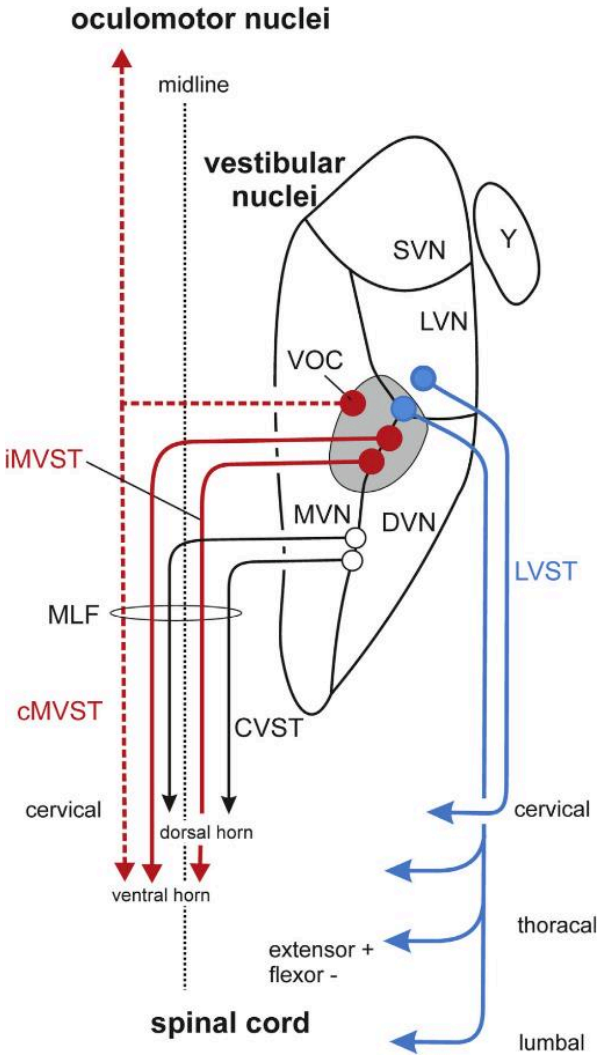

Figure 16 : Voies vestibulo-spinales

Il y a trois faisceaux principaux : le faisceau latéral (LVST – lateral vestibulospinal tract) ; le faisceau médian (MVST – medial vestibulospinal tract) avec ses projections ipsilatérales (i) et contralatérales (c) ; et le faisceau caudal (CVST – caudal vestibulospinal tract) (Horn, 2020)*, provenant d'études chez le singe et le chat.*

1.4.4. Voies vestibulo-cérébelleuses

Il existe de nombreuses connexions afférentes et efférentes entre le système vestibulaire et le cervelet (***Figure 17***). Des neurones vestibulaires primaires projettent vers le nodulus ipsilatéral (principalement canalaires) et l'uvula ipsilatéral (principalement du saccule). Les projections des neurones vestibulaires secondaires existent également bilatéralement vers ces mêmes structures et vers le flocculus. Des connexions afférentes du cervelet aux noyaux vestibulaires proviennent des mêmes structures (Goldberg et al., 2012). Le vestibulo-cervelet joue un rôle essentiel dans l'intégration des informations canalaires et otolithiques, dans la calibration des voies vestibulaires par l'intégration avec d'autres modalités sensorielles (ex : adaptation du réflexe vestibulo-oculaire par le retour visuel), ainsi que dans la discrimination des composantes actives (volontaires, prévisibles) et passives (involontaires, non prévisibles) du mouvement (Angelaki and Cullen, 2008; Mackrous et al., 2019).

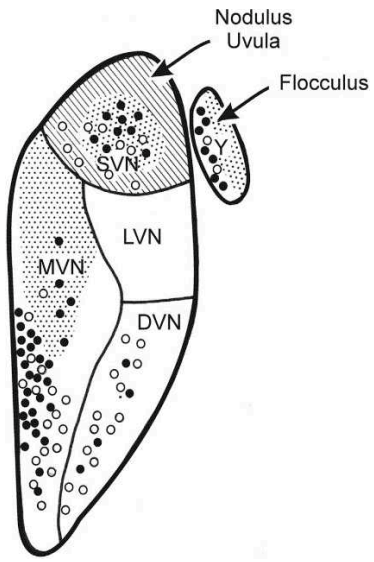

Figure 17 : Connexions entre les neurones vestibulaires secondaires et le cervelet

Les connexions efférentes vers le nodulus et l'uvula sont représentées par des cercles blancs et vers le flocculus par des cercles noirs. Les zones de projection provenant du nodulus et de l'uvula sont représentées en hachuré et du flocculus en pointillé (Büttner-Ennever, 1992)*, provenant d'études chez le singe et le chat.*

1.4.5. Voies vestibulo-végétatives

Le système otolithique participe au maintien de la pression artérielle, des fréquences cardiaques et respiratoires stables pendant les inclinaisons de la tête (Yates and Miller, 1998), ainsi qu'à la régulation du rythme circadien (Martin et al., 2015). Le système vestibulaire participe également à l'homéostasie osseuse en modulant l'activité ostéoblastique et notamment la masse des os qui supportent la structure corporelle (Vignaux et al., 2015, 2013). La voie descendante principale provient des noyaux vestibulaires et innerve les centres végétatifs médullaires, dont le noyaux moteur dorsal du nerf vague. D'autres voies ascendantes et descentes dont certaines sont modulées par le cervelet participent à la régulation homéostasique lors du mouvement (Goldberg et al., 2012; Horn, 2020). Les projections des neurones vestibulaires sur le nerf vague pourraient expliquer les symptômes neuro-végétatifs lors du syndrome vestibulaire (Horn, 2020).

1.4.6. Le cortex vestibulaire

Les neurones vestibulaires secondaires se projettent sur plusieurs régions corticales qui forment le cortex vestibulaire, avec de nombreuses afférences réciproques et interconnexions (***Figure 18***). Les neurones thalamiques intègrent et transmettent la majorité des informations entre les noyaux vestibulaires et différentes zones du cortex, par de nombreuses voies vestibulo-thalamiques différentes. Plus particulièrement, le cortex vestibulaire insulo-pariétal (PIVC) serait une zone importante d'intégration multisensorielle, recevant de nombreuses informations visuelles et somesthésiques (Brandt and Dieterich, 2019). Quatre voies principales ont pu être identifiées entre les noyaux vestibulaires et le cortex vestibulaire : (i) une voie vestibulo-thalamo-corticale qui transmettrait des informations d'orientation spatiale et de rapports entre les objets et le soi vers l'hippocampe; (ii) une voie passant par le noyau thalamique antéro-dorsal et le subiculum qui coderait l'orientation de la tête ; (iii) une voie « theta » qui passerait par le noyau supra-mamillaire jusqu'à l'hippocampe et jouerait un rôle dans la mémoire ; (iv) une voie cérébelleuse passant par le noyau

ventro-latéral du thalamus puis par l'hippocampe qui participerait à l'apprentissage spatial (Hitier et al., 2014).

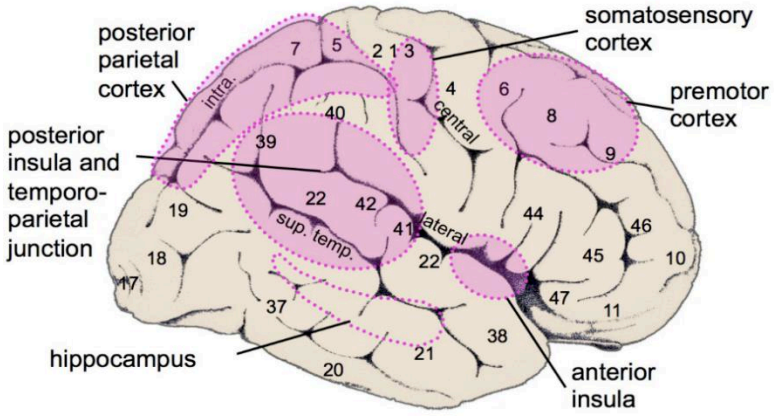

Figure 18 : Cortex vestibulaire

Zones vestibulaires principales dans le cerveau humain, identifiées par imagerie fonctionnelle. Les zones de Brodmann sont identifiées (Lenggenhager and Lopez, 2015).

1.5. Réflexes vestibulo-oculaires (VOR)

1.5.1. Angular VOR (aVOR)

Afin de maintenir la stabilité du regard pendant les mouvements de la tête, les yeux doivent se déplacer exactement à la même vitesse dans le sens opposé (le glissement de l'image rétinienne doit être inférieur à 2°/s pour que la vision reste nette). Ce mouvement réflexe angulaire de l'œil est possible grâce à la voie vestibulo-oculaire entre les canaux semi-circulaires et les motoneurones oculaires. Ce mouvement comporte deux phases bien distinctes : la phase lente qui correspond au mouvement de l'œil en réponse au mouvement de la tête, permettant la stabilité du regard ; la phase rapide dans le sens opposé à la phase lente qui permet le recentrage rapide de l'œil dans l'orbite lorsque celui-ci s'excentre de plus de 30°. L'alternance de ces deux phases constitue le nystagmus du réflexe vestibulo-oculaire. Le sens du nystagmus est nommé par convention en fonction du sens de la phase rapide, car plus simple à constater lors de l'examen clinique, mais c'est bien la phase lente qui correspond à la partie stabilisatrice de l'aVOR (Schubert and Minor, 2004).

Lors d'un mouvement de tête horizontal par exemple, le canal semi-circulaire horizontal ipsilatéral au sens de la rotation va être stimulé et le canal contralatéral inhibé. Les neurones vestibulaires secondaires ipsilatéraux vont stimuler à la fois le noyau abducens (VI) contralatéral et le noyau oculomoteur (III) ipsilatéral pour initier un mouvement oculaire contralatéral en faisant contracter le droit externe contralatéral et droit interne ipsilatéral. Des communications supplémentaires entre des noyaux oculomoteurs permettent d'affiner ce réflexe et de conjuguer le mouvement des deux yeux (notamment entre le noyau abducens vers le noyau oculomoteur contralatéral).

A l'inverse, les neurones vestibulaires secondaires contralatéraux vont être inhibés par la rotation de la tête et vont participer au relâchement des muscles droit interne contralatéral et abducens ipsilatéral. Une véritable relation *push-pull* existe entre les deux canaux semi-circulaires horizontaux,

c'est-à-dire une contribution des deux canaux à l'aVOR même si l'information du canal stimulé prédomine.

L'aVOR vertical des canaux semi-circulaires antérieurs et postérieurs est superposable à celui des canaux horizontaux, avec un effet push-pull entre le canal semi-circulaire antérieur gauche et postérieur droit, et postérieur gauche et antérieur droit.

1.5.2. Le stockage de vitesse (velocity storage)

L'aVOR normal ne peut garantir une performance optimale que pour des mouvements brefs de la tête, et donc permet de prendre en compte les mouvements de haute-fréquence, mais moins les mouvements de basse-fréquence. Cette caractéristique est mise en évidence lors d'une rotation à vitesse continue de la tête, qui montre une décroissance exponentielle de la réponse vestibulaire. La constante de temps est le temps au bout duquel la réponse vestibulaire post-rotatoire n'est plus qu'à 37% de son activité maximale. Chez l'Homme, la constante de temps est de l'ordre de 15-20 secondes (Cohen et al., 1981), alors que lorsqu'elle est mesurée expérimentalement au niveau de la cupule, celle-ci n'est que de 5 secondes (Fernandez and Goldberg, 1971). La différence entre les deux mesures correspond à un stockage de vitesse central, qui permet de prolonger l'aVOR lors des mouvements basse-fréquence. Le *velocity storage* est encodé dans les noyaux vestibulaires centraux et le vestibulo-cervelet (Raphan et al., 1979; Yakushin et al., 2017).

1.5.3. Le réflexe maculo-oculaire pendant l'OVAR ($_{OVAR}$MOR)

Lors d'une rotation à vitesse constante autour d'un axe légèrement incliné par rapport à la verticale, plusieurs réflexes sont mis en évidence, dont l'aVOR et le *velocity storage*. Après épuisement du réflexe canalaire horizontal lié à la rotation continue à vitesse constante, un nystagmus horizontal peut-être identifié avec une phase lente dans le sens opposé à la rotation qui reste constant tant que la rotation est maintenue (Benson and Bodin, 1966). Ce nystagmus est accompagné d'un mouvement oculaire vertical sinusoïdal. Ce réflexe serait principalement dû à une activation otolithique, liée à la

rotation du vecteur gravitationnel entrainant une stimulation séquentielle des cellules ciliées otolithiques (Angelaki, 1992). Le $_{OVAR}$MOR nécessite cependant une intégrité du cervelet (Angelaki and Hess, 1995), et utiliserait un circuit neuronal commun avec le *velocity storage* avec une probable faible participation de l'aVOR (Angelaki and Hess, 1996). Les mécanismes précis sont encore mal compris, mais ce réflexe maculo-oculaire nécessite une intégrité du système vestibulaire périphérique et central.

1.5.4. Translational VOR (TVOR)

Ce réflexe vestibulo-oculaire permet de conserver la stabilité du regard lors de mouvements translationnels de haute fréquence (comme l'AVOR lors de mouvements de rotation) et dépend principalement du système otolithique (Angelaki, 2004; Kutz et al., 2020). A l'inverse de l'AVOR, le TVOR est particulièrement important pour la vision des objets proches car permet de garder l'image focalisée sur la fovea, alors que l'AVOR stabilise l'image rétinienne globale (Wei and Angelaki, 2006). Il a été montré que ce réflexe est faible chez les mammifères n'ayant pas de fovea, comme les souris (Hess and Dieringer, 1991).

1.5.5. Tilt VOR

Le *tilt VOR* survient lorsque la tête est penchée en roulis sur le côté (autour d'un axe antéro-postérieur) ou en tangage (autour de l'axe droite-gauche latéral), l'objectif étant de maintenir l'orientation des yeux dans l'espace. Lors de l'inclinaison statique de la tête, seul le système otolithique et surtout l'utricule est stimulé, entrainant un réflexe maculo-oculaire ($_{tilt}$MOR). Pendant un mouvement d'inclinaison dynamique, il y a une stimulation mixte otolithique et canalaire verticale. Deux composantes principales de ce réflexe sont identifiées :

a. Torsion oculaire : *ocular counter-roll (OCR) :* Il s'agit d'une rotation torsionnelle de l'œil en réponse à l'inclinaison latérale de la tête. L'OCR dynamique entraine un nystagmus torsionnel avec une phase rapide vers le côté d'inclinaison de la tête et une phase lente vers le côté

contralatéral (Collewijn et al., 1985). Lorsque l'inclinaison de la tête est stable, l'OCR statique entraîne une cyclotorsion de l'œil, vers le côté contralatéral, avec un gain estimé entre 0,1 et 0,25 (angle de l'œil / angle de la tête) chez l'Homme (Bockisch and Haslwanter, 2001).

b. Mouvement compensatoire vertical de l'œil : L'œil se déplace verticalement vers le haut lorsque la tête est inclinée ipsilatéralement, et l'œil se déplace vers le bas lorsque la tête est inclinée contralatéralement. L'œil se stabilise dans cette position lors d'une inclinaison statique (Oommen and Stahl, 2008).

A noter que chez les animaux aux yeux frontaux comme le singe, l'OCR est plus important lors de l'inclinaison en roulis (autour de l'axe antéro-postérieur) et le mouvement oculaire vertical lors de l'inclinaison en tangage (inclinaison autour de l'axe droite-gauche) (Bockisch and Haslwanter, 2001). En revanche, chez les animaux aux yeux latéraux dont les souris, le tilt VOR est important (Cohen et al., 2001; Migliaccio et al., 2011). Aussi, le mouvement oculaire vertical est plus important lors de l'inclinaison en roulis, et la torsion lors de l'inclinaison en tangage.

1.6. Réflexes vestibulo-spinaux (VSR)

Deux réflexes principaux, empruntant les voies vestibulo-spinales, ont pour rôle de maintenir une posture verticale du corps et de la tête lors des mouvements de la tête (principalement détectés par le système otolithique). Le réflexe vestibulo-colique (VCR), par le faisceau vestibulo-spinal médian, agit sur les muscles du cou (notamment en contractant les sterno-cleido-mastoïdiens) pour stabiliser les mouvements involontaires de la tête et compenser une inclinaison en maintenant la tête droite et le regard à l'horizontal (Goldberg and Cullen, 2011). Parallèlement, l'objectif du réflexe vestibulo-spinal est de maintenir la posture verticale en fonction des mouvements de la tête en fonction de la perception de la gravité. Lorsqu'un mouvement de la tête est détecté, la stimulation otolithique relayée par le faisceau vestibulo-spinal latéral entraine une stimulation des muscles extenseurs ipsilatéraux et des muscles fléchisseurs contralatéraux.

2. Rôles du système vestibulaire

2.1. La stabilité de la posture

La stabilisation posturale est l'une des fonctions principales du système vestibulaire, participant au maintien de l'équilibre. L'équilibre est une fonction complexe et est le résultat d'une véritable intégration multisensorielle. Le système vestibulaire fait partie des trois entrées principales permettant le maintien de l'équilibre, avec le système visuel et le système proprioceptif. Cette complexité permet également une grande adaptabilité avec de nombreux moyens de compensation en cas de défaillance de l'une des entrées sensorielles.

2.2. La stabilité du regard

Plusieurs réflexes vestibulo-oculaires (AVOR, TVOR, $_{tilt}$VOR) participent avec le réflexe optocinétique (ORK) à la stabilisation du regard. Cet ensemble de réflexes permet les mouvements oculaires compensatoires lors des mouvements de la tête, lesquels permettent de maintenir une vision nette. S'y ajoutent les réflexes qui permettent la stabilité de la tête dans l'espace dont le réflexe vestibulo-colique en interaction avec les réflexes cervico-coliques.

2.3. Fonctions cognitives

2.3.1. Orientation dans l'espace

L'orientation dans l'espace est également le fruit d'une intégration multisensorielle dont le système vestibulaire fait partie. Le déficit vestibulaire a été significativement associé à une diminution des capacités visuo-spatiales (Ayar et al., 2020; Bigelow et al., 2015). Le retentissement sur ces capacités serait en lien avec une atrophie de l'hippocampe secondaire au déficit vestibulaire (Aitken et al., 2018;

Brandt et al., 2005; Smith et al., 2005). Plus spécifiquement, le système otolithique aurait un rôle important dans l'orientation spatiale par sa capacité à déterminer la direction de la gravité (Smith, 2019). Enfin, la fonction vestibulaire et la verticale subjective participerait à la coordination entre l'œil est la main, notamment pour saisir objet (Blouin et al., 2015; Tagliabue et al., 2013; Tagliabue and McIntyre, 2014).

2.3.2. Mémoire

Il a été noté une diminution des capacités cognitives chez le sujet âgé (Semenov et al., 2016), ainsi qu'une altération de la mémoire (Ayar et al., 2020; Bigelow et al., 2016). La dysfonction vestibulaire pourrait être un facteur de risque de démence (Smith, 2017).

2.3.3. Retentissement psychiatrique et psychologique

Un lien entre déficit vestibulaire et atteinte psychologique a été mis en avant par plusieurs grandes études épidémiologiques avec notamment une augmentation globale du risque de comorbidité psychiatrique, dont l'anxiété et la dépression (Ayar et al., 2020; Bigelow et al., 2016; Schmid et al., 2020).

La construction du soi semble également lié à une perception satisfaisante de la verticale subjective (Borel et al., 2008). Certains patients avec déficit vestibulaire rapportent des troubles dissociatifs de type dépersonnalisation/déréalisation, en rapportant des sensations de flottement (Kitahara et al., 2019), ou l'impression de voir son propre corps de l'extérieur (Kaliuzhna et al., 2015; Lopez and Elzière, 2018). Ces troubles ont été étudiés plus en détail par une revue systématique de la littérature.

2.4. Revue 1 : Symptômes de dépersonnalisation/déréalisation dans le syndrome vestibulaire : revue systématique de la littérature et approche phénoménologique

2.4.1. Contexte scientifique

Le trouble de dépersonnalisation/déréalisation est un trouble dissociatif parfois rapporté par des patients lors de crises vestibulaires (sensations de flottement ou de se voir à la troisième personne). Ce trouble est défini, dans le DSM-5 (Spiegel et al., 2013), par une expérience prolongée ou récurrente de détachement de son propre corps ou de son fonctionnent mental, avec l'impression d'être devenu un observateur extérieur de sa propre existence (dépersonnalisation) ou d'être détaché de son environnement (déréalisation). Il s'agit d'une forme de trouble dissociatif surtout retrouvé dans les pathologies psychiatriques telles que l'anxiété (Schlax et al., 2020), la dépression (Paul et al., 2019) ou la schizophrénie (Gonzalez-Torres et al., 2010) mais aussi neurologiques comme l'épilepsie (Heydrich et al., 2019) ou la migraine (Cahill and Murphy, 2004).

Concernant le vestibule, de nombreuses études observationnelles (Deroualle et al., 2017; Kolev et al., 2014; Lopez and Elzière, 2018; Smith and Darlington, 2013; Toupet et al., 2019) sur des patients avec déficit vestibulaire unilatéral ont été réalisées, ainsi que de nombreuses études expérimentales (Aranda-Moreno et al., 2019; Jáuregui-Renaud et al., 2019; Karnath et al., 2019; Schönherr and May, 2016) avec une stimulation vestibulaire (galvanique, calorique, rotation, etc.) cependant les critères de jugement principaux sont hétérogènes et les conclusions parfois contradictoires. L'évaluation de l'importance du trouble dissociatif est forcément subjectif et le questionnaire le plus fréquemment utilisé était le 28-DDI (depersonlization/derealization inventory), développé pour évaluer ces troubles dans l'anxiété (Cox and Swinson, 2002).

Nous avons également cherché à explorer ces symptômes en utilisant du vocabulaire phénoménologique. L'objectif principal de la phénoménologie est l'analyse des phénomènes tels

qu'ils sont perçus subjectivement (sans métaphysique et sans développer de théories sur la causalité sous-jacente). Cette tradition philosophique majeure de la première moitié du 19ème siècle a été développée principalement par les philosophes allemands Edmund Husserl (1859 – 1938) et Martin Heidegger (1889 – 1976), mais aussi par le philosophe français Maurice Merleau-Ponty (1908 – 1961) qui s'est particulièrement intéressé à la phénoménologie du corps. L'utilisation de cette méthodologie semble pertinente pour apporter un nouveau regard sur ces symptômes vestibulaires méconnus.

2.4.2. Buts de l'étude

L'objectif principal de l'étude était de réaliser une revue systématique de la littérature sur les troubles de dépersonnalisation/déréalisation en lien avec un déficit ou une stimulation vestibulaire pour faire ressortir les tendances principales et préciser l'influence du système vestibulaire sur les expériences hors du corps. Pour aider à la compréhension de ces troubles, tant du point de vue du patient que du soignant (ou sujet et observateur), une analyse phénoménologique a été réalisée.

2.4.3. Résumé en français

Une revue systématique de la littérature a été réalisée en suivant les guidelines PRISMA, en recherchant sur les bases de données Medline et Embase. Les mots clés « Embodiment », « disembodiment », « self-consciousness », « out of body experience », « depersonalization », « derealization » and « vestibular », « vestibular disease », « vestibule » ont été recherchés. Les articles publiés entre janvier 2005 et Avril 2020 en anglais ont été inclus. Les articles sélectionnés ont ensuite été analysé pour leur qualité en utilisant le « Newcastle-Ottawa quality assessment scale ». Au total, 47 articles ont été sélectionnés dont 13 études observationnelles, 21 études expérimentales et 13 revues non-systématiques de la littérature ou éditoriaux. Neuf de ces études ont analysé les résultats à un questionnaire (7 ont utilisé le 28-DDI), quatre ont analysé la verticale subjective et quatre un test d'illusion de la main en caoutchouc. Les autres articles ont évalué des tests non standardisés, tels que l'impression de changement de la taille de différentes parties du corps ou

simulation de perspective en troisième personne à l'aide d'avatars. Concernant les 34 articles originaux, 26 avaient un score de qualité moyen et 8 un score mauvais. L'ensemble de preuves statistiquement significatives à la fois expérimentales et observationnels sur patients semble montrer une claire association entre le vestibule et la dépersonnalisation/déréalisation. Que ce soit par stimulation vestibulaire (galvanique, calorique, ou autre) ou lors de déficits vestibulaires, l'intégration multisensorielle avec des entrées vestibulaires perturbées entraine une modulation de l'intégration visuo-proprioceptive avec une augmentation de l'illusion corporelle et une diminution de la capacité de se projeter à la 3ème personne. Les 13 articles de revue/opinion ont tous mis en avant la jonction temporo-pariétale comme étant une région d'intégration multisensorielle et d'interprétation de l'information vestibulaire, pouvant être en cause lors des troubles dissociatifs. L'approche phénoménologique, basée principalement sur le concept de corporéité de Merleau-Ponty, a permis de définir le corps, non seulement comme un organisme physiologique, mais aussi comme étant le moyen d'interaction de l'être avec son environnement. L'altération de la fonction vestibulaire pourrait favoriser une rupture de cette corporéité et la perception de son propre corps comme un objet, se traduisant psychologiquement par un trouble de dépersonnalisation/déréalisation.

2.4.4. Article original

Titre :

The vestibular influence on embodied self-consciousness: systematic literature review and phenomenological approach

Auteurs :

Cassandre DJIAN, Tudi GOZE, Françoise DENOYELLE, Michele TAGLIABUE, Mathieu BERANECK, François SIMON

Etat d'avancement :

A soumettre : *Cortex* (IF = 4.009)

Introduction:

Bodily self-consciousness is defined as the relationship between the physical body and the "self" which, in the physiological state, are experienced as a single "embodied self" or "lived body", whereas spatial self-consciousness is defined as the interaction between the "embodied self" and its immediate environment. Depersonalization-derealization disorder (DPDR) is a typical dissociative disorder induced by the breakdown of bodily and spatial self-consciousness respectively [1], reported in various neurological disorders such as epilepsy [2,3], migraine [4,5], and psychiatric disorders [1] including anxiety [6] or schizophrenia [7,8]. Recent evidence has demonstrated that the vestibular system, and its interaction with visual and somatosensory systems, could play a key role in bodily and spatial self-consciousness [9–17]. Indeed, patients with vestibular impairment often experience DPDR, describing illusory sensations as floating [18] or "seeing themselves from the outside" [19,20]. A better understanding of the role of vestibular signals in embodied self-consciousness and DPDR in pathological situations could lead to more accurate diagnoses and better rehabilitation strategies.

DPDR may be further explored from a phenomenological perspective. Phenomenology refers to the study of "lived experience", that is the subjective dimension of a medical disorder. It stresses the inseparability of the physical body and the self [21], in which the "embodied self" actively perceives and influences its environment [22]. This method, which dominated continental philosophy during the first half of the 20th century, can provide useful heuristic material to understand how experience can be altered from a first-person perspective. As such, phenomenology has a growing audience in psychiatry and cognitive neurosciences, notably because it allows consciousness to be thought of as the close and non-exclusive relationship between the self and the world (intentionality in Edmund Husserl's terms).

The aim of this systematic review was to give an overview of the evidence linking the vestibular system and embodied self-consciousness, out-of-body experience (OBE) or DPDR. A number of recent papers have attempted to clarify the relationship between vestibular disorders or experimental vestibular stimulation and embodied self-consciousness. Also, recent advances in vestibular cortex neuroanatomy and multi-sensory integration may help understand the pathways at hand. Lastly, we will discuss how altered vestibular input may be perceived as a phenomenological rupture between the physical body and the self.

Materials and methods:

Search strategy and selection criteria

The systematic review followed PRISMA guidelines [23]. Studies providing data on the vestibular system and bodily-self-consciousness or spatial self-consciousness, were identified searching Medline and Embase databases. All of the articles published from January 2005 to April 2020, on human subjects and in English, were included. The research strategy included the following search terms: 'Embodiment', 'disembodiment', 'self-consciousness', 'out of body experience', 'depersonalization', 'derealization' and 'vestibular', 'vestibular disease', 'vestibule' (full search strategy detailed in ***Supplementary Table 1***). Interventional and observational studies, general reviews and editorials were included, case reports were excluded. After removal of duplicates, articles were first selected on their title and abstract, then based on the abstract, excluding papers which did not relate to the topic. Final inclusion was based on the full text. References of included articles were checked for any additional studies.

Supplementary Table 1: Extensive overview of search terms: search strategy PubMed

Search number	Query	Search Details	Results
2	(labyrinth vestibule[MeSH Terms]) OR (vestibular[Text Word]) OR (vestibul*[Text Word])	"vestibule, labyrinth"[MeSH Terms] OR "vestibular"[Text Word] OR "vestibul*"[Text Word]	60,034
1	(embodiment[Text Word]) OR (disembodiment[Text Word]) OR (depersonalization[MeSH Terms]) OR (derealization[Text Word]) OR (out of body experience[Text Word]) OR (self-consciousness[Text Word])	"embodiment"[Text Word] OR "disembodiment"[Text Word] OR "depersonalization"[MeSH Terms] OR "derealization"[Text Word] OR "out of body experience"[Text Word] OR "self-consciousness"[Text Word]	5,729
3	(#1) AND (#2)	(("embodiment"[Text Word] OR "disembodiment"[Text Word]) OR "depersonalization"[MeSH Terms]) OR "derealization"[Text Word]) OR "out of body experience"[Text Word]) OR "self-consciousness"[Text Word])) AND (("vestibule, labyrinth"[MeSH Terms] OR "vestibular"[Text Word]) OR "vestibul*"[Text Word])	65

Data extraction

For each included experimental study, the primary outcomes regarding own-body perception or spatial orientation were extracted. Patient characteristics, diagnoses, type of intervention and results

with statistical significance were extracted from the articles. In non-experimental articles or reviews, the neurophysiological hypotheses that were put forward were reported.

Quality assessment

Risk of bias was separately assessed for each study, as defined in the PRISMA guidelines. The Newcastle – Ottawa quality assessment scale for non-randomized studies was used with an overall score ranging from 0 (minimum) to 9 (maximum) points [24]. A risk of bias was assigned to each study, low for 7-9; moderate for 4-6 and low for 1-3 points, (***Supplementary Table 2***).

Supplementary Table 2: Newcastle-Ottawa scale for quality assessment of non-randomized studies

Note: A study can be awarded a maximum of one star for each numbered item within the Selection and Outcome categories. A maximum of two stars can be given Comparability.

Selection

1) Representativeness of the exposed cohort
   a) truly representative of the average subject in the community *
   b) somewhat representative of the average in the community *
   c) selected group of subjects/patients
   d) no description of the derivation of the cohort

2) Selection of the non exposed cohort
   a) drawn from the same community as the exposed cohort *
   b) drawn from a different source
   c) no description of the derivation of the non exposed cohort

3) Ascertainment of exposure
   a) secure record (eg surgical records) *
   b) structured interview *
   c) written self report
   d) no description

4) Demonstration that outcome of interest was not present at start of study
   a) yes *
   b) no

Comparability

1) Comparability of cohorts on the basis of the design or analysis
   a) study controls for vestibular stimulation *
   b) study controls for patients with vestibular disorders

Outcome

1) Assessment of outcome
   a) independent blind assessment *
   b) record linkage *
   c) self report
   d) no description

2) Was follow-up long enough for outcomes to occur
   a) yes *
   b) no

3) Adequacy of follow up of cohorts
   a) complete follow up - all subjects accounted for *
   b) subjects lost to follow up unlikely to introduce bias - small number lost to follow up, or description provided of those lost) *
   c) important lost to follow up rate and no description of those lost
   d) no statement

Results:

A total of 150 articles were initially identified after the database search, of those 47 articles were selected: 34 original research articles and 13 general reviews. The flow diagram of the article selection process is reported in ***Figure 1***.

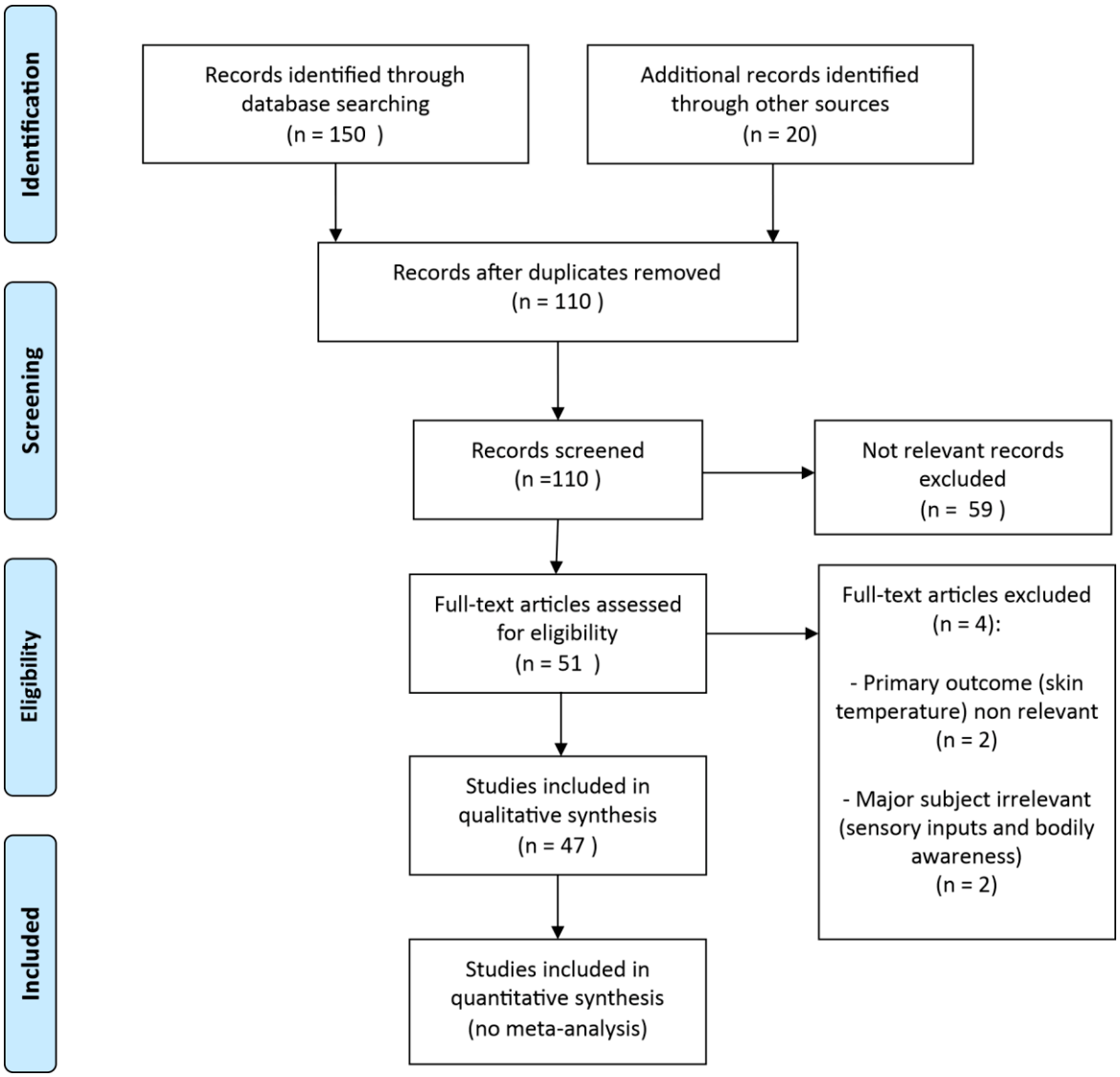

Figure 1: Flow chart according to PRISMA guidelines

Original Research articles

A total of 2183 patients were included in 13 observational and 21 interventional studies. In the observational studies, patients had unilateral or bilateral vestibular disorder. Study characteristics including selection criteria and diagnoses are summarized in ***Table 1***. In the interventional studies,

healthy participants were recruited, and primary outcome was comparison within the same population, before and after vestibular stimulation. Study characteristics are summarized in ***Table 2***. All experimental studies were prospective. No meta-analysis was possible because of primary outcome heterogeneity. Primary outcomes, statistical significance, and bias scores are summarized in ***Table 3***.

Table 1: Characteristics of observational studies

Study	No of patients	Inclusion criteria	Diagnostic testing	Diagnosis	Primary Outcome	BSC	SSC
[20]	210	Acute symptoms of dizziness	Otoneurological exam Caloric testing VHIT, cVEMP MRI	Peripheral VD, Central VD, Unknown	OBE questionnaire	x	x
[25]	319	Chronic dizziness (>3 months)	Clinical exam Caloric testing SVV, HADS	BPPV, Ménière, stress, vestibular migraine, UVL, Unknown	DDI	x	x
[26]	50	Acute VD	Clinical exam Caloric testing	Unilateral canal paresis Bilateral canal paresis BPPV		x	x
[27]	50	Acute or chronic VD	Clinical exam Audiogram Caloric testing	Unilateral canal paresis Bilateral canal paresis BPPV		x	x
[28]	24	Acute VD	Dix and Hallpike Caloric, HADS	Unilateral canal paresis BPPV		x	x
[29]	10	Acute unilateral VD	Clinical exam Caloric testing	Unilateral vestibular disorders		x	x
[30]	56	Otolithic or rotatory vertigo	Clinical exam Caloric testing cVEMP	Oto group: otolithic symptom Rotatory group: rotatory symptom	SVV		x
[31]	23	Idiopathic bilateral VD	Clinical exam Caloric testing VHIT cVEMP Rotatory chair	Idiopathic bilateral vestibular failure	Perspective-taking task	x	x
[32]	20	BPPV Unilateral Vestibular neuritis	Dix and Hallpike maneuver clinical exam Caloric testing VVS	BPPV Vestibular neuritis	Own-body mental rotation / human figure mental rotation tasks		x
[33]	32	Objective / subjective vertigo	Gait task vHIT	Balance disorder	Copied or transformed movements	x	x
[34]	23	Unilateral Vestibular neurectomy	Surgical procedure	Vestibular neurectomy	First or Third person perspective taking task	x	x
[35]	22				Object based mental transformation		x
[36]	11				SVV depending on body position		x

BPPV = benign paroxysmal positional vertigo, BSC = Bodily Self-Consciousness, cVEMP = cervical Vestibular Evoked Myogenic Potentials, DDI = depersonalization / derealization Inventory, HADS = Hospital Anxiety and Depression Scale, MRI = magnetic resonance imagery, OBE = out-of-body experience, SSC = Space Self-Consciousness, SVV = subjective visual vertical, UVL = unilateral vestibular labyrinthectomy, VD = vestibular disease, vHIT = video head impulse test, VVH = visuo-vestibular hypersensitivity, SVV = subjective visual vertical.

Questionnaires were used by nine studies as primary outcome to assess DPDR symptoms, of which seven [25–29,37,38] used the "Depersonalization / Derealization Inventory" (DDI), a standardized 28-item questionnaire used in DPDR (***Supplementary Table 3)*** [39]; two the "Cambridge depersonalization score" [20,40] and one an OBE diagnostic questionnaire [20]. DPDR was assessed in

vestibular impaired patients or during caloric vestibular stimulation (CVS) or galvanic vestibular stimulation (GVS).

Table 2: Characteristics of experimental studies

Study	No of subjects	Vestibular stimulation	Primary outcome	BSC	SSC
[37]	100	Unilateral centrifugation	DDI	x	x
[38]	34			x	x
[41]	26	Galvanic vestibular stimulation	Rubber hand illusion	x	
[16]	26			x	
[42]	16			x	
[43]	22		Perceived arm length	x	
[44]	12		Localization of tactile stimulus	x	
[45]	11		Mental transformations		x
[46]	32		3PP task		x
[47]	18		Graphesthesia task	x	x
[38]	34	Caloric vestibular stimulation	DDI	x	x
[48]	17		Perceived hand size	x	
[40]	16			x	
[49]	13		Non visual rubber hand illusion	x	
[50]	30		Perceived thigh width	x	
[51]	13		Tactile two-point discrimination	x	
[52]	18	Rotatory chair stimulation	Mental body rotation		x
[53]	20		3PP task	x	x
[54]	78	Visuo-vestibular conflict	Full body illusion	x	x
[55]	35			x	x
[56]	9			x	x

3PP = Third person-perspective, BSC = Bodily Self-Consciousness, DDI = depersonalization / derealization inventory, SSC = Space Self-Consciousness.

Patients presenting with acute or chronic vestibular disorders were statistically associated with increased DPDR symptoms compared to control subjects in all observational studies [20,25–29,40], DPDR symptoms being more important in symptomatic vestibular patients. In patients with vestibular disorders, anxiety symptoms were shown to be statistically more frequent and intense in patients with higher DDI scores [25,28] or reporting OBE [20]. DDI scores was also increased after unilateral centrifugation (19) and after CVS in healthy subjects [26]. In patients with DPDR due to a phantom limb syndrome, unilateral centrifugation and CVS decreased DDI scores [38].

Subjective visual vertical (SVV) was used as a primary outcome to assess spatial self-consciousness, analysing in the dark, the mean error in degrees between the SVV from the true vertical. SVV perception was found to increase significantly as DDI score increased [29] and was worse patients with otolithic vertigo (versus rotatory vertigo) [30]. After vestibular neurotomy, SVV was poor, but was reported significantly worse when in supine position, compared to sitting and standing positions, showing the importance of integration of postural and vestibular information to perceive space [36]. SVV and

subjective body orientation were also found to be significantly modified during GVS, by modifying the perceived gravity vector [57], although there was no correlation between the degree or side of SVV and subjective body deviation.

Table 3: Original research results according to primary outcome and quality assessment

Primary outcome	Study	Results	Statistical significance	Risk of bias
OBE questionnaire	[20]	OBE reported in 14% of acute dizziness patients vs 5% control group and higher DPDR scores in dizziness group	$p < 0.001$	Moderate
DDI	[25]	Correlation between visual and vestibular hypersensitivity and higher DDI scores in chronic dizziness	$p < 0.001$	High
	[28]	Higher DDI scores in vestibular impaired patients vs control, especially in patients with anxiety	$p < 0.05$	Moderate
	[26]	Higher DDI score in patients with vestibular disorders compared to control, especially during caloric stimulation	$p < 0.01$	High
	[27]	Higher DDI score in patients with vestibular disorders compared to control, correlated to spatial orientation impairment.	$p < 0.05$	Moderate
	[29]	Higher DDI scores in the first week of unilateral vestibular impairment. Lower DDI scores correlated to better SVV results.	$p < 0.05$	High
	[37]	Increased DDI score after unilateral centrifugation (300°/s)	$p < 0.0001$	Moderate
	[38]	Decreased DDI score and pain from phantom limb after CVS and unilateral centrifugation	$p < 0.05$	Moderate
Cambridge depersonalization score	[40]	Higher depersonalization score in patients with vestibular impaired patients vs control	$p < 0.05$	Moderate
SVV	[30]	Better SVV in rotatory vertigo vs otolithic vertigo	$p < 0.01$	High
	[36]	Better SVV in standing position compared to sitting or lying supine after vestibular neurotomy	$p < 0.0001$	Moderate
	[57]	Deviation of SVV and subjective body orientation during unilateral GVS (either side)	$p < 0.05$	Moderate
Rubber hand illusion	[41]	Increased proprioceptive drift towards the rubber hand during GVS (especially left)	$p = 0.002$	Moderate
	[16]	Increased feeling of ownership towards rubber hand during either side (especially right) GVS	$p < 0.001$	Moderate
	[42]	Increased proprioceptive drift towards the rubber hand during left GVS	ns	Moderate
	[49]	No difference in proprioceptive drift during CVS when visual feedback from the body surface is absent	ns	Moderate
Full body illusion	[54]	Increased full body illusions during visuo-vestibular conflict of looking-down at virtual self while supine	$p < 0.05$	Moderate
	[55]	Decreased full body illusion during body tilt visuo-vestibular conflict	$p < 0.005$	Moderate
	[56]	Supine position may induce illusory changes of self-location due to otolithic ambiguity	$p < 0.05$	Moderate
Perceived body parts	[40], [48]	Increased perceived hand length size during left warm CVS	$p = 0.003$, $p < 0.05$	Moderate
	[43]	Neither GVS nor CVS modified perceived length of arms or legs on a self-representing avatar	ns	Moderate
	[44]	Modified localization (somatoperception) of tactile stimulation after right GVS	$p = 0.026$	Moderate
	[51]	Improved two-point discrimination after left cold CVS	$P = 0.003$	Moderate
	[50]	Decreased perceived thigh width after cold CVS either side	$p < 0.05$	Moderate
Mental rotations	[32]	Higher mean reaction time in mental rotation task in patients with unilateral vestibular impairment	$p < 0.035$	High
	[35]	Higher error rates in object mental representation task in vestibular impaired patients	$p < 0.05$	High
	[52]	Transformation task improved when physical body rotated in the same direction as the mental rotation	$p < 0.05$	Moderate
	[45]	Increased reaction time for correct object mental rotation during GVS	$P = 0.026$	Moderate
Perspective tasks	[31]	No difference between patients with bilateral chronic vestibular disorders and controls	ns	Moderate
	[33]	Higher mean response time for transformed movements in patients with vestibular deficit	$p < 0.05$	Moderate
	[34]	Increased mean reaction time for 3PP task (ball throwing) in patients with left vestibular neurectomy	$p < 0.05$	High
	[53]	Subjects were faster when their physical body rotated in the same direction as the mental rotation needed to take the avatar's 3PP viewpoint	$p < 0.005$	Moderate
	[46]	Left GVS increased mean reaction times in 3PP task versus sham (no difference between right GVS and sham)	$p = 0.0041$	Moderate
	[47]	Left and right GVS increased identification to 1PP rather than 3PP	$p < 0.05$	Moderate

1PP = first person perspective, 3PP = third person perspective, CVS = caloric vestibular stimulation, DDI = depersonalization / derealization inventory, GVS = galvanic vestibular stimulation, NS = non-significant, OBE = out-of-body experience, SVV = subjective visual vertical, VS = vestibular stimulation.

Concerning mental rotation testing, increased reaction time was found in vestibular impaired patients performing own-body (egocentric) or human-figure (allocentric) rotations compared to controls [32] and in subjects during right (and not left) anodal GVS performing object-based mental rotations [45]. In patients after vestibular neurotomy, significantly higher error rates were found compared to controls when performing mental representation tasks such as virtual rotations or translations of objects relative to the environment [35]. More specifically, it was shown that vestibular input influenced self-centred mental imagery: during rotatory chair vestibular stimulation, subjects would accomplish a mental task faster when the physical body was rotating in the same direction as the mental rotation [52,53]. Concerning embodied self-location, vestibular impaired patients made significantly more spatial orientation errors after whole-body rotations in darkness than controls, suggesting a key role of vestibular input [27]. Even in a subject without vestibular deficit, specific body positions such as the supine position, could lead to "otolithic ambiguity", creating illusory self-translation because of a mismatch between the actual position and an internally assumed upright position [56].

Supplementary Table 3: Depersonalization-derealization inventory (DDI) [39]

1. Surroundings seem strange or unreal
2. Time seems to pass very slowly
3. Body feels strange or different in some way
4. Feel like you've been here before (deja vu)
5. Feel as though in a dream
6. Body feels numb
7. Feeling of detachment or separation from surroundings
8. Numbing of emotions
9. People and objects seem far away
10. Feeling detached or separated from your body
11. Thoughts seem blurred
12. Events seem to happen in slow motion
13. Your emotions seem disconnected from yourself
14. Feeling of not being in control of self
15. People appear strange or unreal
16. Dizziness
17. Surroundings appear covered with a haze
18. Vision is dulled
19. Feel as if walking on shifting ground
20. Difficulty understanding what others say to you
21. Difficulty focusing attention
22. Feel as though in a trance
23. The distinction between close and distant is blurred
24. Difficulty concentrating
25. Feel as though your personality is different
26. Feel confused or bewildered
27. Feel isolated from the world
28. Feel ''spacy'' or ''spaced out''

Bodily self-consciousness has repeatedly been studied using illusory body ownership experiments, either full-body illusion setups or rubber hand setups, in which a fake rubber hand is placed in the subject's field of view and touched, simultaneously as the subject's real hand is also touched whilst hidden from direct view, thus creating an illusion of ownership of the rubber hand. A proprioceptive drift can be defined as the perceived shift of the participant's hand towards the rubber hand, measured in centimetres by an examiner, a greater shift corresponding to a stronger illusionary own-body perception. Four studies used the proprioceptive drift in rubber hand illusion as primary outcome by applying left, right or sham GVS. Proprioceptive drift towards the rubber hand was found to be increased during GVS, suggesting an influence of vestibular stimulation on visuo-proprioceptive integration [41,42]. However, when visual feedback from the body surface was absent, CVS lost any influence on the proprioceptive drift [49]. Ferrè *et al* found that left anodal GVS induced a smaller drift than right stimulation [16]. Contrarily, Lopez *et al* reported that left GVS led to significantly increased body ownership of the rubber hand, a multisensory mediating mechanism taking place in the right temporo-parietal junction and posterior insula [42].

CVS induced a significantly increased perception of hand length in both hands whether right or left stimulation [40,48]. Concerning sidedness, left warm CVS was more potent than right, and the left hand was perceived significantly larger than the right [40]. Cold CVS (either side) was shown to induce significantly decreased perceived thigh width [50], whereas left cold CVS improved tactile two-point discrimination [51] and GVS (especially right) modulated somatoperception of a tactile stimulus [44]. However, unilateral (either side) CVS or GVS was not found to modify arm or leg length perception from a third person perspective [43].

Depersonalization by identification to a "full-body illusion" may be induced by generating self-identification towards a virtual body, and then analysed during gravity-related visuo-vestibular conflicts. Visuo-vestibular conflict has been shown to modify body self-consciousness during full-body illusion, however it has been found to enhance the illusion during a downward-looking perspective while in supine position [54,56], and contrarily significantly decrease full body illusion during a body tilt-induced visuo-otolithic conflict [55].

The virtual body was also used for third person perspective (3PP) tests, inducing depersonalization by making a subject act from another person's or an avatar's point of view. Mean reaction times in performing third-person perspective tasks were significantly increased in patients with vestibular disorders [33] and more specifically after left unilateral vestibular neurectomy [34] compared to healthy participants. In patients with chronic bilateral vestibular disorders however, no statistically significant difference was found during 3PP tasks, compared to healthy subjects [31]. In experimental conditions, GVS (left or right) reinforced 1PP rather than 3PP during tactile stimulation [47], left GVS (contrarily to right) significantly increased reaction time in performing 3PP tasks [46] showing how vestibular stimulation interferes with third person perception making.

General reviews and expert opinions

Thirteen general reviews, including one editorial were included, which were all non-systematic literature reviews [9–15,17,58–62]. In all of these studies, the pathophysiological hypothesis explaining the role of the vestibular organs in body and spatial perception was the existence of a visuo-vestibulo-somatosensory convergence in the vestibular nuclei, thalami and temporo-parietal junction. All 13 articles insisted on the importance of the temporo-parietal junction and parieto-insular vestibular cortex (PIVC) for multisensory integration of vestibular inputs and for embodied self-consciousness. All authors agreed on a possible visuo-vestibulo-somatosensory mismatch to explain alterations in bodily or spatial self-consciousness. Three papers [10,15,58] made a distinction between dissociation between personal and extra-personal space caused by a visuo-vestibular mismatch, and dissociation within the personal space caused by visuo-vestibulo-somatosensory mismatch. It has been suggested that a temporal mismatch between an action and the sensory feedback from this action could explain alterations in bodily perceptions [9]. Ferrè *et al* emphasized three degrees of vestibular influence on the bodily representation : somato-sensory inputs (somato-sensation), perception of body parts (somato-perception), first-person perspective and body ownership (somato-representation) [61]. In support of this hypothesis, changes in visuo-spatial perspective and self-location perception have been associated to signal changes in functional MRI [10,12,58] and changes in functional imaging signals have been reported in the temporo-parietal junction during caloric or galvanic vestibular stimulation

[9,12,13,15,62]. Lastly, similarities in neural networks responsible for body representation and the visual vertical perception have been reported [11] as well as between the vestibular cortex and networks likely involved in the perception of gravity [14].

Quality assessment

Of the 34 research articles, 26 had an average risk and 8 a high risk of bias, reported in ***Table 3***. The most common reason for poor methodological quality was lack of comparability between groups and outcome assessment.

Discussion:

This systematic review reports extensive evidence showing a relationship between the vestibular system and bodily or spatial self-consciousness. Modulation of bodily self-consciousness in patients with vestibular disorders or during vestibular stimulation was reported by 31 of the 34 experimental studies [16,20,25–30,32–38,40–42,44–48,50–57] (***Table 1 and 2***). The only study not to find any statistical association assessed patients with chronic bilateral vestibular impairment [31], this is probably due to the fact that multisensory integration is less dependent on vestibular input in these patients, compared to cases with acute unilateral vestibular disorders or intermittent vestibular stimulations [29,63]. Moreover, a bilateral lesion is less likely to result in changes in spatial self-consciousness since a symmetrical vestibular impairment seems to have minor effect on the perception of gravity [64,65]. Thus, DPDR especially occurs in acute vestibular disorders which brutally disrupt a harmonious multi-modal perception of the environment. In such cases, anxiety generated by abrupt and intense vestibular symptoms, could either independently create or reinforce and increase existing DPDR symptoms [28].

When specific SCC stimulation was studied [32,38,40,43,48–53], bodily and spatial self-consciousness were both modified. When specific otolithic alteration were induced [30,37,38,56], spatial self-consciousness was always disrupted whereas bodily self-consciousness modifications were less frequently reported [37,38,56]. Otolithic impairment seems to especially affect spatial self-consciousness by altering proprioceptive and gravity perception [30]. This is particularly true when proprioceptive input is also modulated, as bodily self-consciousness is more severely altered in the

supine position, when the postural feedback is reduced [36,54,56]. Spatial self-consciousness linked to otolithic inputs was assessed using SVV by four studies (***Table 3***), which is a good test to assess the vestibular impact on visuo-proprioceptive integration [36,66] and was significantly correlated to DPDR symptoms [29].

Vestibular inputs also influence bodily self-consciousness by modulating the complex visuo-proprioceptive integration, which may be studied using body illusion and 3PP tests. Vestibular stimulation overall reinforced body illusion, except during body tilt when body illusion was decreased maybe due to the increased posture/proprioceptive feedback induced by the task [55]. Interestingly, vestibular stimulation did not influence proprioceptive perception when no visual feedback was available, indicating that the vestibular system influences the multisensory integration of bodily self-consciousness rather than specific sensory inputs [49]. Conversely, altered vestibular input impaired mental imaging and 3PP capacities and even reduced DPDR symptoms from phantom limb [38]. This could be explained by the hypothesis that while discordant vestibular input alters bodily self-consciousness as seen previously, it also deconstructs spatial self-consciousness of the body and the capacity to extract one's self and self-reflect in an organised manner. This emphasises the important role of the vestibular system in the construction and representation of the bodily self.

The main limit of this systematic review is the lack of standardised tests and heterogeneity of results. Although a direct link between the vestibular system and embodied self-consciousness is undeniable, more precise vestibular organ or stimulation-specific analysis is difficult. For example, anodal GVS, warm CVS or even vestibular neurectomy on the left side were found in 6 studies to specifically alter embodied self-consciousness compared to the right side [31,40–42,46,48]; and right anodal GVS or cold CVS in 3 articles [16,44,51]. This is notable as left- GVS has been shown to activate the right hemisphere (posterior parietal and premotor cortex) and vice-versa [67], however the contradictory evidence at hand cannot support any further analysis.

Neuroanatomy of embodied self-consciousness

Functional imagery (such as MRI or TEP scans) have enabled us to analyse functional cerebral areas of different entities related to embodied self-consciousness such as DPDR, OBE or the vestibular

cortex (***Figure 2***). Two main overlapping areas stand out which are the insula and the temporo-parietal junction. These two areas correspond the parietoinsular vestibular cortex (PIVC) which has been clearly identified as an area of multisensory integration with vestibular, visual and somatosensory input [68–70]. We believe that in all likelihood it is also the area where embodied self-consciousness is constructed, and where altered vestibular inputs can modulate visuo-proprioceptive integration and induce OBE and DPDR symptoms.

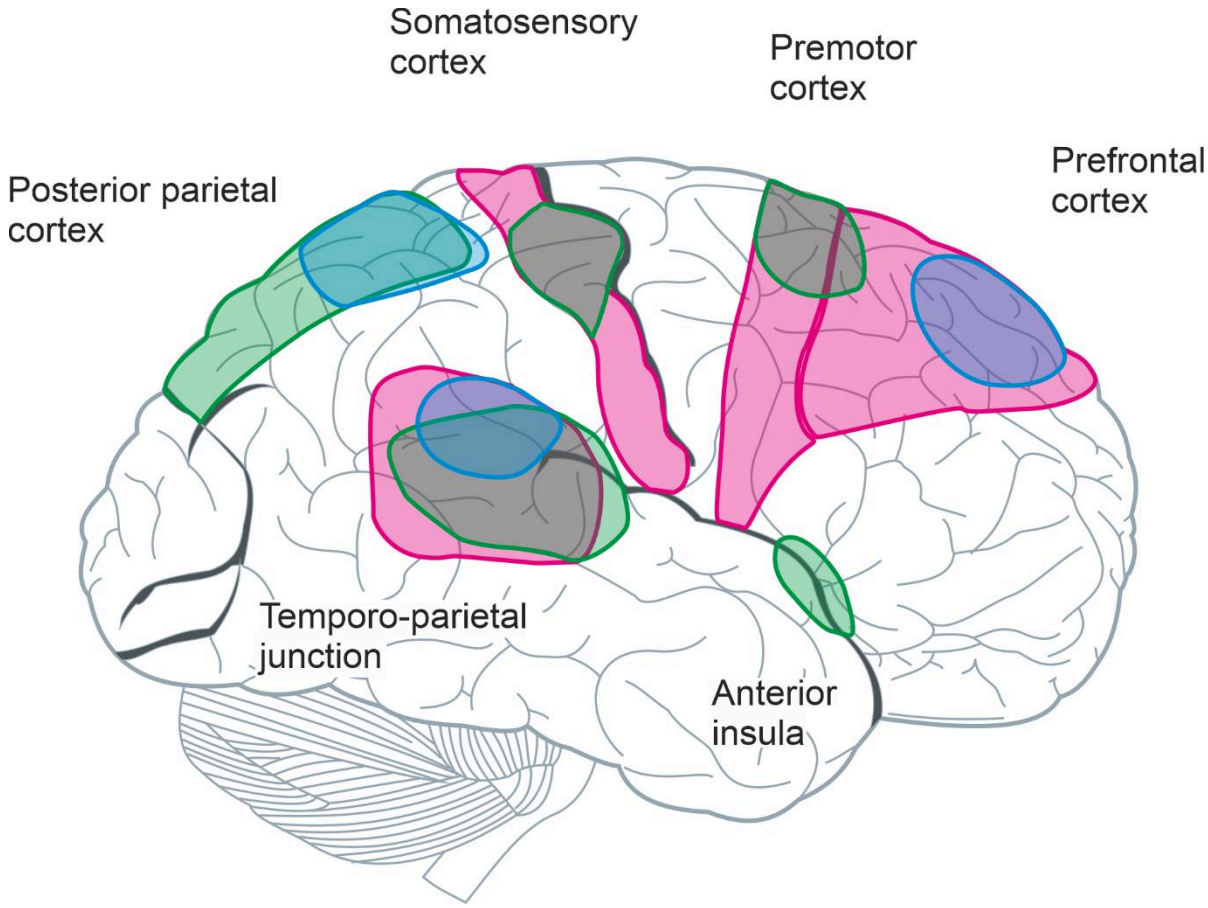

Figure 2: Neuroanatomy of embodied self-consciousness

Different neuroanatomical areas are represented based on the literature. The vestibular cortex in green (are not shown in this figure the hippocampus/parahippocampal gyrus, precuneus and the cingulate gyrus) [70–74]*; Out-of-body-experience areas of increased activity in pink* [67,68,75,76]*; and depersonalization-derealization disorder areas of increased activity in blue* [69,77–80]*. The main overlapping area is the parietoinsular vestibular cortex which encompasses the parieto-temporal junction and the posterior insular areas.*

A phenomenological approach

If from a neurophysiological standpoint, the PIVC is the key area where the vestibular system influences embodied self-consciousness, phenomenology may help explain vestibular induced DPDR from a subjective point of view, to help improve patient management. In contemporary philosophy, phenomenology refers to a method of investigation of what experiencing means and aims at the detailed exploration of lived experience as a basis for empirical science. Edmund Husserl (1859 – 1938), founder of the philosophical movement, insists on the idea that the world and consciousness cannot be considered separately, and that there is always a close relationship between the act of consciousness and the objects constituted by consciousness. This act is called "intentionality" or “the encounter between consciousness and the world” [81], when consciousness implicitly constitutes the surrounding world in an integrated and coherent way.

In this respect, the body is considered by phenomenologists (notably Maurice Merleau-Ponty, 1908-1961) as what mediates the relationship to exteriority. This mediation is however mostly invisible or transparent: the hand taking a cup of coffee is not experienced as such, the cup of coffee is directly reached out to (intentionality). The body is the inapparent condition of consciousness and from the experiential point of view, sensory inputs are not perceived separately and cognitively associated together, but are immediately experienced as a coherent world. What phenomenology calls "corporeality" is thus most often implicit in consciousness.

The body is paradoxical: it is both an object of knowledge (neurophysiological, anatomical, aesthetic, etc.) and a subject knowing, perceiving and feeling, “by which I am present to the world” [22]. Husserl identified the first with the German word *Körper*, meaning the body as property, and the second *Leib*, the body as lived (as a being). Phenomenologically, embodied self-consciousness is implicit and contains both dimensions of the *Körper* and the *Leib* as one bodily self.

The phenomenological approach is interesting to understand vestibular disorders in relation to the mind-body duality. As in neurophysiology, which tends to show a biological continuity between neurological and psychological events, phenomenology does not separate the body and the mind as in classical philosophy, but merges them into a unique bodily self. Indeed, vestibular diseases can induce

dissociative disorders; and conversely psychological issues can trigger vestibular symptoms (for example in Menière's disease).

Phenomenology asserts the primacy of intentionality, which is an active event, an "embodied activity" [81] that relates to one's existence in the surrounding world. Concerning vestibular inputs, intentionality (or the way consciousness acts to experience the world) is always implicit. Gravity for example is perceived by the otolithic system and is integrated with other sensory information to correctly identify SVV without requiring any cognitive analysis. Also, SVV is perceived by the body as a whole and the vestibular gravitational input is not perceived as independent information. To Husserl, the constitution of perception allows things to reveal themselves to our conscience (such as SVV). Thus, one should be interested not in the things themselves, but in the way they are presented to us, as a phenomenon. This can be seen when SVV is perceived differently from standing to supine position [36,56], the phenomenon of gravity is perceived differently (the intentionality has changed due to different sensory conditions) although of course gravitation in itself is identical.

Lastly, according to phenomenology, our perception of things depends on their environment or background, from which the object is "extracted". We never perceive the elements in an "atomic manner", but always as inserted in a context, which Husserl called an "external horizon". This background is passively perceived, but one can constantly change perspective by "extracting" one object after the next from its own background and continue one's "perceiving experience" [82]. In otolithic impairment, SVV is often altered, providing an erroneous frame, a tilted background, that distorts the spatial representation of objects, and so, the perceiving experience. Merleau-Ponty further insisted that embodied perception was global and not an addition of unintegrated sensory inputs. This is of course particularly true concerning vestibular perception, which is integrated with visual and somatosensory perception in the vestibular nuclei, cerebellum and vestibular cortex. Conversely, conflicting vestibular input can induce a phenomenological rupture, or a "failure in bodily self-monitoring" [83]. A very common example of this is motion sickness where a discrepancy between vestibular and other sensory signals induces dizziness and neurovegetative symptoms.

Thus, loss of unity between physical body and self in depersonalisation, "out of body experiences", or changes in own-body perception, loss of coherence between the lived body and the

environment in spatial disorientation or derealization states, and loss of verticality in otolithic impairment can be interpreted in the frame of phenomenological rupture. As such, we are not aware and do not think about our vestibular organs or vestibular inputs in our day to day activities. Yet, vestibular function is a clear determination of one's embodied experience of the world. It is also a multisensory integrated system, which gives a holistic perception of the world, or as would say Martin Heidegger (1889 – 1976), impression of the world.

Conclusion:

This systematic literature review reports 34 research articles and 13 review articles with evidence of a role played by the vestibular system in bodily and spatial self-consciousness. The importance of the vestibular system in body ownership and spatial representation is a relatively new concept and should be further studied. Whether by experimental vestibular stimulation, or pathological vestibular disorder, disrupted vestibular inputs to the multisensory integration increase DPDR symptoms, modulate the visuo-proprioceptive integration and impair the capacity perform mental representation or third person perspective tasks. The neuroanatomical areas of increased activity of each of these aspects of embodied self-consciousness overlap in the PIVC (posterior insula and temporo-parietal junction), which is one of the main centres of multi-sensory integration in the vestibular cortex, including vestibular, visual and somatosensory inputs. From a subjective point of view, the sensory conflict induced by failing vestibular inputs creates a phenomenological rupture, which may explain how vestibular conflict can induce dissociative disorders. Indeed, in acute unilateral vestibular disease with disrupted multisensory integration, patients would tend to observe their own body as an object, rather than implicitly being part of their bodily self with which they experience the world. Understanding bodily self-consciousness from both a neurophysiological standpoint and subjective point of view can give new insight to better managing DPDR symptoms in these patients. Conversely, the vestibular pathophysiology may provide a new scientific case study for phenomenologists, exploring how the vestibular organs may help define our being-in-the-world.

References:

[1] D. Spiegel, R.J. Loewenstein, R. Lewis-Fernández, V. Sar, D. Simeon, E. Vermetten, E. Cardeña, P.F. Dell, Dissociative disorders in DSM-5, Depress. Anxiety. 28 (2011) 824–852. https://doi.org/10.1002/da.20874.

[2] L. Heydrich, G. Marillier, N. Evans, M. Seeck, O. Blanke, Depersonalization- and derealization-like phenomena of epileptic origin, Ann. Clin. Transl. Neurol. 6 (2019) 1739–1747. https://doi.org/10.1002/acn3.50870.

[3] F. Anzellotti, V. Onofrj, V. Maruotti, L. Ricciardi, R. Franciotti, L. Bonanni, A. Thomas, M. Onofrj, Autoscopic phenomena: case report and review of literature, Behav. Brain Funct. 7 (2011) 2. https://doi.org/10.1186/1744-9081-7-2.

[4] C.W. Lippman, Hallucinations of physical duality in migraine, J. Nerv. Ment. Dis. 117 (1953) 345–350. https://doi.org/10.1097/00005053-195304000-00008.

[5] A. Comfort, Out-of-body experiences and migraine, Am. J. Psychiatry. 139 (1982) 1379–1380.

[6] D. Trueman, Anxiety and depersonalization and derealization experiences, Psychol. Rep. 54 (1984) 91–96. https://doi.org/10.2466/pr0.1984.54.1.91.

[7] M.A. Gonzalez-Torres, L. Inchausti, M. Aristegui, B. Ibañez, L. Diez, A. Fernandez-Rivas, S. Bustamante, K. Haidar, M. Rodríguez-Zabaleta, A. Mingo, Depersonalization in patients with schizophrenia spectrum disorders, first-degree relatives and normal controls, Psychopathology. 43 (2010) 141–149. https://doi.org/10.1159/000288635.

[8] G. Stanghellini, A.V. Fernandez, M. Ballerini, S. Blasi, E. Belfiore, J. Cutting, M. Mancini, Abnormal Space Experiences in Persons With Schizophrenia: An Empirical Qualitative Study, Schizophr. Bull. 46 (2020) 530–539. https://doi.org/10.1093/schbul/sbz107.

[9] C. Lopez, A neuroscientific account of how vestibular disorders impair bodily self-consciousness, Front. Integr. Neurosci. 7 (2013) 91. https://doi.org/10.3389/fnint.2013.00091.

[10] C. Lopez, P. Halje, O. Blanke, Body ownership and embodiment: vestibular and multisensory mechanisms, Neurophysiol. Clin. Clin. Neurophysiol. 38 (2008) 149–161. https://doi.org/10.1016/j.neucli.2007.12.006.

[11] C. Lopez, M. Toupet, C. van Nechel, A. Bozorg Grayeli, Editorial: Role of Inner Ear in Self and Environment Perception, Front. Neurol. 11 (2020) 22. https://doi.org/10.3389/fneur.2020.00022.

[12] B. Lenggenhager, S.T. Smith, O. Blanke, Functional and neural mechanisms of embodiment: importance of the vestibular system and the temporal parietal junction, Rev. Neurosci. 17 (2006) 643–657. https://doi.org/10.1515/revneuro.2006.17.6.643.

[13] C. Lopez, C.J. Falconer, D. Deroualle, F.W. Mast, In the presence of others: Self-location, balance control and vestibular processing, Neurophysiol. Clin. Clin. Neurophysiol. 45 (2015) 241–254. https://doi.org/10.1016/j.neucli.2015.09.001.

[14] C. Lopez, Making Sense of the Body: the Role of Vestibular Signals, Multisensory Res. 28 (2015) 525–557. https://doi.org/10.1163/22134808-00002490.

[15] C. Pfeiffer, A. Serino, O. Blanke, The vestibular system: a spatial reference for bodily self-consciousness, Front. Integr. Neurosci. 8 (2014) 31. https://doi.org/10.3389/fnint.2014.00031.

[16] E.R. Ferrè, E. Berlot, P. Haggard, Vestibular contributions to a right-hemisphere network for bodily awareness: combining galvanic vestibular stimulation and the "Rubber Hand Illusion," Neuropsychologia. 69 (2015) 140–147. https://doi.org/10.1016/j.neuropsychologia.2015.01.032.

[17] K. Jáuregui Renaud, Vestibular Function and Depersonalization/Derealization Symptoms, Multisensory Res. 28 (2015) 637–651. https://doi.org/10.1163/22134808-00002480.

[18] T. Kitahara, M. Sakagami, T. Ito, T. Shiozaki, K. Kitano, A. Yamashita, I. Ota, Y. Wada, T. Yamanaka, Ménière's disease with unremitting floating sensation is associated with canal paresis, gravity-sensitive dysfunction, mental illness, and bilaterality, Auris. Nasus. Larynx. 46 (2019) 186–192. https://doi.org/10.1016/j.anl.2018.07.003.

[19] M. Kaliuzhna, D. Vibert, P. Grivaz, O. Blanke, Out-of-Body Experiences and Other Complex Dissociation Experiences in a Patient with Unilateral Peripheral Vestibular Damage and Deficient Multisensory Integration, Multisensory Res. 28 (2015) 613–635. https://doi.org/10.1163/22134808-00002506.

[20] C. Lopez, M. Elzière, Out-of-body experience in vestibular disorders - A prospective study of 210 patients with dizziness, Cortex J. Devoted Study Nerv. Syst. Behav. 104 (2018) 193–206. https://doi.org/10.1016/j.cortex.2017.05.026.

[21] H. Wykretowicz, M. Saraga, C. Bourquin, F. Stiefel, [Multifaceted body. 2. The lived body], Rev. Med. Suisse. 11 (2015) 389–390, 392–393.
[22] A. De Waelhens, La Phénoménologie du corps, Rev. Philos. Louvain. 48 (1950) 371–397. https://doi.org/10.3406/phlou.1950.4299.
[23] L. Shamseer, D. Moher, M. Clarke, D. Ghersi, A. Liberati, M. Petticrew, P. Shekelle, L.A. Stewart, the PRISMA-P Group, Preferred reporting items for systematic review and meta-analysis protocols (PRISMA-P) 2015: elaboration and explanation, BMJ. 349 (2015). https://doi.org/10.1136/bmj.g7647.
[24] G. Wells, The Newcastle-Ottawa Scale (NOS) for assessing the quality of nonrandomised studies in meta-analyses, (n.d.).
[25] M. Toupet, C. Van Nechel, C. Hautefort, S. Heuschen, U. Duquesne, A. Cassoulet, A. Bozorg Grayeli, Influence of Visual and Vestibular Hypersensitivity on Derealization and Depersonalization in Chronic Dizziness, Front. Neurol. 10 (2019) 69. https://doi.org/10.3389/fneur.2019.00069.
[26] F.Y.P. Sang, K. Jáuregui-Renaud, D.A. Green, A.M. Bronstein, M.A. Gresty, Depersonalisation/derealisation symptoms in vestibular disease, J. Neurol. Neurosurg. Psychiatry. 77 (2006) 760–766. https://doi.org/10.1136/jnnp.2005.075473.
[27] K. Jáuregui-Renaud, F.Y.P. Sang, M.A. Gresty, D.A. Green, A.M. Bronstein, Depersonalisation/derealisation symptoms and updating orientation in patients with vestibular disease, J. Neurol. Neurosurg. Psychiatry. 79 (2008) 276–283. https://doi.org/10.1136/jnnp.2007.122119.
[28] O.I. Kolev, S.O. Georgieva-Zhostova, A. Berthoz, Anxiety changes depersonalization and derealization symptoms in vestibular patients, Behav. Neurol. 2014 (2014) 847054. https://doi.org/10.1155/2014/847054.
[29] F.B. Gómez-Alvarez, K. Jáuregui-Renaud, Psychological symptoms and spatial orientation during the first 3 months after acute unilateral vestibular lesion, Arch. Med. Res. 42 (2011) 97–103. https://doi.org/10.1016/j.arcmed.2011.03.004.
[30] G. Clément, M.-J. Fraysse, O. Deguine, Mental representation of space in vestibular patients with otolithic or rotatory vertigo, Neuroreport. 20 (2009) 457–461. https://doi.org/10.1097/wnr.0b013e328326f815.
[31] D. Deroualle, M. Toupet, C. van Nechel, U. Duquesne, C. Hautefort, C. Lopez, Anchoring the Self to the Body in Bilateral Vestibular Failure, PloS One. 12 (2017) e0170488. https://doi.org/10.1371/journal.pone.0170488.
[32] M. Candidi, A. Micarelli, A. Viziano, S.M. Aglioti, I. Minio-Paluello, M. Alessandrini, Impaired mental rotation in benign paroxysmal positional vertigo and acute vestibular neuritis, Front. Hum. Neurosci. 7 (2013) 783. https://doi.org/10.3389/fnhum.2013.00783.
[33] J.H.J. Allum, W. Langewitz, M. Sleptsova, A. Welge-Luessen, F. Honegger, T.H. Schatz, C.L. Biner, C. Maguire, D.A. Schmid, Mental body transformation deficits in patients with chronic balance disorders, J. Vestib. Res. Equilib. Orientat. 27 (2017) 113–125. https://doi.org/10.3233/VES-170613.
[34] D. Deroualle, L. Borel, B. Tanguy, L. Bernard-Demanze, A. Devèze, M. Montava, J.-P. Lavieille, C. Lopez, Unilateral vestibular deafferentation impairs embodied spatial cognition, J. Neurol. 266 (2019) 149–159. https://doi.org/10.1007/s00415-019-09433-7.
[35] P. Péruch, C. Lopez, C. Redon-Zouiteni, G. Escoffier, A. Zeitoun, M. Sanjuan, A. Devèze, J. Magnan, L. Borel, Vestibular information is necessary for maintaining metric properties of representational space: evidence from mental imagery, Neuropsychologia. 49 (2011) 3136–3144. https://doi.org/10.1016/j.neuropsychologia.2011.07.026.
[36] C. Lopez, M. Lacour, J. Léonard, J. Magnan, L. Borel, How body position changes visual vertical perception after unilateral vestibular loss, Neuropsychologia. 46 (2008) 2435–2440. https://doi.org/10.1016/j.neuropsychologia.2008.03.017.
[37] C. Aranda-Moreno, K. Jáuregui-Renaud, Derealization during utricular stimulation, J. Vestib. Res. Equilib. Orientat. 26 (2016) 425–431. https://doi.org/10.3233/VES-160597.
[38] C. Aranda-Moreno, K. Jáuregui-Renaud, J. Reyes-Espinosa, A. Andrade-Galicia, A.E. Bastida-Segura, L.G. González Carrazco, Stimulation of the Semicircular Canals or the Utricles by Clinical Tests Can Modify the Intensity of Phantom Limb Pain, Front. Neurol. 10 (2019) 117. https://doi.org/10.3389/fneur.2019.00117.
[39] B.J. Cox, R.P. Swinson, Instrument to assess depersonalization-derealization in panic disorder, Depress. Anxiety. 15 (2002) 172–175. https://doi.org/10.1002/da.10051.

[40] C. Lopez, E. Nakul, N. Preuss, M. Elzière, F.W. Mast, Distorted own-body representations in patients with dizziness and during caloric vestibular stimulation, J. Neurol. 265 (2018) 86–94. https://doi.org/10.1007/s00415-018-8906-8.
[41] S. Ponzo, L.P. Kirsch, A. Fotopoulou, P.M. Jenkinson, Balancing body ownership: Visual capture of proprioception and affectivity during vestibular stimulation, Neuropsychologia. 117 (2018) 311–321. https://doi.org/10.1016/j.neuropsychologia.2018.06.020.
[42] C. Lopez, B. Lenggenhager, O. Blanke, How vestibular stimulation interacts with illusory hand ownership, Conscious. Cogn. 19 (2010) 33–47. https://doi.org/10.1016/j.concog.2009.12.003.
[43] H.-O. Karnath, S.C. Mölbert, A.K. Klaner, J. Tesch, K.E. Giel, H.Y. Wong, B.J. Mohler, Visual perception of one's own body under vestibular stimulation using biometric self-avatars in virtual reality, PLOS ONE. 14 (2019) e0213944. https://doi.org/10.1371/journal.pone.0213944.
[44] E.R. Ferrè, E. Vagnoni, P. Haggard, Vestibular contributions to bodily awareness, Neuropsychologia. 51 (2013) 1445–1452. https://doi.org/10.1016/j.neuropsychologia.2013.04.006.
[45] B. Lenggenhager, C. Lopez, O. Blanke, Influence of galvanic vestibular stimulation on egocentric and object-based mental transformations, Exp. Brain Res. 184 (2007) 211–221. https://doi.org/10.1007/s00221-007-1095-9.
[46] A. Pavlidou, E.R. Ferrè, C. Lopez, Vestibular stimulation makes people more egocentric, Cortex. 101 (2018) 302–305. https://doi.org/10.1016/j.cortex.2017.12.005.
[47] E.R. Ferrè, C. Lopez, P. Haggard, Anchoring the Self to the Body: Vestibular Contribution to the Sense of Self, Psychol. Sci. 25 (2014) 2106–2108. https://doi.org/10.1177/0956797614547917.
[48] C. Lopez, H.-M. Schreyer, N. Preuss, F.W. Mast, Vestibular stimulation modifies the body schema, Neuropsychologia. 50 (2012) 1830–1837. https://doi.org/10.1016/j.neuropsychologia.2012.04.008.
[49] C. Lopez, C.P. Bieri, N. Preuss, F.W. Mast, Tactile and vestibular mechanisms underlying ownership for body parts: A non-visual variant of the rubber hand illusion, Neurosci. Lett. 511 (2012) 120–124. https://doi.org/10.1016/j.neulet.2012.01.055.
[50] A. Schönherr, C.A. May, Influence of Caloric Vestibular Stimulation on Body Experience in Healthy Humans, Front. Integr. Neurosci. 10 (2016). https://doi.org/10.3389/fnint.2016.00014.
[51] A. Sedda, D. Tonin, G. Salvato, M. Gandola, G. Bottini, Left caloric vestibular stimulation as a tool to reveal implicit and explicit parameters of body representation, Conscious. Cogn. 41 (2016) 1–9. https://doi.org/10.1016/j.concog.2016.01.012.
[52] M. van Elk, O. Blanke, Imagined own-body transformations during passive self-motion, Psychol. Res. 78 (2014) 18–27. https://doi.org/10.1007/s00426-013-0486-8.
[53] D. Deroualle, L. Borel, A. Devèze, C. Lopez, Changing perspective: The role of vestibular signals, Neuropsychologia. 79 (2015) 175–185. https://doi.org/10.1016/j.neuropsychologia.2015.08.022.
[54] C. Pfeiffer, C. Lopez, V. Schmutz, J.A. Duenas, R. Martuzzi, O. Blanke, Multisensory origin of the subjective first-person perspective: visual, tactile, and vestibular mechanisms, PloS One. 8 (2013) e61751. https://doi.org/10.1371/journal.pone.0061751.
[55] C. Thür, M. Roel Lesur, C.J. Bockisch, C. Lopez, B. Lenggenhager, The Tilted Self: Visuo-Graviceptive Mismatch in the Full-Body Illusion, Front. Neurol. 10 (2019) 436. https://doi.org/10.3389/fneur.2019.00436.
[56] L. Schwabe, O. Blanke, The vestibular component in out-of-body experiences: a computational approach, Front. Hum. Neurosci. 2 (2008) 17. https://doi.org/10.3389/neuro.09.017.2008.
[57] F. Mars, J.-L. Vercher, K. Popov, Dissociation between subjective vertical and subjective body orientation elicited by galvanic vestibular stimulation, Brain Res. Bull. 65 (2005) 77–86. https://doi.org/10.1016/j.brainresbull.2004.11.012.
[58] B. Lenggenhager, C. Lopez, Vestibular Contributions to the Sense of Body, Self, and Others, (2015). https://doi.org/10.15502/9783958570023.
[59] S. Dieguez, C. Lopez, The bodily self: Insights from clinical and experimental research, Ann. Phys. Rehabil. Med. 60 (2017) 198–207. https://doi.org/10.1016/j.rehab.2016.04.007.
[60] C. Lopez, The vestibular system: balancing more than just the body, Curr. Opin. Neurol. 29 (2016) 74–83. https://doi.org/10.1097/WCO.0000000000000286.
[61] E.R. Ferrè, P. Haggard, The vestibular body: Vestibular contributions to bodily representations, Cogn. Neuropsychol. 33 (2016) 67–81. https://doi.org/10.1080/02643294.2016.1168390.

[62] Paul F. Smith, Personality changes in patients with vestibular dysfunction, Hum Neurosci 29 Oct. 2013. (n.d.).
[63] T. Brandt, T. Huppert, K. Hüfner, V.C. Zingler, M. Dieterich, M. Strupp, Long-term course and relapses of vestibular and balance disorders, Restor. Neurol. Neurosci. 28 (2010) 69–82. https://doi.org/10.3233/RNN-2010-0504.
[64] C. Lopez, M. Lacour, A.E. Ahmadi, J. Magnan, L. Borel, Changes of visual vertical perception: a long-term sign of unilateral and bilateral vestibular loss, Neuropsychologia. 45 (2007) 2025–2037. https://doi.org/10.1016/j.neuropsychologia.2007.02.004.
[65] M. Toupet, C. Van Nechel, C. Hautefort, U. Duquesne, S. Heuschen, A. Bozorg Grayeli, Subjective Visual Vertical in Idiopathic Bilateral Vestibular Hypofunction: Enhanced Role of Vision, Neck, and Body Proprioception, Otol. Neurotol. Off. Publ. Am. Otol. Soc. Am. Neurotol. Soc. Eur. Acad. Otol. Neurotol. 38 (2017) 1010–1016. https://doi.org/10.1097/MAO.0000000000001462.
[66] A. Böhmer, F. Mast, Assessing otolith function by the subjective visual vertical, Ann.-N. Y. Acad. Sci. 871 (1999) 221–231. https://doi.org/10.1111/j.1749-6632.1999.tb09187.x.
[67] G.R. Fink, J.C. Marshall, P.H. Weiss, T. Stephan, C. Grefkes, N.J. Shah, K. Zilles, M. Dieterich, Performing allocentric visuospatial judgments with induced distortion of the egocentric reference frame: an fMRI study with clinical implications, NeuroImage. 20 (2003) 1505–1517. https://doi.org/10.1016/j.neuroimage.2003.07.006.
[68] O. Blanke, Multisensory brain mechanisms of bodily self-consciousness, Nat. Rev. Neurosci. 13 (2012) 556–571. https://doi.org/10.1038/nrn3292.
[69] D. Simeon, O. Guralnik, E.A. Hazlett, J. Spiegel-Cohen, E. Hollander, M.S. Buchsbaum, Feeling unreal: a PET study of depersonalization disorder, Am. J. Psychiatry. 157 (2000) 1782–1788. https://doi.org/10.1176/appi.ajp.157.11.1782.
[70] M. Dieterich, T. Brandt, The parietal lobe and the vestibular system, Handb. Clin. Neurol. 151 (2018) 119–140. https://doi.org/10.1016/B978-0-444-63622-5.00006-1.
[71] T. Brandt, M. Dieterich, Thalamocortical network: a core structure for integrative multimodal vestibular functions, Curr. Opin. Neurol. 32 (2019) 154–164. https://doi.org/10.1097/WCO.0000000000000638.
[72] I. Indovina, V. Maffei, G. Bosco, M. Zago, E. Macaluso, F. Lacquaniti, Representation of visual gravitational motion in the human vestibular cortex, Science. 308 (2005) 416–419. https://doi.org/10.1126/science.1107961.
[73] T. Miyamoto, K. Fukushima, T. Takada, C. de Waele, P.-P. Vidal, Saccular stimulation of the human cortex: a functional magnetic resonance imaging study, Neurosci. Lett. 423 (2007) 68–72. https://doi.org/10.1016/j.neulet.2007.06.036.
[74] P. Schlindwein, M. Mueller, T. Bauermann, T. Brandt, P. Stoeter, M. Dieterich, Cortical representation of saccular vestibular stimulation: VEMPs in fMRI, NeuroImage. 39 (2008) 19–31. https://doi.org/10.1016/j.neuroimage.2007.08.016.
[75] O. Blanke, C. Mohr, C.M. Michel, A. Pascual-Leone, P. Brugger, M. Seeck, T. Landis, G. Thut, Linking out-of-body experience and self processing to mental own-body imagery at the temporoparietal junction, J. Neurosci. Off. J. Soc. Neurosci. 25 (2005) 550–557. https://doi.org/10.1523/JNEUROSCI.2612-04.2005.
[76] S. Ionta, L. Heydrich, B. Lenggenhager, M. Mouthon, E. Fornari, D. Chapuis, R. Gassert, O. Blanke, Multisensory mechanisms in temporo-parietal cortex support self-location and first-person perspective, Neuron. 70 (2011) 363–374. https://doi.org/10.1016/j.neuron.2011.03.009.
[77] M.L. Phillips, M. Sierra, Depersonalization disorder: a functional neuroanatomical perspective, Stress Amst. Neth. 6 (2003) 157–165. https://doi.org/10.1080/1025389031000138538.
[78] N. Medford, M. Sierra, A. Stringaris, V. Giampietro, M.J. Brammer, A.S. David, Emotional Experience and Awareness of Self: Functional MRI Studies of Depersonalization Disorder, Front. Psychol. 7 (2016) 432. https://doi.org/10.3389/fpsyg.2016.00432.
[79] E. Lemche, A. Anilkumar, V.P. Giampietro, M.J. Brammer, S.A. Surguladze, N.S. Lawrence, D. Gasston, X. Chitnis, S.C.R. Williams, M. Sierra, P. Joraschky, M.L. Phillips, Cerebral and autonomic responses to emotional facial expressions in depersonalisation disorder, Br. J. Psychiatry J. Ment. Sci. 193 (2008) 222–228. https://doi.org/10.1192/bjp.bp.107.044263.

[80] A. Sierk, J.K. Daniels, A. Manthey, J.G. Kok, A. Leemans, M. Gaebler, J.-P. Lamke, J. Kruschwitz, H. Walter, White matter network alterations in patients with depersonalization/derealization disorder, J. Psychiatry Neurosci. JPN. 43 (2018) 347–357.
[81] H. Carel, Phenomenology and its application in medicine, Theor. Med. Bioeth. 32 (2011) 33–46. https://doi.org/10.1007/s11017-010-9161-x.
[82] A. Van Reeth, A la recherche du monde commun, Chemins Philos. (n.d.).
[83] R. Salomon, P. Progin, A. Griffa, G. Rognini, K.Q. Do, P. Conus, S. Marchesotti, F. Bernasconi, P. Hagmann, A. Serino, O. Blanke, Sensorimotor Induction of Auditory Misattribution in Early Psychosis, Schizophr. Bull. 46 (2020) 947–954. https://doi.org/10.1093/schbul/sbz136.

2.4.5. Conclusion

De nombreuses études, à la fois expérimentales en stimulant artificiellement le vestibule ou observationnelles sur des patients avec déficit vestibulaire, ont constaté des troubles de dépersonnalisation/déréalisation, affectant à la fois le rapport subjectif au monde extérieur et à son propre corps. La zone PIVC (posteroinsular vestibuar cortex) est la zone principale d'intégration muli-sensorielle du cortex vestibulaire, qui a également une activité neuronale augmentée lors d'expériences extracorporelles ou de symptômes de dépersonnalisation/déréalisation.

L'approche holiste de la phénoménologie est particulièrement intéressante, en ce qui concerne l'apport des informations vestibulaires à l'intégration multisensorielle. En effet le vestibule permet d'apporter des informations sur le mouvement et la position dans l'espace qui sont complémentaires des autres sens. La cinétose (mal des transports) est une conséquence bien connue de la discordance entre les informations vestibulaires et visuelles. Cependant, les nombreux résultats statistiquement significatifs rapportés par cette revue systématique de la littérature, semblent indiquer que la dysfonction vestibulaire peut également altérer la corporéité. Ce terme phénoménologique développé entre autres par Merleau-Ponty (Florival and Dudley, 1979; Merleau-Ponty, 1945), désigne le corps objectif (organisme avec des fonctions physiologiques) mais aussi le corps propre, c'est-à-dire le corps intentionnel qui interagit avec l'environnement, ou le corps « par quoi nous sommes au monde ». Le déficit vestibulaire, entrainant un conflit multisensoriel, semble créer une véritable rupture phénoménologique : une mise en cause du caractère existential du corps (sa nature ontologique) et une disparition du corps propre au profit du corps objectif. Cet évènement pourrait favoriser l'apparition d'un trouble dissociatif, le patient ayant tendance à voir son corps comme un objet plutôt que faisant partie de son être. Ainsi, le vestibule pourrait être une façon d'aborder la question philosophique millénaire de l'union du corps et de l'âme, permettant de dépasser cette dualité. En termes de retombées cliniques, ce travail renforce la stratégie d'associer dès le début de la crise vestibulaire, une prise en charge psychologique à la rééducation vestibulaire (Yardley et al., 2001; Yardley and Redfern, 2001).

2.5. Particularités chez l'enfant

L'enfant a la particularité d'être en développement, et si des troubles vestibulaires aigus peuvent avoir des effets similaires à ceux observés chez l'adulte (voire moindre grâce à une compensation vestibulaire plus rapide), un certain nombre de patients souffrent de déficit vestibulaire congénital et se développent (ou se construisent au monde) avec une fonction vestibulaire altérée depuis la naissance. Alors que le système vestibulaire est normalement fonctionnel dès la vie fœtale, une déficience peut entrainer des problèmes d'intégration multisensorielle, alors que la posture, les fonctions motrices et la stabilité du regard se calibrent pendant les premiers mois de vie.

Plusieurs études ont montré un retentissement postural et moteur du déficit vestibulaire (Maes et al., 2017), le plus évident étant l'âge de la marche qui est habituellement à l'âge 12 mois ± 5 mois et qui peut être retardé jusqu'à 24 mois en cas de déficit vestibulaire. Il peut y avoir également un retard à la tenue de la nuque (normalement 3 mois) et à l'acquisition de la position assise (normalement 9 mois), la sévérité du retentissement postural étant corrélée à la sévérité du déficit vestibulaire et son apparition à un jeune âge (Wiener-Vacher et al., 2013, 2012). Des comportements de compensation sont parfois mis en place avec une dépendance visuelle ou somesthésique (déplacement sur le dos par exemple pour augmenter la surface de contact). L'absence de détection du mouvement lors de rotations du corps peut entrainer des chutes fréquentes chez ces patients et de moins bons résultats des implants cochléaires (Wolter et al., 2015). La stabilité de la vision peut être altérée avec une diminution de l'acuité visuelle dynamique et la présence d'oscillopsies, entrainant des difficultés de lecture (Braswell and Rine, 2006; de Vargas Romero et al., 2020). La fatigabilité et la diminution de la concentration induites peuvent retentir sur l'apprentissage.

La construction du « soi » peut également être modifiée (Wiener-Vacher et al., 2013), surtout en lien avec la verticale subjective et la détection de la gravité, renvoyant au concept de corporéité discuté précédemment. Enfin, le déficit vestibulaire est associé à une augmentation de l'incidence de comorbidités psychiatriques chez l'enfant (Bigelow et al., 2019).

3. La dysfonction vestibulaire chez l'Homme

3.1. Le syndrome vestibulaire aigu

Lors de symptômes vestibulaires chez l'Homme, il convient toujours de faire un examen neurologique à la recherche d'une lésion centrale et d'évaluer la fonction auditive pour éliminer un syndrome cochléo-vestibulaire. Nous allons rappeler ici brièvement les principales caractéristiques cliniques du syndrome vestibulaire harmonieux non compensé (lésion vestibulaire unilatérale périphérique complète).

3.1.1. Symptômes neurovégétatifs

Les nausées et vomissements sont les symptômes neurovégétatifs les plus fréquents et sont souvent au premier plan des symptômes rapportés par les patients présentant un syndrome vestibulaire aigu. C'est l'une des traductions cliniques les plus fréquentes de conflit neurosensoriel, également retrouvé dans la cinétose (ou mal des transports).

3.1.2. La déviation posturale

Lors d'un syndrome vestibulaire harmonieux, une déviation posturale vers le côté lésionnel est observée. Cette déviation est lente, progressive et aggravée lors de la perte des autres entrées sensorielles (à l'obscurité, sans appui mural ou aide) (Chays et al., 2009). La déviation peut être observée à la marche ou en position statique debout grâce à de nombreux tests cliniques réalisés les yeux fermés (test de Romberg, test de déviation des index, tests de piétinement de Fukuda, etc.).

3.1.3. Le nystagmus

Le nystagmus est un mouvement oculaire composé de deux phases, d'abord une déviation lente vers un côté puis une déviation ou saccade rapide de recentrage dans le sens opposé. Par convention, le sens de la secousse rapide donne son nom au nystagmus. Lors d'un syndrome vestibulaire harmonieux,

un nystagmus horizontal est observé, la secousse rapide battant du côté contralatéral à la lésion, le sens du nystagmus restant stable dans le temps et quelle que soit la position de la tête. Ce mouvement résulte d'une prépondérance directionnelle de la phase lente vers le côté lésionnel, suite à une asymétrie des deux VOR droit et gauche. Cette déviation oculaire est responsable du symptôme de vertige rotatoire.

3.1.4. « Ocular tilt reaction »

L'OTR (*ocular tilt reaction*) est un syndrome clinique qui comprend une inclinaison latérale de la tête et une déviation de la verticale subjective vers le côté lésionnel. Les yeux perdent leur alignement vertical (*skew deviation*) et présentent une cyclotorsion vers la lésion. Ainsi, l'œil du côté ipsilatéral à la lésion est hypotrope et en extorsion, l'œil du côté contralatéral est hypertrope et en intorsion (Halmagyi et al., 1991). Cet ensemble de signes cliniques est l'inverse de ce qui se produit lors du tilt VOR physiologique et serait principalement lié à une atteinte otolithique (Chandrakumar et al., 2011; Wong, 2015).

La *skew deviation* qui correspond au strabisme vertical peut-être recherché cliniquement, mais est surtout présente dans les premiers jours d'un déficit unilatéral sévère (névrite vestibulaire, labyrinthite). Certaines méthodes d'exploration vestibulaire au lit du malade permettent d'explorer le système utriculaire en analysant la déviation verticale de la pupille en fonction de l'inclinaison de la tête (Otero-Millan et al., 2017; Zingler et al., 2006).

Ce signe clinique n'est cependant pas spécifique d'une atteinte vestibulaire et peut survenir lors d'atteintes du tronc cérébral (AVC ou tumeurs) : si la lésion est basse (bulbaire ou ponto-bulbaire) alors l'OTR a une inclinaison vers le côté ipsilatéral à la lésion mais si la lésion est haute (mésencéphalique ou ponto-mésencéphalique) alors l'OTR est incliné vers le côté contralatéral (Brodsky et al., 2006; Wong and Sharpe, 2005).

3.2. Principales pathologies et leur prise en charge

Chez l'adulte ou chez l'enfant, la majorité des patients qui consultent pour trouble de l'équilibre, instabilité ou vertiges ne présentent pas de dysfonctions vestibulaires. Nous allons brièvement présenter les principales pathologies chez l'Homme et les solutions thérapeutiques actuelles.

3.2.1. Principales pathologies

Chez l'adulte, la première cause de vertige est le vertige positionnel paroxystique bénin (VPPB), mais qui correspond à une stimulation mécanique anormale, sans dysfonction clinique des organes vestibulaires (explorations fonctionnelles normales). Parmi les dysfonctions vestibulaires, les premières causes sont les déficits vestibulaires d'origine vasculaire, la maladie de Menière (mécanisme d'hydrops vestibulaire) et la névrite vestibulaire (atteinte le plus fréquemment du nerf vestibulaire supérieur), (***Figure 19***).

Chez l'enfant, la répartition des pathologies est différente (***Figure 20***) comme rapporté dans une étude épidémiologique de 2528 patients (Wiener-Vacher et al., 2018). Seuls 37% des patients pédiatriques adressés pour troubles de l'équilibre avaient un déficit fonctionnel vestibulaire (majorité de migraines et des troubles oculomoteurs), dont 25% avaient une malformation de l'oreille interne associée. Parmi les patients présentant une surdité profonde congénitale avec indication d'implant cochléaire, 30% avaient une dysfonction partielle (uni- ou bilatérale) et 20% une perte de fonction complète bilatérale. La prévalence des dysfonctions vestibulaires chez l'enfant est sans doute sous-évaluée à cause de la difficulté de l'interrogatoire chez l'enfant, la capacité plus important (et donc plus rapide) de compensation centrale multisensorielle, ainsi qu'un accès limité aux explorations vestibulaires.

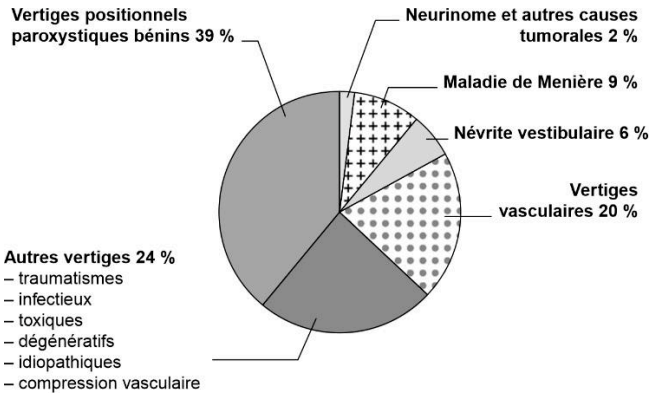

Figure 19 : Principales pathologies vestibulaires chez l'adulte

Il n'est pas représenté sur ce graphique les causes centrales, dont les migraines vestibulaires qui représenteraient 10% des causes de vertige. (Les vertiges, Chays et al., 2009).

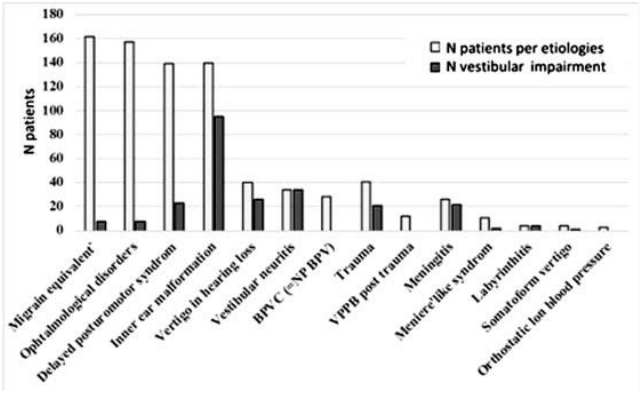

Figure 20 : Principales pathologies vestibulaires chez l'enfant

La majorité des patients pédiatriques adressés pour troubles de l'équilibre n'ont pas de déficit vestibulaire. Cependant parmi ceux qui ont un bilan vestibulaire anormal, la majorité ont des malformations de l'oreille interne correspondant à une vestibulopathie congénitale (Wiener-Vacher et al., 2018).

3.2.2. Principaux traitements et perspectives

En dehors du VPPB pris en charge avec des manœuvres libératoires, les traitements médicamenteux en phase aiguë comprennent souvent un traitement symptomatique antiémétique et une corticothérapie à forte dose pendant quelques jours, pour diminuer l'inflammation labyrinthique ou du nerf vestibulaire. Concernant l'instabilité à moyen ou long terme, certains traitement plus spécifiques existent (notamment pour l'hydrops), mais l'arsenal thérapeutique est pauvre à ce jour.

Le traitement le plus efficace pour réduire les symptômes chroniques est de renforcer le processus de compensation vestibulaire par la rééducation vestibulaire (ou psychomotricité chez les petits enfants), qui permet de solliciter le système vestibulaire résiduel ainsi que le système visuel et somesthésique (Han et al., 2011).

Un projet technologique prometteur est l'implant vestibulaire, qui permettrait (couplé à l'implant cochléaire) de stimuler les afférents vestibulaires en fonction de capteurs de mouvements pour améliorer la stabilité de regard et la posture (Azevedo et al., 2019; Rubinstein et al., 2020). Un autre domaine prometteur est la thérapie génique, principalement orientée vers la réhabilitation auditive des surdités congénitales d'origine génétique, celle-ci permettrait également de rétablir une fonction vestibulaire (Delmaghani and El-Amraoui, 2020). Si les implants vestibulaires sont principalement développés directement chez l'Homme, la thérapie génique demeure pour l'instant un projet de recherche sur modèle animal.

4. Méthodes d'exploration vestibulaire chez l'Homme

Il n'est pas possible d'explorer directement le vestibule (puisque l'organe n'est pas directement visible ou manipulable), mais indirectement en utilisant le VOR ou par électrophysiologie (Starkov et al., 2020). Les principales techniques sont décrites ci-après. Pour explorer l'ensemble de l'oreille interne, des examens audiométriques et une imagerie (IRM et parfois TDM), sont nécessaires.

4.1. Exploration fonctionnelle des canaux semi-circulaires

Les cellules ciliées vestibulaires réagissent à des mouvements ou stimulations mécaniques sur une gamme de fréquence très large (0,01Hz à plus de 4000Hz) (Curthoys and Grant, 2015), cependant les mouvements des yeux ne sont explorés que pour des stimulations allant de 0,01 à 100Hz et les mouvements de la vie quotidienne varient essentiellement entre 0,05Hz et 10Hz (Ulmer et al., 2011). Différents tests fonctionnels peuvent être réalisés pour analyser différentes fréquences (***Figure 21***).

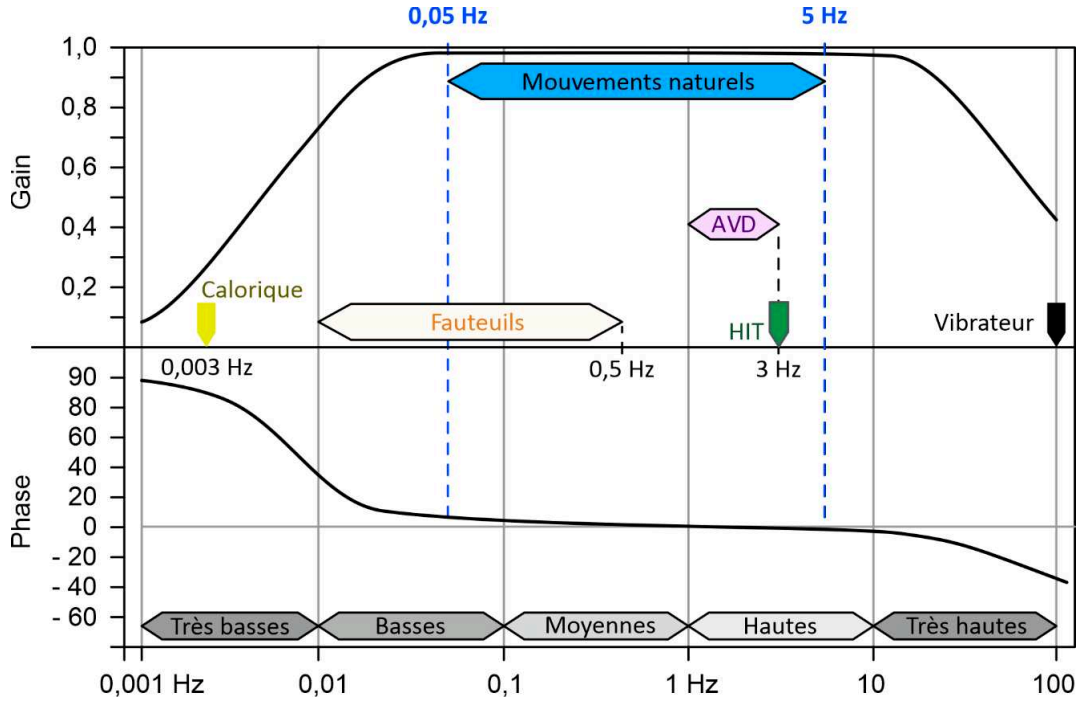

Figure 21 : Tests utilisés pour l'exploration vestibulaire canalaire chez l'Homme

Les gains et les phases dépendent de la fréquence de stimulation. AVD : acuité visuelle dynamique HIT : Head-Impulse Test. Adapté de (Les Vertiges, Chays et al., 2009)

4.1.1. Tests caloriques

Les épreuves caloriques reposent sur le mouvement de convection du liquide endolymphatique induit par une différence de température entre la température corporelle et une température administrée au conduit auditif externe (Bárány, 1906). Ce test permet d'explorer la fonction du canal semi-circulaire latéral aux très basses fréquences. Une vidéonystagmographie dans l'obscurité est réalisée pendant quatre épreuves d'irrigation des conduits auditifs externes alternativement à droite et gauche de liquide (ou d'air) à chaud (44°) puis à froid (30°). La stimulation calorique se fait pendant au moins 30 secondes, avec la tête inclinée de 30° en arrière pour mettre le plan des canaux semi-circulaire latéraux dans un plan vertical. Lors des stimulations caloriques, un nystagmus apparait après une phase de latence, battant ipsilatéralement pour une stimulation chaude (mouvement endolymphatique ampullifuge) et contralatérale ment pour une stimulation froide (mouvement endolymphatique ampullipète). Un logiciel calcule la fréquence et la vitesse maximale de la phase lente au pic de vitesse du nystagmus. Trois indicateurs sont calculés pour interpréter l'examen : la réflectivité, l'hypovalence et la prépondérance directionnelle (Les vertiges, Chays et al., 2009).

La réflectivité correspond, pour une oreille donnée, à la somme des vitesses maximales des phases lentes à chaud et à froid. La réflectivité est très variable d'un individu à l'autre mais est considérée anormale si inférieure à 6°/s.

L'hypovalence est la différence en réflectivité entre les deux oreilles selon la formule de Jongkees et doit être inférieure à 15%, permettant de mettre en évidence une asymétrie de la fonction vestibulaire (OD et OG correspondant à la réflectivité droite et gauche).

$$\text{Hypovalence} = \frac{OD - OG}{OD + OG} \times 100$$

Enfin la prépondérance directionnelle mesure une réponse directionnelle asymétrique entre les nystagmus droit et gauche, permettant de mettre en évidence une hypofonction vestibulaire non-compensée. La prépondérance relative peut être calculée avec la formule de Jongkees (ND et NG

correspond à la somme des vitesses maximales en °/s des phases lentes aux deux stimulations caloriques à droite et à gauche respectivement) :

$$\text{Prépondérance relative} = \frac{ND - NG}{ND + NG} \times 100$$

La prépondérance absolue est plus précise car n'est pas dépendante d'une éventuelle prépondérance thermique d'un individu (sensibilité physiologiquement plus élevée au froid ou au chaud) et calculée selon la formule suivante (ou 1 et 2 correspondent aux stimulations à froid et à chaud) :

$$\text{Prépondérance absolue} = \frac{(ND1 \times ND2) - (NG1 \times NG2)}{ND + NG}$$

La prépondérance directionnelle est présente en cas de déficit vestibulaire non compensé traduisant une dérive pupillaire vers la lésion, la prépondérance relative est considérée normale en dessous de 20% et la prépondérance absolue en dessous de 2°/s. La réflectivité et la prépondérance directionnelle peuvent être visualisées en reportant sur un diagramme (appelé papillon de Freyss) les vitesses des réponses oculaires aux irrigations chaudes et froides à droite et à gauche.

4.1.2. Tests au fauteuil rotatoire

Les tests au fauteuil permettent d'explorer la fonction vestibulaire à plusieurs fréquences physiologiques. Le patient est assis tête fixe dans un fauteuil qui peut tourner dans le plan horizontal à vitesse contrôlée. Une vidéonystagmographie dans l'obscurité est réalisée avec calcul automatisé des mesures de VOR. Deux épreuves principales sont réalisées étudiant la fonction canalaire horizontale : sinusoïdales et rotatoires impulsionnelles.

Les épreuves sinusoïdales correspondent à une rotation horizontale sinusoïdale à fréquence déterminée (*sinusoidal harmonic acceleration test* – SHA). Plusieurs fréquences sont habituellement analysées de 0,05Hz à 0,5Hz (généralement rotation de 180° dans un sens puis dans l'autre). Le gain (rapport de vitesse entre la phase lente et la vitesse de rotation) et la phase (décalage temporel entre

la phase lente et la rotation du fauteuil) sont calculés. Enfin la prépondérance directionnelle (asymétrie du gain vers un côté ou l'autre) est calculée mettant en évidence une asymétrie vestibulaire non compensée si supérieure à 2°/s. Le gain et la phase sont très reproductibles et varient en fonction de la fréquence de stimulation : par exemple à 0,5Hz, le gain est de 0,5 et il y a une avance de phase de 20° ; à 1Hz le gain est de 1 et la phase de 0° (Baloh et al., 1979; Li et al., 1991).

L'épreuve rotatoire impulsionnelle (*velocity-steps test*) est un test rotatoire à vitesse constante (généralement 100°/s) avec accélération initiale rapide et une décélération brutale. La rotation génère un nystagmus dont la secousse rapide bat dans le sens de la rotation (per-rotatoire), puis à l'arrêt une secousse qui bat dans le sens inverse (post-rotatoire). Ces deux nystagmus s'épuisent après un certain temps correspondant au stockage de vitesse. Sont calculés la constante de temps et le gain, rapport entre vitesse de la secousse lente et la vitesse de rotation (Baloh et al., 1979; DiZio and Lackner, 1990; Hain et al., 2018). Une prépondérance directionnelle peut être calculée à partir du gain (notamment en utilisant le diagramme de Freyss et en remplaçant le côté de l'oreille par le sens de rotation, et les deux stimulations caloriques par le nystagmus per et post-rotatoire).

4.1.3. Video Head Impulse Test (vHIT)

Le vHIT permet de filmer et mesurer le mouvement pupillaire lors d'une rotation rapide et brutale de la tête dans les axes de stimulation de chacun des 6 canaux semi-circulaires pendant que le sujet fixe un point immobile devant lui. Sa fiabilité et reproductibilité pour calculer le gain (mouvement oculaire versus mouvement de la tête) à haute fréquence de chaque canal semi-circulaire en fait un examen paraclinique incontournable aujourd'hui pour explorer le système vestibulaire (MacDougall et al., 2009). Chez l'Homme, les normes de gain sont entre 0,9 et 1 pour les canaux horizontaux et 0,8 et 0,9 pour les canaux verticaux, et ne semblent pas évoluer avec l'âge (McGarvie et al., 2015), ainsi un gain inférieur à 0,8 est considéré comme pathologique (Agrawal et al., 2019). Le gain peut varier en fonction de la vitesse de rotation de la tête, et de la distance du point à fixer (Judge et al., 2018; Kim et al., 2018). Il est donc impératif de reproduire le test plusieurs fois pour obtenir un résultat fiable.

Le vHIT permet également de détecter des saccades de refixation précoces (covert) ou tardives (overt) qui sont généralement un argument supplémentaire suggérant une dysfonction canalaire.

4.1.4. Acuité visuelle dynamique

L'acuité visuelle dynamique (AVD) permet d'évaluer la stabilité du regard lors de mouvements rapides de la tête (Schubert et al., 2002). Elle est mesurée par la différence entre l'acuité visuelle statique et dynamique (le caractère dynamique étant induit par la marche ou un mouvement passif ou actif de la tête). En cas d'hypofonction vestibulaire, l'AVD est généralement d'avantage altérée lors des mouvements passifs de la tête (Tian et al., 2002). Une AVD normale nécessite une intégrité du VOR mais aussi d'autres structures (corticlaes ; visuelles) indépendantes du système vestibulaire, la stabilisation de la posture et de la tête ou la présence de covert saccades permettant de limiter les oscillopsies (Brandt et al., 1999; Dietrich and Wuehr, 2019). Ainsi l'AVD permet surtout d'évaluer les aspects de substitutions sensorielles liés à la compensation vestibulaire et n'est pas un examen diagnostic de déficits spécifiquement vestibulaires.

4.2. Exploration fonctionnelle du système otolithique

Plusieurs tests existent pour explorer la fonction otolithique. En routine, il s'agit principalement des tests électromyographiques qui ont l'avantage de pouvoir évaluer indépendamment l'utricule et le saccule de chaque côté, mais ne testent pas leur fonction physiologique. La verticale visuelle subjective et les tests de posture sur plateforme permettent une évaluation plus physiologique de la posture mais leur interprétation doit prendre en compte l'intégration multisensorielle visuelle et somesthésique et proprioceptive, même si celle-ci est minimisée pendant l'examen. Un test de mesure vidéo de la cyclotorsion oculaire lors de l'inclinaison latérale de la tête a été développé mais n'est pas utilisé en routine clinique (Otero-Millan et al., 2017).

4.2.1. Verticale visuelle subjective

Le patient doit estimer sa perception de la verticale dans le noir (pour limiter les informations visuelles). La marge d'erreur normale ne doit pas excéder 4°. En cas de déficit otolithique unilatéral, la verticale subjective est déviée vers le côté malade jusqu'à compensation vestibulaire, traduisant l'effet de la cyclotorsion oculaire sur la verticale perçue (Böhmer and Mast, 1999). Ce test n'est pas spécifique de la fonction vestibulaire et peut également être altéré en cas de lésion du tronc cérébral, tout comme l'OTR (Dieterich and Brandt, 1993).

4.2.2. Potentiels évoqués otolithiques (VEMP)

Les potentiels évoqués otolithiques permettent d'évaluer la fonction sacculaire par les potentiels évoqués otolithiques cervicaux (cVEMP) ou utriculaire par les potentiels évoqués otolithiques oculaires (oVEMP). Ces deux tests mesurent une inhibition musculaire en réponse à une stimulation auditive forte unilatérale (Curthoys and Dlugaiczyk, 2020). Lors des cVEMP, une inhibition du muscle sterno-cleido-mastoïdien ipsilatéral est constaté, et lors des oVEMP le muscle oculaire petit oblique contralatéral. Ainsi pour potentialiser le test, le muscle en question doit être contracté pendant la stimulation, en tournant la tête vers le côté contralatéral pour les cVEMP et en levant les yeux vers le haut pour les oVEMP.

La stimulation sonore peut être réalisée par voie aérienne ou osseuse à des fréquences variables. Elle est habituellement de type *clic* ou *tone burst* (5Hz) à une intensité de 90 à 120dB et à une fréquence de 500Hz. Une stimulation à 1000Hz peut être réalisée notamment pour les pathologies avec suspicion d'hydrops. Deux pics électromyographiques biphasiques d'origine vestibulaire sont enregistrés, correspondant à l'inhibition puis la contraction musculaire, à P13 et N23 ms pour les cVEMP et N10 et P15 ms pour les oVEMP (N pour négatif et P pour positif).

Les résultats sont interprétés en fonction des amplitudes P13-N23 et N10-P15 de chaque oreille, dont le ratio entre les deux côtés ne doit pas dépasser 40% à 500Hz ainsi qu'un respect des latences d'apparition des ondes. Plus spécifiquement pour les cVEMP, un ratio d'amplitude à 1000Hz/500Hz >

85% peut faire évoquer un hydrops labyrinthique, et une diminution des seuils d'apparition des ondes en dessous de 80Hz en faveur d'une troisième fenêtre (Fife et al., 2017; Papathanasiou and Straumann, 2019).

4.2.3. Posturographie

La posturographie statique ou dynamique permet d'évaluer la posture en plaçant un patient debout sur une plateforme, tout en modulant les entrées visuelles (dans le noir, stimulations visuelles) et proprioceptive (plateforme horizontale, penchée, etc.). Des scores composites en fonction tests en différentes conditions permettent d'estimer le retentissement vestibulaire sur la posture en recherchant une latéralisation de celle-ci (Fabre-Adinolfi et al., 2020). Cet examen est très intéressant notamment lors du suivi en rééducation pour évaluer l'intégration multisensorielle et la compensation vestibulaire (Baydan et al., 2020).

4.3. Explorations vestibulaires chez l'enfant

Tous ces tests adultes peuvent être fait en théorie chez l'enfant, mais à moduler en fonction de la tolérance de chaque enfant et du contexte de l'examen (Ciolek et al., 2018; Dhondt et al., 2018; Janky and Rodriguez, 2018).

Les tests caloriques peuvent être moins bien tolérés chez l'enfant mais sont en théorie réalisable à tout âge. La sensation désagréable de vertige induit par le test ainsi que le maintien de l'enfant dans l'obscurité peuvent être anxiogène et parfois nécessiter un examen simple sous vidéonystagmoscopie avec comptage manuel des secousses rapides.

Les tests au fauteuil rotatoire sont faisable dès les premiers mois de vie avec des gains similaires à l'adulte (Maes et al., 2014). Le vHIT également peut être réalisé dès 3 mois de vie, avec des résultats reproductibles (Bachmann et al., 2018; Hamilton et al., 2015; Ross and Helminski, 2016; Wiener-Vacher and Wiener, 2017). Notamment, deux stimulations par CSC peuvent être suffisantes si les courbes sont satisfaisantes (Wenzel et al., 2019). Les gains du vHIT chez les jeunes enfants sont plus bas (norme à 0,65 pour les canaux verticaux et 0,77 pour les horizontaux) pour atteindre la normale adulte vers 16 ans (Wiener-Vacher and Wiener, 2017). Enfin les cVEMP peuvent être réalisés dès 3 mois de vie lorsque l'enfant peut tenir sa tête, une augmentation physiologique de la latence N1 et une diminution du seuil lors des cVEMP ayant été rapporté (Maes et al., 2014). Les oVEMP qui demandent une participation plus importante de l'enfant peuvent être réalisés à partir de l'âge de 3 ans avec des résultats similaires à l'adulte (Kuhn et al., 2018). Concernant les potentiels évoqués myogéniques, il est préférable d'utiliser une stimulation sonore en conduction osseuse pour pallier aux surdités de transmission fréquentes liées aux otites séro-muqueuses, pouvant altérer les résultats (Rodriguez et al., 2018). Des tests posturaux peuvent enfin être réalisés en prenant en compte l'âge (Goulème et al., 2018).

5. Intérêt des modèles murins

5.1. Pourquoi la souris ?

La souris est le modèle mammifère le plus fréquent en laboratoire, du fait de son taux de reproduction rapide, sa petite taille et sa disponibilité. Ce modèle animal est bien connu par la communauté scientifique et sa manipulation facile pour créer de nouveaux mutants génétiques mais aussi obtenir les mêmes lignées reproductibles partout dans le monde (par exemple C57BL/6). Par ailleurs, les techniques d'immunohistochimie sont rendues possibles du fait de la disponibilité de nombreux anticorps à un coût relativement faible. Enfin, le système vestibulaire est une structure ancienne dans l'évolution qui est comparable entre les différentes espèces de vertébrés. Ainsi, le modèle murin est le premier modèle animal de recherche cochléo-vestibulaire depuis 2005 et surpasse en nombre de publications l'ensemble des autres modèles (rat, cochon-d'Inde, chat) depuis 2015 (Ohlemiller et al., 2016). Son essor a conduit au développement de techniques de vidéo-oculographie qui ont révélé des réflexes vestibulo-oculaires proches de l'unité ; la souris constitue donc un modèle animal présentant de nombreux avantages expérimentaux pour mieux caractériser la fonction vestibulaire rencontrée chez les Mammifères, dont l'Homme.

Un exemple concerne l'étude de la surdité congénitale liée à une mutation du gène *SLC26A4*, dont le syndrome de Pendred. En effet cette pathologie, qui se traduit dans la majorité des cas par un déficit cochléo-vestibulaire congénital, est encore mal comprise chez l'Homme, particulièrement d'un point de vue vestibulaire. Le développement et l'exploration d'un modèle murin ont permis de mieux comprendre les mécanismes en jeu.

5.2. Revue 2 : Interprétation du syndrome de Pendred et des surdités congénitales liées à une mutation du gène *SLC26A4* comme un hydrops fœtal

5.2.1. Contexte scientifique

La maladie de Menière est fréquente et bien décrite dans la littérature, même si le mécanisme sous-jacent de l'hydrops endolymphatique est encore mal connu et probablement plurifactoriel. La maladie de Menière est définie comme un deuxième (ou plus) épisode de vertige, d'une durée de 20 minutes à 12 heures, associé à une perte auditive et des symptômes cochléaires (acouphènes, sensation de plénitude de l'oreille), ne pouvant être expliqué par un autre diagnostic (Goebel, 2016). Si la définition clinique de la maladie de Menière est très précise, les pathologies liées à l'hydrops endolymphatique sont beaucoup plus vastes, avec des présentations incomplètes de maladie de Menière parfois uniquement cochléaires ou vestibulaires. L'essor récent des imageries endolymphatiques par IRM (avec acquisition retardée après injection de gadolinium) permettent de visualiser l'hydrops endolymphatique dans la maladie de Menière typique mais aussi dans les hydrops atypiques (Attyé et al., 2017; Lopez-Escamez and Attyé, 2019).

Le syndrome de Pendred est une surdité congénitale associée à un goître, liée à une mutation biallélique du gène *SLC26A4*. Les mutations de *SLC26A4* sont beaucoup plus souvent associées à une surdité isolée DFNB4 (80-90% de surdités isolées et 10-20% de syndromes de Pendred). Cette surdité est typiquement fluctuante et progressive, et associée radiologiquement à une dilatation de l'aqueduc du vestibule bilatérale et parfois à une dysplasie cochléaire de type II (Albert et al., 2006). La pathologie étant rare, ses caractéristiques surtout vestibulaires sont peu décrites dans la littérature. De récentes avancées sur un modèle murin *slc26a4*-KO de surdité fluctuante ont permis de mettre en évidence les mécanismes embryologiques probables de dysfonction labyrinthique avec notamment la

mise en évidence histologique d'un hydrops avant la naissance de la souris (Wangemann and Griffith, 2017).

5.2.2. Buts de l'étude

L'objectif de cette revue de la littérature était de mettre en parallèle les connaissances scientifiques (provenant de données humaines ou animales) concernant les deux atteintes cochléo-vestibulaires de la maladie de Menière et du syndrome de Pendred, et de comparer les deux types d'hydrops sous-jacents.

5.2.3. Résumé en français

La mutation biallélique du gène *SLC26A4* entraine une surdité isolée DFNB4 ou syndromique (syndrome de Pendred) dont l'atteinte vestibulaire est encore mal décrite. En croisant les avancées sur des modèles murins *slc26a4*-KO aux données de patients (notamment les caractéristiques cliniques des crises de vertige ainsi que les données radiologiques), nous avons proposé l'hypothèse qu'un hydrops fœtal pourrait être à l'origine du déficit cochléo-vestibulaire dans ces maladies. De nombreux parallèles ont pu être dressés avec la maladie de Menière, qui est la maladie typiquement associée à l'hydrops endolymphatique dans la littérature. Les deux entités présentent une surdité fluctuante et progressive avec des épisodes de vertiges et d'acouphènes, associé à un hydrops endolymphatique (visible en imagerie ou en histologie). L'étude des modèles murins de syndrome de Pendred a montré que la mutation biallélique du gène *slc26a4* entraine une rétention de Na^+ et d'eau dans l'endolymphe pendant la période périnatale, qui induit une dégénérescence de la strie vasculaire puis une perte de la fonction auditive. En transposant à l'Homme, ces anomalies endolymphatiques surviendraient pendant la vie fœtale et pourraient expliquer les anomalies morphologiques visibles à l'imagerie dès la naissance (dilatation de l'aqueduc du vestibule et dysplasie cochléaire de type II).

5.2.4. Article original

Titre :

Interpreting Pendred syndrome as a foetal hydrops: clinical and animal model evidence

Auteurs :

François SIMON, Françoise DENOYELLE, Mathieu BERANECK

Etat d'avancement :

Soumis le 05/03/2020 à *Journal of Vestibular Research* (IF = 2.816)

Abstract

Background: Menière disease (MD) and *SLC26A4* related deafness (Pendred syndrome (PS) or DFNB4) are two different inner ear disorders which present with fluctuating and progressive hearing loss, which could be a direct consequence of endolymphatic hydrops.

Objective: to present similarities between both pathologies and explore how the concept of hydrops may be applied to PS/DFNB4.

Methods: Review of the literature on MD, PS/DFNB4 and mouse model of PS/DFNB4.

Results: MD and PS/DFNB4 share a number of similarities such as fluctuating and progressive hearing loss, acute episodes with vertigo and tinnitus, MRI and histological evidence of endolymphatic hydrops (although with different underlying mechanisms). MD is usually diagnosed during the fourth decade of life whereas PS/DFNB4 is congenital. The PS/DFNB4 mouse models have shown that biallelic *slc26a4* mutations lead to Na^+ and water retention in the endolymph during the perinatal period, which in turn induces degeneration of the stria vascularis and hearing loss. Crossing clinical/imagery characteristics and animal models, evidence seems to support the hypothesis of PS being a foetal hydrops.

Conclusions: When understanding PS/DFNB4 as a developmental hydrops, treatments used in MD could be repositioned to PS.

Keywords: Menière; Pendred; DFNB4; hydrops; mouse

Introduction

Menière's disease (MD) and endolymphatic hydrops are both very frequently discussed topics in the literature, although the underlying mechanisms are still poorly understood. First described in 1938 by Hallpike and Cairns [1], endolymphatic hydrops corresponds to a dilated endolymphatic sector within the inner ear, and is considered as a histological basis for MD although it has also been found in other inner ear diseases. In addition, it is still debated whether endolymphatic hydrops is a cause or consequence of MD. Genetics seem to play a role in some sporadic and familial cases but are of a complex and polygenic nature [2].

SLC26A4 mutations are the cause of two autosomal recessive diseases, which share the same audiometric phenotype of progressive and fluctuating hearing loss (HL): Pendred syndrome (PS), a rare syndrome deafness associated with thyroid disorders and DFNB4, an isolated deafness (*SLC26A4* related deafness hereinafter referred to as PS/DFNB4). Recent studies on a mouse model of PS/DFNB4 have shown evidence of endolymphatic hydrops which could draw parallels with the better-known hydrops described in MD patients. Both MD and PS/DFNB4 correspond to internationally defined entities, yet may easily be confused with other types of fluctuating HL of idiopathic origin. Thus, for the sake of clarity, this paper will only discuss clinical presentations of definite MD (as defined by the American Academy of Otolaryngology-Head and Neck Surgery) and PS/DFNB4 with confirmed biallelic *SLC26A4* mutations. The objective of this paper is to present similarities between both entities and explore how the concept of hydrops may be applied to PS/DFNB4.

Menière *versus* Pendred, similarities and differences

MD and PS/DFNB4 are two different inner ear disorders, which share a number of similarities and differences as reported in **Table 1**.

MD, first described by Prosper Menière in 1861, is the typical clinical example of hydrops. It has a very strict clinical definition, which was recently updated in 2015 [3]. Briefly, a patient must present with two or more spontaneous episodes of vertigo, ranging from 20 minutes to 12 hours long, with low to medium frequency sensorineural HL and aural symptoms (tinnitus or aural fullness), which cannot be

accounted for by any other vestibular diagnosis. Symptoms which do not exactly correspond to this definition may be linked to endolymphatic hydrops and be considered as probable or possible MD. MD may have very different presentations from one patient to the other, but the key aspect is the fluctuating and progressive HL which spans out over several years. Over time, the HL worsens at all tested frequencies and becomes constant, usually stabilizing between 50 and 70 dB. Symptoms are usually unilateral, but up to half of patients present with bilateral symptoms, and the majority have bilateral electrophysiological or imagery anomalies (regardless of the contralateral ear being symptomatic or not) [4, 5]. This is an adult's disease, with most cases diagnosed in the fourth or fifth decade of life. Juvenile MD has been described in case reports in the literature, but remains extremely rare and linked to family history of MD [6]. The most frequent diagnosis in the child is vestibular migraine [7], but the clinical symptoms also resemble the rarer PS/DFNB4.

Table 1: Main differences and similarities between MD and PS/DFNB4

Differences	*Similarities*
- Typical age of onset (MD in 40s; PS prelingual) - Typical long-term HL severity (MD: moderate HL; PS: profound to severe) - HL frequencies (MD: low-medium frequencies; PS: non-specific) - CT-scan bony modifications (MD: normal; PS: EVA and Mondini)	- Fluctuating and progressive HL - Acute HL episodes with vertigo and tinnitus - Enlarged endolymphatic space on MRI - Histological evidence of endolymphatic hydrops (cadaveric studies in MD and mouse in PS)

EVA Enlarged vestibular aqueduct ; *HL* Hearing Loss ; *MD* Menière disease; *PS* Pendred Syndrome

Vaughan Pendred first described Pendred syndrome in 1896, reporting an Irish family with congenital deafness and thyroid goitre. The disease has since then been linked to the *SLC26A4* (or *PDS*) gene which codes for the pendrin protein (Na^+ independent Cl^-/Iodine/$HCO3^-$ exchanger) [8]. Biallelic recessive mutation can cause DNFB4 isolated deafness or the Pendred syndrome when associated to a goitre (10-20% of cases) and is estimated to be responsible for 5-15% of congenital HL [9–14]. The prevalence of *SLC26A4* mutations is higher in China (carry rate 2.02% I la population of 2627 new-borns) [14]. Clinically, the same triad can be found as in MD, with episodes of fluctuating HL (although not

specifically low to medium frequencies), vertigo and tinnitus. An auditory bone-gap can be found in low frequencies, probably due to a third-window effect, but may as in some MD patients be due to decreased stapes mobility entailed by excessive endolymphatic pressure [15–17]. Symptoms vary from one patient to another, with unilateral or bilateral HL, and severity at birth ranging from cophosis to normal hearing. HL is however prelingual and progressive in the majority of cases (50-60% and 70-90% respectively) [11, 12, 18, 19].

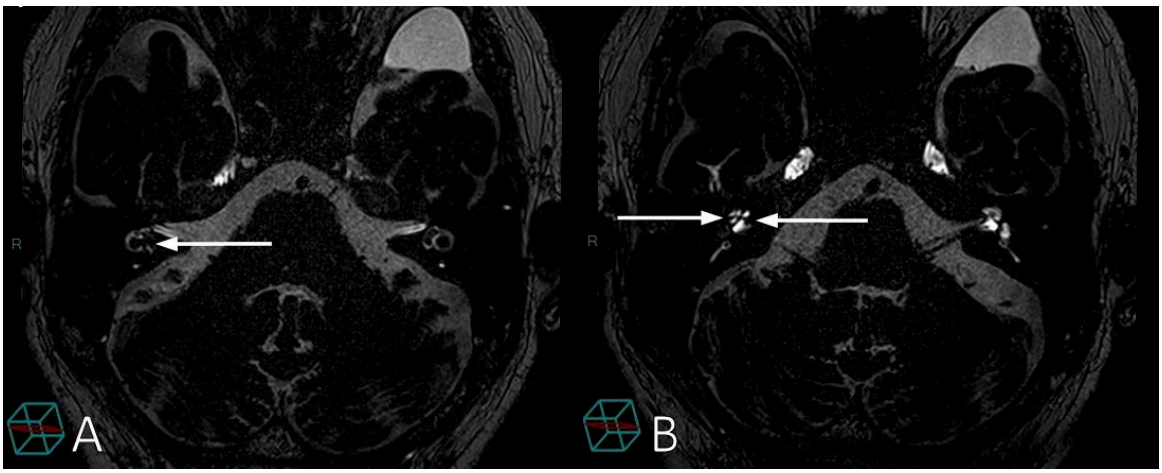

Fig 1. MRI of hydrops in Menière disease
MRI 3D-FLAIR sequence 4h after intravenous gadolinium injection. Imagery of a patient with right Menière disease. The MRI shows endolymphatic hydrops of vestibular and cochlear sectors in the right ear (and normal left ear). In the inner ear, the perilymph appears in hypersignal and endolymph in hyposignal. A: arrow shows utricular hydrops. B: left-to-right arrow shows cochlear hydrops; right-to-left arrow shows saccular hydrops. Curtesy from Michael Eliezer (Lariboisière Hospital, APHP, Paris, France)

Concerning imagery, both vestibular disorders show signs of increased endolymphatic volume, although the aspect and mechanism are quite different. In MD, CT-scan is normal, MRI can show endolymphatic hydrops concerning both cochlear and vestibular sectors (see **Figure 1**), however saccular hydrops seems to be one of the most reproducible markers [20–24]. In PS/DFNB4, bilateral enlarged vestibular aqueduct (EVA), containing endolymph, is a constant feature in patients with biallelic mutations and may sometimes be associated with cochlear incomplete partition type II (Mondini dysplasia), as shown in **Figure 2**. Both malformations can also be diagnosed on a CT-scan or MRI and are often-indicators of PS/DFNB4 that usually precede genetic confirmation.

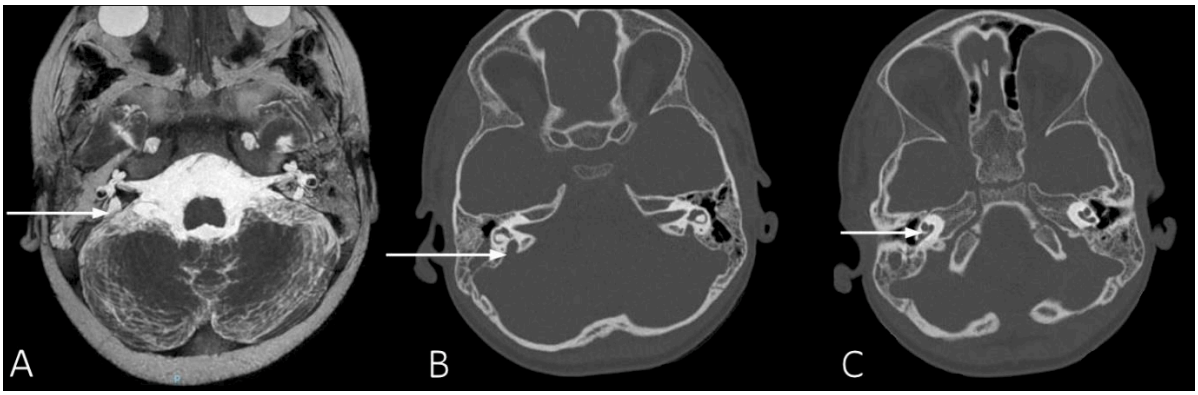

Fig 2. CT-scan and MRI of hydrops in Pendred syndrome
Imagery of a patient with Pendred syndrome, with bilateral enlarged vestibular aqueduct (EVA), and cochlear incomplete partition type II (Mondini dysplasia). A: MRI T2 sequence, arrow shows the right EVA. B: CT-scan, arrow showing the right EVA with the large bony canal. C: CT-scan showing right Mondini dysplasia in the cochlea (only two turns).

Vestibular function in MD is remarkable as there is, in most cases, a dissociation between caloric tests and vHIT [25–27]. This is probably due to the fact that while endolymphatic hydrops distorts the volume of the lateral semi-circular canal, thus inducing caloric hyporeflexia, the semi-circular canals still respond normally to high speed physiological stimulation. In the later stages of MD, the proportion of normal canal function (vHIT) and otolith function (cVEMP and oVEMP) decrease [27–29]. Literature on the vestibular function in PS/DFNB4 is to date very poor due to its rarity, one study reporting canal paresis in 49% using caloric test [30]. Studies on EVA series (including PS/DFNB4 patients but not specific to SLC26A4 mutations) report abnormally low cVEMP (at 250 and 500Hz) thresholds and high amplitudes probably due to a third-window effect [15, 31, 32].

Animal models

Lacking any unique genetic background or universally accepted histopathological hypothesis, it has been difficult to develop a specific animal model of MD [2]. A large number of models have been developed to try and mimic endolymphatic hydrops and fluctuating HL, usually requiring surgical endolymphatic sac destruction (to reduce endolymphatic resorption) or administration of medication to increase endolymphatic production (such as aldosterone) [33–36]. These models rely on artificial disruption of the endolymphatic homeostasis. PS/DFNB4, on the other hand, has been clearly linked to

a biallelic mutation of the *SCL26A4* gene, and mouse models specific of this disease have been recently developed to understand underlying mechanisms.

It is first important to specify that in the mouse, development of the inner ear occurs throughout the perinatal period, starting at E9 (embryo day 9) with the otic placode and ending with a final adult structure at P20 (20 days after birth), whereas the human inner ear formation exclusively takes place during the foetal life ranging from 23 days to 8 months, respectively [37]. More precisely, key steps in mouse inner ear development are as follows: opening of endolymphatic sac lumen at E10.5; opening of cochlear lumen at E14.5; utricule and saccule are formed by E17; neuronal elements continue to develop during a period of differenciation and speciation from E17 to P7; mature endolymph produced at P3; endolymphatic potential matures from P7 to P15; with the onset of auditory function generally at P12; as well as the functional maturation of the vestibulo-ocular reflex which occurs after the opening of the eye at P12 [37–40].

The first *slc26a4* mouse biallelic knock-out model was developed in 1999 but showed a more severe phenotype than in humans, with congenital complete bilateral deafness and vestibular deficit behaviour. Pendrin expression was first detected at E13 in the duct and sac, and then at E15 in the utricule, saccule and cochlea. Enlarged endolymphatic space was demonstrated at E15 with secondary cochlea hair cell and macula destruction from P7 to P45 [41–43]. Further studies reported that pendrin in itself was not essential for hearing but defective pendrin caused HL via secondary mechanisms such as the degeneration, oxidative stress and macrophagic invasion of the stria vascularis [39, 43, 44]. Pendrin was demonstrated to be key in the endolymphatic homeostasis: lack of the $Cl^-/HCO3^-$ exchanger pendrin would decrease the endolymphatic pH as soon as E15.5 and thereby increase Ca^{2+} and Na^+ retention (by reducing the current that drives Na^+ reabsorption through Na^+ channels in the endolymphatic sac) [45–47]. Increased Na^+ endolymphatic concentration would in turn induce reduced endolymphatic potential and retain water creating endolymphatic hydrops. Finally, the mechanical effect of endolymphatic hydrops and increased cellular stress would entail cochlea stria vascularis degeneration around P10 (no data available for the vestibular system) [38, 48]. Other mice models have been developed with similar results, also showing a decreased amount of otoconia and giant or ectopic otoconia probably due to the

altered endolymphatic calcium homeostasis [49–51]. Histological exploration and imagery of these mice models clearly showed endolymphatic hydrops.

Studies of the pendrin action timeframe were conducted on a dox-dependent mouse knock-out model, developed in 2011[52]. It was shown that absence of expression *slc26a4* expression (no pendrin) before E16.5 or after P2 did not alter auditory brainstem responses (ABR) in these mice. However, absence of *slc26a4* expression between E16.5 and E18.5 led to a decreased endolymphatic potential and pH, although with normal ABR. Finally, absence of *slc26a4* expression between E18.5 and P2 entailed a more severe state with abnormal ABR [52]. From these results, a model reproducing the human cochlea-vestibular phenotype of PS/DFNB4 was developed, with *slc26a4* expression deactivated from E17.5 to P2, leading to fluctuating abnormal ABR and a progressive hearing loss at 6 months (vestibular function was not assessed) [53]. From this model, hypothesis was drawn that the pendrin expression in the endolymphatic sac would be necessary in the mouse to allow acquisition of normal hearing in the perinatal period [54, 55].

A foetal hydrops

PS/DFNB4 in the mouse model seems to be secondary to modification of endolymphatic fluid absorption in the developing inner ear. Although the exact molecular mechanisms may differ in human PS/DFNB4, the process is probably comparable. The timing of these events in the human inner ear is unknown, but by comparing the timetable of mouse and human ear development, we may suppose they could take place during the human foetal and early postnatal life, with the most sensitive moment (corresponding to the mouse perinatal period) taking place in a 3 to 4-month-old foetus, well before birth [37]. Although gene therapy seems promising [56, 57], this timing causes great difficulties, first in terms of diagnostic opportunities, and then of treatment strategies.

Crossing results from the animal model with children's imagery, we could hypothesise that foetal endolymphatic hydrops, may induce inner ear bulging before cranial ossification occurs, thus rendering the cochleo-vestibular malformations visible on the CT-scan at birth. This foetal hydrops may be already advanced at birth, with congenital bilateral cophosis, in which case management would have to rely (as

it does today) on auditory rehabilitation such as cochlear implant. In the cases where congenital hydrops is associated with residual to normal hearing, specific treatment, yet to be developed, may become key: on one hand, gene therapy or inner ear medication (research on animal models) and on the other hand, repositioning of established hydrops treatment (currently used in MD) to treat fluctuating episodes.

Conclusion:

MD and PS/DFNB4 are two different inner ear disorders linked to endolymphatic hydrops. MD is more common and its literature abundant whereas PS/DFNB4 remains poorly described, especially its vestibular characteristics. The main common feature is fluctuating and progressive HL, which could be a direct consequence of endolymphatic hydrops, with fluctuating hydrops on one hand and progressive degeneration of the cochlea on the other. The PS/DFNB4 mouse models developed in the past two decades have helped identify the role of pendrin and how biallelic slc26a4 mutation lead to Na^+ and water retention in the endolymph. When understanding PS/DFNB4 as a developmental hydrops, treatments which have been proven to improve MD symptoms could be repositioned to PS/DFNB4, for which large-scale studies are difficult to organise due to its rarity. Conversely, parallels may be drawn between mechanisms highlighted in the mouse PS/DFNB4 model and physiopathological hypothesis in MD. Exchanges between different fields, from paediatric and adult otolaryngologists to researchers developing animal models should be encouraged. More broadly, further links should be established between congenital fluctuating inner ear disorders, with unilateral or bilateral EVA, and the larger diagnosis of possible or probable MD.

References:

[1] C. S. Hallpike and H. Cairns, Observations on the pathology of Meniere's syndrome, *J. Laryngol. Otol.* **53**(10) (1938), 625–655.

[2] A. Gallego-Martinez and J. A. Lopez-Escamez, Genetic architecture of Meniere's disease, *Hear. Res.* (2019), 107872.

[3] J. A. Goebel, 2015 Equilibrium Committee Amendment to the 1995 AAO-HNS Guidelines for the Definition of Ménière's Disease, *Otolaryngol.--Head Neck Surg. Off. J. Am. Acad. Otolaryngol.-Head Neck Surg.* **154**(3) (2016), 403–404.

[4] C.-H. Huang and Y.-H. Young, Bilateral Meniere's disease assessed by an inner ear test battery, *Acta Otolaryngol. (Stockh.)* **135**(3) (2015), 233–238.

[5] K. Morimoto, T. Yoshida, S. Sugiura, M. Kato, K. Kato, M. Teranishi, *et al.*, Endolymphatic hydrops in patients with unilateral and bilateral Meniere's disease, *Acta Otolaryngol. (Stockh.)* **137**(1) (2017), 23–28.

[6] C. Wang, C.-H. Wu, P.-W. Cheng, and Y.-H. Young, Pediatric Meniere's disease, *Int. J. Pediatr. Otorhinolaryngol.* **105** (2018), 16–19.

[7] S. R. Wiener-Vacher, J. Quarez, and A. L. Priol, Epidemiology of Vestibular Impairments in a Pediatric Population, *Semin. Hear.* **39**(3) (2018), 229–242.

[8] L. A. Everett, B. Glaser, J. C. Beck, J. R. Idol, A. Buchs, M. Heyman, *et al.*, Pendred syndrome is caused by mutations in a putative sulphate transporter gene (PDS), *Nat Genet* **17**(4) (1997), 411–22.

[9] X. C. Li, L. A. Everett, A. K. Lalwani, D. Desmukh, T. B. Friedman, E. D. Green, *et al.*, A mutation in PDS causes non-syndromic recessive deafness, *Nat. Genet.* **18**(3) (1998), 215–217.

[10] C. Aimoni, A. Ciorba, L. Cerritelli, S. Ceruti, P. H. Skarzynski, and S. Hatzopoulos, Enlarged vestibular aqueduct: Audiological and genetical features in children and adolescents, *Int J Pediatr Otorhinolaryngol* **101** (2017), 254–258.

[11] M. Miyagawa, S. Y. Nishio, and S. Usami, Mutation spectrum and genotype-phenotype correlation of hearing loss patients caused by SLC26A4 mutations in the Japanese: a large cohort study, *J Hum Genet* **59**(5) (2014), 262–8.

[12] H. Suzuki, A. Oshima, K. Tsukamoto, S. Abe, K. Kumakawa, K. Nagai, *et al.*, Clinical characteristics and genotype-phenotype correlation of hearing loss patients with SLC26A4 mutations, *Acta Otolaryngol* **127**(12) (2007), 1292–7.

[13] S. Albert, H. Blons, L. Jonard, D. Feldmann, P. Chauvin, N. Loundon, *et al.*, SLC26A4 gene is frequently involved in nonsyndromic hearing impairment with enlarged vestibular aqueduct in Caucasian populations, *Eur J Hum Genet* **14**(6) (2006), 773–9.

[14] Y. Fang, M. Gu, C. Wang, F. Suo, G. Wang, and Y. Xia, GJB2 as Well as SLC26A4 Gene Mutations are Prominent Causes for Congenital Deafness, *Cell Biochem Biophys* **73**(1) (2015), 41–4.

[15] G. Zhou and Q. Gopen, Characteristics of vestibular evoked myogenic potentials in children with enlarged vestibular aqueduct, *Laryngoscope* **121**(1) (2011), 220–5.

[16] Y. J. Seo, J. Kim, and J. Y. Choi, Correlation of vestibular aqueduct size with air-bone gap in enlarged vestibular aqueduct syndrome, *Laryngoscope* **126**(7) (2016), 1633–8.

[17] S. Sugimoto, T. Yoshida, M. Teranishi, Y. Okazaki, S. Naganawa, and M. Sone, The relationship between endolymphatic hydrops in the vestibule and low-frequency air-bone gaps, *The Laryngoscope* **128**(7) (2018), 1658–1662.

[18] Y. Okamoto, H. Mutai, A. Nakano, Y. Arimoto, T. Sugiuchi, S. Masuda, *et al.*, Subgroups of enlarged vestibular aqueduct in relation to SLC26A4 mutations and hearing loss, *Laryngoscope* **124**(4) (2014), E134-40.

[19] J. W. van Nierop, W. J. Huinck, R. J. Pennings, R. J. Admiraal, E. A. Mylanus, and H. P. Kunst, Patients with Pendred syndrome: is cochlear implantation beneficial?, *Clin Otolaryngol* **41**(4) (2016), 386–94.

[20] F. Simon, J. P. Guichard, R. Kania, J. Franc, P. Herman, and C. Hautefort, Saccular measurements in routine MRI can predict hydrops in Meniere's disease, *Eur. Arch. Oto-Rhino-Laryngol. Off. J. Eur. Fed. Oto-Rhino-Laryngol. Soc. EUFOS Affil. Ger. Soc. Oto-Rhino-Laryngol. - Head Neck Surg.* **274**(12) (2017), 4113–4120.

[21] A. Attyé, M. Eliezer, N. Boudiaf, I. Tropres, D. Chechin, S. Schmerber, *et al.*, MRI of endolymphatic hydrops in patients with Meniere's disease: a case-controlled study with a simplified classification based on saccular morphology, *Eur. Radiol.* **27**(8) (2017), 3138–3146.

[22] A. Attyé, M. Eliezer, M. Medici, I. Tropres, G. Dumas, A. Krainik, *et al.*, In vivo imaging of saccular hydrops in humans reflects sensorineural hearing loss rather than Meniere's disease symptoms, *Eur. Radiol.* **28**(7) (2018), 2916–2922.

[23] A. Venkatasamy, F. Veillon, A. Fleury, M. Eliezer, M. Abu Eid, B. Romain, *et al.*, Imaging of the saccule for the diagnosis of endolymphatic hydrops in Meniere disease, using a three-dimensional T2-weighted steady state free precession sequence: accurate, fast, and without contrast material intravenous injection, *Eur. Radiol. Exp.* **1**(1) (2017), 14.

[24] J. A. Lopez-Escamez and A. Attyé, Systematic review of magnetic resonance imaging for diagnosis of Meniere disease, *J. Vestib. Res. Equilib. Orientat.* **29**(2–3) (2019), 121–129.

[25] F. Rubin, F. Simon, B. Verillaud, P. Herman, R. Kania, and C. Hautefort, Comparison of Video Head Impulse Test and Caloric Reflex Test in advanced unilateral definite Menière's disease, *Eur. Ann. Otorhinolaryngol. Head Neck Dis.* **135**(3) (2018), 167–169.

[26] I. P. Hannigan, M. S. Welgampola, and S. R. D. Watson, Dissociation of caloric and head impulse tests: a marker of Meniere's disease, *J. Neurol.* (2019),.

[27] B. F. van Esch, K. Abolhosseini, S. Masius-Olthof, H. J. van der Zaag-Loonen, P. P. G. van Benthem, and T. D. Bruintjes, Video-head impulse test results in patients with Menière's disease related to duration and stage of disease, *J. Vestib. Res. Equilib. Orientat.* **28**(5–6) (2018), 401–407.

[28] T. Okumura, T. Imai, Y. Takimoto, N. Takeda, T. Kitahara, A. Uno, *et al.*, Assessment of endolymphatic hydrops and otolith function in patients with Meniere's disease, *Eur. Arch. Otorhinolaryngol.* **274**(3) (2017), 1413–1421.

[29] L. Chen, H. Xu, W. Wang, Q. Zhang, Q. Lv, and X. Song, Evaluation of the otolith function using c/oVEMPs in patients with Ménière's disease, *J. Otolaryngol.-Head Neck Surg.* **45**(1) (2016), 39.

[30] J. Jung, Y. W. Seo, J. Y. Choi, and S. H. Kim, Vestibular function is associated with residual low-frequency hearing loss in patients with bi-allelic mutations in the SLC26A4 gene, *Hear Res* **335** (2016), 33–39.

[31] C. K. Zalewski, W. W. Chien, K. A. King, J. A. Muskett, R. E. Baron, J. A. Butman, *et al.*, Vestibular Dysfunction in Patients with Enlarged Vestibular Aqueduct, *Otolaryngol Head Neck Surg* **153**(2) (2015), 257–62.

[32] C. J. Yang, V. Lavender, J. K. Meinzen-Derr, A. P. Cohen, M. Youssif, M. Castiglione, *et al.*, Vestibular pathology in children with enlarged vestibular aqueduct, *Laryngoscope* **126**(10) (2016), 2344–50.

[33] R. Kimura and H. Schuknecht, Membranous hydrops in the inner ear of the guinea pig after obliteration of the endolymphatic sac, *Orl* **27**(6) (1965), 343–354.

[34] K. C. Horner, Auditory and vestibular function in experimental hydrops, *Otolaryngol. Neck Surg.* **112**(1) (1995), 84–89.

[35] E. Ferrary and O. Sterkers, Mechanisms of endolymph secretion., *Kidney Int. Suppl.* **65** (1998), S98-103.

[36] E. Dunnebier, J. Segenhout, H. Wit, and F. Albers, Two-phase endolymphatic hydrops: a new dynamic guinea pig model, *Acta Otolaryngol. (Stockh.)* **117**(1) (1997), 13–19.

[37] R. J. Gorlin, R. J. Gorlin, H. V. Toriello, and M. M. Cohen, Hereditary hearing loss and its syndromes,. Oxford University Press, USA 1995.

[38] P. Wangemann, The role of pendrin in the development of the murine inner ear, *Cell Physiol Biochem* **28**(3) (2011), 527–34.

[39] P. Wangemann, E. M. Itza, B. Albrecht, T. Wu, S. V. Jabba, R. J. Maganti, *et al.*, Loss of KCNJ10 protein expression abolishes endocochlear potential and causes deafness in Pendred syndrome mouse model, *BMC Med* **2** (2004), 30.

[40] M. Beraneck, F. M. Lambert, and S. G. Sadeghi, Functional development of the vestibular system: Sensorimotor pathways for stabilization of gaze and posture, in *Development of auditory and vestibular systems*, Elsevier, 2014, 449–487.

[41] L. A. Everett, I. A. Belyantseva, K. Noben-Trauth, R. Cantos, A. Chen, S. I. Thakkar, *et al.*, Targeted disruption of mouse Pds provides insight about the inner-ear defects encountered in Pendred syndrome, *Hum Mol Genet* **10**(2) (2001), 153–61.

[42] L. A. Everett, H. Morsli, D. K. Wu, and E. D. Green, Expression pattern of the mouse ortholog of the Pendred's syndrome gene (Pds) suggests a key role for pendrin in the inner ear, *Proc Natl Acad Sci U A* **96**(17) (1999), 9727–32.

[43] I. E. Royaux, I. A. Belyantseva, T. Wu, B. Kachar, L. A. Everett, D. C. Marcus, *et al.*, Localization and functional studies of pendrin in the mouse inner ear provide insight about the etiology of deafness in pendred syndrome, *J Assoc Res Otolaryngol* **4**(3) (2003), 394–404.

[44] S. V. Jabba, A. Oelke, R. Singh, R. J. Maganti, S. Fleming, S. M. Wall, *et al.*, Macrophage invasion contributes to degeneration of stria vascularis in Pendred syndrome mouse model, *BMC Med* **4** (2006), 37.

[45] H. M. Kim and P. Wangemann, Failure of fluid absorption in the endolymphatic sac initiates cochlear enlargement that leads to deafness in mice lacking pendrin expression, *PLoS One* **5**(11) (2010), e14041.

[46] H. M. Kim and P. Wangemann, Epithelial cell stretching and luminal acidification lead to a retarded development of stria vascularis and deafness in mice lacking pendrin, *PLoS One* **6**(3) (2011), e17949.

[47] X. Li, J. D. Sanneman, D. G. Harbidge, F. Zhou, T. Ito, R. Nelson, *et al.*, SLC26A4 targeted to the endolymphatic sac rescues hearing and balance in Slc26a4 mutant mice, *PLoS Genet* **9**(7) (2013), e1003641.

[48] R. Singh and P. Wangemann, Free radical stress-mediated loss of Kcnj10 protein expression in stria vascularis contributes to deafness in Pendred syndrome mouse model, *Am J Physiol Ren. Physiol* **294**(1) (2008), F139-48.

[49] Y. C. Lu, C. C. Wu, W. S. Shen, T. H. Yang, T. H. Yeh, P. J. Chen, *et al.*, Establishment of a knock-in mouse model with the SLC26A4 c.919-2A>G mutation and characterization of its pathology, *PLoS One* **6**(7) (2011), e22150.

[50] A. A. Dror, Y. Politi, H. Shahin, D. R. Lenz, S. Dossena, C. Nofziger, *et al.*, Calcium oxalate stone formation in the inner ear as a result of an Slc26a4 mutation, *J Biol Chem* **285**(28) (2010), 21724–35.

[51] A. A. Dror and K. B. Avraham, The Slc26a4 loop Mouse Model for Pendred's Syndrome and Nonsyndromic Deafness, in *The Role of Pendrin in Health and Disease*, Springer, 2017, 23–36.

[52] B. Y. Choi, H. M. Kim, T. Ito, K. Y. Lee, X. Li, K. Monahan, *et al.*, Mouse model of enlarged vestibular aqueducts defines temporal requirement of Slc26a4 expression for hearing acquisition, *J Clin Invest* **121**(11) (2011), 4516–25.

[53] T. Ito, X. Li, K. Kurima, B. Y. Choi, P. Wangemann, and A. J. Griffith, Slc26a4-insufficiency causes fluctuating hearing loss and stria vascularis dysfunction, *Neurobiol Dis* **66** (2014), 53–65.

[54] A. Nishio, T. Ito, H. Cheng, T. S. Fitzgerald, P. Wangemann, and A. J. Griffith, Slc26a4 expression prevents fluctuation of hearing in a mouse model of large vestibular aqueduct syndrome, *Neuroscience* **329** (2016), 74–82.

[55] T. Ito, A. Nishio, P. Wangemann, and A. J. Griffith, Progressive irreversible hearing loss is caused by stria vascularis degeneration in an Slc26a4-insufficient mouse model of large vestibular aqueduct syndrome, *Neuroscience* **310** (2015), 188–97.

[56] M.-A. Kim, S. H. Kim, N. Ryu, J.-H. Ma, Y.-R. Kim, J. Jung, *et al.*, Gene therapy for hereditary hearing loss by SLC26A4 mutations in mice reveals distinct functional roles of pendrin in normal hearing, *Theranostics* **9**(24) (2019), 7184.

[57] H. J. Choi, H. J. Lee, J. Y. Choi, I. H. Jeon, B. Noh, S. Devkota, *et al.*, DNAJC14 ameliorates inner ear degeneration in the DFNB4 mouse model, *Mol. Ther.-Methods Clin. Dev.* **17** (2020), 188–197.

5.2.5. Conclusion

La maladie de Menière et le syndrome de Pendred sont deux dysfonctions vestibulaires différentes liées à un hydrops endolymphatique, l'une apparaissant chez l'adulte et l'autre congénitale. Dans les deux cas, une surdité fluctuante avec des crises vestibulaires est rapportée, évoluant vers une aggravation progressive de la fonction cochléo-vestibulaire.

Le syndrome Menière est très bien décrit dans la littérature, avec de nombreuses études évaluant la fonction vestibulaire ainsi que la morphologie du secteur endolymphatique. Le mécanisme de l'hydrops est cependant encore mal compris et son origine probablement plurifactorielle. Le syndrome de Pendred est beaucoup plus rare, et la littérature à son sujet comparativement très pauvre. Le retentissement fonctionnel vestibulaire et la morphologie vestibulaire endolymphatique est notamment méconnu. L'intérêt du modèle murin est clair dans ce type de pathologie monogénique, puisqu'il permet d'envisager des hypothèses physiopathologiques sur la formation de l'hydrops dans le syndrome de Pendred qui sont impossible à tester chez l'Homme.

6. Objectifs de la thèse

La dimension vestibulaire des pathologies cochléo-vestibulaire est mal comprise, surtout chez l'enfant où l'interrogatoire, l'examen clinique et paraclinique peuvent être difficiles. Le modèle murin, comme nous l'avons vu, peut permettre de progresser dans la compréhension des pathologies, notamment congénitales, et le développement de nouvelles thérapeutiques. Cette thèse est translationnelle et à partir de la constatation de la difficulté de prise en charge des pathologies vestibulaires, sa finalité était de mieux comprendre la physiologie et physiopathologie vestibulaire pour pouvoir participer au développement de nouvelles stratégies diagnostiques et thérapeutiques.

Ce travail expérimental s'inscrit dans un projet plus large autour du vestibule de l'enfant, dont des études cliniques : validation en français de questionnaires diagnostics, développement de stratégies diagnostiques innovantes par IRM, études rétrospectives sur des cohortes de patients (mutations du gène *SLC26A4*, retentissement de l'implantation cochléaire, etc.).

Les deux objectifs de la thèse sont de :

(i) Valider sur le plan vestibulaire des modèles murins de pathologie cochléo-vestibulaire et d'explorer l'efficacité de thérapie génique

(ii) Mieux comprendre la physiologie vestibulaire et les mécanismes de compensation vestibulaire, à partir de modèles murins présentant des lésions vestibulaires spécifiques

Partie 2 : Matériel et méthodes

1. Animaux

La manipulation expérimentale des animaux a nécessité la validation d'une « formation destinée aux personnes concevant ou réalisant les procédures expérimentales chez le rongeur », délivrée par la Faculté de Pharmacie de l'Université de Paris Descartes le 19 Janvier 2017.

Les animaux expérimentaux étaient hébergés sur le site des Saints-Pères de l'Université de Paris. Les souris étaient hébergées à 4 par cage, sauf pendant des périodes post-opératoires qui conduisaient à un isolement de 24h. En dehors des procédures expérimentales, le bien-être des animaux était assuré par les animaliers. Les besoins vitaux et physiologiques étaient couverts et surveillés quotidiennement.

Pour chaque procédure expérimentale, un accord du comité éthique local et du ministère a été obtenu.

Compte tenu du système d'oculographie utilisé (nécessitant un contraste suffisant pour détecter la pupille à la lumière infra-rouge), nous n'avons pu travailler qu'avec des souris pigmentées. Les souris C57BL/6 étaient la lignée de souris de choix pour l'exploration vestibulaire.

2. Etude comportementale du syndrome vestibulaire chez la souris

Le syndrome vestibulaire chez la souris entraine des symptômes oculo-moteurs, posturo-locomoteurs, cognitifs (orientation spatiale) et végétatifs (salivation – les rongeurs ne peuvent vomir). Les études comportementales se concentrent sur l'observation des symptômes posturo-locomoteurs et cognitifs.

Suite à une lésion vestibulaire aigüe et brutale, la souris va présenter des symptômes intenses qui vont diminuer jusqu'à leur compensation complète quelques semaines après la lésion (Simon et al., 2020). Le signe le plus intense est le *tumbling*, lorsque la souris fait des tonneaux de façon répétée vers le côté ipsilatéral à la lésion. Il est également possible de constater une hypotonie de l'hémicorps ipsilatéral à la lésion, un torticolis ipsilatéral (OTR ipsilatéral), un *circling* (mouvements locomoteurs circulaires répétés), un *head bobbing* (instabilité de la tête) ainsi qu'une perte de la capacité à nager.

Chez des modèles murins de dysfonction vestibulaire congénitale, les symptômes sont moins importants. L'analyse de la nage reste un élément important pour distinguer un déficit sévère et modéré (noyade immédiate, différée, nage en *circling* et inclinaison de la tête). Une analyse du comportement de la souris suspendue par la queue et notamment le comportement à la chute est intéressant : une souris normale aura tendance à avoir un tronc en extension en cherchant un support et à tomber sur ses pattes. Une souris avec déficit vestibulaire est plutôt fléchie sur elle-même lors de la suspension et la réception à la chute est mauvaise (Cassel et al., 2018). D'autres tests peuvent être utilisés, comme une analyse par vidéo-tracking du nombre de *circling* réalisés pendant une durée de 120 secondes ou une analyse de l'équilibre en positionnement la souris sur une petite plateforme de 7 x 7cm en comptabilisant le nombre de chutes pendant 60 secondes (Emptoz et al., 2017).

Si ces tests comportementaux sont très faciles à mettre en place, ils ne sont pas spécifiques et sont difficilement quantifiable avec précision. Seule l'exploration vestibulaire par vidéo-oculographie permet d'avoir une analyse fine et spécifique du système vestibulaire de la souris.

3. Méthodes d'exploration vestibulaire chez la souris

3.1. Montage expérimental

3.1.1. Plateforme rotatoire

Une plateforme rotatoire est utilisée pour explorer la fonction vestibulaire de la souris, permettant d'incliner et tourner la souris selon différents axes avec un enregistrement des mouvements de la table. Les mouvements sont générés par un logiciel dédié qui régule les fréquences et vitesse de rotation de la table vestibulaire. Au cours de ce test, l'animal est placé tête fixe dans un tube en plexiglas, lequel est disposé au centre d'une table qui peut tourner dans différents plans de l'espace (***Figure 22***).

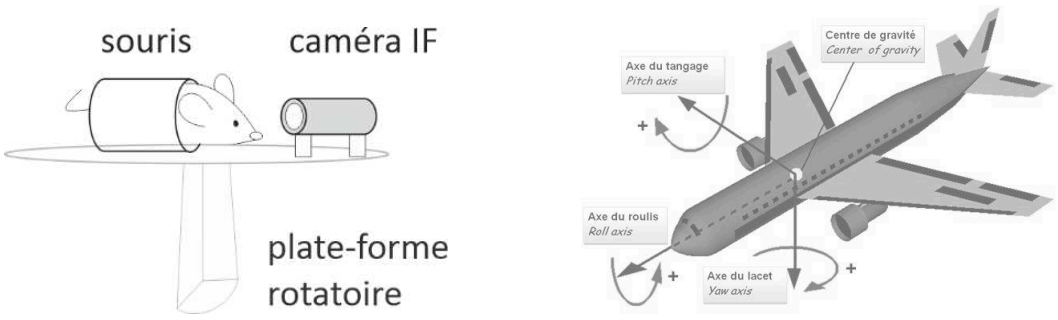

Figure 22 : Plateforme rotatoire

A gauche : La souris est installée dans un tube en plexiglass, tête-fixe, lui-même fixé à une plateforme rotatoire. L'ensemble du dispositif est placé dans le noir, et le mouvement pupillaire horizontal et vertical est enregistré par une caméra infra-rouge. A droite : La plateforme peut être manipulée dans les différents plans de l'espace, l'axe principal de rotation lors des stimulations étant celui du lacet.

La mesure des mouvements oculaires en réponse aux stimulations permet d'évaluer différents types de VOR et d'avoir une vision large de la fonction vestibulaire. Le mouvement oculaire est enregistré grâce à la vidéo-oculographie, une technique non invasive qui consiste à filmer les mouvements de la

pupille (Stahl et al., 2000). Cet enregistrement est réalisé dans le noir (sous un couvercle dans une pièce avec lumière éteinte, < 0,02 lux) avec une caméra infra-rouge (ETL-200, ISCAN, Burlington MA), en suivant la position de la pupille et du reflet cornéen (obtenu par un générateur infrarouge fixé à la caméra), permettant d'obtenir une nystagmographie. La tête de la souris est fixée avec un angle de 30° vers le bas pour aligner le plan des canaux semi-circulaires horizontaux avec celui du plan de rotation horizontal de la table (Beraneck and Cullen, 2007).

Il est nécessaire d'appliquer une goutte oculaire (0,05 mL de pilocarpine), environ cinq minutes avant la mesure pour entrainer un myosis d'une durée allant jusqu'à 40 minutes. La souris doit être la moins stressée possible pour maintenir les yeux ouverts et permettre l'enregistrement. En cas de stress important, la souris peut se débattre, et une sécrétion de larmes épaisses peut être constaté devant faire interrompre l'expérimentation.

La vidéonystagmographie est d'abord enregistrée sans stimulation dans le noir et à la lumière pour rapporter le sens et le nombre de nystagmus spontanés par minute. Puis différentes stimulations sont appliquées pour analyser les différents aspects fonctionnels du VOR (***Tableau 2***), détaillées ci-après.

Tableau 2: Différents réflexes vestibulaires analysés chez la souris

Stimulation	Réflexe analysé	Mesure	Fonction analysée	Equivalent chez l'Homme
Rotation sinusoïdale dans le plan horizontal	*αVOR*	Gain et phase	Canal semi-circulaire horizontal	*SHA* sur fauteuil rotatoire
Off-vertical axis rotation (OVAR)	$_{OVAR}$*MOR*	Biais	Intégrité du système otolithique, canalaire et central	*OVAR* sur fauteuil rotatoire
Inclinaison statique de la tête en roulis (*static roll head tilt*)	$_{tilt}$*MOR*	Gain (position verticale oculaire sur l'angle d'inclinaison de la tête)	Système otolithique surtout utricule	*vOCR*
Rotation impulsionnelle dans le plan horizontal (*hsteps*)	*velocity storage*	Constante de temps et gain	Intégrité du système canalaire et central	Rotation impulsionnelle sur fauteuil rotatoire

L'ensemble de ces tests se font à tête fixe et dans le noir

3.1.2. Calibration des mouvements enregistrés

Les positions de la tête et de l'œil sont enregistrées avec un filtre passe-bas à 250 Hz puis amplifiées à 1 kHz (CED power1401 MkII) en utilisant le logiciel Spike 2 puis exportées dans Matlab (Matlab, The MathWorks) pour l'analyse (Beraneck et al., 2012).

Les positions horizontales et verticales pupillaires (en pixels) sont calibrées en angle oculaire horizontaux et verticaux dans Matlab en utilisant une méthode trigonométrique (Beraneck and Cullen, 2007; Stahl, 2004). Cette conversion se base sur des calculs de mouvements théoriques de la pupille et du reflet cornéen lors de rotations de la caméra autour de l'œil de l'animal à des angles donnés.

3.1.3. Implantation de la casquette et technique opératoire

La casquette ou « headpost » est fondamentale pour pouvoir réaliser les examens à tête fixe et permettre l'enregistrement pupillaire. Il s'agit d'un petit fixateur collé sur le crâne de la souris et permettant d'immobiliser la tête de la souris dans un tube de plexiglas par des vis dans la casquette (***Figure 23***). L'implantation doit être réalisée au minimum 48h avant une exploration vestibulaire.

La procédure est la suivante (França de Barros et al., 2019): anesthésie à l'isoflurane et analgésie par buprénorphine pré-opératoire. Après vérification de l'absence de réflexe podal, une incision médiane entre les oreilles et descendant entre les yeux est réalisée pour exposer le crâne. La casquette est cimentée (C&B Metabond) à l'os du crâne juste en avant la fontanelle lambda. Une résine protectrice est déposée sur le ciment puis la peau rabattue autour de la casquette et suturée au fil résorbable.

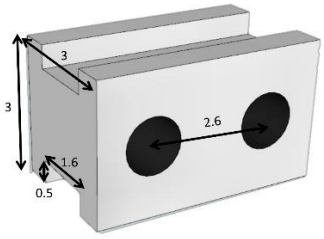

Figure 23 : Casquette

Schéma et mensurations (en mm) de la casquette. Pour l'exploration, les deux trous sont placés dans un plan frontal, permettant de fixer la tête de la souris le temps des examens vestibulaires, en vissant la casquette au montage avec le tube de plexiglas. Une vidéo de l'implantation disponible en ligne (França de Barros et al., 2019).

3.2. Méthode d'exploration des VOR chez la souris

3.2.1. Rotation sinusoïdale dans le plan horizontal

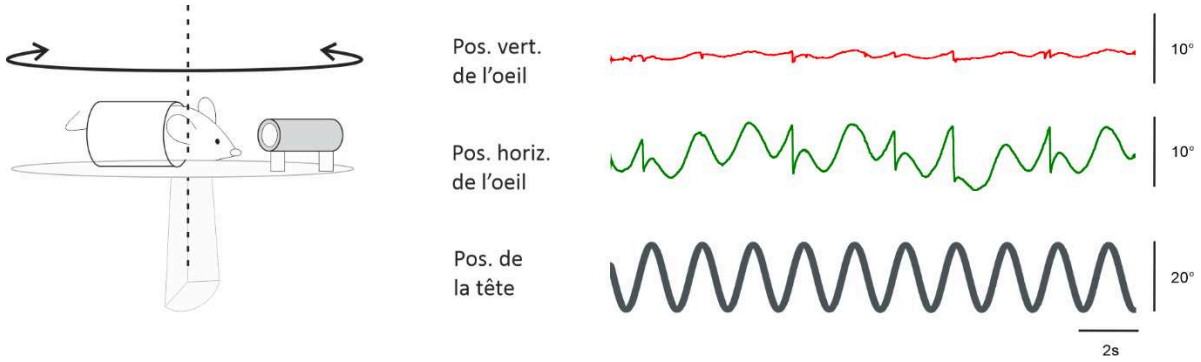

Figure 24 : Rotation sinusoïdale horizontale

A gauche : Schéma de rotation sinusoïdale de la souris, sur la plateforme de rotation. Dans ce travail, la vitesse maximale de rotation est fixée à 30°/s et de fréquence variable. A droite : tracés bruts analysés. En bas la position de la tête (qui correspond à la position de la table la souris étant tête fixe), et en haut la position horizontale et verticale de l'œil (position de la pupille par rapport au reflet cornéen fixe). La courbe de la position horizontale de l'œil est comparée à la position de la tête pour calculer le gain et la phase de l'aVOR.

Ce test évalue la fonction canalaire horizontale en rapportant le gain et la phase des mouvements oculaires par rapports aux mouvements de la tête (***Figure 24***). Le gain correspond au rapport entre le mouvement de l'œil et de la tête. La phase représente le décalage temporel entre la position de l'œil et celle de la tête et mesurée en décalage de cycle de phase (360° correspondant à un cycle complet). Normalement l'œil doit à n'importe quel moment donné être à l'opposé de la position de la tête, ainsi idéalement avec un gain égal à 1 et la phase à 0.

La méthodologie pour obtenir ces valeurs est bien décrite depuis plusieurs années chez la souris (Beraneck et al., 2012; Iwashita et al., 2001; Sakatani and Isa, 2004; Stahl et al., 2000). L'enregistrement est réalisé pendant au moins dix cycles, à plusieurs fréquences (0,2 ; 0,5 ; 0,8 ; 1 ; 1,5 ou 2 Hz), puis les phases lentes sont analysées (exclusion des phases rapides). Le gain et la phase sont calculées à partir d'une méthode des moindres carrés selon la formule suivante :

$$EH_v(t) = g \cdot \{[HH_v \cdot (t - t_d)] + C^{te}\}$$

Dans cette formule, $EH_v(t)$ correspond à la vitesse horizontale de l'œil, g est le gain, $HH_v(t)$ la vitesse horizontale de la tête, *td* le temps de latence dynamique (en millisecondes) du mouvement oculaire par rapport au mouvement de la tête et C^{te} une constante. La valeur *td* est utilisée pour calculer la phase (en degrés) de la vitesse de l'œil par rapport à la vitesse de la tête.

La variance (VAF – Variance-Accounted-For) permet d'évaluer la fiabilité des mesures, avec la formule suivante :

$$VAF = \left\{1 - \left[\frac{var\ (est) - EH_v}{var\ (EH_v)}\right]\right\}$$

La *var* correspond à la variance, *est* à la vitesse oculaire modélisée et EH_v la vitesse oculaire horizontale réelle. Les valeurs sont typiquement comprises entre 0,7 et 1 (1 correspondant à une modélisation parfaite). Les enregistrements avec une VAF < 0,5 sont exclus des analyses.

3.2.2. Off-axis vertical rotation (OVAR)

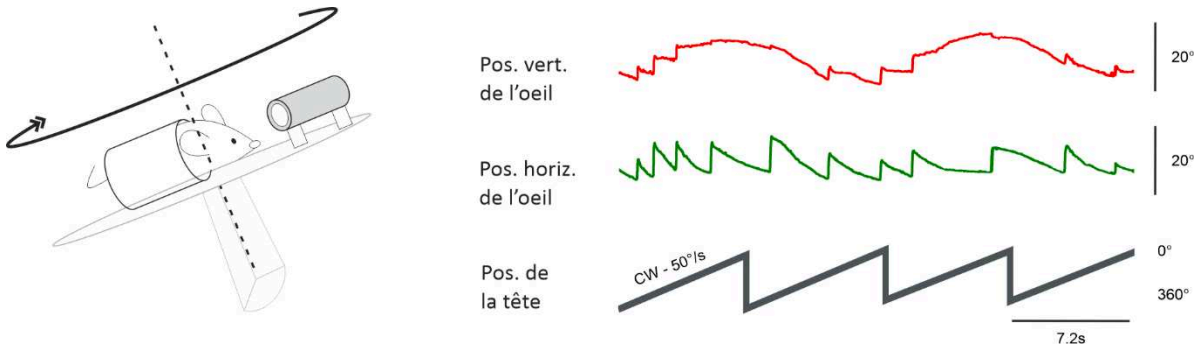

Figure 25 : OVAR

A gauche : Schéma de rotation continue de la souris autour d'un axe décalé par rapport à la verticale, sur la plateforme de rotation. Dans ce travail, la vitesse maximale de rotation est fixée à 50°/s, dans un sens puis dans l'autre. A droite : tracés bruts analysés. Dans cet exemple il s'agit d'une rotation horaire (CW). En bas la position de la tête (qui correspond à la position de la table la souris étant tête fixe), et en haut la position horizontale et verticale de l'œil (position de la pupille par rapport au reflet cornéen fixe). La courbe de la position horizontale de l'œil est comparée à la position de la tête pour calculer le biais du OVARMOR.

Ce test permet de calculer l'$_{OVAR}$MOR et donc d'évaluer la fonction otolithique mais aussi l'intégrité du système vestibulaire canalaire, otolithique et central (lien avec le stockage de vitesse). Il a été décrit chez différentes espèces, en particulier chez le rat (Hess and Dieringer, 1990), puis plus récemment chez la souris, les réponses des deux espèces étant comme attendu assez similaires (Beraneck et al., 2012). Une rotation à vitesse constante de 50°/s autour de l'axe en lacet incliné sur le côté à 17° est réalisée pendant au moins 10 cycles de 360°. L'inclinaison à 17° garantit lors de la stimulation une inclinaison maximale de la souris entre 13° et 47° en tangage et une inclinaison en roulis de ± 17° (Beraneck et al., 2012).

Suite à la stimulation, le VOR entraine un mouvement pupillaire dans l'axe horizontal et vertical (***Figure 25***), seule la composante horizontale est analysée. La vitesse des phases lentes est modulée (modulation, µ) autour d'un bias constant (β). Ces deux paramètres sont calculés à partir d'un modèle sinusoïdal des moindres carrés selon la formule suivante :

$$SP(t) = \beta + \mu \cdot \sin\left[2\pi \cdot f_0 \cdot (t + t_d)\right]$$

SP(t) est la vitesse de la phase lente, β le biais de la vitesse lente, μ la modulation de la vitesse lente et f_0 la fréquence de la rotation de la table.

3.2.3. Rotation impulsionnelle dans le plan horizontal (hsteps)

Ce test permet d'évaluer l'accumulateur de vitesse et la fonction canalaire horizontale et a été perfectionné. Lors d'une accélération brutale sous forme d'impulsion (step), suivie d'une rotation à vitesse constante, la vitesse de la phase lente du nystagmus atteint un maximum précoce, puis décroit de façon exponentielle (***Figure 26***). La constante de temps *tau* correspond au temps au bout duquel la vitesse des phases lentes décroit d'environ 2/3 de la valeur maximale (***Figure 27***).

Ces mesures sont effectuées après stimulation par une rotation à 50°/s dans le plan horizontal (trois cycles de 360°) à départ et arrêt brutal (horizontal steps). La décroissance de la vitesse des phases lentes de nystagmus est modélisée par une courbe exponentielle $f(x) = a \cdot exp^{bx}$ et la constante de

temps τ était calculée suivant la formule $\tau = \frac{-1}{b}$. Un gain de VOR horizontal peut également être calculé correspondant au ratio :

$$gain = \frac{vitesse\ oculaire\ maximale\ phase\ lente}{vitesse\ de\ rotation\ de\ la\ table}$$

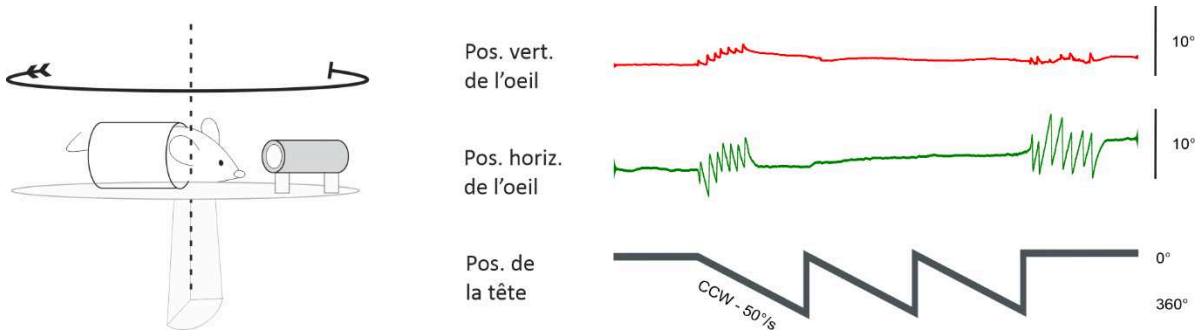

Figure 26 : rotations impulsionnelles horizontales

A gauche : Schéma de rotation impulsionnelle dans un plan horizontal de la souris autour d'un axe de lacet. La vitesse maximale de rotation est fixée à 50°/s, dans un sens puis dans l'autre, avec des impulsions de 3 cycles de 360°. A droite : tracés bruts analysés. Dans cet exemple il s'agit d'une rotation anti-horaire (CWW). En bas la position de la tête, et en haut la position horizontale et verticale de l'œil (position de la pupille par rapport au reflet cornéen fixe). La pente des phases lentes des nystagmus per-rotatoires et post-rotatoires sur la courbe de la position horizontale de l'œil est analysée en fonction de la vitesse de rotation pour calculer un gain et la constante de temps τ (voir figure27).

Les valeurs de gain et de constante de temps sont calculées au début (nystagmus per-rotatoire) et à l'arrêt (nystagmus post-rotatoire) des deux cycles de rotation en sens horaire (CW) et sens anti-horaire (CCW), obtenant quatre valeurs. La moyenne des valeurs CCW-per-rotatoire et CW-post-rotatoire ainsi que CCW-post-rotatoire et CW-per-rotatoire peuvent être calculées pour évaluer les fonctions vestibulaires gauches ou droites, respectivement. Pour évaluer la fonction globale de *velocity storage*, la moyenne des quatre valeurs est calculée. Une prépondérance directionnelle peut être recherchée à partir de la comparaison des gains lors des rotations droites et gauches.

$$\text{Prépondérance directionnelle} = \frac{gain\ \text{gauche} - gain\ \text{droit}}{gain\ \text{gauche} + gain\ \text{droit}}$$

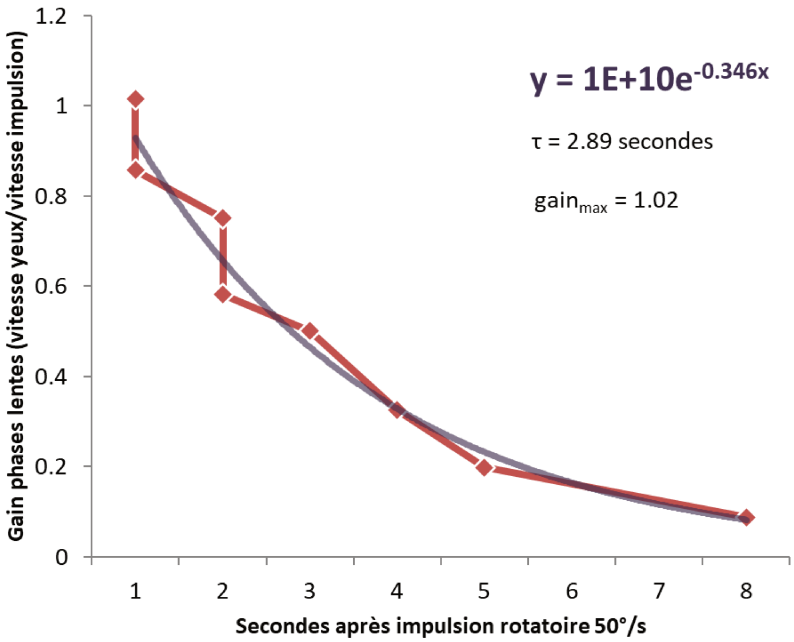

Figure 27 : Exemple de calcul de la constante de temps chez une souris normale

La courbe représente la phase lente des différents nystagmus post-impulsion (ici 8 nystagmus), le gain est calculé en faisant le rapport entre la vitesse de la phase lente sur la vitesse de l'impulsion rotationnelle de la table (qui est constante à 50°/s dans notre cas). La décroissance de la vitesse suit une courbe exponentielle dont la formule est représentée en haut à droite, avec le gain maximal et la constante de temps tau.

3.2.4. *Inclinaison statique de la tête en roulis*

Ce test permet d'évaluer la fonction otolithique mais surtout la fonction utriculaire et la réponse tonique associée. Comme chez l'Homme, la cyclotorsion de l'œil peut également être mesurée mais chez la souris la composante verticale ($_{tilt}$MOR statique) est bien supérieure dans cet axe d'inclinaison.

L'inclinaison statique en roulis a été étudiée avec des inclinaisons allant de -180° à 180° (Migliaccio et al., 2011; Oommen and Stahl, 2008) qui ont montré un rapport sinusoïdal entre l'angle d'inclinaison de la tête et la position angulaire verticale de l'œil. Ces deux études ont cependant montré que le gain était maximal et suivait une droite sur la portion -40° à 40°. Ainsi, à ces angles d'inclinaison, le gain correspond à la pente *m* de la courbe (position pupillaire/inclinaison de la tête) selon la formule $y = m\,x + b$. Au-delà de ces angles, le gain du $_{tilt}$MOR statique diminuait plus l'angle d'inclinaison augmentait, dû au fait que ces angles correspondent à des positions peu naturelles de la tête.

La manipulation se déroule comme suit : la souris est d'abord maintenue dans le plan horizontal, avec mesure de la position verticale pupillaire à 0° qui sert de référence pour la suite. La souris est ensuite lentement inclinée à droite puis à gauche de 10°, 20°, 30°, 40° et parfois 50° (***Figure 28***). La souris est maintenue dans chaque position le temps de la stabilisation de la position verticale de la pupille (environ 15 secondes), seul l'œil gauche est enregistré. L'angle vertical pupillaire est calculé pour chaque angle d'inclinaison de la tête, les valeurs normalisées en fonction de la position de départ à 0° et la courbe correspondante tracée. La pente est calculée pour l'inclinaison à gauche (40° à 0°), à droite (-40° à 0°) et l'examen complet (40° à -40°) pour obtenir les gains $_{tilt}$MOR ipsilatéraux, contralatéraux et moyens, respectivement.

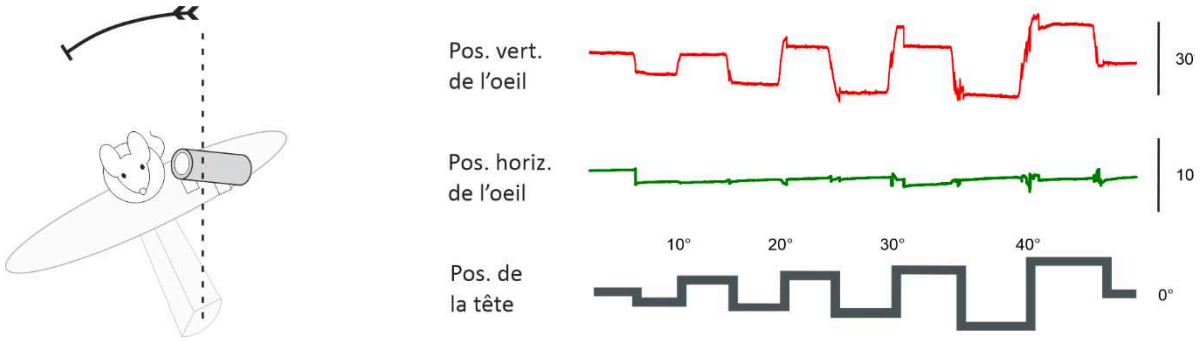

Figure 28 : Inclinaison de la tête en roulis

A gauche : Schéma d'inclinaison en roulis de la souris, sur la plateforme de rotation. La table peut être basculée jusqu'à 50° sur le côté. A droite : tracés bruts analysés. En bas la position de la tête (qui correspond à la position de la table la souris étant tête fixe), avec des inclinaisons statiques à différents degrés croissants en maintenant la position fixe de la souris pendant au moins 15 secondes. En haut, la position horizontale et verticale de l'œil (position de la pupille par rapport au reflet cornéen fixe). Le mouvement pupillaire horizontal est très faible, mais il est possible de distinguer des plateaux de position verticale pupillaire en fonction de la position de la tête.

Les inclinaisons dynamiques de la tête en roulis peuvent également être réalisées mais leur interprétation est complexe : en effet le mouvement oculaire vertical mesuré dépend en partie d'une stimulation des canaux semi-circulaires verticaux antérieurs et postérieurs. Concernant l'utricule, alors que la stimulation statique sollicite la composante tonique persistante, la stimulation dynamique

dépend également de la composante phasique. Pour ce test dynamique, une inclinaison sinusoïdale en roulis de part et d'autre du plan horizontal est réalisée, à une fréquence donnée (par exemple 0,5Hz), et à une inclinaison maximale de la tête donnée (de -20° à 20° par exemple). L'amplitude maximale de la sinusoïde du mouvement angulaire vertical pupillaire est ensuite calculé pour des inclinaisons latérales de 10°, 20° et 30°. Le gain (*dynamic $_{tilt}$VOR gain*) augmente lorsque l'inclinaison augmente, selon la formule suivante :

$$\text{dynamic }_{\text{tilt}}\text{VOR gain} = \frac{amplitude\ de\ la\ position\ verticale\ oculaire}{amplitude\ de\ l'inclinaison\ de\ la\ tête}$$

3.2.5. Stimulation visuelle sinusoïdale

La mesure du réflexe opto-cinétique, fonctionnellement complémentaire du VOR, est réalisée afin d'éliminer une possible dysfonction rétinienne qui pourrait entraîner des déficits vestibulaires secondaires (défaut de calibration du VOR). Aucun mouvement n'est imposé à la plateforme et les souris sont exposées à une stimulation visuelle rotatoire sinusoïdale à différentes fréquences (***Figure 29***) entrainant un mouvement sinusoïdal oculaire dont le gain diminue avec l'augmentation de la fréquence (Kretschmer et al., 2017).

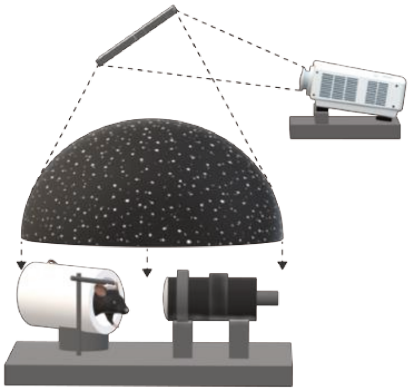

Figure 29 : Stimulation visuelle sinusoïdale

La souris est dans le noir et exposée à un stimulation visuelle rotatoire par points lumineux. La caméra infra-rouge recueille les mouvements de l'œil en réponse à la stimulation (D'après Barros et al. 2020).

4. Prélèvement des organes vestibulaires

Après exploration fonctionnelle, les organes vestibulaires peuvent être prélevés pour analyse et corrélation entre la morphologie et la fonction vestibulaire (Parker et al., 2016). L'analyse morphologique peut être réalisée à l'aide d'un microscope confocal ou électronique, et est réalisé par d'autres équipes dans le cadre de collaborations.

Une fixation corps-entier et labyrinthique est réalisée pour prélever le rocher, partie de l'os temporal comprenant les organes vestibulaires. Une perfusion intra-cardiaque d'un agent fixateur permet de préserver le contenu moléculaire et la morphologie des tissus. La procédure consiste à remplacer le sang de l'animal par un tampon phosphate salin puis d'échanger ce tampon par une solution de fixation. Après anesthésie profonde par un mélange xylazine (10mg/kg) - kétamine (85mg/kg), une incision est réalisée au niveau du sternum. Le thorax est ouvert, la cage thoracique et le diaphragme incisés afin d'exposer le cœur. Une incision est réalisée au niveau du ventricule gauche pour y insérer l'aiguille de la pompe péristaltique. L'aiguille est clampée, puis une perfusion de solution saline réalisée. Une incision de l'oreillette droite permet de favoriser le drainage. Une fois le sang éliminé, une perfusion de solution de fixation (PFA 4%) est réalisée. Ensuite une incision médiane du crâne permet d'identifier la face interne du rocher, avant de retirer délicatement tous les tissus adhérents à celui-ci. Une fois les deux rochers isolés, un trou infra-millimétrique est creusé dans la cochlée et le prélèvement déposé dans une solution de PFA 4% pendant 4h pour fixation complémentaire. Après de multiples lavages, le rocher fixé peut être conservé plusieurs mois.

Une autre stratégie est de prélever directement les organes vestibulaires en isolant le rocher sans fixation préalable. Le rocher est ensuite déposé dans une solution de PFA 4% et disséqué pour en extraire les canaux semi-circulaires et les otolithes. Les prélèvements sont fixés pendant une heure puis peuvent être stockés.

Partie 3 : Résultats

1. Modèles murins de mutations génétiques à retentissement cochléo-vestibulaire

La première partie des résultats expérimentaux traite de modèles murins de mutations génétiques. Ceux-ci peuvent être des modèles de maladies génétiques connues chez l'Homme (syndrome de Usher), ou de mutations de gènes ayant un rôle dans la fonction cochléo-vestibulaire. Dans les deux cas, l'objectif principal est de mieux comprendre le fonctionnement vestibulaire et, concernant les modèles de maladies génétiques, comparer le modèle murin à la présentation clinique chez l'Homme.

1.1. Article 1 : Rôles des protéines clarine-1 et clarine-2 dans la fonction cochléo-vestibulaire et évaluation de l'efficacité de la thérapie génique

1.1.1. Contexte scientifique

Chez l'Homme, la clarine-1 est une protéine dont le déficit est associé à la maladie de Usher de type III. Le syndrome de Usher est un groupe de maladies génétiques autosomiques récessives qui associe un déficit cochléo-vestibulaire progressif de gravité variable et une rétinite pigmentaire (perte de la vision nocturne et rétrécissement du champ visuel évoluant vers la cécité). Il existe trois types de syndrome de Usher classés par gravité et par âge de survenue, avec de nombreux gènes identifiés (Ahmed et al., 2003), présentés dans le ***Tableau 3***.

Tableau 3 : Différents syndromes de Usher

Type	Gènes fréquents	Audition	Equilibre	Vision
Type I	*MYO7A* (myosine VIIa) *USH1C* (harmonin) *CDH23* (cadhérine 23) *PCDH15* (protocadhérine 15) *USH1G* (sans)	Surdité sévère à profonde congénitale	Retard à la marche et troubles de l'équilibre	RP débutant dans l'enfance
Type II	*USH2A* (usherin)	Surdité moyenne à sévère congénitale avec aggravation progressive jusqu'à l'âge adulte	Aucuns troubles	RP débutant à l'adolescence
Type III	*CLRN1* (clarine-1)	Audition normale à la naissance et dégradation progressive à partir de l'adolescence	Atteinte variable	RP débutant à l'adolescence

Le gène *MYO7A* correspond à la maladie USH1B, *CDH23* à USH1D, *PCDH15* à USH1F et *CLRN1* à USH3A. RP : rétinite pigmentaire

L'équipe de Saaid SAFIEDDINE (Institut Pasteur, Unité Génétique et Physiologie de l'Audition, dirigée par le Pr Christine PETIT) a déjà travaillé en collaboration avec l'équipe de Mathieu BERANECK sur un modèle de souris de Usher type IG (Emptoz et al., 2017), en montrant une efficacité de l'injection trans-tympanique néonatale de thérapie génique (AAV) sur la fonction vestibulaire et une restauration partielle de l'audition. Un projet comparable est mené en collaboration avec l'équipe d'Aziz EL-

AMRAOUI (Institut Pasteur, Unité Génétique et Physiologie de l'Audition, dirigée par le Pr Christine PETIT) autour de dysfonction de la protéine clarine-1 et son interaction avec la clarine-2.

Des modèles murins *clrn1*$^{-/-}$ ont déjà pu être étudiés, montrant chez la souris une surdité progressive et une atteinte visuelle variable selon les modèles (Alagramam et al., 2016; Dinculescu et al., 2016; Geller et al., 2009; Geng et al., 2017; Tian et al., 2016). Des troubles d'équilibre progressifs ont été décrits mais aucune exploration vestibulaire quantifiée n'a été réalisée. Des tentatives de thérapies géniques périnatales ont déjà été efficaces pour la restauration de l'audition (Geng et al., 2017; György et al., 2019). La clarine-1 est une molécule transmembranaire présente dans les cellules ciliées, au niveau des stéréocils et des synapses à ruban (Dulon et al., 2018; Zallocchi et al., 2009). Son absence entraine chez la souris une dégénérescence progressive de la touffe ciliaire (malposition de la touffe ciliaire et régression du stéréocil) et une perte de la mécanotransduction (Dulon et al., 2018; Geller et al., 2009; Geng et al., 2017, 2012).

La clarine-2 est une protéine également impliquée dans l'intégrité de la touffe ciliaire dans l'oreille interne (Dunbar et al., 2019). Dans ce modèle murin *clrn2*$^{-/-}$, il a été noté une surdité progressive avec une perte de la transduction mécano-électrique et une perte du stéréocil, en revanche la clarine-2 ne semblait pas nécessaire au développement de la touffe ciliaire. Il n'a pas été retrouvé d'anomalie à l'électrorétinogramme, ni de trouble vestibulaire locomoteur. La fonction vestibulaire n'a pas été étudiée. Aucune étude n'a pour l'instant évalué les interactions des protéines clarine-1 et clarine-2 et le retentissement vestibulaire d'un déficit dans chacune de ces protéines n'a été évalué que par des observations des comportements locomoteurs et d'équilibration, non spécifiques de la fonction vestibulaire.

1.1.2. Buts de l'étude

Le premier objectif était de caractériser le rôle dans la fonction vestibulaire des protéines clarine-1 et clarine-2 ainsi que leur interaction à partir de modèle double-KO ou simple-KO murins. Ces

explorations ont été faites sur des modèles de souris clarine-1 et clarine-2 sans atteinte rétinienne (Dulon et al., 2018; Dunbar et al., 2019).

1.1.3. Résumé en français

La mutation du gène *clrn1* est responsable du syndrome cochléo-vestibulaire de Usher type III. Des modèles murins avec invalidation des gènes *clrn1*, *clrn2* ou des deux ont été développés par l'équipe de l'Institut Pasteur pour mieux comprendre le rôle de ces molécules et étudier l'efficacité d'une thérapie génique péri-natale Au total 51 souris ont été explorées à l'âge de 3 mois. Les souris double-KO *clrn1*$^{-/-}$*clrn2*$^{-/-}$ présentent un déficit complet des réflexes vestibulo-oculaires canalaire et otolithique, avec un déficit locomoteur/postural associé objectivable dès P10. Les autres souris simple KO mono ou hétérozygotes avaient toutes une dysfonction vestibulaire, sauf *clrn1*$^{+/+}$ *clrn2*$^{-/-}$. Au total la clarine-1 semble nécessaire au bon fonctionnement vestibulaire, avec une dysfonction canalaire ($p < 0,001$) et utriculaire ($p < 0,001$) en son absence malgré une expression biallélique du gène *clrn2*. En l'absence de clarine-2, une expression bi-allélique *clrn1* permet de garantir un fonctionnement normal vestibulaire (pas de différence significative avec la souris contrôle). L'expression monoallélique de *clrn1* ou de *clrn2* (avec knock-out complet de *clrn2* ou *clrn1* respectivement), permet de conserver une fonction vestibulaire altérée comparable entre ces deux cas. La redondance fonctionnelle entre ces deux protéines n'est donc que partielle.

1.1.4. Article original

Titre :

Functional evaluation of the vestibulo-ocular reflex of single and double *clarine-1* and *clarine-2* knock-out mice and restauration after gene therapy

Auteurs :

François SIMON, Françoise DENOYELLE, Mathieu BERANECK

En collaboration avec Pranav PATNI (doctorant) et l'équipe d'Aziz EL-AMRAOUI (Institut Pasteur, Unité Génétique et Physiologie de l'Audition, dirigée par le Pr Christine PETIT)

Etat d'avancement :

Deux articles en cours de préparation (sur la clarine-1 et son interaction avec la clarine-2 ; et sur la fonction vestibulaire de la clarine-2)

Introduction

In humans, Usher syndrome type 3 is an autosomal recessive genetic condition which induces progressive hearing loss with variable vestibular impairment and retinitis pigmentosa, usually starting after adolescence. It is the rarest form of Usher syndromes, especially prevalent in the Finnish population or people of Ashkenazi descent [1, 2]. It is linked to a mutation in the *CLRN1* gene, which normally codes CLARIN-1, a protein necessary for proper cochlear and vestibular hair cell function [3–5]. Another protein of the same family, CLARIN-2, has also been linked to progressive hearing loss [6].

The objective of this study was to assess the interaction between both clarin-1 and clarin-2 proteins in hair cells of the mouse inner ear. More specifically, the vestibular function of different mouse models expressing a combination of clarin-1 or clarin-2 was assessed using vestibulo-ocular reflex quantification to specify the role of both proteins, and their interaction, in the vestibular system.

Material and Methods

Animals were used in accordance with the European Communities Council Directive 2010/63/EU. All efforts were made to minimize suffering and reduce the number of animals included in the study. All procedures were approved by the ethical committee for animal research of the University of Paris (CEEA.34). Mice were provided by l'Institut Pasteur and had *clrn-1* and *clrn-2* mutations as previously described [3, 6]. The mice were crossed to obtain 5 different knock-out groups ($clrn1^{-/-}clrn2^{-/-}$, $clrn1^{-/-}clrn2^{+/-}$, $clrn1^{-/-}clrn2^{+/+}$, $clrn1^{+/-}clrn2^{-/-}$, $clrn1^{+/+}clrn2^{-/-}$) and compared to wild type (WT). None of the mice had retinal impairment. For increased clarity in tables and figures, $clrn1^{-/-}clrn2^{-/-}$ is represented in red, $clrn1^{-/-}clrn2^{+/+}$ in blue, $clrn1^{+/+}clrn2^{-/-}$ in gold and c$lrn1^{+/+}clrn2^{+/+}$ in green.

To perform pupil position recording with a fixed head, a head post was implanted at least 48h before vestibular exploration to the skull [7–9]. All eye movements recordings were made in the dark using an infrared video system (ETL-200, ISCAN, Burlington MA), recording pupil and corneal reflection (CR) position [7, 8, 10, 11]. Eye movements were recorded using non-invasive video-oculography [12]. The experimental set-up, apparatus and methods of data acquisition were similar to those described previously [8, 13, 14]. Briefly, mice were head-fixed at a ~30° nose-down position to

align the horizontal canals with the yaw plane [15]. Myosis was induced with topical 2% pilocarpine applied 10 minutes before experimentation. Recorded eye and head position signals were sampled at 1 kHz, digitally recorded (CED power1401 MkII) using Spike 2 software and later exported into the Matlab programming environment for off-line analysis (Matlab, The MathWorks). Videonystagmography recorded spontaneous eye movement without vestibular stimulation and eye movement with the three following stimulations: sinusoidal rotation for horizontal angular vestibulo-ocular reflex (aVOR); off-vertical axis rotation (OVAR) for maculo-ocular reflex ($_{OVAR}$MOR) and static head tilt for $_{tilt}$MOR [8, 16, 17].

Briefly, aVOR was tested during horizontal sinusoidal rotation of the turntable (at 0.2; 0.5; 0.8; 1 and 1.5Hz; peak velocity 30°/s), analysing gain and phase. The gain was the ratio between the amplitude of the eye (response) and head (stimulus) rotations. Since the animal was head-fixed to the rotating table, head movements and table movements were identical. The phase was the temporal shift between the eye and table rotations, expressed in degrees as ratio of the sinusoidal cycle (2 pi). Details for gain and phase calculation were reported in Carcaud et al. 2017 [13]. Values with VAF (Variance-accounted-for) under 0.5 were discarded [7]. During OVAR for $_{OVAR}$MOR, [18] axis of rotation was tilted from the vertical by 17°. Rotations were performed at constant speed (50°/s) for at least 10 rotations both in clockwise (CW) and counterclockwise (CCW) directions. During rotations, the velocity of horizontal slow phases is modulated around a constant bias. The bias is reported here as $_{OVAR}$MOR, which corresponds to an otolithic response, but also depends on an efficient central vestibular system [8, 18]. The $_{tilt}$MOR tests more specifically the static utricular function. Vertical pupil position according to the head tilt angle was measured first with the mouse maintained at a 0° horizontal position. The platform was then tilted into different roll positions, at 10°, 20°, 30° and 40° alternatively to the right and to the left. Measurements were made in a static position during at least 15 seconds to identify the stable pupil position. The vertical eye angle was then calculated from the raw vertical CR and pupil position [19]. The slope of a linear regression of both variables (vertical eye angle and head tilt degree) was calculated.

Mice were observed during swimming and were scored as following: 0 – normal swimming; 1 – swimming with head tilt; 2 – floating followed by drowning; 3 – immediate drowning.

Statistical analysis was made using XLstats (Addinsoft, New York, NY). All data are reported as mean and standard deviation. Two-way ANOVA was used to compare aVOR gain and phase (mouse type and frequency), one-way ANOVA for $_{OVAR}$MOR and $_{tilt}$MOR. Post-hoc comparisons were performed where appropriate using the Tukey HSD test. Ordinal logistic regression was performed for association between $_{tilt}$MOR slope and drowning score. Values of $p < 0.05$ were considered significant.

Results

A total of 51 mice were tested at 3 months of age, all groups are presented in ***Table 1***. Single-KO mice (*clrn1*$^{+/+}$*clrn2*$^{-/-}$ and *clrn1*$^{-/-}$*clrn2*$^{+/+}$) were also tested at 2 and 4 months of age.

Table 1: Different groups of mice tested

Type of mice	Number of mice	Age (weeks) when tested	Number of mice drowning
clrn1$^{-/-}$*clrn2*$^{-/-}$	8	13 ± 0	8 (100)
clrn1$^{-/-}$*clrn2*$^{+/-}$	7	14 ± 1	3 (43)
clrn1$^{-/-}$*clrn2*$^{+/+}$	8	14 ± 3	0 (0)
clrn1$^{+/-}$*clrn2*$^{-/-}$	8	14 ± 1	4 (44)
clrn1$^{+/+}$*clrn2*$^{-/-}$	9	14 ± 2	0 (0)
clrn1$^{+/+}$***clrn2***$^{+/+}$	10	15 ± 1	0 (0)

Age reported as mean ± standard deviation, drowning as number (percentage).

Videonystagmography recording spontaneous eye movements without any vestibular stimulation was normal for all mice except *clrn1*$^{-/-}$*clrn2*$^{-/-}$ which presented with an unstable eye position (flutter). An overview of the vestibular function of all 6 groups can be found in ***Figure 1***. Horizontal aVOR gain and phase are reported in ***Table 2***. Double-KO mice had near-zero gain and phase was therefore not measurable (VAF < 0.5). $_{tilt}$MOR and $_{OVAR}$MOR values are reported in ***Table 3***. A two-way ANOVA model ($F(29)=32.6$, $p<0.0001$) compared aVOR gain values and another ($F(24)=38.8$, $p<0.0001$) compared phase values, according to mouse group and frequency, p values are reported in ***Table 4***.

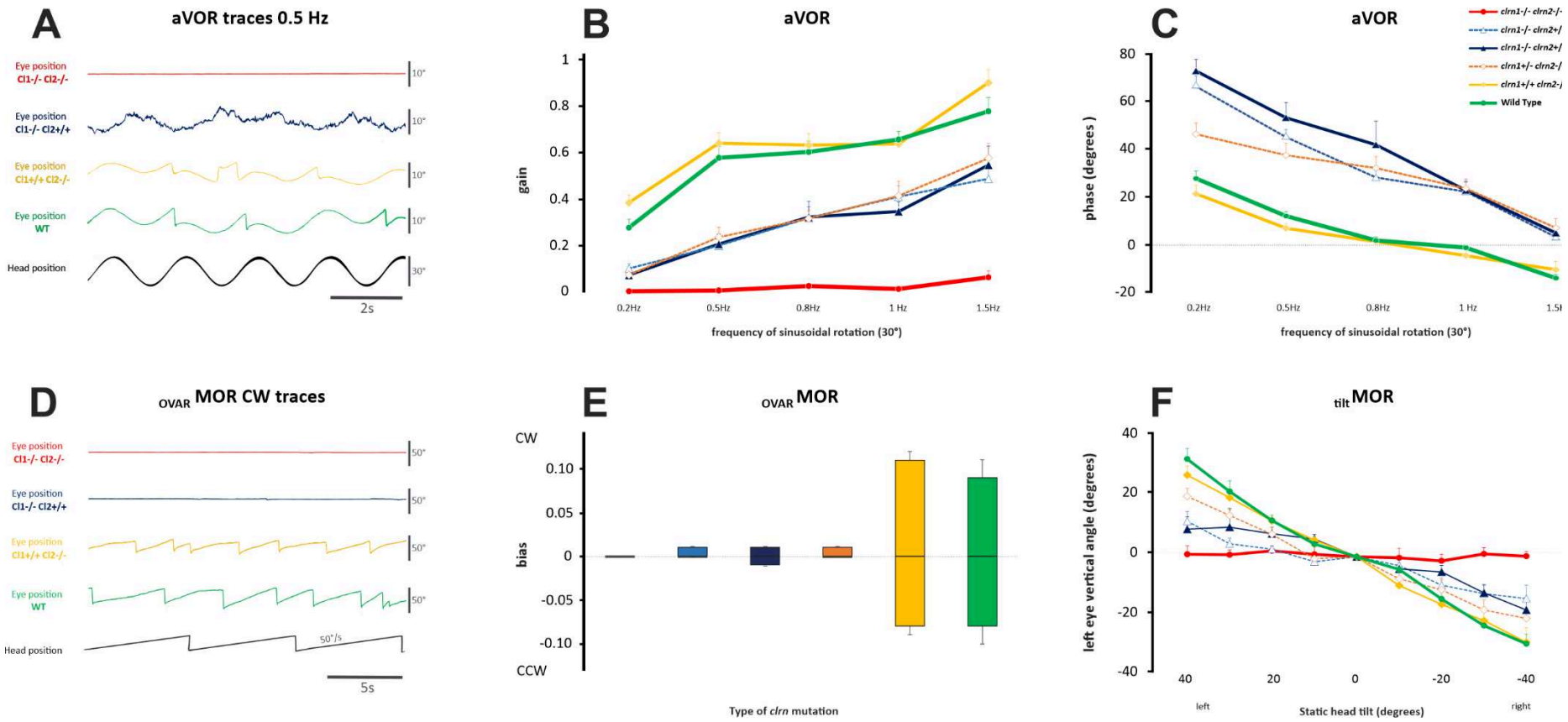

Figure 1: Overview of vestibule-ocular reflex of the six clarin groups

A. Traces of the sinusoidal rotation at 0.5Hz and 30°/s peak velocity. Wild type and *clrn1*$^{+/+}$*clrn2*$^{-/-}$ mice have normal traces with slow phases compensatory for head movements and normal fast phases that recenter the eye in orbit. *clrn1*$^{-/-}$*clrn2*$^{+/+}$ has no fast phase and slow phases which are not correlated to head movement. *clrn1*$^{-/-}$*clrn2*$^{-/-}$ had no compensatory eye movements during head movement. **B.** Horizontal aVOR gain during sinusoidal rotation stimulation. Gain of *clrn1*$^{-/-}$*clrn2*$^{-/-}$ mice was close to 0. **C.** Horizontal aVOR phase during sinusoidal rotation stimulation, no phase was measurable for *clrn1*$^{-/-}$*clrn2*$^{-/-}$ mice. **D.** Traces of the OVAR at 50°/s and 17° tilt. Wild type and *clrn1*$^{+/+}$*clrn2*$^{-/-}$ mice have normal traces with slow phases corresponding to MOR bias. *clrn1*$^{-/-}$*clrn2*$^{+/+}$ and *clrn1*$^{-/-}$*clrn2*$^{-/-}$ had no compensatory eye movement during head movement. **E.** CCW and CW MOR bias during OVAR. **F.** Vertical left eye angle during static head tilt ranging from 40° (left head tilt) to -40° (right head tilt). The static head tilt induces a MOR and especially requires utricular function. *CCW* counter-clockwise *CW* clockwise *MOR* maculo-ocular reflex *OVAR* off-vertical axis rotation *aVOR* angular vestibulo-ocular reflex *WT* Wild Type. Values shown correspond to mean and SEM. For eye position, up is right; head position is inverted for ease of reading

$_{tilt}$MOR slopes were compared using a one-way ANOVA model, ($F(5)=22.1$, $p<0.0001$) and $_{OVAR}$MOR bias using another ($F(5)=32.4$, $p<0.0001$) according to mouse group and *p* values are reported in ***Table 4***. Briefly, *clrn1*$^{+/+}$*clrn2*$^{-/-}$ and WT groups did not have any statistically significant difference in any aVOR, $_{tilt}$MOR or $_{OVAR}$MOR values. Also, *clrn1*$^{-/-}$*clrn2*$^{+/+}$, *clrn1*$^{-/-}$*clrn2*$^{+/-}$ and *clrn1*$^{+/-}$*clrn2*$^{-/-}$ groups did not have any statistically significant difference in any aVOR, $_{tilt}$MOR or $_{OVAR}$MOR values. The double-KO mice did not have any measurable vestibular reflex, concerning aVOR, $_{tilt}$MOR or $_{OVAR}$MOR values.

Table 2: Horizontal angular vestibulo-ocular reflex

Frequency	0.2Hz	0.5Hz	0.8Hz	1Hz	1.5Hz
aVOR gain					
clrn1$^{-/-}$*clrn2*$^{-/-}$	0.01±0.01	0.01±0.01	0.03±0.02	0.02±0.01	0.07±0.08
clrn1$^{-/-}$*clrn2*$^{+/-}$	0.10±0.05	0.20±0.10	0.32±0.13	0.41±0.12	0.49±0.16
clrn1$^{-/-}$*clrn2*$^{+/+}$	0.08±0.05	0.21±0.12	0.32±0.19	0.35±0.12	0.55±0.23
clrn1$^{+/-}$*clrn2*$^{-/-}$	0.08±0.04	0.24±0.12	0.32±0.10	0.42±0.19	0.58±0.19
clrn1$^{+/+}$*clrn2*$^{-/-}$	0.39±0.10	0.64±0.13	0.63±0.15	0.64±0.14	0.90±0.17
***clrn1*$^{+/+}$*clrn2*$^{+/+}$**	0.28±0.12	0.58±0.15	0.60±0.15	0.66±0.11	0.78±0.19
aVOR phase					
clrn1$^{-/-}$*clrn2*$^{-/-}$	-	-	-	-	-
clrn1$^{-/-}$*clrn2*$^{+/-}$	68.5±13.9	44.7±5.0	28.1±7.7	22.2±12.1	3.3±10.4
clrn1$^{-/-}$*clrn2*$^{+/+}$	72.5±13.6	49.0±12.4	41.7±27.8	22.7±9.7	5.0±5.4
clrn1$^{+/-}$*clrn2*$^{-/-}$	45.3±10.7	40.1±11.8	32.0±14.1	23.5±12.2	7.1±11.8
clrn1$^{+/+}$*clrn2*$^{-/-}$	21.3±10.8	7.0±5.6	1.4±6.3	-4.4±6.4	-10.3±10.7
***clrn1*$^{+/+}$*clrn2*$^{+/+}$**	27.7±9.6	12.1±5.8	1.9±4.8	-1.1±3.5	-13.8±4.8

All values are represented as mean ± SD (standard deviation). Phase was not measurable for *clrn1*$^{-/-}$*clrn2*$^{-/-}$ mice. *aVOR* angular Vestibular-ocular reflex.

Table 3: tilt- and OVAR- maculo-vestibular reflexes

MOR	$_{tilt}$MOR			$_{OVAR}$MOR		
	50° left	50° right	slope	CCW	CW	Overall
clrn1$^{-/-}$*clrn2*$^{-/-}$	-0.7±5.9	-4.1±8.1	0.02±0.03	0.00±0.00	0.00±0.01	0.01±0.00
clrn1$^{-/-}$*clrn2*$^{+/-}$	14.5±4.1	-16.0±13.0	0.28±0.11	0.00±0.01	0.01±0.01	0.01±0.00
clrn1$^{-/-}$*clrn2*$^{+/+}$	13.9±8.4	-16.8±8.1	0.31±0.14	-0.01±0.01	0.01±0.01	0.01±0.01
clrn1$^{+/-}$*clrn2*$^{-/-}$	23.9±7.7	-23.1±10.1	0.46±0.12	0.00±0.00	0.01±0.01	0.01±0.01
clrn1$^{+/+}$*clrn2*$^{-/-}$	29.1±11.6	-31.3±14.8	0.62±0.23	-0.08±0.04	0.11±0.04	0.09±0.03
***clrn1*$^{+/+}$*clrn2*$^{+/+}$**	28.1±9.6	-30.6±11.9	0.63±0.13	-0.08±0.05	0.09±0.05	0.08±0.01

All values are represented as mean ± SD (standard deviation). $_{tilt}$MOR is reported as the left eye vertical angle at 50° static head tilt to the left and to the right and slope value (vertical eye angle and head tilt degree). $_{OVAR}$MOR is reported with the bias value, during CCW and CW stimulations, and overall mean. *CCW* counter-clockwise *CW* clockwise *MOR* maculo-ocular reflex *OVAR* off-vertical axis rotation.

The proportion of mice drowning is reported in ***Table 1***. All mice *clrn1*$^{+/+}$*clrn2*$^{-/-}$ and WT groups swam normally and all mice in the *clrn1*$^{-/-}$*clrn2*$^{-/-}$ group drowned immediately (score 3/3). Mice in the remaining groups scored variously from normal swimming to immediate drowning, as detailed in ***Figure 2***. An ordinal logistic regression was calculated ($\chi 2$ (3) = 65.1, p>0.0001) between the drowning score and aVOR 0.5Hz gain, $_{tilt}$MOR slope and $_{OVAR}$MOR bias. $_{tilt}$MOR slope was the only statistically significant factor, OR=-12.5 [95CI -20.8;-4.1], p=0.003. Lower $_{tilt}$MOR slope values were significantly associated with poorer swimming capacities, as shown in ***Figure 2***, suggesting that both tests score utricular function

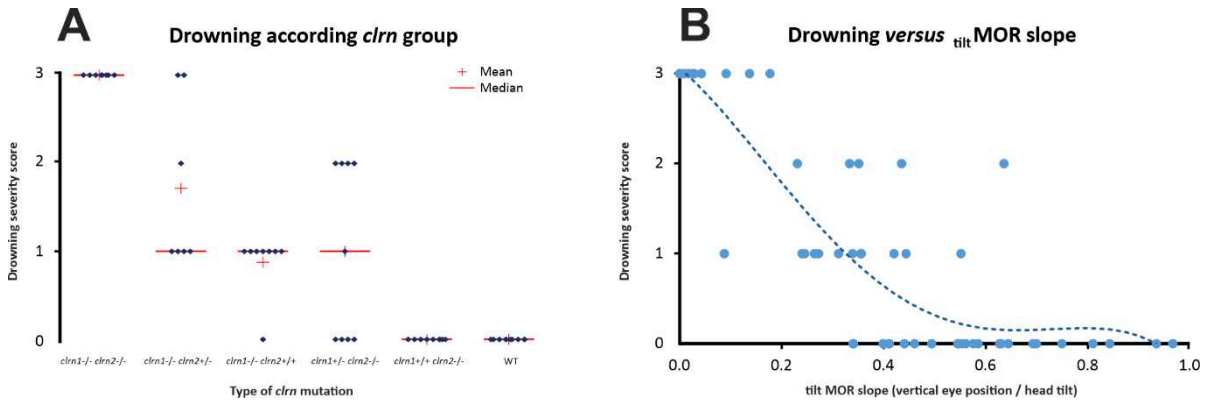

Figure 2: Severity of drowning according to mouse group and utricular function
A. Severity of drowning according to *clrn* mutations, from 0 (no drowning) to 3 (immediate drowning). **B.** Drowning severity according to utricular function (based on $_{tilt}$MOR slope values) polynomial trendline curve, across all genetic groups. All immediate drowning mice have a $_{tilt}$MOR slope below 0.3. *MOR* maculo-ocular reflex.

Vestibular function according to *clrn1* expression is detailed in ***Figure 3***. In brief, *clrn1*$^{-/-}$*clrn2*$^{+/+}$ mice have statistically significative hypofunction of horizontal aVOR and $_{tilt}$MOR compared to WT but near-to-zero $_{OVAR}$MOR. In a *clrn2* knockout background, *clrn1* biallelic expression maintains full vestibular function, and monoallelic expression enables aVOR hypofunction (statistically different from double-KO as well as WT) but near-to-zero $_{OVAR}$MOR bias. *clrn1*$^{+/-}$*clrn2*$^{-/-}$ $_{tilt}$MOR slope was statistically different from double-KO mice, but was not statistically different from WT or *clrn1*$^{+/+}$*clrn2*$^{-/-}$ groups.

Table 4: Statistical significance when comparing different clarin mice groups

Reflex tested	aVOR 0.2Hz		aVOR 0.5Hz		aVOR 0.8Hz		aVOR 1Hz		aVOR 1.5Hz		$_{tilt}$MOR	$_{OVAR}$MOR
Measurement	Gain	Phase	Gain	Phase	Gain	Phase	Gain	Phase	Gain	Phase	Slope	Bias
clrn1$^{+/+}$clrn2$^{+/+}$ *vs clrn1$^{-/-}$clrn2$^{+/-}$*	0.614	**< 0,0001**	**< 0,0001**	**< 0,0001**	**0.006**	**0.001**	**0.048**	**0.005**	**0.004**	0.196	**0.000**	**< 0,0001**
clrn1$^{+/+}$clrn2$^{+/+}$ *vs clrn1$^{-/-}$clrn2$^{+/+}$*	0.220	**< 0,0001**	**< 0,0001**	**< 0,0001**	**0.004**	**< 0,0001**	**0.000**	**0.002**	0.065	0.056	**0.000**	**< 0,0001**
clrn1$^{+/+}$clrn2$^{+/+}$ *vs clrn1$^{+/-}$clrn2$^{-/-}$*	0.173	0.081	**< 0,0001**	**< 0,0001**	**0.001**	**< 0,0001**	**0.023**	**0.000**	0.182	**0.008**	0.128	**< 0,0001**
clrn1$^{+/+}$clrn2$^{+/+}$ *vs clrn1$^{+/+}$clrn2$^{-/-}$*	0.995	1.000	1.000	1.000	1.000	1.000	1.000	1.000	0.968	1.000	1.000	0.752
clrn1$^{+/+}$clrn2$^{+/+}$ *vs clrn1$^{-/-}$clrn2$^{-/-}$*	**0.006**	**-**	**< 0,0001**	**-**	**< 0,0001**	-	**< 0,0001**	-	**< 0,0001**	-	**< 0,0001**	**< 0,0001**
clrn1$^{-/-}$clrn2$^{-/-}$ vs clrn1$^{-/-}$clrn2$^{+/-}$	1.000	-	0.511	-	**0.008**	-	**< 0,0001**	-	**< 0,0001**	-	**0.012**	1.000
clrn1$^{-/-}$clrn2$^{-/-}$ vs clrn1$^{-/-}$clrn2$^{+/+}$	1.000	-	0.364	-	**0.003**	-	**0.000**	-	**< 0,0001**	-	**0.003**	0.994
clrn1$^{-/-}$clrn2$^{-/-}$ vs clrn1$^{+/-}$clrn2$^{-/-}$	1.000	-	0.091	-	**0.003**	-	**< 0,0001**	-	**< 0,0001**	-	**< 0,0001**	1.000
clrn1$^{-/-}$clrn2$^{-/-}$ vs clrn1$^{+/+}$clrn2$^{-/-}$	**< 0,0001**	-	**< 0,0001**	-	**< 0,0001**	-	**< 0,0001**	-	**< 0,0001**	-	**< 0,0001**	**< 0,0001**
clrn1$^{-/-}$clrn2$^{+/+}$ vs clrn1$^{-/-}$clrn2$^{+/-}$	1.000	1.000	1.000	1.000	1.000	0.738	1.000	1.000	1.000	1.000	0.999	0.999
clrn1$^{-/-}$clrn2$^{+/+}$ vs clrn1$^{+/-}$clrn2$^{-/-}$	1.000	**0.000**	1.000	0.993	1.000	0.979	1.000	1.000	1.000	1.000	0.275	1.000
clrn1$^{-/-}$clrn2$^{+/+}$ vs clrn1$^{+/+}$clrn2$^{-/-}$	**0.001**	**< 0,0001**	**< 0,0001**	**< 0,0001**	**0.001**	**< 0,0001**	**0.003**	**0.000**	**< 0,0001**	0.375	**0.001**	**< 0,0001**
clrn1$^{+/+}$clrn2$^{-/-}$ vs clrn1$^{-/-}$clrn2$^{+/-}$	**0.009**	**< 0,0001**	**< 0,0001**	**< 0,0001**	**0.001**	**0.001**	0.146	**0.001**	**< 0,0001**	0.689	**0.000**	**< 0,0001**
clrn1$^{+/+}$clrn2$^{-/-}$ vs clrn1$^{+/-}$clrn2$^{-/-}$	**0.000**	**0.001**	**< 0,0001**	**< 0,0001**	**0.000**	**< 0,0001**	0.088	**< 0,0001**	**0.000**	0.114	0.211	**< 0,0001**
clrn1$^{-/-}$clrn2$^{+/-}$ vs clrn1$^{+/-}$clrn2$^{-/-}$	1.000	**0.008**	1.000	1.000	1.000	1.000	1.000	1.000	1.000	1.000	0.167	1.000

Statistically significant values are in bold. aVOR values were compared using a two-way ANOVA and post-hoc Tukey test, Gain model ($F(29)=32.6$, $p<0.0001$) and phase model ($F(24)=38.8$, $p<0.0001$). Phase was not measurable for *clrn1$^{-/-}$clrn2$^{-/-}$* mice. $_{tilt}$MOR and $_{OVAR}$MOR were each compared with a one-way ANOVA model, ($F(5)=22.1$, $p<0.0001$) and ($F(5)=32.4$, $p<0.0001$), respectively. *aVOR* angular vestibular-ocular reflex *MOR* maculo-ocular reflex *OVAR* off-vertical axis rotation.

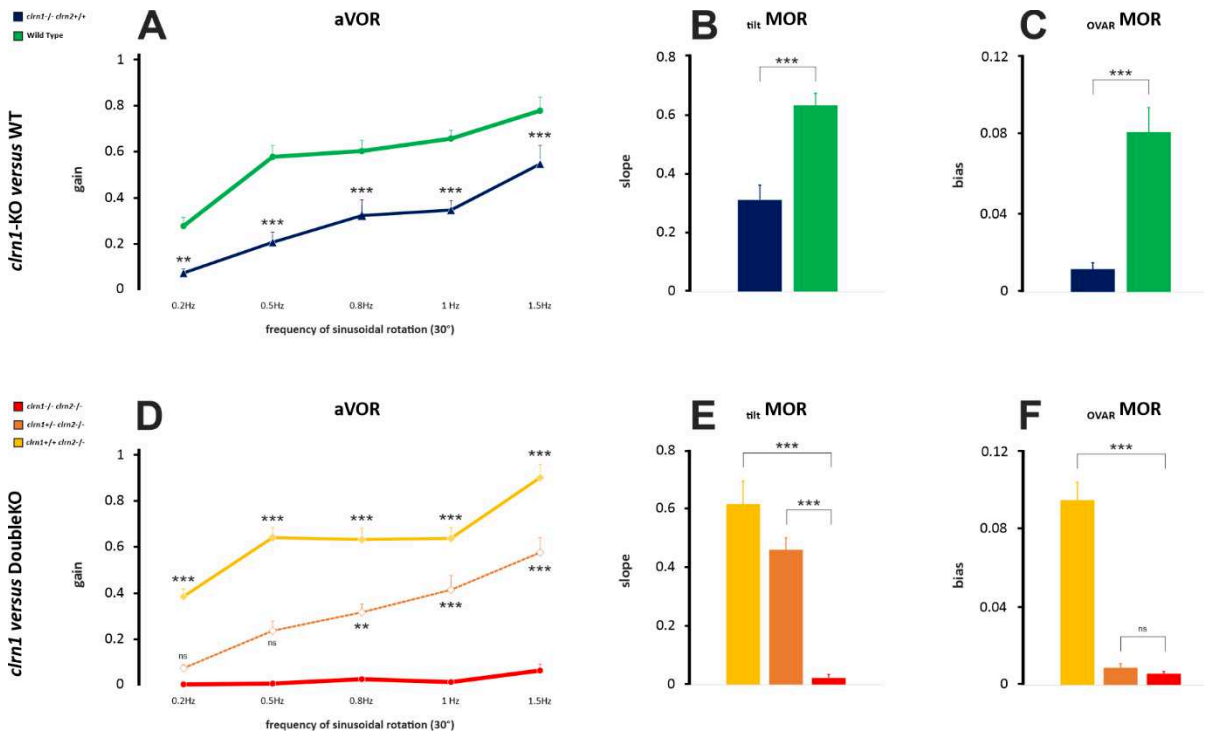

Figure 3: Mice vestibular functions according to *clrn1* expression
clrn1$^{-/-}$*clrn2*$^{+/+}$ *versus wild type:* **A.** Horizontal aVOR at different frequencies. **B.** $_{tilt}$MOR slope. **C.** $_{OVAR}$MOR bias (overall mean of clockwise and counter-clockwise measures). *clrn1*$^{+/+}$*clrn2*$^{-/-}$ *or clrn1*$^{+/-}$*clrn2*$^{-/-}$ *versus clrn1*$^{-/-}$*clrn2*$^{-/-}$*:* **D.** Horizontal aVOR at different frequencies. **E.** $_{tilt}$MOR slope. **F.** $_{OVAR}$MOR bias (mean of clockwise and counter-clockwise measures). Significance: ns >0.05; * < 0.05; ** < 0.01: *** < 0.001. MOR maculo-ocular reflex *OVAR* off-vertical axis rotation *aVOR* angular vestibulo-ocular reflex *WT* Wild Type.

Vestibular function according to clarin-2 expression is detailed in ***Figure 4***. In brief, in a *clrn1* knockout background, *clrn2* biallelic and monoallelic expression were statistically non-different, with near-to-zero $_{OVAR}$MOR bias and aVOR and $_{tilt}$MOR hypofunction (statistically different from double-KO as well as WT).

During single-KO mice (*clrn1*$^{+/+}$*clrn2*$^{-/-}$ and *clrn1*$^{-/-}$*clrn2*$^{+/+}$) follow-up at 2, 3 and 4 months, no time-related statistically significant trends were reported, regarding aVOR, $_{tilt}$MOR or $_{OVAR}$MOR. ANOVA models were applied and no significant difference was found between values at 2 months and 4 months of age.

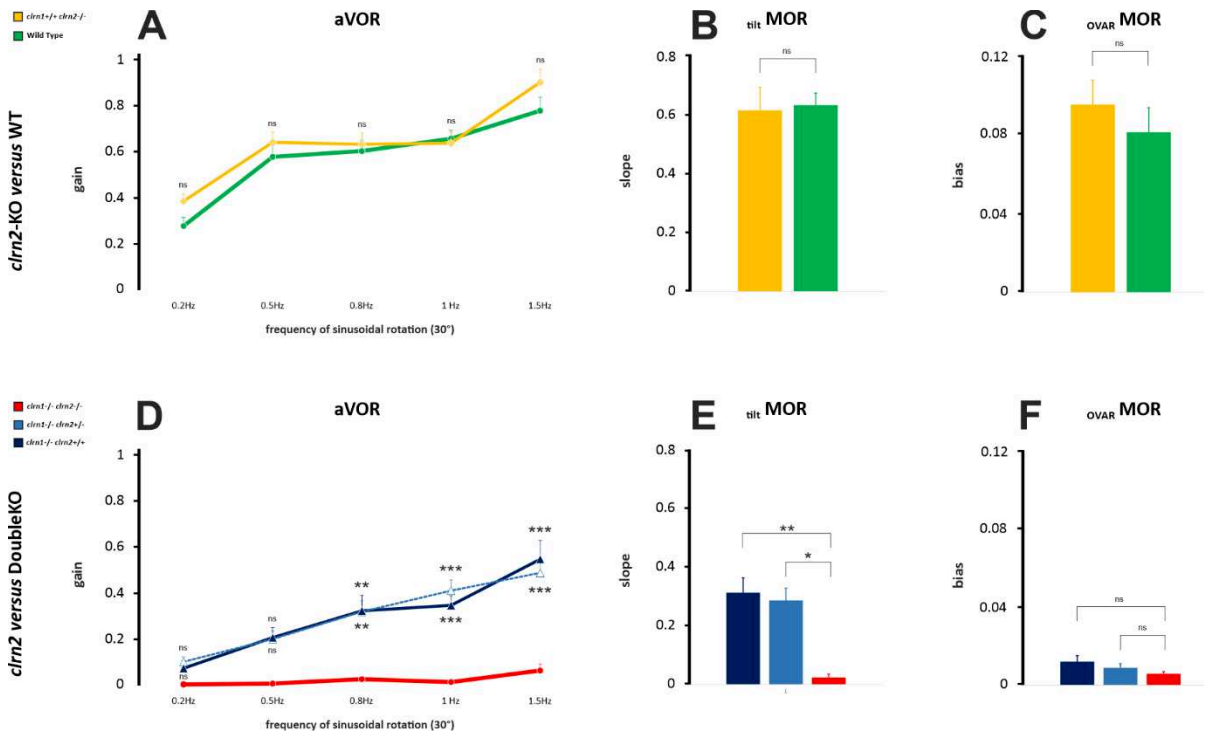

Figure 4: Mice vestibular functions according to *clrn2* expression
clrn1$^{+/+}$*clrn2*$^{-/-}$ *versus wild type:* **A.** Horizontal aVOR at different frequencies. **B.** $_{tilt}$MOR slope. **C.** $_{OVAR}$MOR bias (overall mean of clockwise and counter-clockwise measures). *clrn1*$^{-/-}$*clrn2*$^{+/+}$ *or clrn1*$^{-/-}$*clrn2*$^{+/-}$ *versus clrn1*$^{-/-}$*clrn2*$^{-/-}$*:* **D.** Horizontal aVOR at different frequencies. **E.** $_{tilt}$MOR slope. **F.** $_{OVAR}$MOR bias (mean of clockwise and counter-clockwise measures). Significance: ns >0.05; * < 0.05; ** < 0.01: *** < 0.001. *MOR* maculo-ocular reflex *OVAR* off-vertical axis rotation *aVOR* angular vestibulo-ocular reflex *WT* Wild Type.

Discussion

A summary of the vestibular function of each mouse group can be found in ***Table 5***. As the $_{OVAR}$MOR bias requires not only an efficient otolithic system, but also an overall satisfactory canalar and central vestibular system [20, 21], it is not surprising that all but WT and *clrn1*$^{+/+}$*clrn2*$^{-/-}$ groups were found to have near-to-zero bias values.

Clrn1$^{+/+}$*clrn2*$^{-/-}$ mice maintained normal vestibular function, which corresponds to previous observations of normal vestibular behavioural testing in P28 and P60 *clrn2*$^{-/-}$ mice [6]. A hypothesis would be that biallelic expression of *clrn1* may compensate *clrn2* deficit in these mice. Interestingly, when *clrn2* was deactivated, monoallelic expression of *clrn1* was sufficient to guarantee a near-normal utricular function, although canalar function was decreased and the overall integration of the vestibular system was not functional ($_{OVAR}$MOR bias close to zero). This may be due to the fact that in the utricle,

the clarin-1 protein may be compensated by another protein less present in the ampullae, or that the utricular sensory type II hair cells (stimulated during static head tilt) are less dependent on clarin-1 to function. This has to be moderated by the fact that although *clrn1*$^{+/-}$*clrn2*$^{-/-}$ mice's $_{tilt}$MOR was not statistically different from wild type, 44% of those mice did drown (all grade 2 after initial floating) which accounts for bilateral utricular malfunction in those cases.

Table 5: Summary of vestibular function according to genetic background

Type of mice	Semi-circular canals	Otolithic system (utricle)	Central integration
clrn1$^{-/-}$*clrn2*$^{-/-}$	*null*	*null*	*null*
clrn1$^{-/-}$*clrn2*$^{+/-}$	decreased	decreased	*null*
clrn1$^{-/-}$*clrn2*$^{+/+}$	decreased	decreased	*null*
clrn1$^{+/-}$*clrn2*$^{-/-}$	decreased	**normal**	*null*
clrn1$^{+/+}$*clrn2*$^{-/-}$	**normal**	**normal**	**normal**
***clrn1*$^{+/+}$*clrn2*$^{+/+}$**	**normal**	**normal**	**normal**

Semi-circular canal function is based on horizontal aVOR, otolithic system function on $_{tilt}$MOR and central integration on $_{OVAR}$MOR. Function was considered normal if statistically different from doubleKO and non-different from WT, decreased if statistically different from both doubleKO and WT, and null if non-different from doubleKO and statistically different from WT (doubleKO = *clrn1*$^{-/-}$*clrn2*$^{-/-}$ and WT = *clrn1*$^{+/+}$*clrn2*$^{+/+}$).

Although clarin-2 seems not to be necessary for normal vestibular function in the mouse, it may partially compensate clarin-1 loss, similarly with either biallelic or monoallelic expression, thus maintaining a basic canalar and utricular function (no statistical difference was found between *clrn1*$^{-/-}$ *clrn2*$^{+/+}$ and *clrn1*$^{-/-}$*clrn2*$^{+/-}$ mice).

The capacity of mice to swim and maintain a horizontal position when floating in water seems specifically correlated to utricular function, more specifically $_{tilt}$MOR which corresponds to the capacity of the vestibular system to detect static head (or body) tilt. Even in mice which did not drown, a head tilt (drowning score 1) was often noted which was not observed in the cage. These results are not surprising but the association should be further explored to develop more precise and relevant behavioural scores.

Conclusion:

Clarin-1 and clarin-2 are both present in the vestibular hair cells and have a quantifiable role in the function of vestibule-ocular reflexes. Clarin-1 seems to be the most important protein of the two, as its loss cannot be compensated by clarin-2, whereas biallelic *clrn1* expression seems to be able to fully compensate *clrn2* knock-out. Furthermore, *clrn1* expression seems to be more important in the ampullae compared to the maculae, as utricular function is almost normal even in $clrn1^{+/-}clrn2^{-/-}$ mice. In *clrn1* knock-out mice, the clarin-2 protein can maintain a basic vestibular hypofunction, whereas double-knockout ($clrn1^{-/-}clrn2^{-/-}$) have no measurable vestibular function whatsoever.

References:

[1] R. F. Plantinga, L. Kleemola, P. L. M. Huygen, T. Joensuu, E.-M. Sankila, R. J. E. Pennings, *et al.*, Serial audiometry and speech recognition findings in Finnish Usher syndrome type III patients, *Audiol. Neurootol.* **10**(2) (2005), 79–89.

[2] S. L. Ness, T. Ben-Yosef, A. Bar-Lev, A. C. Madeo, C. C. Brewer, K. B. Avraham, *et al.*, Genetic homogeneity and phenotypic variability among Ashkenazi Jews with Usher syndrome type III, *J. Med. Genet.* **40**(10) (2003), 767–772.

[3] D. Dulon, S. Papal, P. Patni, M. Cortese, P. F. Vincent, M. Tertrais, *et al.*, Clarin-1 gene transfer rescues auditory synaptopathy in model of Usher syndrome, *J. Clin. Invest.* **128**(8) (2018), 3382–3401.

[4] M. Zallocchi, D. T. Meehan, D. Delimont, C. Askew, S. Garige, M. A. Gratton, *et al.*, Localization and expression of clarin-1, the Clrn1 gene product, in auditory hair cells and photoreceptors., *Hear. Res.* **255**(1–2) (2009), 109–120.

[5] R. Geng, S. Melki, D. H.-C. Chen, G. Tian, D. N. Furness, T. Oshima-Takago, *et al.*, The mechanosensory structure of the hair cell requires clarin-1, a protein encoded by Usher syndrome III causative gene., *J. Neurosci. Off. J. Soc. Neurosci.* **32**(28) (2012), 9485–9498.

[6] L. A. Dunbar, P. Patni, C. Aguilar, P. Mburu, L. Corns, H. R. Wells, *et al.*, Clarin-2 is essential for hearing by maintaining stereocilia integrity and function, *EMBO Mol. Med.* **11**(9) (2019), e10288.

[7] M. Beraneck and K. E. Cullen, Activity of vestibular nuclei neurons during vestibular and optokinetic stimulation in the alert mouse, *J. Neurophysiol.* **98**(3) (2007), 1549–1565.

[8] M. Beraneck, M. Bojados, A. Le Seac'h, M. Jamon, and P. P. Vidal, Ontogeny of mouse vestibulo-ocular reflex following genetic or environmental alteration of gravity sensing, *PLoS One* **7**(7) (2012), e40414.

[9] F. França de Barros, J. Carcaud, and M. Beraneck, Long-term Sensory Conflict in Freely Behaving Mice, *J. Vis. Exp. JoVE* (144) (2019),.

[10] M. Beraneck and F. M. Lambert, Impaired perception of gravity leads to altered head direction signals: what can we learn from vestibular-deficient mice?, *J Neurophysiol* **102**(1) (2009), 12–4.

[11] M. Beraneck and E. Idoux, Reconsidering the Role of Neuronal Intrinsic Properties and Neuromodulation in Vestibular Homeostasis, *Front. Neurol.* **3** (2012),.

[12] J. S. Stahl, L. Averbuch-Heller, and R. J. Leigh, Acquired nystagmus, *Arch. Ophthalmol. Chic. Ill 1960* **118**(4) (2000), 544–549.

[13] J. Carcaud, F. França de Barros, E. Idoux, D. Eugène, L. Reveret, L. E. Moore, *et al.*, Long-Lasting Visuo-Vestibular Mismatch in Freely-Behaving Mice Reduces the Vestibulo-Ocular Reflex and Leads to Neural Changes in the Direct Vestibular Pathway, *eNeuro* **4**(1) (2017),.

[14] E. Idoux, M. Tagliabue, and M. Beraneck, No Gain No Pain: Relations Between Vestibulo-Ocular Reflexes and Motion Sickness in Mice, *Front. Neurol.* **9** (2018), 918.

[15] D. R. Calabrese and T. E. Hullar, Planar relationships of the semicircular canals in two strains of mice, *J. Assoc. Res. Otolaryngol. JARO* **7**(2) (2006), 151–159.

[16] F. Simon, D. Pericat, C. Djian, D. Fricker, F. Denoyelle, and M. Beraneck, Surgical techniques and functional evaluation for vestibular lesions in the mouse: unilateral labyrinthectomy (UL) and unilateral vestibular neurectomy (UVN), *J. Neurol.* (2020),.

[17] R. Romand, W. Krezel, M. Beraneck, L. Cammas, V. Fraulob, N. Messaddeq, *et al.*, Retinoic acid deficiency impairs the vestibular function, *J Neurosci* **33**(13) (2013), 5856–66.

[18] B. J. M. Hess and N. Dieringer, Spatial Organization of the Maculo-Ocular Reflex of the Rat: Responses During Off-Vertical Axis Rotation, *Eur. J. Neurosci.* **2**(11) (1990), 909–919.

[19] B. S. Oommen and J. S. Stahl, Eye orientation during static tilts and its relationship to spontaneous head pitch in the laboratory mouse, *Brain Res.* **1193** (2008), 57–66.

[20] D. E. Angelaki and B. J. Hess, Lesion of the nodulus and ventral uvula abolish steady-state off-vertical axis otolith response, *J. Neurophysiol.* **73**(4) (1995), 1716–1720.

[21] D. E. Angelaki and B. J. Hess, Three-dimensional organization of otolith-ocular reflexes in rhesus monkeys. II. Inertial detection of angular velocity, *J. Neurophysiol.* **75**(6) (1996), 2425–2440.

1.1.5. Conclusion

Chez la souris, les protéines clarine-1 et clarine-2 participent toutes les deux à la fonction vestibulaire. La clarine-1 semble plus importante que la clarine-2 puisque chez des souris *clarine-2*$^{-/-}$, l'expression biallélique du gène *clarine-1* permet de garantir seule une fonction vestibulaire normale. A l'inverse, chez les souris *clarine-1*$^{-/-}$, l'expression biallélique du gène *clarine-2* ne permet que de conserver une hypofonction vestibulaire suffisante pour la nage sans noyade. Au total, si la clarine-2 semble non-essentielle à la fonction vestibulaire, elle permet de palier une absence de clarine-1 pour garantir une fonction vestibulaire minimale.

1.2. Article 2 : Etude des conséquences fonctionnelles vestibulaires de malpositions ciliées à partir d'un modèle déficitaire en celsr1

1.2.1. Contexte scientifique

Même en l'absence de dégénérescence des touffes ciliaires vestibulaires, leur désorganisation peut altérer la fonction vestibulaire. En effet, la polarisation des cellules ciliées vestibulaires peut se faire à plusieurs niveaux : à l'échelle cellulaire avec une orientation croissante de la touffe ciliaire jusqu'au kinocil, mais aussi par rapport aux cellules voisines les touffes ciliaires étant orientées dans la même direction et enfin dans le système otolithique par rapport à la striole maculaire. Cette organisation des cellules ciliées semble nécessaire à la bonne transduction mécano-électrique, chaque cellule ciliée ayant une sensibilité directionnelle spécifique qui correspond à l'axe de sa touffe ciliaire permettant une dépolarisation de la cellule (Shotwell et al., 1981).

Cette polarité cellulaire planaire est un système clé dans l'ensemble des organismes vertébrés, grâce à la présence de protéines de la polarité planaire qui permettent aux cellules ciliées de communiquer et de s'orienter avec les cellules de soutien, ainsi que les cellules de soutien entre-elles (Deans, 2013). Plusieurs protéines trans-membranaires permettent de créer des ponts entre les cellules. Parmi celles-ci, la protéine celsr1 (Cadherin EGF LAG Seven-pass G-type Receptor 1) est une protéine répartie de façon asymétrique autour de la cellule en fonction de la position du kinocil (Duncan et al., 2017).

La protéine celsr1, comme toute protéine de la polarité planaire, a un rôle majeur pendant la fermeture du tube neural, ainsi la majorité des souris avec une mutation celsr1 ne sont pas viable, mourant *in utero* ou dans les premiers jours de vie avec des malformations sévères du tube neural (Greene et al., 2009). Les souris qui survivent présentent souvent un enroulement de la queue (loop-tail) ou des mauvaises orientations des poils. Chez l'Homme, la mutation du gène *CELSR1* est peu décrite mais rapportée dans des séries de patients avec spina bifida (Allache et al., 2012; Lei et al., 2014; Zhan et al., 2016).

Aucun déficit vestibulaire ou cochléaire n'a été rapporté dans la littérature concernant les patients avec mutation du gène *CELSR1* et troubles de la fermeture du tube neural.

Un modèle de souris *Celsr1*$^{-/-}$ a été développé avec un mutation stop empêchant la traduction du domaine cytoplasmique de la protéine (Ravni et al., 2009). Ces souris développent une audition normale ainsi qu'une morphologie des cellules ciliées cochléaires normales (Curtin et al., 2003; Duncan et al., 2017). Elles présentent cependant des troubles de la polarisation des cellules ciliées vestibulaires, principalement au niveau des canaux semi-circulaires (***Figure 30***).

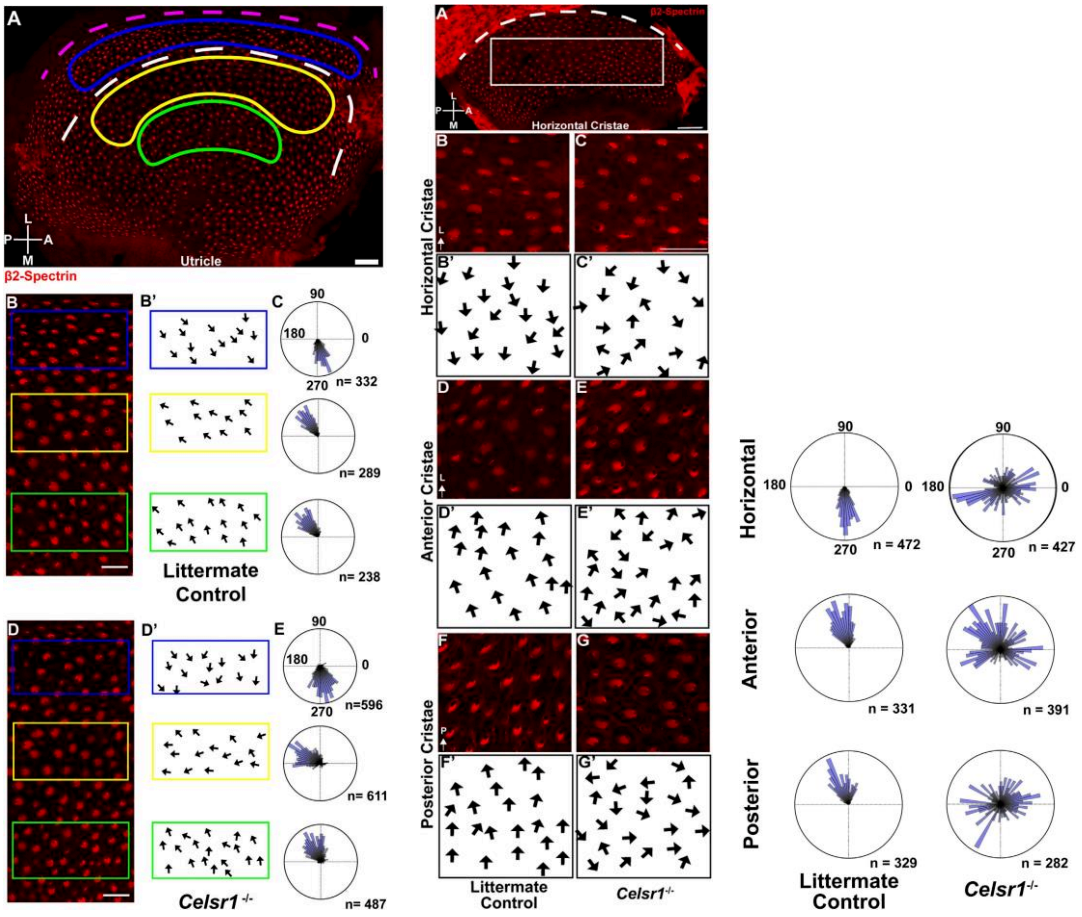

Figure 30 : Modification de la polarisation des cellules ciliées en cas de mutation *Celsr1*

A gauche : Microscopie des cellules ciliées utriculaires (microscopie confocale, repérage de ß2-Spectrine en rouge) montrant un trouble de la polarité modéré. Au milieu et à droite : Microscopie des cellules ciliées des canaux semi-circulaires, montrant une dépolarisation importante des cellules ciliées. (Duncan et al., 2017)

Cette dépolarisation est concordante avec un phénotype comportement de *circling*, instabilité de la tête et *twirling* lors de la suspension par la queue, compatible avec une déficit vestibulaire (Duncan et al., 2017), cependant aucune exploration vestibulaire de ces souris n'a pu être réalisé.

1.2.2. Buts de l'étude

L'objectif de l'étude est de caractériser la fonction vestibulaire des souris présentant une mutation hétérozygote *ceslr1 KO* et de corréler la perte de polarité ciliée à la fonction canalaire et otolithique.

1.2.3. Résumé en français

Une question essentielle de neurophysiologie concerne le rôle joué par l'organisation ciliaires des macules otolithiques et des cupules canalaires. La mutation du gène *celsr1* est associée à une malposition des cils des récepteurs de l'oreille interne avec un phénotype vestibulaire (*circling*, difficultés à la nage) et des défauts de fermeture du tube neural (spina bifida). La désorganisation ciliaire concerne essentiellement les cupules et à un degré moindre les macules. L'étude fonctionnelle de 10 souris *celsr1*-KO et 10 souris contrôles a montré chez les souris mutantes une hypo-fonction canalaire importante (50% de gain aVOR résiduel) associée une avance de phase sur les basses fréquences. Ceci pourrait montrer une dépendance importante du système tonique à la bonne polarisation planaire des cellules ciliées. Il a également été retrouvé un déficit otolithique (66% de gain $_{tilt}$MOR utriculaire résiduel) malgré l'atteinte morphologique limité. Ceci pourrait suggérer que la polarité ciliaire est un facteur particulièrement critique de la physiologie otolithique.

1.2.4. Article original

Titre :

Disorganisation of vestibular hair cells polarisation impairs the vestibulo-ocular reflexes in *celsr1*$^{-/-}$ mice

Auteurs :

François SIMON, Fadel TISSIR, Vincent MICHEL, Ghizlene LAHLOU, Françoise DENOYELLE, Michael DEANS, Mathieu BERANECK

En collaboration avec Vincent MICHEL et Ghizlene LAHLOU (Institut Pasteur, Unité Génétique et Physiologie de l'Audition, dirigée par le Pr Christine PETIT), Fadel TISSIR (Université Catholique de Louvain) et Michael DEANS (University of Utah School of Medicine)

Etat d'avancement :

Article en cours de préparation (corrélation à la polarisation cellulaire à réaliser)

Introduction

Sensory hair cells play a key role in the vestibular system as they enable the transduction of mechanical head movements into the electrical signals that will inform the brain about the head movements and position in 3D space. This is made possible by the organisation and polarisation of the stereociliary bundle, a group of stereocilia on the apical hair cell surface which are arranged in rows of increasing height leading up to a microtubule based kinocilium. Mechanical movement may deflect the bundle towards the kinocilium, placing tension on the tip-links (which link each stereocilia) and opening mechanoelectrical transducers (MET) channels, thus depolarising the hair cell and sending an excitatory signal to the vestibular neurons. Movement away from the kinocilium would conversely close MET and result in an inhibitory stimulus. Each hair cell therefore has a specific directional sensitivity which corresponds to its polarity axis [1]. In both the semi-circular canals (SCC) and otolithic system, hair cells are arranged and coordinated according to their neighbouring cells. In the SCC, the stereociliary bundles are all orientated in the same direction parallel to the SCC axis and are thus all stimulated at the same time. In the utricular and saccular maculae, orientation of the hair cells cover 360° and are all organized in a mirror-like fashion around the striola, also called Line of Polarity Reversal (LPR), which runs along the centre of the macula [2].

This complex organisation, termed Planar Cell Polarity (PCP), may be found on different levels: intra-cellular level with the stereociliary bundle, inter-cellular level where hair cell orientation depends on its neighbours' and in the otolithic system on a macular level, where each head movement combines an excitatory and inhibitory stimulus on either side of the LPR [2]. PCP proteins are key in all vertebrate systems to enable cell communication and coordination between hair cells and supporting cells, as well as between supporting cells [2]. The Celsr1 molecule (Cadherin EGF LAG Seven-pass G-type Receptor 1), a PCP protein, has been reported to cause auditory hair cell misorientation when mutated [3]. Consistent with PCP protein role, *Celsr1* mouse mutants also presented with severe neural tube defects, [4] ranging from craniorachischisis to loop-tails.

Celsr1$^{-/-}$ mice have been developed introducing a frameshift and premature stop preventing translation of the cytoplasmic domain. Most *Celsr1* KO mice are not viable due to neural tube defects: 20% die *in utero* and more than half of the remaining die before weaning [5]. Concerning the labyrinth, *Celsr1* KO mice were not found to have any auditory impairment but presented with classical vestibular postural and locomotor disorders such as head bobbing, circling and spinning when suspended by the tail [3, 6]. This was further confirmed by electronic microscopic analysis of the vestibular organs, which showed that in the absence of Celsr1, stereociliary bundles were misoriented relative to their neighbours, especially in the SCC. On the other hand, the orientation at the level of the maculae were found to be only mildly affected [6]. To which extend does the processing of vestibular information depend on the precise orientation of the population of hair cells in the ampullae and maculae remains completely unexplored.

The objective of this study was therefore to precisely quantify in the *Celsr1* KO adult mice how the disorganisation of the vestibular hair cells polarity affects the canalar- and otolithic-dependent features of the vestibulo-ocular reflexes.

Material and Methods

Animals were used in accordance with the European Communities Council Directive 2010/63/EU. All efforts were made to minimize suffering and reduce the number of animals included in the study. All procedures were approved by the ethical committee for animal research of the University of Paris (CEEA.34). Animals from the *Celsr1* KO line [5] were provided by the University Catholique de Louvain. Ten *Celsr1*$^{-/-}$ and ten littermate control mice were analysed.

To perform pupil position recording with a fixed head, a head post was implanted at least 48h before vestibular exploration to the skull [7–9]. All eye movements recordings were made in the dark using an infrared video system (ETL-200, ISCAN, Burlington MA), recording pupil and corneal reflection (CR) position [7, 8, 10, 11]. Eye movements were recorded using non-invasive video-oculography [12]. The experimental set-up, apparatus and methods of data acquisition were similar to those described previously [8, 13, 14]. Briefly, mice were head-fixed at a ~30° nose-down position to

align the horizontal canals with the yaw plane [15]. Myosis was induced with topical 2% pilocarpine applied 10 minutes before experimentation. Recorded eye and head position signals were sampled at 1 kHz, digitally recorded (CED power1401 MkII) using Spike 2 software and later exported into the Matlab programming environment for off-line analysis (Matlab, The MathWorks). Videonystagmography recorded spontaneous eye movement without vestibular stimulation and eye movement with the three following stimulations: sinusoidal rotation for horizontal angular vestibulo-ocular reflex (aVOR); off-vertical axis rotation (OVAR) for maculo-ocular reflex ($_{OVAR}$MOR) and static and dynamic head tilt roll for $_{tilt}$MOR [8, 16, 17].

Briefly, aVOR was tested during horizontal sinusoidal rotation of the turntable (at 0.2; 0.5; 0.8; 1 and 1.5Hz; peak velocity 30°/s), analysing gain and phase. The gain was the ratio between the amplitude of the eye (response) and head (stimulus) rotations. Since the animal was head-fixed to the rotating table, head movements and table movements were identical. The phase was the temporal shift between the eye and table rotations, expressed in degrees as ratio of the sinusoidal cycle (2 pi). Details for gain and phase calculation were reported in Carcaud et al. 2017 [13]. Values with VAF (Variance-accounted-for) under 0.5 were discarded [7]. During OVAR for $_{OVAR}$MOR, [18] axis of rotation was tilted from the vertical by 17°. Rotations were performed at constant speed (50°/s) for at least 10 rotations both in clockwise (CW) and counter-clockwise (CCW) directions. During rotations, the velocity of horizontal slow phases is modulated around a constant bias. The bias is reported here as $_{OVAR}$MOR, which corresponds to an otolithic response, but also depends on an efficient central vestibular system [8, 18]. The static $_{tilt}$MOR tests more specifically the static utricular function. Vertical pupil position according to the head tilt angle was measured first with the mouse maintained at a 0° horizontal position. The platform was then tilted into different roll positions, at 10°, 20°, 30° and 40° alternatively to the right and to the left. Measurements were made in a static position during at least 15 seconds to identify the stable pupil position. The vertical eye angle was then calculated from the raw vertical CR and pupil position [19]. The $_{tilt}$MOR gain was calculated corresponding to the slope of a linear regression of both variables (vertical eye angle and head tilt degree). Dynamic roll head tilt was also tested during sinusoidal roll motion at 0.5Hz from left to right at three different roll angles: -10° to 10°, -20° to 20°

and -30° to 30° corresponding to three different roll amplitudes: 20°, 40° and 60°. Maximal amplitude of the sinusoidal vertical pupil position was calculated for each condition and dynamic $_{tilt}$VOR gain was calculated corresponding to the amplitude of the vertical eye position on amplitude of the roll rotation. Finally, angular velocity steps in the horizontal plane (hsteps) were performed at a speed of 50°/s. The horizontal slow phase velocity decay was fitted to an exponential curve (f(x) = a*exp(b*x)) and the time constant τ was then calculated as τ=-1/b. Gain was calculated from the peak slow phase velocity on table velocity. The time constant of the slow phase exponential velocity decay and gain was calculated for per-rotatory and post-rotatory nystagmus for CW and CCW rotations. CCW per-rotatory and CW post-rotatory values; and CCW post-rotatory and CW per-rotatory values, were combined to assess left and right vestibular functions, respectively. Directional preponderance was calculated using the Jongkees formula and gain value: $DP = Left\ gain - Right\ gain / Left\ gain + Right\ gain$

Mice were observed during swimming and were scored as following: 0 – normal swimming; 1 – swimming with head tilt; 2 – floating followed by drowning; 3 – immediate drowning.

After vestibular exploration, mice were euthanised. The temporal bone was dissected and an opening made in the apex of the cochlea before fixation in 2.5% glutaraldehyde in cacodylate buffer pH 7.4 at 4°C for 2 hours. Vestibular organs were later microdissected for scanning electronic microscopy examination of hair cell morphology. Functional vestibular results were correlated to hair cell morphology.

Statistical analysis was made using XLstats (Addinsoft, New York, NY). All data are reported as mean and standard deviation. Two-way ANOVA was used to compare aVOR gain and phase (mouse type and frequency). One-way ANOVA was used to compare static and dynamic roll head tilt amplitudes. Post-hoc comparisons were performed where appropriate using the Tukey HSD test. A student t-test was used for $_{OVAR}$MOR, static $_{tilt}$MOR and dynamic $_{tilt}$VOR, if distribution was normal. Values of $p < 0.05$ were considered significant.

Results

A total of 10 *Celsr1*$^{-/-}$ (KO mice) and 10 wild type were tested, characteristics of both groups are reported in ***Table 1***. Concerning the KO mice, none of the mice drowned but 5 showed a circling behaviour and all had a lateral head tilt when floating. When held by the tail, 6 mice twirled spontaneously and only one reached out (9 mice showed body hyperflexion). Behaviour was normal for all WT mice.

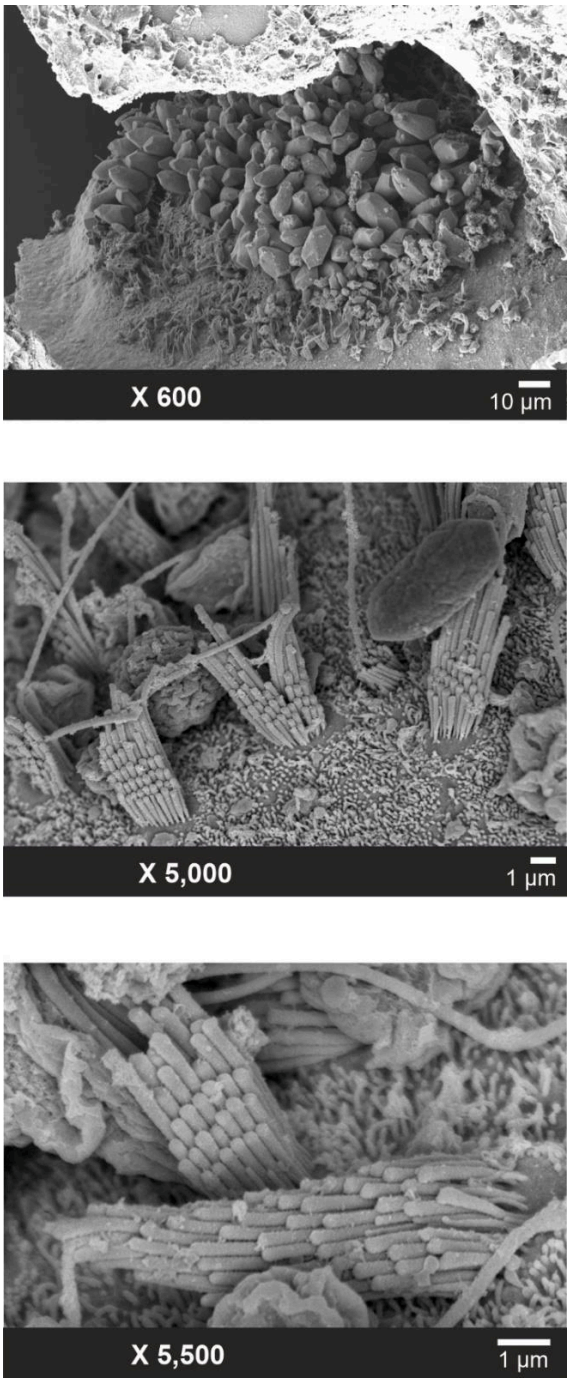

Figure 1: Hair cell stereocilia bundle in the saccular macula.
Scanning electronic microscope of the saccular macula of a KO mouse. x600 image shows an overall maintained saccular structure with otoconia and sensory hair cells beneath. x5000 image shows mostly stereociliary bundles and x5,500 image shows a clear misalignment of two neighbouring hair cells.

Cell morphology was examined using scanning electronic microscope in 4 KO and 2 WT mice, qualitatively confirming a loss of spatial polarisation of the hair cells (example in ***Figure 1***).

Table 1: Characteristics of mice tested

Type of mice	Number of mice	Number of males	Age (weeks) when tested	Number of loop-tails
Celsr1$^{-/-}$	10	2	13 ± 9	6
WT	10	6	15 ± 9	0

Age reported as mean ± standard deviation

Videonystagmography recording spontaneous eye movements without any vestibular stimulation showed spontaneous nystagmus in the KO group only. Five mice showed unilateral nystagmus and five a nystagmus in both directions. KO group had 10.8 ± 7 nystagmus beating per minute (regardless of direction). An overview of the canalar vestibular function, including sinusoidal rotations and hsteps can be found in ***Figure 2***. Horizontal aVOR gain and phase are reported in ***Table 2***. KO mice had significantly lower gain over all frequencies (two-way ANOVA model, $F(9,100)=17.1$, $p<0.001$), whereas significant phase lead was observed in the lower frequencies only (two-way ANOVA model, $F(9,100)=37.9$, $p<0.001$).

Table 2: Horizontal angular vestibulo-ocular reflex

Frequency	0.2Hz	0.5Hz	0.8Hz	1Hz	1.5Hz
aVOR gain					
Celsr1 KO	0.24±0.22	0.42±0.24	0.55±0.21	0.55±0.27	0.77±0.27
WT	0.56±0.13	0.84±0.19	0.91±0.24	0.97±0.22	1.20±0.22
p	***0.044***	***0.002***	***0.015***	***0.002***	***0.002***
aVOR phase					
Celsr1 KO	48.7±16.2	28.0±10.4	11.4±10.4	6.1±11.7	-11.6±3.8
WT	20.3±11.5	1.0±10.7	0.4±5.7	-3.8±4.7	-11.8±6.6
p	***< 0.001***	***< 0.001***	*0.266*	*0.423*	*1*

All values are represented as mean ± SD (standard deviation). *aVOR* angular Vestibular-ocular reflex.

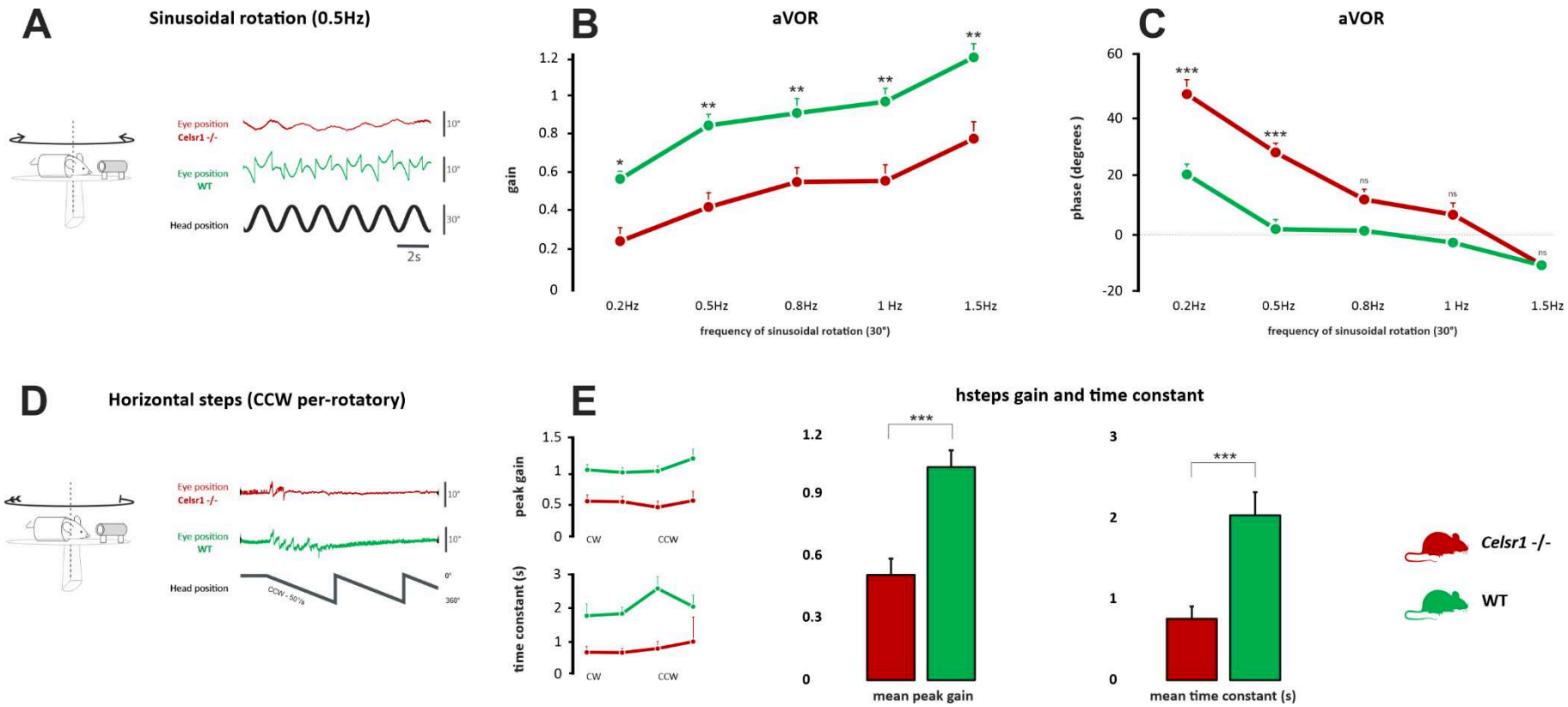

Figure 2: Semi-circular canal function.

The horizontal semi-circular canal (SCC) was tested. **A:** Horizontal sinusoidal rotation tested for aVOR. Traces show head position (corresponding to table position) and horizontal eye movement. KO mice show clear reduction in the amplitude of the eye movement. **B:** aVOR gain for maximum 30°/s velocity according to frequency of stimulation. **C:** aVOR phase for maximum 30°/s velocity according to frequency of stimulation. **D:** Horizontal steps at 50°/s. Traces show head position and horizontal eye position, during per-rotatory nystagmus at the start of a CCW stimulation. KO mouse only has 2 compensatory nystagmus compared to 7 for the WT in this example. **E:** Left: peak gain and time constant for hsteps at 50°/s, for per- and post-rotatory nystagmus during CW and CCW steps. Right: Mean (of all four values) peak gain and time constant. *aVOR* angular vestibulo-ocular reflex *CW* Clockwise *CCW* Counter-clockwise *hsteps* horizontal steps *WT* Wild type.

Hsteps results are reported in ***Table 3***. Briefly, overall peak-velocity gain and time constant were significantly reduced in KO mice. Directional preponderance was significantly increased in KO mice compared to WT, regardless of the direction.

Table 3: Horizontal steps

	Left gain	Right gain	Left τ	Right τ	Overall Gain	Overall τ	Directional preponderance
Celsr1 KO	0.48±0.22	0.53±0.31	0.70±0.50	0.81±0.50	0.51±0.25	0.76±0.48	0.18±0.11
WT	0.97±0.22	1.08±0.31	2.18±0.82	1.88±1.05	1.03±0.26	2.03±0.90	0.06±0.06
p	-	-	-	-	***< 0.001***	***0.001***	***0.009***

All values are represented as mean ± SD (standard deviation). Overall gain and τ values correspond to the mean value of CCW and CW per- and post-rotatory values. τ is in seconds. Absolute values were used to calculate directional preponderance mean. Statistical comparison was made using a student t-test (normal distribution). *τ* time constant.

Results from roll head tilt and OVAR stimulation results are reported in ***Figure 2***. Static $_{tilt}$MOR gain and $_{OVAR}$MOR bias are reported in ***Table 4***, which were both significantly reduced in KO mice. Based on the static head tilt results, the amplitude of the vertical eye position angle during static roll head tilts were calculated for the 20° (-10 to 10); 40° (-20 to 20) and 60° (-30 to 30) amplitudes. Mean amplitude gain (vertical eye amplitude / tilt amplitude) was 0.34 ± 0.07 versus 0.57 ± 0.20, p = 0.062, for KO and WT mice, respectively. The mean gain was calculated for dynamic head roll tilts during 0.5Hz sinusoidal rotations and found 0.40 ± 0.19 versus 0.93 ± 0.31, p < 0.001, for KO and WT mice, respectively (ANOVA model F(3,40) = 17.5, p<0.001).

Table 4: static tilt- and OVAR- maculo-vestibular reflexes

MOR	Static $_{tilt}$MOR			$_{OVAR}$MOR		
	40° left	40° right	gain	CCW	CW	Overall
Celsr1 KO	14.7±8.2	-16.9±8.1	0.37±0.09	-0.02±0.03	0.04±0.04	0.03±0.03
WT	17.7±7.4	-29.0±13.0	0.56±0.17	-0.17±0.10	0.17±0.11	0.17±0.10
p	-	-	***0.008***	-	-	***< 0.001***

All values are represented as mean ± SD (standard deviation). $_{tilt}$MOR is reported as the left eye vertical angle at 40° static head tilt to the left and to the right and gain (slope value of vertical eye angle and head tilt degree). $_{OVAR}$MOR is reported with the bias value, during CCW and CW stimulations, and overall mean. Statistical comparison was made using a student t-test (normal distribution). *CCW* counter-clockwise *CW* clockwise *MOR* maculo-ocular reflex *OVAR* off-vertical axis rotation.

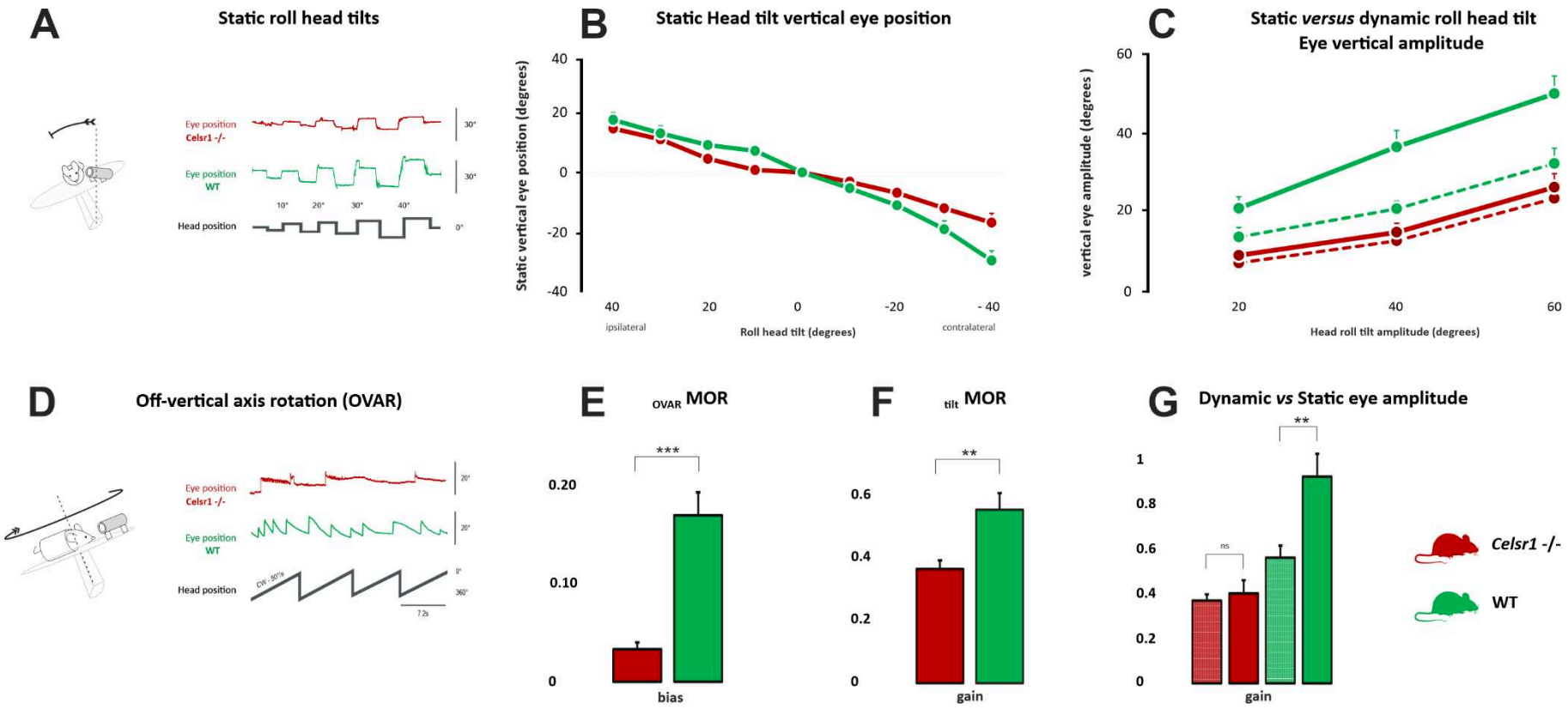

Figure 3: Otolithic system function.

A: Static roll head tilts to determine $_{tilt}$MOR corresponding to utricular function. Traces show head position (corresponding to table position) and vertical eye movement. KO mouse had preserved function with slightly poorer gain. **B:** Vertical eye position in degrees according to roll head tilt degree. The left eye pupil position was measured, tilts with positive degrees were towards the left side and with negative degrees towards the right side. **C:** Amplitude in degrees of vertical eye movement according to amplitude of head tilt (from left to right), for static tilts (dotted lines) and dynamic sinusoidal 0.5Hz tilts (solid lines). **D:** Off-vertical axis rotations at 50°/s. Traces show head position and horizontal eye position, during CW stimulation. KO mouse in this example has poor response, seen as the absence of the MOR nystagmus. **E:** $_{OVAR}$MOR bias, which is significantly reduced in KO mice. **F:** $_{tilt}$MOR gain, which is significantly reduced in KO mice. **G:** Comparison of vertical eye amplitude during static (dashed fill) and dynamic (solid fill) head tilts. In KO mice, the amplitude was not significantly changed between static and dynamic stimulations, whereas it was in WT mice. *CW* Clockwise *CCW* Counter-clockwise *MOR* Maculo-ocular reflex *OVAR* Off-vertical axis rotation *WT* Wild type.

No correlation was found between directional preponderance, spontaneous nystagmus direction, CCW or CW $_{OVAR}$MOR, left or right hsteps gains, left or right time constants or side of head tilt.

Discussion

Celsr1 KO mice are an excellent model of planar cell polarisation loss in the vestibular system. It has previously been shown that in *Celsr1* KO mice, SCC ampullar hair cells were particularly disorganised, with less than 20% of hair cells coordinated in the right direction, whereas the depolarisation was less important in the otolithic system with more than 80% of hair cells in the appropriate direction [6]. Although morphological, locomotor and postural behavioural studies had already been undertaken, the effect of stereociliary bundle polarity loss on the capacity of the vestibular system to encode precise directional signals during angular or linear acceleration had not yet been studied.

In our study on 10 *Celsr1* KO mice, canalar function was found to be severely altered, with aVOR gain approximately half of that of WT mice on all frequencies. A statistically significant phase lead was however only found in the lower frequencies at 0.2 and 0.5Hz, and became progressively identical to WT phases at high frequencies (>1.5Hz). This tends to show that loss of cell polarity particularly impairs function at lower frequencies. A hypothesis to explain this result would be that, angular velocities being lower at those frequencies, the misoriented hair cells are likely not stimulated or stimulated to a lower extent, leading to a decreased population encoding of the movement. This probably impairs the capacity of central vestibular neurons to appropriately encode the amplitude of the head movement and distinguish it from background noise. In higher frequencies, a larger proportion of hair cells would be stimulated, facilitating the event detection of movement and enabling a VOR response with a normal phase. Whichever the frequency, the reduced number of correctly aligned stereocilia bundles depolarised during canalar stimulation, could explain the reduced gain even in the higher frequencies. Overall, it should be noted that despite a complete disorganization of the hair cells orientation in the ampullae, the signals originating from one SCC can be centrally interpreted as a directional activation in the plane of the canal, thus preserving the directionality of the generated eye movement

Another aspect is the significantly greater directional preponderance found in *Celsr1* KO mice (as well as multiple bilateral spontaneous nystagmus), although no correlation was found between the direction of the preponderance and any ipsilateral vestibular function. This could be interpreted as a severely impaired tonic vestibular signal in the absence of, or during low-velocity stimulations. As previously described [6], if some hair cells maintain a physiological orientation in the ampulla, a small proportion of depolarised hair cells are orientated in the opposite direction, thus transmitting excitatory information instead of inhibitory and vice-versa. This impaired push-pull system could explain the alternating slow VOR phases, which could be overrun at high frequency stimulations when a sufficient amount of coherent information is being processed by the vestibular nuclei.

Utricular function was significantly decreased in the *Celsr1* KO mice but the residual function was sufficient to maintain a static $_{tilt}$MOR gain (approximately two thirds of WT mice gain) and swimming abilities. Considering the minor loss of hair cell polarisation in the utricle morphologically [6], functional loss may be considered excessive compared to the ampulla (half of the gain remaining with less than 20% of hair cells correctly orientated). This may be due to the fact that the otolithic system contains less redundancy in hair cell direction, compared to the ampulla where all hair cells are orientated in the same direction [2]. This result demonstrates that the spatial organisation of the hair cells in the maculae is a critical factor allowing the precise decoding of the spatial directionality of the head movements by central vestibular structures. Thus, in the otolithic system, a small proportion of dispolarised hair cells may incur major functional impairment.

A number of others tests assessed more integrated and complex vestibular functions, such as the velocity storage (which requires SCC function and the integrity of a central vestibular and cerebellar neural circuit), OVAR (the bias corresponding to a complex otolithic response, but which also requires the integrity of canalar and velocity storage system) and the dynamic roll head tilt (which recruits both utricular and vertical canal function). In each of these tests, differences between KO and WT mice were strongly significant, which suggests that the vestibular nuclei are not able to compensate by integrating different vestibular afferent information.

The reduced time constant could be related to an impaired velocity storage or to a reduced aVOR gain. However, in mice the velocity storage is considered "leaky" [20], the reduced encoding at the level of the ampullae would therefore constitute the most parcimonious explanation for this reduction. Similarly, $_{OVAR}$MOR bias significantly lower value in KO mice is probably due to combination of the decreased canalar and otolithic functions. Lastly, concerning dynamic roll tilt, in the WT mice, the significant difference between static and dynamic tilt might be due to the addition of vertical canal push-pull information, and/or to the recruitment of phasic utricular type I cells. It is interesting that in the KO mice, the $_{tilt}$VOR gain was similar to the static amplitude gain, which could be due either to a deficit in the integration of spatially-convergent canalar and utricular information, or to a deficit in the recruitment of type I utricular hair cells.

Conclusion:

This study first confirms the previous morphological results [6], showing that in *Celsr1* KO mice, planar hair cell polarisation is more severely disorganised in the semi-circular canal hair cells than in the otolithic hair cells. Our results show that loss of hair cell polarity particularly impairs angular VOR at low frequencies, with a strong phase lead and decrease in amplitude. The deficit at low frequencies shows that population coding is particularly important when vestibular stimulation is weak. Surprisingly however, the major ampullar disorganization led to a reduction but not to a complete loss of angular coding capacities. In addition, the spatial-tuning of the horizontal angular VOR was preserved, suggesting that the canalar spatial tuning does not depend on hair cells polarization. On the other hand, the utricular function seems greatly affected relatively to the morphological study. This may be due to the specific three-layered hair cell polarisation (intra-cellular, inter-cellular and macula level). Specifically, these results demonstrate that the highly organized polarisation of otolithic hair cells is a critical factor for the accurate encoding of the head movement and that the loss of a small fraction of the population is likely to have major functional consequences.

Although *CELSR1* mutations have been reported in neural tube defect papers [21–24], vestibular function in these patients has never been reported. Considering their neurological background, exploration of vestibular function may not be sufficiently considered in patients with neural tube defects

who present with posture, reaching or orientation issues. Bearing in mind our results, we believe that clinical research studies should assess vestibular function in patients with neural tube defects and especially with *CELSR1* mutations, as vestibular disorders may be diagnosed and appropriate rehabilitation prescribed.

References:

[1] S. L. Shotwell, R. Jacobs, and A. J. Hudspeth, Directional sensitivity of individual vertebrate hair cells to controlled deflection of their hair bundles, *Ann. N. Y. Acad. Sci.* **374** (1981), 1–10.

[2] M. R. Deans, A balance of form and function: planar polarity and development of the vestibular maculae, *Semin Cell Dev Biol* **24**(5) (2013), 490–8.

[3] J. A. Curtin, E. Quint, V. Tsipouri, R. M. Arkell, B. Cattanach, A. J. Copp, *et al.*, Mutation of Celsr1 disrupts planar polarity of inner ear hair cells and causes severe neural tube defects in the mouse, *Curr. Biol. CB* **13**(13) (2003), 1129–1133.

[4] N. D. E. Greene, P. Stanier, and A. J. Copp, Genetics of human neural tube defects, *Hum. Mol. Genet.* **18**(R2) (2009), R113-129.

[5] A. Ravni, Y. Qu, A. M. Goffinet, and F. Tissir, Planar cell polarity cadherin Celsr1 regulates skin hair patterning in the mouse, *J. Invest. Dermatol.* **129**(10) (2009), 2507–2509.

[6] J. S. Duncan, M. L. Stoller, A. F. Francl, F. Tissir, D. Devenport, and M. R. Deans, Celsr1 coordinates the planar polarity of vestibular hair cells during inner ear development, *Dev Biol* **423**(2) (2017), 126–137.

[7] M. Beraneck and K. E. Cullen, Activity of vestibular nuclei neurons during vestibular and optokinetic stimulation in the alert mouse, *J. Neurophysiol.* **98**(3) (2007), 1549–1565.

[8] M. Beraneck, M. Bojados, A. Le Seac'h, M. Jamon, and P. P. Vidal, Ontogeny of mouse vestibulo-ocular reflex following genetic or environmental alteration of gravity sensing, *PLoS One* **7**(7) (2012), e40414.

[9] F. França de Barros, J. Carcaud, and M. Beraneck, Long-term Sensory Conflict in Freely Behaving Mice, *J. Vis. Exp. JoVE* (144) (2019),.

[10] M. Beraneck and F. M. Lambert, Impaired perception of gravity leads to altered head direction signals: what can we learn from vestibular-deficient mice?, *J Neurophysiol* **102**(1) (2009), 12–4.

[11] M. Beraneck and E. Idoux, Reconsidering the Role of Neuronal Intrinsic Properties and Neuromodulation in Vestibular Homeostasis, *Front. Neurol.* **3** (2012),.

[12] J. S. Stahl, L. Averbuch-Heller, and R. J. Leigh, Acquired nystagmus, *Arch. Ophthalmol. Chic. Ill 1960* **118**(4) (2000), 544–549.

[13] J. Carcaud, F. França de Barros, E. Idoux, D. Eugène, L. Reveret, L. E. Moore, *et al.*, Long-Lasting Visuo-Vestibular Mismatch in Freely-Behaving Mice Reduces the Vestibulo-Ocular Reflex and Leads to Neural Changes in the Direct Vestibular Pathway, *eNeuro* **4**(1) (2017),.

[14] E. Idoux, M. Tagliabue, and M. Beraneck, No Gain No Pain: Relations Between Vestibulo-Ocular Reflexes and Motion Sickness in Mice, *Front. Neurol.* **9** (2018), 918.

[15] D. R. Calabrese and T. E. Hullar, Planar relationships of the semicircular canals in two strains of mice, *J. Assoc. Res. Otolaryngol. JARO* **7**(2) (2006), 151–159.

[16] F. Simon, D. Pericat, C. Djian, D. Fricker, F. Denoyelle, and M. Beraneck, Surgical techniques and functional evaluation for vestibular lesions in the mouse: unilateral labyrinthectomy (UL) and unilateral vestibular neurectomy (UVN), *J. Neurol.* (2020),.

[17] R. Romand, W. Krezel, M. Beraneck, L. Cammas, V. Fraulob, N. Messaddeq, *et al.*, Retinoic acid deficiency impairs the vestibular function, *J Neurosci* **33**(13) (2013), 5856–66.

[18] B. J. M. Hess and N. Dieringer, Spatial Organization of the Maculo-Ocular Reflex of the Rat: Responses During Off-Vertical Axis Rotation, *Eur. J. Neurosci.* **2**(11) (1990), 909–919.

[19] B. S. Oommen and J. S. Stahl, Eye orientation during static tilts and its relationship to spontaneous head pitch in the laboratory mouse, *Brain Res.* **1193** (2008), 57–66.

[20] A. M. van Alphen, J. S. Stahl, and C. I. De Zeeuw, The dynamic characteristics of the mouse horizontal vestibulo-ocular and optokinetic response, *Brain Res.* **890**(2) (2001), 296–305.

[21] R. Allache, P. De Marco, E. Merello, V. Capra, and Z. Kibar, Role of the planar cell polarity gene CELSR1 in neural tube defects and caudal agenesis, *Birt. Defects Res. A. Clin. Mol. Teratol.* **94**(3) (2012), 176–181.

[22] Y. Lei, H. Zhu, W. Yang, M. E. Ross, G. M. Shaw, and R. H. Finnell, Identification of novel CELSR1 mutations in spina bifida, *PloS One* **9**(3) (2014), e92207.

[23] A. Robinson, S. Escuin, K. Doudney, M. Vekemans, R. E. Stevenson, N. D. E. Greene, *et al.*, Mutations in the planar cell polarity genes CELSR1 and SCRIB are associated with the severe neural tube defect craniorachischisis, *Hum. Mutat.* **33**(2) (2012), 440–447.

[24] Y.-H. Zhan, Q.-C. Luo, X.-R. Zhang, N.-A. Xiao, C.-X. Lu, C. Yue, *et al.*, CELSR1 Is a Positive Regulator of Endothelial Cell Migration and Angiogenesis, *Biochem. Biokhimiia* **81**(6) (2016), 591–599.

1.2.5. Conclusion

La polarité des cellules ciliées a un rôle important notamment pour les stimulations rotatoires basses fréquences et dans le système otolithique qui comprend trois niveaux polarité cellulaire planaire (intra-cellulaire, inter-cellulaire et maculaire) et a donc moins de redondance directionnelle des cellules ciliées. Inversement, la polarité des touffes ciliaires ne semble pas essentielle à un fonctionnement vestibulaire minimal, car les gains sont modérément affectés et d'un point de vue comportement, les souris parviennent à conserver une nage efficace et ont un comportement pathologique vestibulaire très modéré par rapport aux souris avec agénésie des cils (les souris clarines par exemple de l'étude 1).

Aucune donnée dans la littérature n'a pu être retrouvé cherchant chez l'Homme un lien entre pathologie de la fermeture du tube neural et dysfonction vestibulaire. Il serait intéressant de réaliser systématiquement des bilans vestibulaires aux patients qui ont une pathologie en lien avec une anomalie des protéines de la polarité cellulaire planaire, dont CELSR1. Si ces patients présentent un déficit vestibulaire comme chez la souris, il est possible que certains symptômes vestibulaires soient mis sur le compte du syndrome neurologique, alors qu'ils pourraient bénéficier d'une rééducation vestibulaire plus ciblée.

1.3. Article 3 : Rôles de la protéine snap25 dans la fonction cochléo-vestibulaire et évaluation de l'efficacité de la thérapie génique

1.3.1. Contexte scientifique

Les cellules ciliées vestibulaires et cochléaires possèdent des synapses particulières, dites à ruban, qui ont la capacité de libérer du glutamate avec une précision temporelle et une intensité importante même lors de stimulation prolongée (Moser and Beutner, 2000; Safieddine et al., 2012). Comme décrit précédemment, la mécano-transduction électrique a lieu lorsqu'une stimulation mécanique des cellules ciliées entraine une dépolarisation de la cellule, puis une entrée massive de Ca^{2+}. Cette chaine d'évènements aboutit à la fusion des vésicules synaptiques avec la membrane plasmatique présynaptique, appelée exocytose, et la libération dans la fente synaptique du glutamate qu'elles contiennent (***Figure 31***). Comme dans d'autres synapses du système nerveux central, la migration de la vésicule, sa fusion membranaire et l'exocytose sont possible grâce au complexe SNARE (SNAP Receptor) qui comprend plusieurs dizaines de protéines. Le complexe SNARE est composé de deux entités, le v-SNARE (qui est incorporé dans la membrane vésiculaire) et le t-SNARE (pour *target* ou cible), dont fait partie la protéine SNAP-25 qui se trouve sur la membrane cellulaire et qui va permettre de guider le v-SNARE. Le complexe SNARE est complètement formé lorsque les deux entités se rejoignent et fusionnent

Le rôle de snap-25 dans les cellules ciliées cochléaires est controversé, car il y a été rapporté que dans des cultures organotypiques des cellules ciliées internes des organes de Corti de souris, la suppression du gène *snap-25* n'avait aucun effet sur l'exocytose synaptique (Nouvian et al., 2011). Ainsi il a été suggéré que l'exocytose dans ces cellules ciliées dépendait d'un mécanisme différent que dans les synapses des autres cellules du système nerveux central. L'exploration de cette hypothèse sur modèle animal a été difficile à mettre en œuvre car les souris avec délétion *snap-25* ne sont pas viables et

présentent une détresse respiratoire à la naissance (absence de contraction diaphragmatique) (Washbourne et al., 2002).

Pour mieux comprendre le rôle de snap-25 dans les cellules ciliées labyrinthiques chez la souris, un nouveau modèle KO conditionnel a été développé par l'équipe de l'Institut Pasteur (Dr Saaid SAFIEDDINE, Institut Pasteur, Unité Génétique et Physiologie de l'Audition, dirigée par le Pr Christine PETIT), permettant une suppression spécifique et temporelle de l'exon 4 du gène *snap-25* dans les cellules labyrinthiques en période néonatale. Il a été constaté une surdité profonde et un comportement anormal compatible avec une atteinte vestibulaire (*circling*, *head-bobbing*), correspondant à une dégénérescence très importante des cellules ciliées (travaux en cours de publication). Les cellules ciliées résiduelles présentent une importante réduction de la fusion rapide des vésicules lors de l'exocytose. Les atteintes cochléaires et vestibulaires semblent cependant décalées dans le temps, la surdité étant constatée dès P14-P17 avec des potentiels évoqués auditifs effondrés, alors que les anomalies comportementales sont constatées à partir de P30 (tests comportementaux normaux à P16-17).

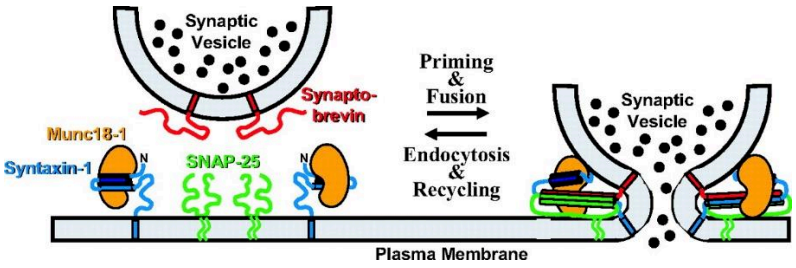

Figure 31 : Exocytose des vésicules synaptiques dans les cellules ciliées

La protéine snap-25 (en vert) est une protéine du complexe SNARE et a un rôle essentiel pour permettre la fusion des vésicules synaptiques et l'exocytose (D'après Dulubova et al., 2007).

L'analyse morphologique des cellules ciliées internes cochléaires à P8 (avant le développement de l'audition) montre une cellule ciliée normale, ce qui semble indiquer que snap-25 n'est pas essentielle

au développement des cellules ciliées avant le développement de l'audition. Le transfert viral de *snap-25* à P2 (par injection dans la fenêtre ronde) permet la restauration partielle de la fonction auditive (testée à P20) et une normalisation du comportement (testé à P30), ce qui semblerait indiquer que les cellules ciliées labyrinthiques utilisent un mécanisme SNARE similaire à celui des synapses neuronales.

1.3.2. Buts de l'étude

Il s'agit d'évaluer le rôle de la protéine snap-25 dans les cellules ciliées vestibulaires de la souris, notamment la fonction vestibulaire en l'absence de la protéine et après transfert génique.

1.3.3. Résumé en français

La molécule snap-25 est une protéine transmembranaire présente dans l'oreille interne et impliquée dans le mécanisme d'exocytose synaptique des cellules ciliées. Au total 22 souris ont été étudiées dont 6 souris *snap-25 cKO*, 8 souris *snap-25 cKO* (KO conditionnel) ayant bénéficié d'un transfert viral de *snap-25* à P2 et 8 souris normales recevant également le transfert génique (sham). Une évaluation comportementale et fonctionnelle du système vestibulaire a été réalisée (réflexe vestibulo-oculaire canalaire et utriculaire). Les souris *snap-25 cKO* sans injection étaient incapable de nager et leurs explorations vestibulaires ont montré des déficits canalaires et otolithiques complets. Les souris SHAM et *snap-25* cKO avec transfert génique étaient statistiquement comparables entre-elles et significativement supérieures au groupe *snap-25* cKO, concernant l'ensemble des tests de réflexe vestibulo-oculaire. La protéine snap-25 du complexe SNARE semble indispensable a une fonction vestibulaire normale. La normalité des explorations vestibulaires dans groupe cKO traité par thérapie génique semble indiquer que la protéine snap-25 n'est pas essentielle à l'organogénèse vestibulaire.

1.3.4. Article original

Titre :

Role of the snap-25 protein on vestibular function

Auteurs :

François SIMON, Françoise DENOYELLE, Mathieu BERANECK

En collaboration avec Charlotte CALVET (doctorante) et l'équipe de Saaid SAFIEDDINE (Institut Pasteur, Unité Génétique et Physiologie de l'Audition, dirigée par le Pr Christine PETIT)

Etat d'avancement :

Article en cours de préparation

Introduction

Ribbon synapses can be found in the auditory inner hair cells and vestibular hair cells [1]. They enable the sensory hair cells to encode information with a high temporal precision and sensitivity, which is essential to correctly transmit auditory or head movement information to the auditory and vestibular neurons. The ribbon is a presynaptic organelle which is surrounded by synaptic vesicles, whose role is to transfer neurotransmitters (such as glutamate) into the synaptic cleft during cell depolarisation. Synaptic vesicle trafficking and membrane fusion in central nervous system synapses depends on a group of proteins, forming the SNARE complex, including snap-25. The role of snap-25 in the labyrinthic hair cells is controversial, as in an organotypic culture of organs of Corti derived from *snap-25* null mice embryos, it has been suggested that cochlear inner hair cells exocytosis was not impaired by the absence of snap-25 and that mature hair cell synapses may operate without neural SNAREs [2]. Initially, this has been difficult to confirm in mice models as *snap-25* null mice die at birth [3].

Hair cell specific *snap-25* conditional knock-out (cKO) mice (Snap-25flox/flox PMyo15-hCre+/KI) have been developed and were viable, showing profound deafness and complete loss of cochlear hair cells (at post-natal day 14-17). It was found however that before hearing onset (at P8-10), auditory hair cells had normal morphology, suggesting that snap-25 is necessary for mature hair cell function and even survival, but not for organogenesis.

The objective of this study was to complete the evaluation of the labyrinthic hair cells and precisely quantify vestibular function in *Snap-25* cKO mice compared to controls, and in cKO mice after gene transfer.

Material and Methods

Animals were used in accordance with the European Communities Council Directive 2010/63/EU. All efforts were made to minimize suffering and reduce the number of animals included in the study. All procedures were approved by the ethical committee for animal research of the University of Paris (CEEA.34). Snap-25 flox/flox mice were generated to enable selective deletion of the *Snap-25* gene in cells expressing Cre recombinase. In this mouse model, exon 4 of *Snap-25* was flanked by two P-lox

sites. These mice were then crossed with PMyo15-hCre+/KI mice, in which the Cre recombinase expression is restricted to the cochlear and the vestibular hair cells due to the Myosin 15 promoter [4].

Three groups of mice were analysed: *Snap-25* cKO mice without any gene transfer (cKO), *snap-25* cKO with gene transfer (cKO-GT) and sham controls (wild type mice with gene transfer). Mouse behaviour was analysed during swimming and tail hanging test, as well as vestibular canalar and otolithic function.

To perform pupil position recording with a fixed head, a head post was implanted at least 48h before vestibular exploration to the skull [5–7]. All eye movements recordings were made in the dark using an infrared video system (ETL-200, ISCAN, Burlington MA), recording pupil and corneal reflection (CR) position [5, 6, 8, 9]. Eye movements were recorded using non-invasive video-oculography [10]. The experimental set-up, apparatus and methods of data acquisition were similar to those described previously [6, 11, 12]. Briefly, mice were head-fixed at a ~30° nose-down position to align the horizontal canals with the yaw plane [13]. Myosis was induced with topical 2% pilocarpine applied 10 minutes before experimentation. Recorded eye and head position signals were sampled at 1 kHz, digitally recorded (CED power1401 MkII) using Spike 2 software and later exported into the Matlab programming environment for off-line analysis (Matlab, The MathWorks). Videonystagmography recorded spontaneous eye movement without vestibular stimulation and eye movement with the three following stimulations: sinusoidal rotation for horizontal angular vestibulo-ocular reflex (aVOR); off-vertical axis rotation (OVAR) for maculo-ocular reflex ($_{OVAR}$MOR) and static and dynamic head tilt roll for $_{tilt}$MOR [6, 14, 15].

Briefly, aVOR was tested during horizontal sinusoidal rotation of the turntable (at 0.2; 0.5; 0.8; 1 and 1.5Hz; peak velocity 30°/s), analysing gain and phase. The gain was the ratio between the amplitude of the eye (response) and head (stimulus) rotations. Since the animal was head-fixed to the rotating table, head movements and table movements were identical. The phase was the temporal shift between the eye and table rotations, expressed in degrees as ratio of the sinusoidal cycle (2 pi). Details for gain and phase calculation were reported in Carcaud et al. 2017 [11]. Values with VAF (Variance-accounted-for) under 0.5 were discarded [5]. During OVAR for $_{OVAR}$MOR, [16] axis of rotation was

tilted from the vertical by 17°. Rotations were performed at constant speed (50°/s) for at least 10 rotations both in clockwise (CW) and counter-clockwise (CCW) directions. During rotations, the velocity of horizontal slow phases is modulated around a constant bias. The bias is reported here as $_{OVAR}$MOR, which corresponds to an otolithic response, but also depends on an efficient central vestibular system [6, 16]. The static $_{tilt}$MOR tests more specifically the static utricular function. Vertical pupil position according to the head tilt angle was measured first with the mouse maintained at a 0° horizontal position. The platform was then tilted into different roll positions, at 10°, 20°, 30° and 40° alternatively to the right and to the left. Measurements were made in a static position during at least 15 seconds to identify the stable pupil position. The vertical eye angle was then calculated from the raw vertical CR and pupil position [17]. The $_{tilt}$MOR gain was calculated as the slope of a linear regression of both variables (vertical eye angle and head tilt degree). Dynamic roll head tilt was also tested during sinusoidal roll motion at 0.5Hz from left to right at three different roll angles: -10° to 10°, -20° to 20° and -30° to 30° corresponding to three different roll amplitudes: 20°, 40° and 60°. Maximal amplitude of the sinusoidal vertical pupil position was calculated for each condition and dynamic $_{tilt}$VOR gain was calculated corresponding to the amplitude of the vertical eye position on amplitude of the roll rotation. Finally, angular velocity steps in the horizontal plane (hsteps) were performed at a speed of 50°/s. The horizontal slow phase velocity decay was fitted to an exponential curve ($f(x) = a*\exp(b*x)$) and the time constant τ was then calculated as $\tau=-1/b$. Gain was calculated from the peak slow phase velocity on table velocity. The time constant of the slow phase exponential velocity decay and gain was calculated for per-rotatory and post-rotatory nystagmus for CW and CCW rotations. CCW per-rotatory and CW post-rotatory values; and CCW post-rotatory and CW per-rotatory values, were combined to assess left and right vestibular functions, respectively.

Statistical analysis was made using XLstats (Addinsoft, New York, NY). All data are reported as mean and standard deviation. Two-way ANOVA was used to compare aVOR gain and phase (mouse type and frequency). One-way ANOVA was used to compare $_{OVAR}$MOR, static $_{tilt}$MOR, time constant and peak-velocity aVOR gain. Post-hoc comparisons were performed where appropriate using the Tukey HSD test. A paired student t-test was used to compare $_{OVAR}$MOR, static $_{tilt}$MOR, time constant

and peak-velocity aVOR gain from both left and right sides. Values of $p < 0.05$ were considered significant.

Results

A total of 14 *Snap-25*$^{-/-}$ (cKO mice) and 8 sham mice were tested. All SHAM and a group of 8 cKO mice received snap-25 viral gene transfer, injected through the round window at P2 (cKO-GT group), a summary of the different groups are reported in ***Table 1***. Concerning behaviour, all cKO mice, were unable to swim or to stay afloat horizontally. All had vestibular behaviour during tail hanging test (folding of the body instead of reach out). Behaviour was normal for all SHAM and cKO-GT mice.

Concerning spontaneous nystagmography in the dark without any vestibular stimulation, all cKO mice had pupil instability and three had spontaneous nystagmus in both directions. SHAM and cKO-GT had not spontaneous nystagmus and pupil was stable.

Table 1: Characteristics of mice tested

Type of mice	Number of mice	Age (weeks) when tested	Gene transfer
Snap-25 cKO	6	12 ± 1	No
Snap-25 cKO -GT	8	19 ± 6	Yes
SHAM	8	24 ± 4	Yes

Age reported as mean ± standard deviation

An overview of the vestibular function can be found in ***Figure 1***. Horizontal aVOR gain and phase are reported in ***Table 2***. cKO mice had significantly lower gain over all frequencies compared to cKO-GT and SHAM mice (two-way ANOVA model, $F(14,110)=36.9$, $p<0.001$). Angular VOR gain was not statistically different between cKO-GT and SHAM groups; neither was aVOR phase (two-way ANOVA model, $F(9,80)=28.8$, $p<0.001$).

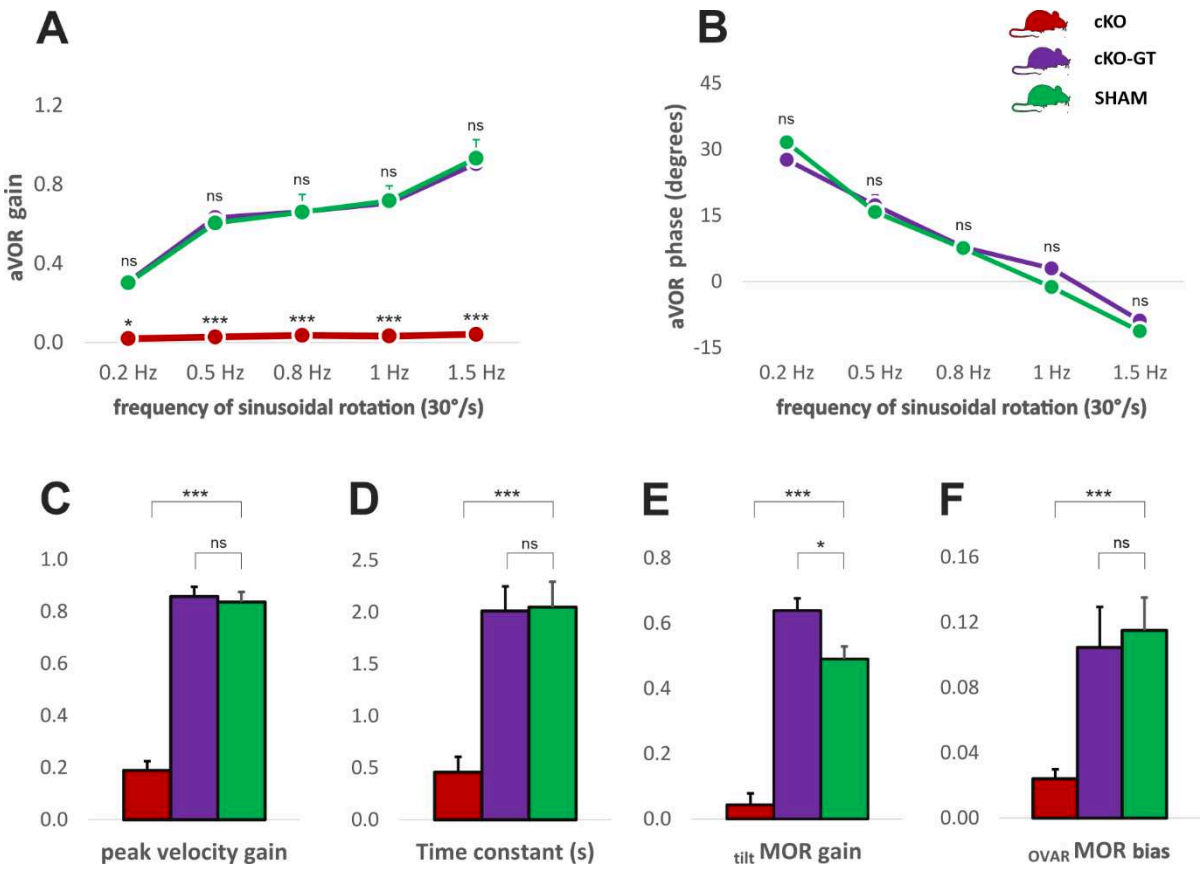

Figure 1: Vestibular function of *snap-25* cKO, cKO-GT and SHAM mice
A: aVOR gain for maximum 30°/s velocity according to frequency of stimulation. Statistical comparison shown versus SHAM. **B:** aVOR phase for maximum 30°/s velocity according to frequency of stimulation. cKO values are not reported because VAF < 0.5. **C:** Peak velocity gain for hsteps at 50°/s. (Mean of CCW and CW per- and post-rotatory nystagmus). **D:** Peak time constant in seconds for hsteps at 50°/s. (Mean of CCW and CW per- and post-rotatory nystagmus). **E:** $_{tilt}$MOR gain during roll static head tilt. **F:** Mean MOR bias (CCW and CW rotations at 50°/s) during OVAR. *aVOR* angular vestibulo-ocular reflex *CW* Clockwise *CCW* Counter-clockwise *hsteps* horizontal steps *MOR* maculo-ocular reflex *OVAR* Off-vertical axis rotation.

Results of the horizontal steps, static roll head tilt and OVAR stimulations are reported in ***Table 3***. Briefly, overall peak-velocity gain and time constant were significantly reduced in cKO mice, $F(2,22)=32.0$, $p<0.001$) and $F(2,22)=14.4$, $p<0.001$), respectively. $_{tilt}$MOR gains were all significantly different between each group $F(2,22)=60.8$, $p<0.001$). $_{OVAR}$MOR bias of cKO group was significantly lower than cKO-GT and SHAM groups $F(2,22)=5.3$, $p=0.015$).

Table 2: Horizontal sinusoidal rotation

Frequency	0.2Hz	0.5Hz	0.8Hz	1Hz	1.5Hz
aVOR gain					
cKO	0.02±0.02	0.03±0.04	0.04±0.05	0.03±0.01	0.04±0.03
cKO-GT	0.31±0.08	0.63±0.09	0.66±0.12	0.71±0.11	0.91±0.19
SHAM	0.30±0.11	0.61±0.16	0.66±0.25	0.72±0.21	0.93±0.26
cKO versus cKO-GT	***0.036***	***<0.001***	***<0.001***	***<0.001***	***<0.001***
cKO versus SHAM	***0.043***	***<0.001***	***<0.001***	***<0.001***	***<0.001***
cKO-GT versus SHAM	*1*	*1*	*1*	*1*	*1*
aVOR phase					
cKO-GT	27.6±9.4	17.3±6.7	7.8±5.6	3.0±2.9	-8.9±4.8
SHAM	31.6±10.4	15.8±15.8	7.6±9.5	-1.3±4.0	-11.3±4.2
cKO-GT versus SHAM	*0.988*	*1*	*1*	*0.981*	*1*

All values are represented as mean ± SD (standard deviation). *aVOR* angular Vestibular-ocular reflex. Phase values of cKO are not reported because VAF < 0.5.

Table 3: Horizontal steps, static roll head tilt and OVAR

	Peak-velocity gain	Time constant	$_{tilt}$MOR	$_{OVAR}$MOR
cKO	0.19±0.18	0.46±0.36	0.04±0.09	0.02±0.01
cKO-GT	0.86±0.19	2.01±0.67	0.64±0.11	0.10±0.07
SHAM	0.84±0.15	2.05±0.69	0.49±0.11	0.12±0.06
cKO versus cKO-GT	***<0.001***	***<0.001***	***<0.001***	***0.017***
cKO versus SHAM	***<0.001***	***<0.001***	***<0.001***	***0.037***
cKO-GT versus SHAM	*0.969*	*0.992*	***0.024***	*0.924*

All values are represented as mean ± SD (standard deviation). Overall gain and time constant values correspond to the mean value of counter-clockwise and clockwise per- and post-rotatory values. Time constant is in seconds. $_{tilt}$MOR is reported as gain (slope value of vertical eye angle and head tilt degree). $_{OVAR}$MOR is reported with the mean bias value of CCW and CW rotations. *OVAR* Off-vertical axis rotation *MOR* maculo-ocular reflex.

Left and right peak-velocity gain were not statistically different (p=0.268), neither were left and right time constants (p=0.375), nor left and right $_{tilt}$MOR gains (p=0.185), nor clockwise and counter-clockwise $_{OVAR}$MOR bias, (p=0.239).

Discussion

In this model of *snap-25* cKO mice, we show that as for the cochlear system, the absence of snap-25 profoundly impairs vestibular function. This deficit was found in all VOR tests, including semi-circular canal function (aVOR), utricular function ($_{tilt}$MOR) and more complex vestibular function including velocity storage and $_{OVAR}$MOR. The cKO mice displayed coherent vestibular behaviour with the inability to swim or float and a body fold behaviour during tail hanging. Residual (very poor) function was quantified especially during the horizontal steps and OVAR stimulations compared to mice models of vestibular surgical destruction [14]. Both these tests use high velocity rotations (50°/s) and show that some form of baseline synaptic hair cell function is preserved, possibly thanks to other SNARE proteins.

After *snap-25* viral gene transfer in cKO mice, vestibular function was found to be statistically similar to SHAM mice, also in all of the VOR tests undertaken. No statistical difference was found concerning sidedness which confirms identical bilateral viral transfer after a unilateral trans-tympanic injection. Thus, gene transfer was a success bilaterally when administered at P2, suggesting that snap-25 is dispensable for vestibular organogenesis in the mouse, at least until the perinatal period.

Conclusion:

Our results show profound vestibular impairment in *snap-25* cKO mice, which can explain the severe behavioural anomalies. Mature vestibular hair cells seem to rely on the same SNARE complex for synaptic vesicular trafficking and membrane fusion, as the cochlear inner hair cells and especially the central neural system synapses. We also show a very clear success of gene transfer concerning vestibular function, which added to the rescued auditory function, is very promising for future treatment of inner ear synaptopathies linked to SNARE proteins.

References:

[1] S. Safieddine, A. El-Amraoui, and C. Petit, The auditory hair cell ribbon synapse: from assembly to function, *Annu. Rev. Neurosci.* **35** (2012), 509–528.

[2] R. Nouvian, J. Neef, A. V. Bulankina, E. Reisinger, T. Pangršič, T. Frank, *et al.*, Exocytosis at the hair cell ribbon synapse apparently operates without neuronal SNARE proteins, *Nat. Neurosci.* **14**(4) (2011), 411–413.

[3] P. Washbourne, P. M. Thompson, M. Carta, E. T. Costa, J. R. Mathews, G. Lopez-Benditó, *et al.*, Genetic ablation of the t-SNARE SNAP-25 distinguishes mechanisms of neuroexocytosis, *Nat. Neurosci.* **5**(1) (2002), 19–26.

[4] E. Caberlotto, V. Michel, I. Foucher, A. Bahloul, R. J. Goodyear, E. Pepermans, *et al.*, Usher type 1G protein sans is a critical component of the tip-link complex, a structure controlling actin polymerization in stereocilia, *Proc. Natl. Acad. Sci. U. S. A.* **108**(14) (2011), 5825–5830.

[5] M. Beraneck and K. E. Cullen, Activity of vestibular nuclei neurons during vestibular and optokinetic stimulation in the alert mouse, *J. Neurophysiol.* **98**(3) (2007), 1549–1565.

[6] M. Beraneck, M. Bojados, A. Le Seac'h, M. Jamon, and P. P. Vidal, Ontogeny of mouse vestibulo-ocular reflex following genetic or environmental alteration of gravity sensing, *PLoS One* **7**(7) (2012), e40414.

[7] F. França de Barros, J. Carcaud, and M. Beraneck, Long-term Sensory Conflict in Freely Behaving Mice, *J. Vis. Exp. JoVE* (144) (2019),.

[8] M. Beraneck and F. M. Lambert, Impaired perception of gravity leads to altered head direction signals: what can we learn from vestibular-deficient mice?, *J Neurophysiol* **102**(1) (2009), 12–4.

[9] M. Beraneck and E. Idoux, Reconsidering the Role of Neuronal Intrinsic Properties and Neuromodulation in Vestibular Homeostasis, *Front. Neurol.* **3** (2012),.

[10] J. S. Stahl, L. Averbuch-Heller, and R. J. Leigh, Acquired nystagmus, *Arch. Ophthalmol. Chic. Ill 1960* **118**(4) (2000), 544–549.

[11] J. Carcaud, F. França de Barros, E. Idoux, D. Eugène, L. Reveret, L. E. Moore, *et al.*, Long-Lasting Visuo-Vestibular Mismatch in Freely-Behaving Mice Reduces the Vestibulo-Ocular Reflex and Leads to Neural Changes in the Direct Vestibular Pathway, *eNeuro* **4**(1) (2017),.

[12] E. Idoux, M. Tagliabue, and M. Beraneck, No Gain No Pain: Relations Between Vestibulo-Ocular Reflexes and Motion Sickness in Mice, *Front. Neurol.* **9** (2018), 918.

[13] D. R. Calabrese and T. E. Hullar, Planar relationships of the semicircular canals in two strains of mice, *J. Assoc. Res. Otolaryngol. JARO* **7**(2) (2006), 151–159.

[14] F. Simon, D. Pericat, C. Djian, D. Fricker, F. Denoyelle, and M. Beraneck, Surgical techniques and functional evaluation for vestibular lesions in the mouse: unilateral labyrinthectomy (UL) and unilateral vestibular neurectomy (UVN), *J. Neurol.* (2020),.

[15] R. Romand, W. Krezel, M. Beraneck, L. Cammas, V. Fraulob, N. Messaddeq, *et al.*, Retinoic acid deficiency impairs the vestibular function, *J Neurosci* **33**(13) (2013), 5856–66.

[16] B. J. M. Hess and N. Dieringer, Spatial Organization of the Maculo-Ocular Reflex of the Rat: Responses During Off-Vertical Axis Rotation, *Eur. J. Neurosci.* **2**(11) (1990), 909–919.

[17] B. S. Oommen and J. S. Stahl, Eye orientation during static tilts and its relationship to spontaneous head pitch in the laboratory mouse, *Brain Res.* **1193** (2008), 57–66.

1.3.5. Conclusion

Ce travail montre que la protéine snap-25 est essentielle au bon fonctionnement vestibulaire mais aussi que le vestibule peut fonctionner normalement malgré l'absence de la protéine pendant l'organogénèse. Ces résultats sont complémentaires à ceux réalisés par l'équipe de l'Institut Pasteur sur les cellules ciliées internes cochléaires, qui montrent un effondrement des seuils auditifs chez la souris KO et une récupération partielle de la fonction auditive après transfert du gène *snap-25*.

Au total ces résultats montrent que la protéine snap-25 est essentielle pour la neurotransmission rapide des cellules ciliées labyrinthiques et que leur mécanisme SNARE est similaire à celui des autres synapses du système nerveux central.

2. Modèles murins de lésion vestibulaire

Cette deuxième partie de résultats expérimentaux concerne l'étude de l'altération de la fonction vestibulaire chez des souris *wild type*. Il s'agit d'entrainer des lésions vestibulaires par chirurgie ou par injection de produit ototoxique, soit pour valider un modèle de déficit vestibulaire chez la souris, soit pour étudier la fonction vestibulaire post-lésionnelle.

2.1. Article 4 : Description et comparaison des techniques chirurgicales de lésion vestibulaire chez la souris : labyrinthectomie et neurectomie du VIII

2.1.1. Contexte scientifique

L'étude la compensation vestibulaire est importante pour comprendre l'intégration multisensorielle, mais aussi pour explorer de nouvelles pistes thérapeutiques pour aider les patients présentant un déficit vestibulaire unilatéral. Plusieurs modèles de lésion vestibulaire unilatérale existent, notamment peu invasifs avec injection de produits ototoxiques par voie trans-tympanique. La lésion chirurgicale vestibulaire est plus lourde mais permet d'obtenir avec certitude une lésion totale et permanente de l'oreille interne. L'amélioration comportementale et vestibulaire post-lésionnelle est donc entièrement liée à la compensation vestibulaire dans ces modèles, sans aucune participation résiduelle ou guérison du côté lésionnel.

Les techniques opératoires ont déjà été rapportés sur plusieurs modèles animaux comme les grenouilles (Lambert and Straka, 2012), les poussins (Pollack et al., 2004), les rats (Hitier et al., 2016; Li et al., 2015; Péricat et al., 2017) ou les chats (Dutheil et al., 2009; Gacek and Schoonmaker, 1997; Schuknecht, 1982) ; mais aucune description détaillée n'a été réalisée chez la souris alors que ce modèle animal est l'un des plus utilisé dans le monde.

2.1.2. Buts de l'étude

Nous souhaitons décrire étape par étape la technique chirurgicale de labyrinthectomie unilatérale et neurectomie vestibulaire unilatérale chez la souris puis comparer ces deux méthodes chirurgicalement et concernant l'évolution post-lésionnelle de la fonction vestibulaire.

2.1.3. Résumé en français

Les lésions chirurgicales vestibulaires chez la souris permettent d'induire une perte unilatérale totale et définitive de la fonction vestibulaire, pour étudier les mécanismes et des pistes thérapeutiques lors

de la compensation vestibulaire. La technique la plus utilisée dans la littérature est la labyrinthectomie unilatérale (UL), mais il est également possible de réaliser une neurectomie vestibulaire unilatérale (UVN). Les deux techniques chirurgicales ont été réalisées sur deux groupes de 6 souris. La technique par UVN est plus lourde (taux de décès de 40%) que l'UL (15%) et avec un retentissement locomoteur plus important. La durée de la chirurgie de l'UL était également plus courte (16 minutes versus 21 minutes). Il n'y avait pas de différence significative de réflexe vestibulo-oculaire entre les deux groupes à J1 jusqu'à J28 post-lésion. Après un mois, le gain du VOR angulaire horizontal était stable autour de 0,4 pour les deux groupes, ains qu'un nystagmus résiduel battant du côté opposé à la lésion à environ 5 battements par minute. La fonction utriculaire montrait un début de récupération de la fonction contralatérale à la lésion à un mois. Pour étudier la compensation vestibulaire chez le rongeur, la lésion vestibulaire la plus simple à réaliser est la UL. La UVN est une méthode plus difficile et plus invasive permettant de détruire le ganglion de Scarpa, ce qui induit des mécanismes centraux de compensation plus important, avec notamment une dégénérescence wallérienne du nerf vestibulaire et une réaction inflammatoire du noyau vestibulaire.

2.1.4. Article original

Titre :

Surgical techniques and functional evaluation for vestibular lesions in the mouse: unilateral labyrinthectomy (UL) and unilateral vestibular neurectomy (UVN)

Auteurs :

François SIMON, David PERICAT, Cassandre DJIAN, Desdemona FRICKER, Françoise DENOYELLE, Mathieu BERANECK

Etat d'avancement :

Publié le 17/06/2020 : *Journal of Neurology* (IF = 4.204), (Simon et al., 2020)

doi: 10.1007/s00415-020-09960-8

Lien vers la vidéo des techniques chirurgicales :

https://link.springer.com/article/10.1007/s00415-020-09960-8#Sec16

Journal of Neurology
https://doi.org/10.1007/s00415-020-09960-8

ORIGINAL COMMUNICATION

Surgical techniques and functional evaluation for vestibular lesions in the mouse: unilateral labyrinthectomy (UL) and unilateral vestibular neurectomy (UVN)

François Simon[1,2] · David Pericat[3] · Cassandre Djian[1] · Desdemona Fricker[1] · Françoise Denoyelle[2] · Mathieu Beraneck[1]

Received: 3 April 2020 / Revised: 26 May 2020 / Accepted: 28 May 2020

Abstract

Objective Unilateral labyrinthectomy (UL) and unilateral vestibular neurectomy (UVN) are two surgical methods to produce vestibular lesions in the mouse. The objective of this study was to describe the surgical technique of both methods, and compare functional compensation using vestibulo-ocular reflex-based tests.

Methods UL and UVN were each performed on groups of seven and ten mice, respectively. Main surgical landmarks were the facial nerve, the external auditory canal and the sternomastoid and digastric muscles. For UL, the sternomastoid muscle was elevated to expose the mastoid, which was drilled to destroy the labyrinth. For UVN, the bulla was drilled opened and a transcochlear approach enabled the identification of the vestibulo-cochlear nerve exiting the brainstem, which was sectioned and the ganglion of Scarpa suctioned. Behaviour and vestibular function were analysed before surgery and at 1, 4, 7 days and at 1 month postlesion using sinusoidal rotation, off-vertical axis rotation, static head tilts and angular velocity steps.

Results UL is a faster and safer procedure than UVN (operative time 16.3 vs 20.5 min, $p=0.19$; survival rate 86% vs 60%, $p=0.25$). UVN was more severe with significantly worse behavioural scores at day 4 and day 7 ($p<0.001$). Vestibular compensation was overall similar during the first week and at 1 month (non-statistically significant difference).

Conclusion Both UL and UVN procedures can routinely be performed in the mouse with similar post-operative recovery and behavioural compensation. The operative risk of vascular or neurological damage is smaller in UL compared to UVN. UVN may be required for specific research protocols studying central cellular process specifically related to the destruction of the ganglion of Scarpa and following vestibular nerve degeneration.

Keywords Unilateral vestibular neurectomy · Unilateral labyrinthectomy · Mouse · Vestibular compensation · Surgery

Introduction

The first description by Flourens in 1824 of the behavioural symptoms that follow an inner ear lesion is a starting point in the field of vestibular research [1]. The study of vestibular lesions and compensation in different vertebrate species has helped to understand vestibular physiology and the capacity of the brain to cope with the loss of a sensory function [2–10]. Unilateral labyrinthectomy (UL) and unilateral vestibular neurectomy (UVN) are two surgical methods to produce vestibular lesions. These are more invasive than pharmacological methods but are also more radical and definite lesions which may be required in certain research protocols [11]. Surgical techniques need to be described in detail to be reproducible [12–18]. Some articles report the surgical methods for UL or UVN in other animal models (e.g. frogs

Electronic supplementary material The online version of this article (https://doi.org/10.1007/s00415-020-09960-8) contains supplementary material, which is available to authorized users.

✉ François Simon
f.simon@aphp.fr

✉ Mathieu Beraneck
Mathieu.beraneck@parisdescartes.fr

1 CNRS, Integrative Neuroscience and Cognition Center, Université de Paris, 75006 Paris, France

2 Department of Paediatric Otolaryngology, Hôpital Necker-Enfants Malades, AP-HP.Centre, Université de Paris, 75015 Paris, France

3 Laboratoire de Neurosciences Sensorielles et Cognitives, CNRS, UMR 7260, Aix Marseille Université, 13331 Marseille, France

Published online: 17 June 2020

[19], chicks [20], rats [21–23], or cats [24–26]) but not in the mouse. Yet mouse models are currently the most used worldwide, due to ease of use for genetic engineering or breeding, and ethical limitations when working with larger mammals. Surgery in the mouse is challenging due to its small size and specific anatomy. Here we provide a detailed step-by-step description of both UL and UVN in adult mice. Video-oculography was used to assess vestibular function following successful surgery, and to monitor vestibular compensation by quantitative measurements of the vestibulo-ocular reflex [11, 14, 27]. The objective of this study was an update of existing protocols for vestibular lesions, allowing the investigator to improve their effectiveness and safety, and reduce the duration of the surgery, critical for survival. We discuss differences in the two approaches to help choose between UL and UVN as adequate methods for a vestibular lesion.

Materials and methods

Ethics statement

A total of 17 male C57/BL6J mice, aged 10–30 weeks, was operated on, seven mice for UL and ten for UVN. Animals were used in accordance with the European Communities Council Directive 2010/63/EU. All efforts were made to minimize suffering and reduce the number of animals included in the study. All procedures were approved by the ethical committee for animal research of the University of Paris (CEEA.34).

Anaesthesia and peri-operative care

Anaesthesia and peri-operative care were identical for either UL or UVN procedure. A stock solution of anaesthesia was prepared including 1 ml Ketamine 100 mg/ml (Virbac, Carros, France), 500 µl Rompun® 2% (Bayer Vital GmbH, Leverkusen, Germany), and 8.5 ml physiological saline solution. A dosage of 100 mg/kg ketamine and 10 mg/kg xylazine, warmed to body temperature, was administered intraperitoneally at a volume of 10 µl/g of body weight.

After anaesthesia, sub-cutaneous injection of buprenorphine 0.3 mg/ml (Buprecare, Axience, Patin, France) was administered at a dose of 0.08 mg/kg of body weight. Local anaesthesia using Laocaïne® 2% (MSD Santé Animale, Beaucouzé, France) was administered sub-cutaneously at the surgical site at a dose of 2 mg/kg of body weight.

Artificial tears (Ocry-gel, TVM lab, Lempdes, France) were administered to both eyes. Loss of pedal withdrawal reflex of both hind paws was verified before incision, and was monitored during surgery. The cervical skin immediately below the ear was shaved and cleaned (Vétédine Solution, Vetoquinol, Magny-Vernois, France). Subcutaneous hydration was performed after the surgery and twice daily for 2 days.

Behaviour evaluation

Mouse behaviour was assessed before and after surgery on day 1, day 4, day 7 and day 28. Normal locomotor mouse behaviour was assessed: ability to swim (over a 30-s-long period), to groom, to move in the cage and to reach for food or water. Vestibular postural and locomotor impaired behaviour was assessed: head tilt (inclination of the head towards the lesioned side), tumbling (mouse rolling around its longitudinal axis towards the lesioned side), twirl (while the mouse is being held by the tail) and circling (stereotyped movement in circles around the mouse's hip). All eight items were quantified with a scale from 0 (normal behaviour, no deficit) to 3 (highest degree of abnormal behaviour), with a maximum deficit score of 24.

Vestibular function exploration using video-oculography

To perform head restrained vestibular exploration, a head post was surgically implanted 2 weeks before the vestibular lesion. Head implant surgery and peri-operative care have been described previously [28, 29]. Briefly, under gas anaesthesia (isoflurane), a small custom-built head holder was cemented (C&B Metabond) to the skull just anterior to the lambda landmark (see França de Barros et al. 2019 for a video tutorial [30]).

Vestibular function was explored before vestibular surgery and after surgery at day 1, day 4, day 7 and long-term day 28. As reported previously, [9, 28, 29, 31] all eye movements recordings were made in the dark using an infrared video system (ETL-200, ISCAN, Burlington, MA, USA), recording pupil and corneal reflection (CR) position.

Eye movements were recorded using non-invasive video-oculography [32]. The experimental set-up, apparatus and methods of data acquisition were similar to those described previously [29, 33, 34]. Briefly, mice were head-fixed at a ~ 30° nose-down position to align the horizontal canals with the yaw plane [35]. Animals were placed in a custom-built Plexiglas tube secured on the superstructure of a vestibular stimulator. The VOR tests were performed in a temperature-controlled room (21 °C) with all sources of light turned off except for computer screens. The turntable was further enclosed in a box to isolate the animal from any remaining light, with a final luminance inside the box < 0.02 lx. Myosis was induced with topical 2% pilocarpine applied 10 min before experimentation. Recorded eye and head position signals were sampled at 1 kHz, digitally recorded (CED power1401 MkII) using Spike 2 software

and later exported into the Matlab programming environment for off-line analysis (Matlab, The MathWorks).

i. Videonystagmography first recorded spontaneous eye movements without any vestibular stimulation, and number and direction of the nystagmus rate per minute were reported.
ii. Then, the angular horizontal vestibulo-ocular reflex (aVOR) was tested during horizontal sinusoidal rotation of the turntable (at 0.2; 0.5; 1 and 1.5 Hz; peak velocity 30°/s). Analysis was made on at least 10 cycles. Two parameters were extracted from the recordings: the gain and the phase. The gain was the ratio between the amplitude of the eye (response) and head (stimulus) rotations. Since the animal was head-fixed to the rotating table, head movements and table movements were identical. The phase was the temporal shift between the eye and table rotations, expressed in degrees as the ratio of the sinusoidal cycle (2 pi). Details for gain and phase calculation were reported in Carcaud et al. [33]. Values with VAF (variance-accounted-for) under 0.5 were discarded [28].
iii. The eye movements evoked by a specific stimulation of the otolith organs (maculo-ocular reflexes, MOR) were tested [36] using an off-vertical axis rotation (OVAR) as previously described [29]. Briefly, the axis of rotation was tilted from the vertical by 17°. Rotations were performed at a constant speed (50°/s) for at least 10 rotations both in clockwise (CW) and counter-clockwise (CCW) directions. Due to the inertial nature of the angular movement detection, a rotation at constant speed elicits a combined canalar and otolithic response at the onset of movement, however, after a few seconds only the otolithic component remains [29, 37]. Since gravitational acceleration acts vertically, this stimulation is equivalent to a continuous rotation (at 0.14 Hz) around the mouse's head of a 17° tilted constant linear acceleration stimulus (see Fig. 2b in Beraneck et al. [29]). For horizontal OVAR responses, quick-phases of reflexive eye movements were identified and not considered for analysis. During rotations, the velocity of horizontal slow phases is modulated (modulation, μ) around a constant bias (β). Both parameters (μ and β) were calculated from the sinusoidal fit of eye horizontal slow-phase velocity using the least-squares optimization of the equation:

$$SP(t) = \beta + \mu \bullet \sin\left[2\pi \bullet f_0 \bullet \left(t + t_d\right)\right]$$

where SP(t) is the slow-phase velocity, β is the steady-state bias slow phase velocity, μ is the modulation of eye velocity, f_0 is the frequency of table rotation, t_d is the dynamic lag time (in msec) of the eye movement with respect to the head movement. The bias (Maculo-ocular reflex Bias; MOR_B) is reported here as the main index of the otolithic response [29, 36]. Notably, MOR requires normal otolith function but also an efficient central velocity storage network.
iv. Static ocular counterroll (OCR) was studied: vertical pupil position according to the head tilt angle was measured first with the mouse maintained at a 0° horizontal position. The platform was then tilted into different roll positions, at 10°, 20°, 30°, 40° and 50° alternatively to the right and to the left. The platform was rotated manually and slowly to limit semi-circular canal stimulation. Measurements were made in a static position during at least 15 s to identify the stable pupil position. The vertical eye angle was then calculated from the raw vertical CR and pupil position [38]. The slope of a linear regression of both variables (vertical eye angle and head tilt degree) was calculated, for ispilesional (− 50°–0°) and contralateral (0°–50°) sides.
v. Finally, angular velocity steps in the horizontal plane (hsteps) were performed at a speed of 50°/s. The horizontal slow phase velocity decay was fitted to an exponential curve ($f(x) = a^*\exp(b^*x)$) and the time constant τ was then calculated as $\tau = -1/b$. The time constant of the slow phase exponential velocity decay was calculated at the start and stop of CW and CCW rotations. CCW-start and CW-stop, CCW-stop and CW-start, were combined to assess left and right vestibular functions, respectively.

Statistical analysis

Statistical analysis was made using XLstats (Addinsoft, New York, NY, USA). All data are reported as mean and standard deviation. Non-parametric means were compared with the Mann–Whitney test and proportions with the Fisher test. Repeated measures ANOVA was used, three-way to compare aVOR (lesion, time and frequency), two-way for ipsilateral and contralateral OVAR, angular velocity and static head-tilt stimulations and one-way for the behaviour score and nystagmus frequency count. Post-hoc comparisons were performed where appropriate using the Tukey HSD test. Values of $p < 0.05$ were considered significant.

Surgical techniques

Unilateral labyrinthectomy (UL) step-by-step surgical technique

The anaesthetised mouse was put in a side-lying position. A posterior incision of the skin following the external auditory

canal anteriorly was performed (Fig. 1). The sub-cutaneous fat was incised immediately to find the cartilaginous external auditory canal, to dissect along with it in an avascular plane. Four retractors were positioned to open the cavity.

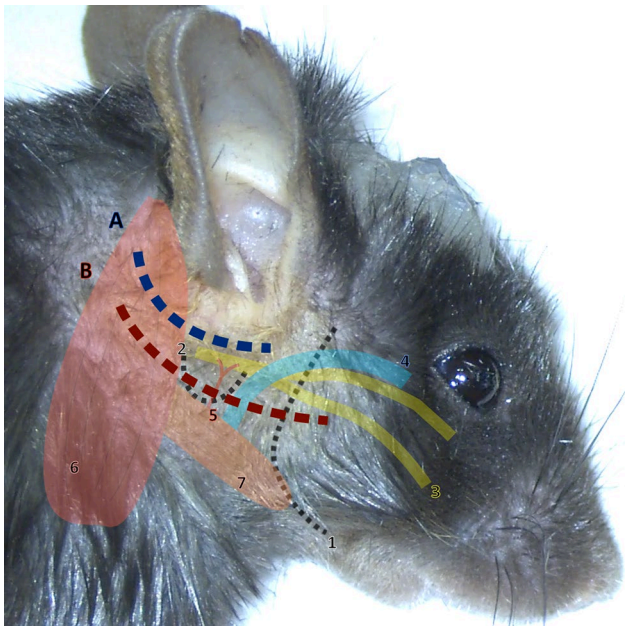

Fig. 1 Incisions and main anatomical landmarks. **a** (In blue): posterior incision for labyrinthectomy, **b** (in red): inferior incision for neurectomy. 1: mandible; 2: bulla; 3: facial nerve; 4: superficial temporal vein; 5: temporal artery; 6: sternomastoid muscle; 7: digastric muscle. The superficial temporal vein is one of the two main bleeding risks with the stapedial artery (not shown on this image). The mandible, facial nerve, sternomastoid and digastric muscles are key landmarks to find the bulla. The head post is visible on the mouse's skull, to be able to maintain the head in a fixed position during vestibular tests

The first visible anatomical landmarks were the facial nerve, external auditory canal and sternomastoid muscle. The facial nerve pointed towards the mastoid which was at this stage hidden beneath the sternomastoid muscle. Thus, the sternomastoid muscle was elevated from the bone, using a cautery to prevent bleeding. The muscle was then retracted posteriorly to expose the mastoid bone (Fig. 2a).

A 0.5 mm cutting burr was used to drill the mastoid, immediately posteriorly to the facial nerve foramen. The bone was not be drilled too posteriorly or superiorly as the cranial cavity would otherwise have been opened.

As the posterior semi-circular canal was opened (Fig. 2b), perilymphatic liquid oozed out and was suctioned as it can sometimes impair vision. The cavity was further opened with pointed instruments such as a hook or forceps. The drill would have been dangerous at this stage as it could have damaged the stapedial artery anteriorly or breached the cranial cavity posteriorly.

The contents (utricule, saccule and cupula) were suctioned until a clear and empty vestibular cavity was visible (Fig. 2c). The ganglion of Scarpa was left intact.

An absorbable gelatin compressed sponge was packed in the cavity and the skin was closed using simple interrupted absorbable 4–0 Vicryl (Ethicon, Somerville, NJ, USA).

Unilateral vestibular neurectomy (UVN) step-by-step surgical technique

The technique was adapted from the previously published neurectomy procedure in the rat [21]. The anaesthetised

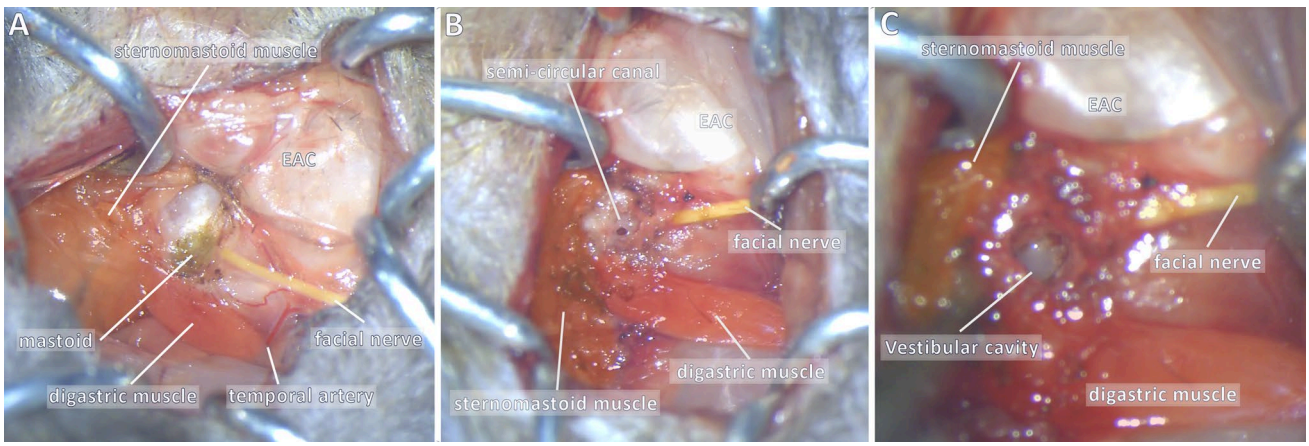

Fig. 2 Unilateral labyrinthectomy: key steps. Key steps are shown: **a** exposure of the mastoid bone, **b** drilling of the mastoid, **c** opening of the vestibular cavity. The mastoid bone (shown in green) can be exposed after elevation of the sternomastoid muscle posteriorly. The following anatomical landmarks stand out: sternomastoid muscle posteriorly (orange), digastric muscle inferiorly (red) and external auditory canal (EAC) superiorly (white). The facial nerve is of particular interest as the mastoid is immediately posterior to its foramen, and may be used as a guide to find the mastoid in an anterio-posterior direction. Great care must be taken not do damage the stapedial artery which is immediately anterior to the cavity. Full size figures are available online (Supplementary Figs. 1, 2, 3)

mouse was put in a side-lying position. A ventral incision (Fig. 1) was performed, from the posterior limit of the external auditory canal to the mandible. After initial dissection of the subcutaneous fat, the first anatomical landmarks encountered were the jaw and masseter muscle, upon which lay the two branches of the facial nerve. Four retractors were put in place to open the surgical field. The superior branch of the nerve was parallel and close to the superficial temporal vein, which was retracted anteriorly to be protected. The superior retractor retracted the skin above the masseter, and the posterior retractor retracted the sternomastoid muscle (Fig. 3a).

The bulla was found by following the facial nerve posteriorly: the facial nerve passed horizontally between the insertion of the cartilaginous external auditory canal and the bulla.

The two major anatomical landmarks to locate the bulla were the digastric muscle inferiorly and the external auditory canal (and facial nerve) superiorly. The digastric muscle masked the posterior half of the bulla and was retracted. The bulla was also immediately beneath and slightly posterior to the Y-shaped temporal artery (Fig. 3a), which was cauterised to prevent bleeding. The bony surface of the bulla was exposed using a pointed instrument such as a hook or forceps.

The bulla was drilled using a 0.5 mm cutting burr, the two main vascular risks being the superficial temporal vein anteriorly and the stapedial artery in the middle ear cavity posteriorly. The bulla was cautiously opened until the stapedial artery was visualised (Fig. 3b).

Next, the cochlea was drilled with the same burr, carefully so as not to damage the stapedial artery. Perilymphatic fluid was suctioned to find the cochlear nerve. Residual bone was cleared using a hook and the cochlear nerve was then followed to reach the vestibulo-cochlear nerve and the brainstem. The VIIIth nerve was sectioned using a hook and the ganglion of Scarpa suctioned (Fig. 3c), great care was taken not to damage the brainstem underneath. The ganglion of Scarpa was visible as a bulge of the nerve, and the procedure was thus a neurectomy of the vestibular ganglion neurons (and not a neurotomy).

Gelfoam was packed in the cavity and the skin was closed using simple interrupted absorbable 4–0 Vicryl (Ethicon, Somerville, NJ, USA).

Results

A total of seven mice underwent UL and ten underwent UVN. The survival rate was higher for UL (6/7 mice, 86%) than for UVN procedure (6/10 mice, 60%; $p = 0.252$). Concerning UL, one mouse did not wake up after anaesthesia, probably due to cardiogenic shock (no major bleeding during surgery). Concerning UVN, two mice died per-operatively, one immediately due to vascular damage and intense bleeding, and the other never woke up, with suspected continuous internal bleeding. The two other mice died post-operatively on day 3 and day 4, possibly due to neurological damage or cardiogenic shock. In none of the cases was there evidence for an infectious cause.

The mean age at surgery was 3.8 (range 2.5–6.3) and 4.5 (range 1.7–7.6) months, for UL and UVN, respectively. Mean operative time (from incision to closure) was 16.3 min (range 11–27) for UL and 20.5 min (range 18–25) for UVN, $p = 0.199$. 50% of UL and 100% of UVN had post-operative total right facial paralysis, although none of the nerves

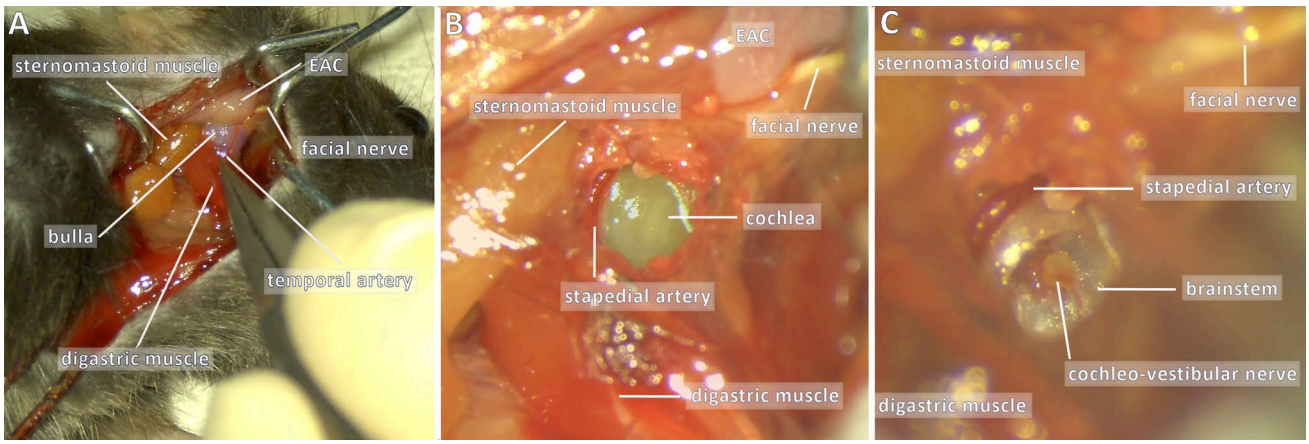

Fig. 3 Unilateral vestibular neurectomy: key steps. Key steps are shown: **a** exposing the bulla, **b** opening the bulla and **c** exposition the vestibulo-cochlear nerve. An important anatomical landmark is the facial nerve, which can be followed backwards and which runs superiorly to the bulla (purple). Other anatomical landmarks include inferiorly the digastric muscle (red), posteriorly the sternomastoid muscle (orange) and the external auditory canal (EAC). The temporal artery also marks the bulla as it runs immediately superficially to the bulla, and must be cauterised to correctly drill the bulla. Full size figures are available online (Supplementary Figs. 4, 5, 6)

were deliberately cut. Partial recuperation at 1 month was observed.

UL and UVN clinical follow-up

Initial clinical follow-up was identical in both UL and UVN mice. Before the animal regained full consciousness after anaesthesia, the following signs demonstrated a successful procedure: head tilted > 45° and body leaning towards the operated side, also the tail 90° bent towards the lesioned side. In the hours after surgery, the main behaviour indicating vestibular impairment was intense and frequent spontaneous tumbling (towards the operated side). The behavioural score was not statistically different at day 1 or after 1 month (Table 1), even though UL mice tended to recover more quickly than UVN mice (Fig. 4a). At day 4, all mice from both groups were able to reach for food and drink autonomously. The first vestibular symptom to disappear was tumbling (0/6 UL mice and 1/6 UVN mice at day 4). At 1 month, circling behaviour had completely disappeared in both groups, while all mice still had a noticeable head tilt (< 45°) and twirled when held by the tail towards the side of the lesion. None were able to swim or float (all presented with underwater tumbling).

UL and UVN functional follow-up

Recordings of spontaneous eye movements always showed a nystagmus with the rapid beat towards the opposite side of the lesion (no nystagmus reported before surgery).

Table 1 Behavioural score and nystagmus count

Lesion	UL	UVN	*p*
Behavioural score			
Before	0	0	–
Day 1	21.7 ± 1.2	21.3 ± 1.4	*0.522*
Day 4	**11.5 ± 1.4**	**14.8 ± 0.8**	**< 0.001**
Day 7	**7.2 ± 0.4**	**11.8 ± 1.2**	**< 0.001**
Day 28	5.0 ± 0.6	5.5 ± 0.5	*0.339*
Nystagmus count (beats per minute)			
Before	0	0	–
Day 1	**19 ± 11**	**31 ± 16**	***0.005***
Day 4	12 ± 9	18 ± 12	*0.161*
Day 7	7 ± 2	9 ± 5	*0.544*
Day 28	5 ± 1	8 ± 3	*0.746*

All values are represented as mean ± SD (standard deviation). Statistically significant values are in bold. Nystagmus count was calculated during spontaneous eye movement in the dark. Behavioural score and nystagmus count values were each compared between UL and UVN mice populations, using a two-way repeated ANOVA and post-hoc Tukey test, both model characteristics were (40, $p < 0.0001$)

UL unilateral labyrinthectomy, *UVN* unilateral vestibular neurectomy

Beats/min were maximal at day 1 (statistically higher after UVN lesions) and progressively decreased (Fig. 4b) for both UL and UVN lesions (Table 1). Sinusoidal rotations at 30°/s were overall not statistically different between UL and UVN lesions concerning gain or phase (Table 2). The gain values were at their lowest at day 1 with an improvement during the first week followed by a stabilisation (Fig. 4c). The gain was lower at day 28 compared to prelesion, for UL ($p = 0.095$, $p < 0.001$, $p = 0.001$) and for UVN ($p = 0.011$, $p < 0.001$, $p < 0.001$), at 0.2 Hz, 0.5 Hz and 1 Hz, respectively. Phase values were not interpretable at day 1 and day 4 with VAF < 0.5, and thus were excluded from the analysis (Table 2).

Static ocular counterroll as well as responses to off-vertical axis rotation (OVAR) and angular velocity steps were analysed during rotation towards the ipsilesional and contralesional sides (Table 3). Briefly, static ocular counterroll was reduced at day 28 compared to prelesion (Fig. 4d), for tilts towards the ipsi- and contralesional side in UL mice ($p < 0.001$, $p = 0.027$) and UVN mice ($p = 0.003$, $p = 0.159$). At day 28, concerning UL, the ocular counterroll measured during inclination towards the contralesional side was statistically greater than when measured during inclination towards the ipsilesional side (0.42 vs 0.19, $p = 0.033$). This difference in the ocular counterroll observed during rotation toward the ipsilateral or contralateral side did not reach significance for UVN (0.47 vs 0.34, $p = 0.220$). We noted an important skew deviation (with the contralesional eye moving upwards) at day 1 and day 4 in both UVN and UL.

Concerning OVAR, MOR gain was lowest at day 1, and remained statistically lower at day 28 compared to prelesion (Fig. 4e), for rotation towards the ipsilateral side but not towards the contralesional side for UL ($p < 0.001$, $p = 0.746$) and UVN ($p < 0.001$, $p = 0.729$). At day 28, gain for rotation towards the contralesional side was statistically higher than during rotations towards the ipsilesional side for UL (0.06 vs 0.00, $p = 0.011$) and for UVN (0.09 vs 0.01, $p < 0.001$). There was no statistically significant difference between UVN and UL mice (except at day 4 concerning rotation towards the contralesional side).

Lastly, angular velocity steps showed time constants of the velocity decay lowest at day 1, which remained significantly lower at day 28 compared to prelesion (Fig. 4e), for both rotations towards ipsi- and contralesional sides in UL ($p < 0.001$, $p = 0.013$) and in UVN mice ($p < 0.001$, $p < 0.001$). At day 28, in UL mice, the contralesional time constant was significantly higher than the ipsilesional time constant (2.51 vs 1.21, $p = 0.028$) but not for UVN (1.71 vs 1.07, $p = 0.277$). There was no statistically significant difference between UVN and UL mice.

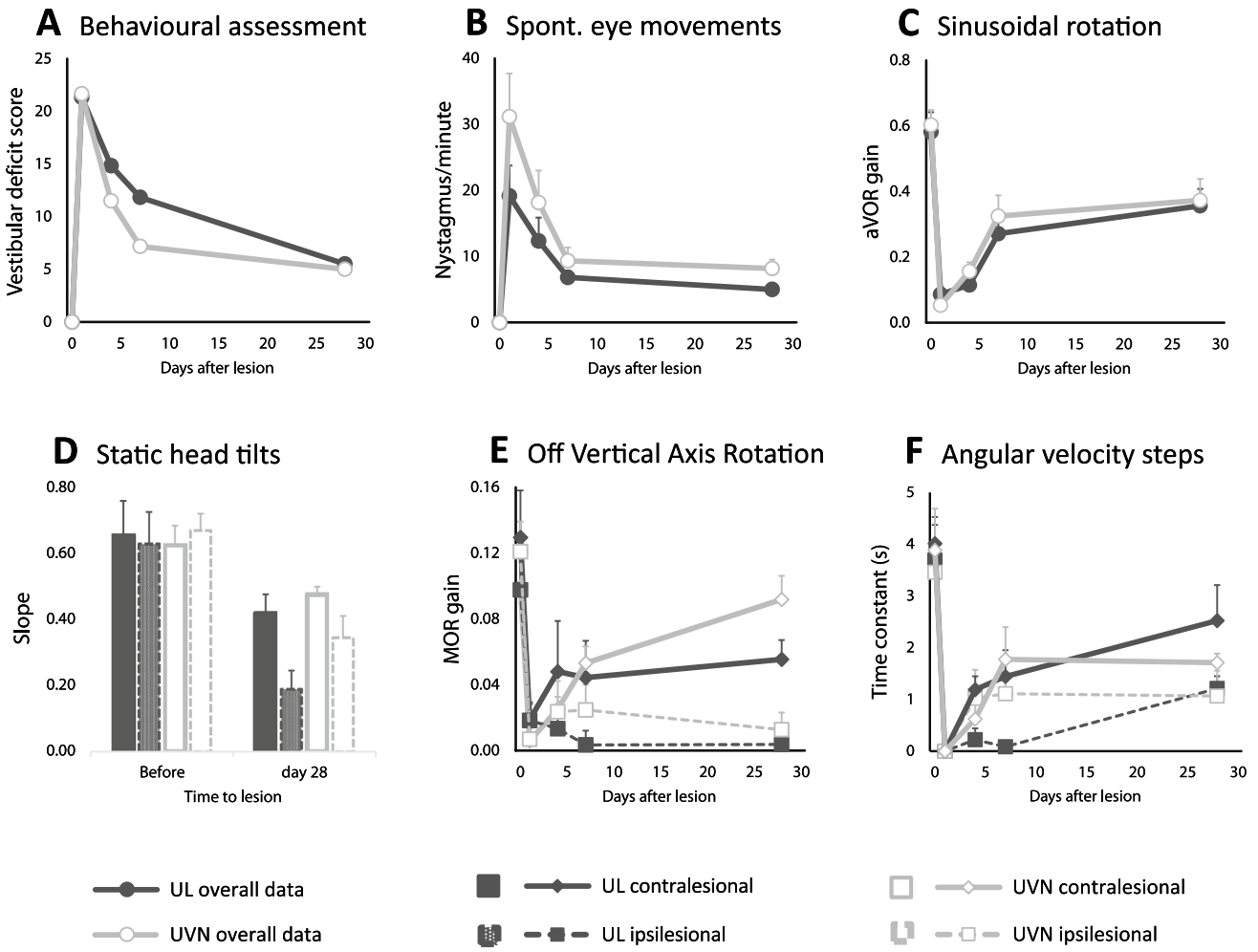

Fig. 4 Vestibular function and behaviour of unilateral vestibular neurectomy vs labyrinthectomy. All graphs show the five time points, before surgical lesion, and during follow-up at day 1, day 4, day 7 and day 28 after lesion. Points represented are mean value with SEM (standard error of the mean). Statistical comparisons are reported in Tables 1, 2 and 3. **a** Behavioural assessment: vestibular deficit score is represented (maximum score of 24). **b** Spontaneous eye movements: spontaneous recording of the pupil in the dark, reporting the number of nystagmus in 1 min. Fast-beating component was always directed towards the contralateral side of the lesion (left side). **c** Sinusoidal rotation: results showing aVOR gain for a 0.5 Hz and 30°/s stimulation, demonstrating horizontal semi-circular canal function. **d** Static ocular counterroll: the slope of a linear equation is reported, of static lateral tilt degree and vertical position of the pupil, corresponding to utricular function. Only the reliable post-lesion results are shown at day 28. **e** Off Vertical Axis Rotation: clockwise and counter-clockwise rotations in yaw plane of a 17° tilted platform at a rotation of speed of 50°/s. MOR gain is reported, which corresponds to a complex integration of otolithic function and velocity storage. **f** Angular velocity steps: horizontal steps including three full rotations in yaw plane at 50°/s were analysed for exponential velocity decay time constant (at start and stop of clockwise and counter-clockwise rotations). Ipsilesional stimulation (right side) corresponds to CW-start and CCW-stop, contralesional stimulation corresponds to CCW-start and CW-stop stimulations

Discussion

Two different surgical strategies to achieve complete vestibular lesions may be used in the mouse, UL (preganglionic lesion) which destroys the peripheral labyrinthine organs and UVN (postganglionic lesion) which destroys the first order vestibular neurons in the ganglion of Scarpa (and is thus a neurectomy of the VIIIth nerve). A summary of the differences is presented in Table 4.

In both cases, surgical landmarks are key, mainly the facial nerve, the external auditory canal and sternomastoid and digastric muscles, to swiftly find the mastoid (UL) or bulla (UVN). It is also important to operate with a good quality microscope (especially for the neurectomy step) and with an electric cautery. Ketamine-xylazine general anaesthesia was preferred as isoflurane is known to induce vasodilation [39]. In addition, in the mouse, manipulation of the head during surgery may be difficult with a facial mask or intubation necessary for isoflurane. Post-operative care is

Table 2 Canalar function (sinusoidal rotation at 30°/s): aVOR gain and phase

Frequency	0.2 Hz			0.5 Hz			1 Hz		
Lesion	UL	UVN	*p*	UL	UVN	*p*	UL	UVN	*p*
aVOR gain									
Before	0.25 ± 0.09	0.35 ± 0.12	*0.107*	0.58 ± 0.15	0.60 ± 0.11	*0.712*	0.66 ± 0.17	0.74 ± 0.20	*0.192*
Day 1	0.04 ± 0.04	0.03 ± 0.02	*0.865*	0.09 ± 0.05	0.05 ± 0.03	*0.570*	0.17 ± 0.11	0.10 ± 0.07	*0.294*
Day 4	0.05 ± 0.05	0.07 ± 0.06	*0.887*	0.12 ± 0.07	0.16 ± 0.07	*0.478*	**0.16 ± 0.07**	**0.29 ± 0.09**	***0.030***
Day 7	0.12 ± 0.08	0.16 ± 0.12	*0.514*	0.27 ± 0.12	0.33 ± 0.16	*0.364*	0.42 ± 0.21	0.48 ± 0.18	*0.335*
Day 28	0.16 ± 0.06	0.20 ± 0.07	*0.478*	0.36 ± 0.13	0.37 ± 0.16	*0.776*	0.47 ± 0.16	0.49 ± 0.13	*0.820*
aVOR phase									
Before	29.3 ± 8.3	24.5 ± 10.6	*0.649*	9.9 ± 8.7	10.2 ± 3.9	*0.982*	−2.2 ± 4.3	−0.2 ± 3.6	*0.855*
Day 1*	–	–	–	–	–	–	–	–	–
Day 4*	–	–	–	–	–	–	–	–	–
Day 7	39.6 ± 9.4	31.8 ± 22.0	*0.457*	39.2 ± 25.6	23.1 ± 13.2	*0.126*	23.2 ± 14.6	16.0 ± 25.0	*0.492*
Day 28	43.6 ± 6.3	26.3 ± 41.9	*0.102*	27.9 ± 6.1	25.0 ± 11.4	*0.393*	5.8 ± 7.5	6.8 ± 4.4	*0.925*

All values are represented as mean ± SD (standard deviation). Statistically significant values are in bold. Gain and phase values were each compared between UL and UVN mice populations, using a three-way repeated ANOVA and post-hoc Tukey test, gain model (150, $p < 0.0001$) and Phase model (90, $p < 0.0001$)

aVOR angular vestibular-ocular reflex, *UL* unilateral labyrinthectomy, *UVN* unilateral vestibular neurectomy

*Phase was not measurable at day 1 or day 4

Table 3 Velocity storage and otolithic function

Stimulation	Ipsilesional			Contralesional		
Lesion	UL	UVN	*p*	UL	UVN	*p*
Static head tilt, slope*						
Before	0.63 ± 0.24	0.67 ± 0.12	*0.701*	0.65 ± 0.25	0.62 ± 0.14	*0.781*
Day 1	0.16 ± 0.26	0.37 ± 0.27	*0.053*	0.57 ± 0.20	0.42 ± 0.28	*0.169*
Day 4	0.15 ± 0.11	0.28 ± 0.14	*0.221*	0.31 ± 0.28	0.34 ± 0.15	*0.814*
Day 7	0.19 ± 0.07	0.22 ± 0.12	*0.811*	0.41 ± 0.23	0.25 ± 0.18	*0.144*
Day 28	0.19 ± 0.14	0.34 ± 0.16	*0.493*	0.42 ± 0.14	0.47 ± 0.06	*0.143*
Off-vertical-axis rotation, MOR gain						
Before	0.10 ± 0.07	0.12 ± 0.04	*0.312*	0.13 ± 0.07	0.10 ± 0.05	*0.197*
Day 1	0.02 ± 0.02	0.01 ± 0.01	*0.274*	0.02 ± 0.03	0.01 ± 0.02	*0.292*
Day 4	0.01 ± 0.03	0.02 ± 0.02	*0.110*	**0.05 ± 0.08**	**0.03 ± 0.04**	***0.002***
Day 7	0.00 ± 0.02	0.02 ± 0.04	*0.222*	0.04 ± 0.05	0.05 ± 0.02	*0.702*
Day 28	0.00 ± 0.01	0.01 ± 0.03	*0.694*	0.06 ± 0.03	0.09 ± 0.04	*0.114*
Angular velocity steps, time constant (seconds)						
Before	3.69 ± 1.67	3.46 ± 1.27	*0.690*	4.01 ± 1.26	3.88 ± 1.97	*0.826*
Day 1	0.00 ± 0.00	0.00 ± 0.00	*1*	0.00 ± 0.00	0.00 ± 0.00	*1*
Day 4	0.22 ± 0.54	1.02 ± 1.35	*0.176*	1.19 ± 0.63	0.62 ± 0.91	*0.336*
Day 7	0.08 ± 0.15	1.11 ± 1.62	*0.084*	1.44 ± 1.24	1.77 ± 1.53	*0.576*
Day 28	1.21 ± 0.58	1.07 ± 1.20	*0.807*	2.52 ± 1.68	1.71 ± 0.43	*0.170*

All values are represented as mean ± SD (standard deviation). Statistically significant values are in bold. Static head tilt, Off-vertical-axis rotation (OVAR) and angular velocity steps values were each compared between UL and UVN mice populations, using a three-way repeated ANOVA and post-hoc Tukey test, all three model characteristics were (100, $p < 0.0001$)

UL unilateral labyrinthectomy, *UVN* unilateral vestibular neurectomy

*Slope of a linear regression of both variables (vertical eye angle and head tilt degree)

Table 4 Summary of differences between unilateral labyrinthectomy and unilateral vestibular neurectomy

Lesion	UL	UVN
Surgical procedure length	Shortest (16 min)*	Longest (21 min)*
Mouse survival rate	Satisfactory (86%)*	Poor (60%)*
Cochlea	Intact	Destroyed
Vestibular labyrinth	Destroyed	Intact
Ganglion of Scarpa	Intact	Destroyed (suctioned)
Type of lesion	Preganglionic lesion	Postganglionic lesion
Degeneration of afferent fibres	No	Yes
Behavioural score	Shorter recovery	Longer recovery
Vestibular function	Similarly impaired	Similarly impaired

*No statistically significant difference

paramount in both surgeries but especially UVN, to prevent dehydration (as mice are unable to drink on their own due to tumbling during the first 48 h) but also to prevent ipsilateral keratitis if the facial nerve was damaged. The auditory function cannot be preserved due to the surgical destruction of the labyrinth, especially in the UVN procedure and its transcochlear approach (thus was not tested in this study).

UVN surgery seemed more severe and aggressive than UL: the behavioural score was significantly higher at day 4 and 7 and the number of nystagmus beats per minute was higher; however, vestibular compensation followed a comparable time course, both after 1 week and at 1 month.

Thus, for the same overall vestibular deficit, in our hands UL is preferred, as the procedure is shorter and bleeding and neurological per-operative risks are reduced with higher survival rates compared to UVN.

The destruction of the vestibular neurons in UVN (postganglionic lesion) induces Wallerian degeneration of the entire vestibular nerve and an inflammatory response reaching the vestibular nuclei [21, 40, 41]. Indeed degeneration of afferent fibres seems to take place after post- but not preganglionic lesions [42]. Such intense inflammation may be key in certain research protocols, in which case the choice of UVN over UL is justified. This has been shown in research on central vestibular neurogenesis, where the neurogenic potential has been identified after UVN but not after UL or pharmacological vestibular lesions [24, 43–45].

Although this was not the main objective of the study, the small number of mice limits the fine interpretation of functional results especially concerning ipsilesional and contralesional data. Some hypothesis may be drawn from our statistics, as contralesional stimulation partially recuperated in most cases at 1 month, in line with previous reports [14]. Concerning overall vestibular function after a unilateral vestibular lesion, this study confirms other papers showing a fast functional compensation period which corresponds to rapid behavioural improvement during the first post-operative week (especially during the first 3 days), which tends to stabilise with a prolonged hypofunction and near-normal behaviour at 1 month, except swimming which did not recuperate [11, 28]. After initial poor bilateral MOR gain, gain improved in both UVN and UL mice at 1 month when the contralesional side was stimulated. The mechanism is unclear (it may reflect asymmetric otolith input to the central nervous system or interactions between semicircular canal-ocular and otolith-ocular reflexes) but it has been reported previously that the bias component remains either small or in an inappropriate direction during OVAR ipsilesional stimulation [46, 47]. Skew deviation is a well described vertical contralesional pupil elevation after peripheral vestibular lesions, whether of surgical, pharmacological or pathological origin [48, 49]. Regarding vertical eye position during static head tilt, skew deviation limited the capacity to measure the response, especially during tilts towards the contralesional side from day 1 to 4. Thus, the impairment was greatest at day 4 (UL) or 7 (UVN), and then partially recuperated. Lastly, concerning the canalar time constant measured during horizontal steps, there was no statistically significant difference between UL and UVN mice. However, UL contralesional values almost returned to perilesional values and were statistically different from ipsilesional values; whereas in UVN, ipsi- and contralesional values were not statistically different at 1 month. It is possible that the Wallerian degeneration of the nerve in UVN, inducing central vestibular nuclei inflammation, may impact velocity storage bilaterally, while UL remaining peripheral inputs allows for restoration of the response during rotation towards the contralesional side at 1 month. These hypotheses should be verified by dedicated studies.

Conclusion

UL and UVN are two reproducible surgical techniques to induce definite and total unilateral vestibular lesions. In both cases, surgical landmarks are key to quickly identify the vestibular system and protect blood vessels and the cranial cavity. These are mainly the facial nerve, the external auditory

canal and the sternomastoid and digastric muscles. UVN and UL induce similar behavioural and functional vestibular deficits during a 1-month follow-up period. Thus, UL should be preferred in most cases as the procedure seems technically safer and quicker, with a higher survival rate. UVN can, however, be required in certain research protocols as the ganglion of Scarpa is destroyed, and Wallerian degeneration may spread inflammation to the central vestibular nuclei.

Acknowledgements This work was supported by the University of Paris and the CNRS. MB and FS received support from Marc Boulet Audition. CD received support from the Association Française d'Otologie et Oto-neurologie (AFON). This study contributes to the IdEx Université de Paris ANR-18-IDEX-0001.

This manuscript is part of a supplement supported by the German Federal Ministry of Education and Research within the funding initiative for integrated research and treatment centers.

Compliance with ethical standards

Conflicts of interest The authors do not have any commercial or other association that might pose a conflict of interest.

References

1. Flourens P (1842) Recherches expérimentales sur les propriétés et les fonctions du système nerveux dans les animaux vertébrés. Ballière
2. Fluur E (1960) Vestibular compensation after labyrinthine destruction. Acta Otolaryngol 52:367–375. https://doi.org/10.3109/00016486009123163
3. Precht W, Shimazu H, Markham CH (1966) A mechanism of central compensation of vestibular function following hemilabyrinthectomy. J Neurophysiol 29:996–1010. https://doi.org/10.1152/jn.1966.29.6.996
4. Smith PF, Curthoys IS (1989) Mechanisms of recovery following unilateral labyrinthectomy: a review. Brain Res Brain Res Rev 14:155–180. https://doi.org/10.1016/0165-0173(89)90013-1
5. Dieringer N (1995) "Vestibular compensation": neural plasticity and its relations to functional recovery after labyrinthine lesions in frogs and other vertebrates. Prog Neurobiol 46:97–129
6. Dieringer N (2003) Activity-related postlesional vestibular reorganization. Ann N Y Acad Sci 1004:50–60
7. Curthoys IS (2000) Vestibular compensation and substitution. Curr Opin Neurol 13:27–30. https://doi.org/10.1097/00019052-200002000-00006
8. Cullen KE, Minor LB, Beraneck M, Sadeghi SG (2009) Neural substrates underlying vestibular compensation: contribution of peripheral versus central processing. J Vestib Res 19:171–182. https://doi.org/10.3233/VES-2009-0357
9. Beraneck M, Idoux E (2012) Reconsidering the role of neuronal intrinsic properties and neuromodulation in vestibular homeostasis. Front Neurol. https://doi.org/10.3389/fneur.2012.00025
10. Straka H, Zwergal A, Cullen KE (2016) Vestibular animal models: contributions to understanding physiology and disease. J Neurol 263(Suppl 1):S10–23. https://doi.org/10.1007/s00415-015-7909-y
11. Cassel R, Bordiga P, Carcaud J et al (2019) Morphological and functional correlates of vestibular synaptic deafferentation and repair in a mouse model of acute onset vertigo. Dis Model Mech. https://doi.org/10.1242/dmm.039115
12. Faralli A, Dagna F, Albera A et al (2016) Modifications of perineuronal nets and remodelling of excitatory and inhibitory afferents during vestibular compensation in the adult mouse. Brain Struct Funct 221:3193–3209. https://doi.org/10.1007/s00429-015-1095-7
13. Yamaoka Y, Abe C, Morita H (2018) Comparison among ultrasonic, electrical apparatus, and toxic chemicals for vestibular lesion in mice. J Neurosci Methods 295:58–67. https://doi.org/10.1016/j.jneumeth.2017.11.021
14. Beraneck M, McKee JL, Aleisa M, Cullen KE (2008) Asymmetric recovery in cerebellar-deficient mice following unilateral labyrinthectomy. J Neurophysiol 100:945–958. https://doi.org/10.1152/jn.90319.2008
15. Hubner PP, Khan SI, Migliaccio AA (2017) The mammalian efferent vestibular system plays a crucial role in vestibulo-ocular reflex compensation after unilateral labyrinthectomy. J Neurophysiol 117:1553–1568. https://doi.org/10.1152/jn.01049.2015
16. Gacek RR, Khetarpal U (1998) Neurotrophin 3, not brain-derived neurotrophic factor or neurotrophin 4, knockout mice have delay in vestibular compensation after unilateral labyrinthectomy. Laryngoscope 108:671–678. https://doi.org/10.1097/00005537-199805000-00009
17. Eron JN, Davidovics N, Della Santina CC (2015) Contribution of vestibular efferent system alpha-9 nicotinic receptors to vestibulo-oculomotor interaction and short-term vestibular compensation after unilateral labyrinthectomy in mice. Neurosci Lett 602:156–161. https://doi.org/10.1016/j.neulet.2015.06.060
18. Aleisa M, Zeitouni AG, Cullen KE (2007) Vestibular compensation after unilateral labyrinthectomy: normal versus cerebellar dysfunctional mice. J Otolaryngol 36:315–321
19. Lambert FM, Straka H (2012) The frog vestibular system as a model for lesion-induced plasticity: basic neural principles and implications for posture control. Front Neurol 3:42. https://doi.org/10.3389/fneur.2012.00042
20. Pollack SM, Popratiloff A, Peusner KD (2004) Vestibular ganglionectomy and otolith nerve identification in the hatchling chicken. J Neurosci Methods 138:149–155. https://doi.org/10.1016/j.jneumeth.2004.04.023
21. Péricat D, Farina A, Agavnian-Couquiaud E et al (2017) Complete and irreversible unilateral vestibular loss: a novel rat model of vestibular pathology. J Neurosci Methods 283:83–91. https://doi.org/10.1016/J.JNEUMETH.2017.04.001
22. Li P, Ding D, Gao K, Salvi R (2015) Standardized surgical approaches to ear surgery in rats. J Otol 10:72–77. https://doi.org/10.1016/j.joto.2015.03.004
23. Hitier M, Sato G, Zhang Y et al (2016) Anatomy and surgical approach of rat's vestibular sensors and nerves. J Neurosci Methods 270:1–8. https://doi.org/10.1016/j.jneumeth.2016.05.013
24. Dutheil S, Brezun JM, Leonard J et al (2009) Neurogenesis and astrogenesis contribution to recovery of vestibular functions in the adult cat following unilateral vestibular neurectomy: cellular and behavioral evidence. Neuroscience 164:1444–1456. https://doi.org/10.1016/J.NEUROSCIENCE.2009.09.048

25. Gacek RR, Schoonmaker JE (1997) Morphologic changes in the vestibular nerves and nuclei after labyrinthectomy in the cat: a case for the neurotrophin hypothesis in vestibular compensation. Acta Otolaryngol 117:244–249. https://doi.org/10.3109/00016489709117780
26. Schuknecht HF (1982) Behavior of the vestibular nerve following labyrinthectomy. Ann Otol Rhinol Laryngol Suppl 97:16–32
27. Faulstich M, van Alphen AM, Luo C et al (2006) Oculomotor plasticity during vestibular compensation does not depend on cerebellar LTD. J Neurophysiol 96:1187–1195. https://doi.org/10.1152/jn.00045.2006
28. Beraneck M, Cullen KE (2007) Activity of vestibular nuclei neurons during vestibular and optokinetic stimulation in the alert mouse. J Neurophysiol 98:1549–1565. https://doi.org/10.1152/jn.00590.2007
29. Beraneck M, Bojados M, Le Seac'h A et al (2012) Ontogeny of mouse vestibulo-ocular reflex following genetic or environmental alteration of gravity sensing. PLoS ONE 7:e40414. https://doi.org/10.1371/journal.pone.0040414
30. França de Barros F, Carcaud J, Beraneck M (2019) Long-term sensory conflict in freely behaving mice. J Vis Exp. https://doi.org/10.3791/59135
31. Beraneck M, Lambert FM (2009) Impaired perception of gravity leads to altered head direction signals: what can we learn from vestibular-deficient mice? J Neurophysiol 102:12–14. https://doi.org/10.1152/jn.00351.2009
32. Stahl JS, Averbuch-Heller L, Leigh RJ (2000) Acquired nystagmus. Arch Ophthalmol 118:544–549. https://doi.org/10.1001/archopht.118.4.544
33. Carcaud J, França de Barros F, Idoux E et al (2017) Long-lasting visuo-vestibular mismatch in freely-behaving mice reduces the vestibulo-ocular reflex and leads to neural changes in the direct vestibular pathway. eNeuro. https://doi.org/10.1523/ENEURO.0290-16.2017
34. Idoux E, Tagliabue M, Beraneck M (2018) No gain no pain: relations between vestibulo-ocular reflexes and motion sickness in mice. Front Neurol 9:918. https://doi.org/10.3389/fneur.2018.00918
35. Calabrese DR, Hullar TE (2006) Planar relationships of the semicircular canals in two strains of mice. J Assoc Res Otolaryngol 7:151–159. https://doi.org/10.1007/s10162-006-0031-1
36. Hess BJM, Dieringer N (1990) Spatial organization of the maculo-ocular reflex of the rat: responses during off-vertical axis rotation. Eur J Neurosci 2:909–919
37. Romand R, Krezel W, Beraneck M et al (2013) Retinoic acid deficiency impairs the vestibular function. J Neurosci 33:5856–5866. https://doi.org/10.1523/jneurosci.4618-12.2013
38. Oommen BS, Stahl JS (2008) Eye orientation during static tilts and its relationship to spontaneous head pitch in the laboratory mouse. Brain Res 1193:57–66. https://doi.org/10.1016/j.brainres.2007.11.053
39. Lenzarini F, Di Lascio N, Stea F et al (2016) Time course of isoflurane-induced vasodilation: a doppler ultrasound study of the left coronary artery in mice. Ultrasound Med Biol 42:999–1009. https://doi.org/10.1016/j.ultrasmedbio.2015.11.026
40. Gaudet AD, Popovich PG, Ramer MS (2011) Wallerian degeneration: gaining perspective on inflammatory events after peripheral nerve injury. J Neuroinflammation 8:110. https://doi.org/10.1186/1742-2094-8-110
41. Conforti L, Gilley J, Coleman MP (2014) Wallerian degeneration: an emerging axon death pathway linking injury and disease. Nat Rev Neurosci 15:394–409. https://doi.org/10.1038/nrn3680
42. Kunkel AW, Dieringer N (1994) Morphological and electrophysiological consequences of unilateral pre- versus postganglionic vestibular lesions in the frog. J Comp Physiol A 174:621–632. https://doi.org/10.1007/BF00217383
43. Dutheil S, Lacour M, Tighilet B (2011) Neurogenic potential of the vestibular nuclei and behavioural recovery time course in the adult cat are governed by the nature of the vestibular damage. PLoS ONE 6:e22262. https://doi.org/10.1371/journal.pone.0022262
44. Dutheil S, Escoffier G, Gharbi A et al (2013) GABA(A) receptor agonist and antagonist alter vestibular compensation and different steps of reactive neurogenesis in deafferented vestibular nuclei of adult cats. J Neurosci 33:15555–15566. https://doi.org/10.3389/fnint.2013.00087
45. Tighilet B, Chabbert C (2019) Adult neurogenesis promotes balance recovery after vestibular loss. Prog Neurobiol 174:28–35. https://doi.org/10.1016/j.pneurobio.2019.01.001
46. Furman JM, Schor RH, Kamerer DB (1993) Off-vertical axis rotational responses in patients with unilateral peripheral vestibular lesions. Ann Otol Rhinol Laryngol 102:137–143. https://doi.org/10.1177/000348949310200211
47. Sugita-Kitajima A, Koizuka I (2014) Evaluation of the vestibulo-ocular reflex using sinusoidal off-vertical axis rotation in patients with canal paresis. Auris Nasus Larynx 41:22–26. https://doi.org/10.1016/j.anl.2013.04.014
48. Vibert D, Häusler R, Safran AB, Koerner F (1996) Diplopia from skew deviation in unilateral peripheral vestibular lesions. Acta Otolaryngol 116:170–176. https://doi.org/10.3109/00016489609137816
49. Ng D, Fouladvand M, Lalwani AK (2011) Skew deviation after intratympanic gentamicin therapy. Laryngoscope 121:492–494. https://doi.org/10.1002/lary.21279

2.1.5. Conclusion

La labyrinthectomie unilatérale et la neurectomie vestibulaire unilatérale sont deux techniques reproductibles et fiables de lésion chirurgicale, complète et définitive, du vestibule chez la souris. La labyrinthectomie est la technique la plus rapportée dans la littérature, étant la plus facile à réaliser et la moins traumatique. Cependant la neurectomie vestibulaire est une lésion post-ganglionnaire induisant une dégénérescence du neurone primaire vestibulaire, nécessaire dans certains protocoles expérimentaux. D'un point de vu chirurgical, les deux techniques nécessitent une bonne connaissance de l'anatomie pour limiter le risque de lésion vasculaire et réussir une lésion vestibulaire en limitant la durée du geste.

2.2. Article 5 : Développement d'un modèle de lésion vestibulaire transitoire chimique au kaïnate et comparaison à une lésion chirurgicale par neurectomie du VIII

2.2.1. Contexte scientifique

Les cliniciens manquent de traitements efficaces et spécifiques pour prendre en charge les vertiges vestibulaires. Dans le même temps, les chercheurs ne disposent pas de modèles animaux reproduisant fidèlement les différentes étiologies vestibulaires. Pour répondre à ces deux défis, il convient de développer des modèles animaux représentatifs des troubles vestibulaires aigus ou chroniques rencontrés chez l'Homme en caractérisant comment une affection de l'oreille interne conduit à des troubles oculomoteurs et posturaux plus ou moins persistants, puis en décrivant les atteintes neurales associées au niveau périphérique (organes vestibulaires) et central (nerf vestibulaire, cervelet et tronc cérébral).

La neuroinflammation est la principale hypothèse physiopathologique pouvant expliquer les atteintes vestibulaire périphérique, avec des différentes localisations possibles sur le trajet du nerf vestibulaire jusqu'au vestibule (Rauch, 2001; Richard and Linthicum, 2012). Par ailleurs la synapse, zone de contact entre le nerf afférent et la cellule ciliée a été considérée comme l'une des zones les plus fragiles de l'oreille interne (Hegemann and Wenzel, 2017; Lysakowski and Goldberg, 1997).

Pour créer un nouveau modèle de souris permettant de simuler une atteinte neuroinflammatoire transitoire, des lésions chroniques excitotoxiques du vestibule seront réalisées chez des souris adultes. L'excitotoxicité est un mécanisme fréquent de destruction neuronale lié à une surexcitation des neurones et à l'afflux de calcium intracellulaire. L'injection de Kaïnate (TTK), un agoniste de récepteur glutamate, dans l'oreille interne par voie trans-tympanique, entrainerait des lésions synaptiques et pourrait constituer un modèle expérimental d'invalidation temporaire de la

transduction vestibulaire. Ces invalidations temporaires permettraient de mimer des crises aiguës de vertiges.

2.2.2. Buts de l'étude

Développer un nouveau modèle murin de lésion vestibulaire partielle et transitoire par désafférentation synaptique des cellules ciliées et le comparer au modèle de lésion chirurgicale complète et définitive par neurectomie du VIII.

2.2.3. Résumé en français

Un nouveau modèle de lésion vestibulaire partielle et temporaire par une injection rétro-tympanique de kaïnate (TTK) a été développé pour permettre l'étude de différents mécanismes de compensation ou de nouvelles thérapeutiques accélérant la compensation vestibulaire. L'étude a comparé 11 souris avec injection unilatérale de TTK et 6 souris avec neurectomie unilatérale du VIII (UVN), contrôlés par 4 et 6 souris SHAM respectivement (injection rétro-tympanique de NaCl pour le TTK et chirurgie jusqu'à l'ouverture de la bulle pour les UVN). Le TTK (agoniste de récepteur glutamate) entraine une désafférentation sélective des synapses entre les cellules ciliées et le neurone vestibulaire primaire, confirmé par analyse microscopique par immunomarquage. L'étude montre que la lésion chimique par injection trans-tympanique de TTK est un bon modèle de lésion partielle et réversible du système vestibulaire périphérique. Ces souris présentaient une diminution des réflexes vestibulo-oculaires ainsi que des troubles posturaux et locomoteurs. Les gains des VOR ont chuté d'approximativement 50% quatre heures après l'injection avec une récupération progressive de la fonction vestibulaire dès J1 jusqu'à une récupération complète à J7. Leur récupération était complète, à la fois en termes de disparition du nystagmus spontané, récupération des fonctions canalaires et otolithiques. Les souris avec neurectomie du VIII avaient une fonction vestibulaire significativement pire ($p<0,001$) avec une fonction nulle à J1 et une récupération partielle de la fonction vestibulaire évaluée à 45% à 3 semaines.

2.2.4. Article original

Titre :

Morphological and functional correlates of vestibular synaptic deafferentation and repair in a mouse model of acute-onset vertigo

Auteurs :

Raphaelle CASSEL, Pierrick BORDIGA, Julie CARCAUD, François SIMON, Mathieu BERANECK, Anne LE GALL, Anne BENOIT, Valentine BOUET, Bruno PHILOXENE, Stéphane BESNARD, Isabelle WATABE, David PERICAT, Charlotte HAUTEFORT, Axel ASSIE, Alain TONETTO, Jonas DYHRFJELD-JOHNSEN, Jordi LLORENS , Brahim TIGHILET, Christian CHABBERT

En collaboration avec Christian CHABBERT (Aix Marseille Université, CNRS, UMR 7260, Laboratoire de Neurosciences Sensorielles et Cognitives - Equipe Physiopathologie et Thérapie des Désordres Vestibulaires, Marseille, 13000 France)

Etat d'avancement :

Publié le 15/07/2019 : *Disease Models & Mechanisms* (IF = 4.028), (Cassel et al., 2019)

doi: 10.1242/dmm.039115

© 2019. Published by The Company of Biologists Ltd | Disease Models & Mechanisms (2019) 12, dmm039115. doi:10.1242/dmm.039115

RESEARCH ARTICLE

Morphological and functional correlates of vestibular synaptic deafferentation and repair in a mouse model of acute-onset vertigo

Raphaelle Cassel[1,*], Pierrick Bordiga[1,*], Julie Carcaud[2], François Simon[2,3], Mathieu Beraneck[2,3], Anne Le Gall[4], Anne Benoit[4], Valentine Bouet[4], Bruno Philoxene[4], Stéphane Besnard[4], Isabelle Watabe[1], David Pericat[1], Charlotte Hautefort[5], Axel Assie[6], Alain Tonetto[6], Jonas Dyhrfjeld-Johnsen[7], Jordi Llorens[8], Brahim Tighilet[1] and Christian Chabbert[1,‡]

ABSTRACT

Damage to cochlear primary afferent synapses has been shown to be a key factor in various auditory pathologies. Similarly, the selective lesioning of primary vestibular synapses might be an underlying cause of peripheral vestibulopathies that cause vertigo and dizziness, for which the pathophysiology is currently unknown. To thoroughly address this possibility, we selectively damaged the synaptic contacts between hair cells and primary vestibular neurons in mice through the transtympanic administration of a glutamate receptor agonist. Using a combination of histological and functional approaches, we demonstrated four key findings: (1) selective synaptic deafferentation is sufficient to generate acute vestibular syndrome with characteristics similar to those reported in patients; (2) the reduction of the vestibulo-ocular reflex and posturo-locomotor deficits mainly depends on spared synapses; (3) damaged primary vestibular synapses can be repaired over the days and weeks following deafferentation; and (4) the synaptic repair process occurs through the re-expression and re-pairing of synaptic proteins such as CtBP2 and SHANK-1. Primary synapse repair might contribute to re-establishing the initial sensory network. Deciphering the molecular mechanism that supports synaptic repair could offer a therapeutic opportunity to rescue full vestibular input and restore gait and balance in patients.

KEY WORDS: Vestibule, Synapses, Excitotoxicity, Plasticity, Vestibular disorders

INTRODUCTION

Acute unilateral vestibulopathy (AUV) has well-defined clinical features, including severe vertigo attacks, static and dynamic imbalances, spontaneous nystagmus, nausea and vomiting (Strupp et al., 2004; Strupp and Magnusson, 2015). Information is still lacking on the aetiology, the pathophysiological processes involved and the specific anatomical substrate that is affected, as well as on the correlation between tissue lesions and the occurrence of the various symptoms that constitute the vestibular syndrome. The neuroinflammatory hypothesis has been largely proposed based on the suspicion of inflammatory foci along the different branches of the vestibular nerve (Ruttin, 1909; Rauch, 2001; Richard and Linthicum, 2012). With the evolution of methods for vestibular functional evaluation, questions have been increasingly raised regarding the precise anatomical locations of the lesions that cause AUV symptoms. Recently, the hypothesis of an intralabyrinthine origin has been proposed (Hegemann and Wenzel, 2017).

The area of contact between the inner ear hair cells and the fibres forming the eighth cranial nerve is considered the most vulnerable area of the inner ear (Liberman and Kujawa, 2017). In the cochlea, selective damage to the primary auditory synapses has been implicated in acquired sensorineural hearing loss. A recent histopathological quantitative analysis of the aged human inner ear confirmed previous observations in animals, which suggested that cochlear synaptopathy and the degeneration of cochlear nerve peripheral axons (despite near-normal hair cell populations) might be an essential component of human age-related hearing loss (Viana et al., 2015). In the vestibule, direct evidence of primary synapse damage under pathological conditions or as a result of ageing is lacking. It has been proposed, however, that the impairment of primary synapses might be involved in vestibular neuritis, labyrinthitis, vertigo of ischaemic origin and Menière disease (Rauch, 2001; Halmagyi et al., 2010; Foster and Breeze, 2013).

Aiming to decipher the correlation between selective damage to the primary vestibular synapses and the occurrence of AUV symptoms, we induced unilateral vestibular excitotoxic lesions in young adult mice through the transtympanic administration of kainic acid (TTK), as previously reported (Cassel et al., 2018). Using light and transmission electron microscopy (TEM), we performed a thorough histological analysis of the damage within the inner ear at different time points, over a period spanning the first hours following lesion induction and up to 3 weeks later. To quantitatively evaluate the proportion of deafferented synapses following the TTK administration, we performed immunostaining for CtBP2 (RIBEYE) and SHANK-1, two synaptic proteins present, respectively, in the inner ear hair cells presynaptic ribbons (Khimich et al., 2005) and in the glutamatergic postsynaptic density (PSD) of their cognate afferent fibres (Huang et al., 2012; Braude et al., 2015). In parallel, video-oculography was used to quantify the occurrence of the nystagmus, as well as the angular vestibulo-ocular reflex (aVOR) and maculo-ocular reflex (MOR), at each time point following the induction of the vestibular excitotoxic lesion, according to previously described protocols (Beraneck and Idoux, 2012; Carcaud et al., 2017). Alterations in gait and balance and in

[1]Aix Marseille Université, CNRS, UMR 7260, Laboratoire de Neurosciences Sensorielles et Cognitives - Equipe Physiopathologie et Thérapie des Désordres Vestibulaires, Marseille, 13000 France. [2]Integrative Neuroscience and Cognition Center, UMR 8002, CNRS, 75006 Paris, France. [3]Sorbonne Paris Cité, Université Paris Descartes, 75006 Paris, France. [4]INSERM U1075, Caen, France. [5]Hôpital Lariboisière, 75010 Paris, France. [6]Aix-Marseille Université, CNRS, Centrale Marseille, FSCM (FR1739), PRATIM, Marseille, 13000 France. [7]Sensorion, Montpellier, 34000 France. [8]Universitat de Barcelona, 08907 Barcelona, Spain.
*These authors contributed equally to this work

‡Author for correspondence (christian.chabbert@univ-amu.fr)

J.L., 0000-0002-3894-9401; C.C., 0000-0003-3932-0223

Received 29 January 2019; Accepted 6 June 2019

Disease Models & Mechanisms (2019) 12, dmm039115. doi:10.1242/dmm.039115

the general behaviour of the animals were also evaluated by specific behavioural testing following previously described methods (Cassel et al., 2018). The two types of functional evaluation were also performed in adult mice after unilateral vestibular neurectomy (UVN) to compare the functional consequences of transient versus permanent unilateral vestibular loss.

The parallel analysis of the temporal evolution of vestibular histological lesions and the resulting functional alterations allows for the evaluation of the specific contribution of peripheral synaptic plasticity to the occurence of the vertigo syndrome. The data demonstrate that synaptic deafferentation is sufficient to produce vertigo symptoms and its associated deficits with a time course of development and recovery that resembles the clinical situation. In turn, the study highlights the primary vestibular synapses as areas that are highly exposed to excitotoxic damage and sets the stage for future pharmacological studies on the development of efficient therapeutic countermeasures.

RESULTS

Induction of peripheral vestibular excitotoxic lesions

TTK administration was performed in adult mice of both sexes, according to a recently described method (Cassel et al., 2018). Histological and functional evaluations were performed on groups of naive and lesioned animals at several time points (4 h, 24 h, 48 h, 72 h, 1 week, 2 weeks and 3 weeks) following vestibular excitotoxicity induction (Fig. 1).

TTK administration induces the transient deafferentation of primary vestibular synapses

Light microscopy and TEM examination of fixed tissue from the vestibular endorgans revealed histological features characteristic of excitotoxic damage in both the utricle (Fig. 2 and Fig. S1) and the crista ampullaris (Fig. S2). Utricles from the sham-injected ears (which received vehicle without kainic acid) and contralateral ears showed normal ultrastructural features (Fig. 2A,B). By 4 h after TTK administration, most of the afferent nerve terminals of the Scarpa's ganglion neurons were highly swollen, with large vacuoles evident along the hair cell membranes throughout the sensory epithelia (Fig. 2C). Many hair cells were distorted owing to the size of the swollen nerve terminals and were sometimes no longer identifiable as type I or type II hair cells with regard to their morphology. Supporting cells were also squeezed, although their nuclei remained in the normal position. Membrane disruptions in damaged afferent terminals were often observed (Fig. S1). These histopathological features of excitotoxic damage were no longer visible in the utricle 1 week after the onset of the lesion, and the two types of hair cells were easily recognisable by their respective calyx and bouton afferent contacts and were morphologically distinct from the supporting cells (Fig. 2D). A detailed examination revealed normal ultrastructural features in both bouton (Fig. 2E) and calyx (Fig. 2F) afferents; however, some of the calyx endings showed discontinuity or a fragmented appearance (Fig. S1). In the cristae (Fig. S2), substantial swelling of afferents was observed 4 h after TTK administration, but this swelling was concentrated in the central part of the sensory epithelium. As in the utricle, the lesions in the crista were largely repaired 1 week after TTK administration. Together, these observations confirmed that, as previously reported in the rat (Brugeaud et al., 2007; Dyhrfjeld-Johnsen et al., 2013; Gaboyard-Niay et al., 2016), TTK administration in adult mice induced transient and specific damage to the synaptic contacts between the vestibular hair cells and their cognate nerve fibres arising from primary vestibular neurons.

To quantitatively assess the magnitude of synapse deafferentation following TTK administration, fixed tissue from the vestibular endorgans was immunostained for CtBP2 (a component of the inner-ear hair cells presynaptic ribbons) and SHANK-1 (a scaffold protein of the glutamatergic postsynaptic density of excitatory synapses). Using 3D confocal microscopy acquisition and image analysis, we extracted the position of each CtBP2-positive fluorescent spot and evaluated its distance from the nearest neighbouring SHANK-1-positive fluorescent spot within observation fields of $4.5e^{-03}$ mm^2, chosen in the central part of both the utricle (extra-striolar region) and the hemi-crista. Figure 3 illustrates the CtBP2 and SHANK-1 expression at a schematically represented vestibular bouton synapse (Fig. 3A), the location of a selected observation field in the utricular macula (Fig. 3B), the fluorescent spots detected using *z*-stack compilation 3D reconstruction with IMARIS software in a representative observation field (Fig. 3C) and the characteristic expression of the CtBP2 and SHANK-1 fluorescence at a calyx synapse (Fig. 3D), both distantly localised and colocalised (Fig. 3E,F). The analysis of the distances between all CtBP2- and SHANK-1-labelled pre- and postsynaptic structures revealed a subpopulation of fluorescent spots separated by 1 µm or less (Fig. 3G). A previous evaluation of the distances between presynaptic dense bodies and the postsynaptic densities in the rodent vestibular endorgans (Sadeghi et al., 2014) suggests that this population corresponds to pre- and postsynaptic proteins at intact primary vestibular synapses. In the sham vehicle-injected mice, 40% of the distances between pre- and postsynaptic proteins in the utricle were ≤1 µm and 75% were ≤2 µm (Fig. 3H). By 4 h after vestibular TTK lesion, only 15% of the co-labelling was ≤1 µm apart, 50% was ≤2 µm apart and 80% was ≤3 µm apart. Conversely, 3 weeks after

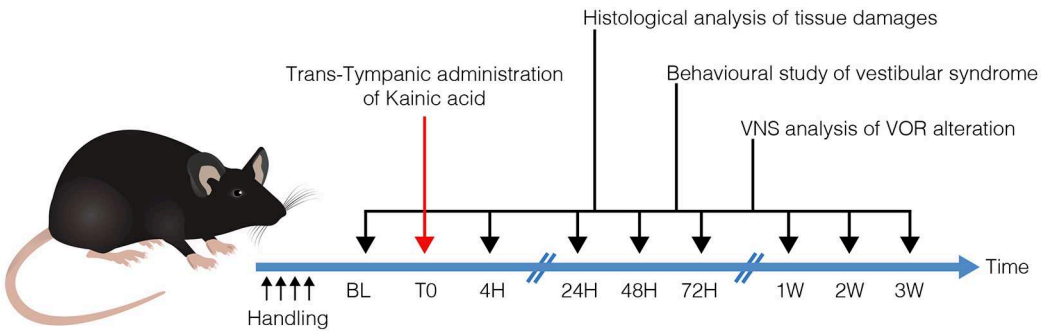

Fig. 1. Operational diagram used in the study. Following TTK (T0), histological and functional analyses were performed at each of the indicated time points. Histological analysis of inner ear tissues was performed using TEM. Assessment of posturo-locomotor alterations was performed using specific behavioural testing. aVOR alterations were measured using video-oculography. BL, base line; VNS, videonystagmoscopy.

Disease Models & Mechanisms (2019) 12, dmm039115. doi:10.1242/dmm.039115

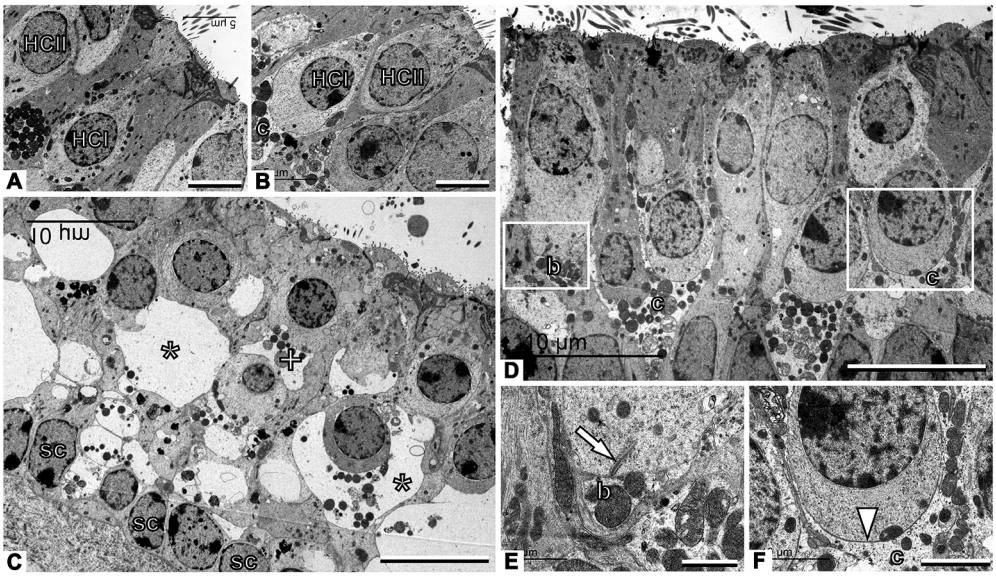

Fig. 2. TEM observation of vestibular primary synapses following TTK in the utricle. (A,B) Sham vestibular epithelium. Type I hair cells (HCI) are recognised by their amphora-like shape and the calyx afferent (c) encasing the cell body. Type II hair cells (HCII) have a more cylindrical shape and no calyx afferent. (C) Afferents are greatly swollen and the structure of the epithelium is completely distorted 4 h after TTK. Some swollen afferents probably corresponded to calyx terminals (*), whereas others are more likely to correspond to bouton terminals (+). Note the row of supporting cell nuclei (sc) just above the basal membrane of the epithelium. (D) The epithelium has grossly recovered a control-like appearance 1 week after TTK. (E) Higher magnification of the area marked with the left box in D, showing control-like ultrastructure including a presynaptic ribbon (arrow) in a type II hair cell facing a postsynaptic bouton afferent (b). (F) Higher magnification of the area marked with the right box in D, showing a contact between a type I hair cell and the calyx afferent contacting it. The arrowhead points to the calyceal junction, a prominent characteristic of this contact in healthy and mature epithelia. Sample: n=3 in each group. Scale bars: 5 µm (A,B), 10 µm (C,D), 1 µm (E) and 2 µm (F).

the induction of vestibular lesion, 40% and 80% of the co-labelling were once again found to be ≤1 µm apart and ≤2 µm apart, respectively. Together, these observations demonstrated that, after the induction of an excitotoxic synaptic lesion, the distance between the pre- and postsynaptic proteins increased significantly, probably signifying the deafferentation of vestibular hair cells. This deafferentation spontaneously recovered in the weeks after injury, as the expression pattern of CtBP2 and SHANK-1 returned to the pre-lesion state after 3 weeks.

The observation of the pre- and postsynaptic protein expression following the induction of the excitotoxic lesion demonstrated a dramatic reduction in both the expression of CtBP2 (F_7=7.263, P<0.001) and SHANK-1 (F_7=5.445, P<0.001) immediately after lesion induction (Fig. 3I-L). In the utricle, the proportion of CtBP2 fluorescent spots decreased from 100±5% (n=5) to 63±9% (P<0.05; n=4) and 33±6% (P<0.001; n=6) 4 h and 48 h after TTK administration, respectively (Fig. 3I). In parallel, the expression of SHANK-1 decreased from 100±6% (n=5) to 49±2% (P<0.01; n=4) and 52±13% (P<0.01; n=6) at 4 h and 48 h, respectively (Fig. 3K). In the crista, the proportion of CtBP2 spots decreased (F_7=5.911, P<0.001) from 100±14% (n=5) to 38±4% (P<0.001; n=6) and 30±8% (P<0.001; n=5) 4 h and 48 h after TTK administration, respectively (Fig. 3J). Similarly, the expression of SHANK-1 significantly decreased (F_7=2.293, P<0.05) from 100±14% (n=5) to 39±5% (P<0.01; n=6) and 51±11% (P<0.05; n=5) by 4 h and 48 h, respectively (Fig. 3L). Beginning at 1 week, we observed an increase in the levels of the two synaptic proteins in the two vestibular endorgans. By 3 weeks after the induction of the excitotoxic lesion, CtBP2 and SHANK-1 expression in the utricle recovered to 88±16% (n=5) and 93±8% (n=5) of the initial expression levels, respectively. At this time point, the expression of these two proteins was no longer significantly different from that in the sham group. CtBP2 and SHANK-1 expression in the crista recovered to 63±6% (n=6) and 76±14% (n=6) of the initial expression levels, respectively. Although SHANK-1 expression was not significantly different from that in the sham group, CtBP2 expression was still significantly reduced (P<0.01) (Fig. 3J,L).

We also quantified the percentage of colocalised CtBP2 and SHANK-1 (i.e. the percentage of CtBP2- and SHANK-1-positive fluorescent spots less than 1 µm apart). Following injury, in the utricle there was a reduction in the percentage of colocalisations (F_7=5.794, P<0.001): from 72±2% to 25±3% (P<0.001) and 37±9% (P<0.01) between 4 h and 48 h after TTK administration, respectively. This observed reduction was followed by an increase to 46±11% at 1 week (P=0.06) and a recovery to the pre-lesional level at 2 and 3 weeks (no statistically significant difference; Fig. 3M). In the crista, the percentage colocalisation was reduced (F_7=7.072, P<0.001) from 61±3% to 18±3% at 4 h after administration (P<0.001), followed by an increase up to 43±8% and 39±4% at 72 h and 1 week (P=0.06 and P<0.05, respectively). From 2 and 3 weeks onwards, the percentage colocalisation again increased to reach a near pre-lesion state (no statistically significant difference; Fig. 3N). The gross values of CtBP2 and SHANK-1 expression are shown in Table 1. Together, these observations indicated that the dynamic reafferentation of the vestibular mechanoreceptors occurred in the vestibular endorgans following excitotoxically induced deafferentation.

Deafferentation of vestibular primary synapses evokes a transient alteration of the vestibulo-ocular reflex

In the clinic, an imbalance of activity between opposite vestibules can be diagnosed by the presence of abnormal gaze stabilisation referred to as spontaneous vestibular nystagmus (SVN). In mice, the occurrence and characteristics of SVN were analysed at different time points following TTK administration (Fig. 4A,B). In the absence of vestibular stimulation and in complete darkness, 24 h

Disease Models & Mechanisms (2019) 12, dmm039115. doi:10.1242/dmm.039115

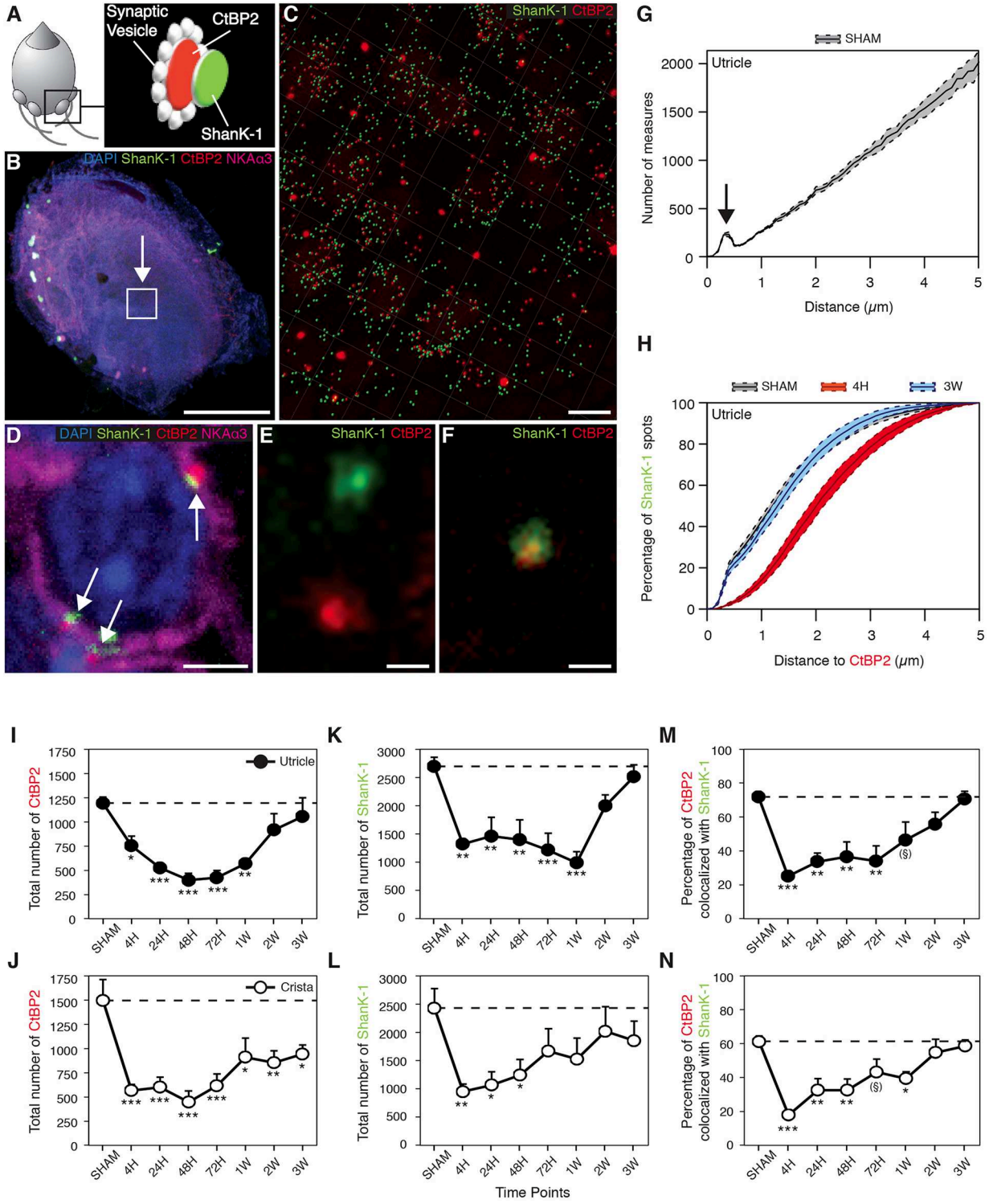

Fig. 3. Evaluation of synaptic protein expression following TTK administration. (A) Schematised vestibular bouton synapses with the respective locations of immunostained CtBP2 (red) and SHANK-1 (green) proteins. (B) Observation field (arrowed box) of $4.5e^{-03}$ mm^2, which includes about 75-100 hair cells in the centre of a utricle. (C) CtBP2 and SHANK-1 fluorescent spots semi-automatically detected within the observation field using IMARIS software. (D) Characteristic expression of fluorescent spots at a calyx terminal (white arrows). (E) Distant and (F) colocalised spots at high magnification. (G) Repartition of the distances between all CtBP2 and SHANK-1 fluorescent spots highlighting a specific subpopulation of spots, the interdistances of which are located within 1 μm (arrow). Images in B-D,F,G: control utricles. (H) Cumulative distances between CtBP2 and SHANK-1 before (sham), 4 h and 3 weeks after TTK application. Note that the gray sham data overlap with the 3 week data. (I-N) Expression of CtBP2 (I,J), SHANK-1 (K,L) and the percentage of their colocalisation (M,N) at each time point before and after TTK application in both the utricle (black circles; *n*=6 for 48 h, 72 h and 2 weeks; *n*=5 for sham, 24 h and 3 weeks; *n*=4 for 4 h and 1 week) and crista ampullaris (white circles; *n*=6 for 4 h, 72 h and 3 weeks; *n*=5 for sham, 24 h, 48 h, 1 week and 2 weeks). The ribbon counts were normalised relative to the observation field described in the Materials and Methods section. Results are expressed as mean±s.e.m. Dotted lines represent sham values. ANOVA followed by Dunnett post-hoc analyses were performed to compare each time point to the sham: **P*<0.05; ***P*<0.01; ****P*<0.001; (§)*P*=0.6. Scale bars: 200 μm (B), 5 μm (C), 2 μm (D) and 0.5 μm (E,F).

Disease Models & Mechanisms (2019) 12, dmm039115. doi:10.1242/dmm.039115

Table 1. Gross values of CtBP2 and SHANK-1 expression

Groups	CtBP2 utricle	SHANK-1 utricle	CtBP2 crest	SHANK-1 crest
Sham	1193.40±64.55	2697.80±162.08	1496.60±216.72	2431.20±344.65
4 h	750.75±102.69	1321.50±45.65	566.67±60.68	952.17±131.43
24 h	522.60±46.40	1460.20±333.75	599.20±105.88	1067.60±237.22
48 h	398.83±67.81	1398.17±354.33	446.20±117.13	1246.20±275.34
72 h	424.17±72.77	1212.33±304.03	612.17±125.10	1666.50±396.19
1 week	570.00±35.26	986.25±197.92	910.00±198.69	1523.80±371.61
2 weeks	917.83±167.16	1994.67±199.24	853.20±124.50	2018.00±435.06
3 weeks	1052.80±195.72	2514.80±208.36	944.00±92.78	1855.33±344.11

Gross results expressed as mean±s.e.m. per observation field and plotted in Fig. 3 for CtBP2 and SHANK-1. The ribbon counts were normalised relative to the observation field described in the Materials and Methods section. In the utricle, n=6 for 48 h, 72 h and 2 weeks; n=5 for sham, 24 h and 3 weeks; n=4 for 4 h and 1 week. In the crest, n=6 for 4 h, 72 h and 3 weeks; n=5 for sham, 24 h, 48 h, 1 week and 2 weeks.

after the lesion onset SVN was observed in 81% of the TTK-administered mice (n=9), but was not observed in any of the vehicle-treated sham mice (n=4). The slow phase of the nystagmus was always directed towards the ipsilesional side. The initial intensity of SVN (the number of beats/min) was variable between individuals at 4 h (mean±s.e.m. 18.6±11.1) and 24 h (mean±s.e.m. 10.0±2.7) and ranged from 1.5 to 24.7 beats/min. The frequency of SVN significantly decreased during the following 48 h in all TTK-administered mice and completely disappeared after 1 week in all but one mouse (Fig. 4C). When the same assessment was performed on mice that underwent UVN, SVN was observed in all lesioned animals at 24 h (it was not measurable at 4 h owing to skew deviation, i.e. post-lesion vertical ocular deviation); SVN occurred significantly more frequently (32.2±7; range 11-57; F_{13}=10.567; P<0.001) in mice that underwent UVN than in the TTK-administered mice. SVN frequency also improved over the following days, but at a slower rate than in TTK-administered mice (intergroup differences are reported in Fig. 4 at the bottom of panels B, D and F). SVN was still observed in all (100%) animals after 1 week (12.8±3.4) and persisted in four animals (67%) beyond 3 weeks (13.3±3.9). The comparison of the TTK-administered mice and the UVN-lesioned mice therefore showed clear differences in both the initial intensity of SVN and in the dynamics of SVN recovery.

To assess semicircular canal function, video-oculography was performed in the dark during rotations in the horizontal plane

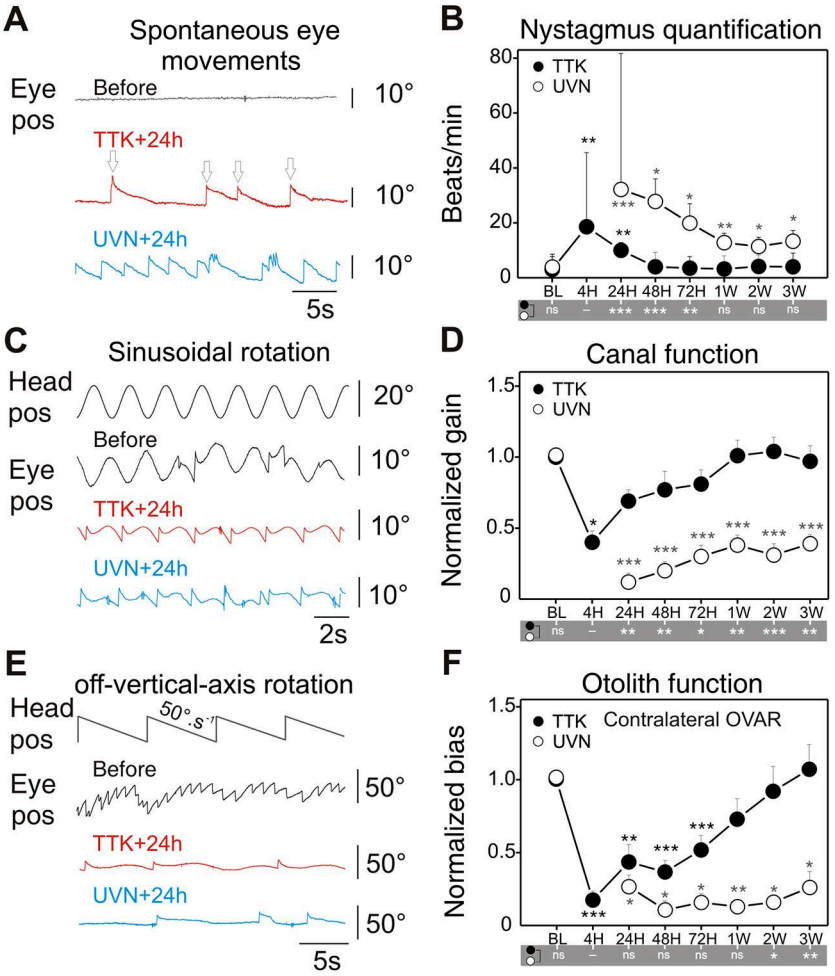

Fig. 4. Analysis of nystagmus, canal and otolith function alterations after TTK administration and UVN. (A) Spontaneous eye movements were recorded in the dark before lesion and 24 h after TTK administration or UVN. Recordings show spontaneous eye drift (slow phase) and multiple quick phases (arrows) corresponding to pathological nystagmus. (B) Comparison of the nystagmus quantified from the TTK (n=11) and UVN (n=6) mice groups during the 3 weeks following the lesion. (C) Raw traces of eye movements observed during sinusoidal table rotation in yaw plane at 0.5 Hz and 30°/s sinusoidal rotation, before and 24 h after TTK or UVN. Note the reduction in amplitude of the eye movements and asymmetry in the response towards the ipsilesional side or contralateral rotation (here ipsi is up). (D) Quantification of the aVOR gain following TTK and UVN. To ease comparison, data are normalised to the pre-lesion values (raw values are reported in Table 2). (E) MOR were measured during off-vertical axis rotation at 50°/s. At 24 h after TTK and UVN, note the absence of the horizontal beating of the eye normally observed. (F) Quantification of the MOR bias following TTK and UVN. Data are normalised to the pre-lesion values. Results are presented as mean±s.e.m. If present, statistical significance is shown comparing each value to the base line (BL) value (repeated measures ANOVA and post-hoc Tukey tests, see Materials and Methods section). In the grey area under B, D and F, statistical differences between UVN and TTK values are reported (two- or three-way ANOVA and post-hoc Tukey tests, see Materials and Methods section). Statistics are represented as *P<0.05; **P<0.01; ***P<0.001; n.s., not specified. In all cases, the TTK population improved after 1 week and fully recovered after 3 weeks, whereas UVN mice remained pathological.

Disease Models & Mechanisms (2019) 12, dmm039115. doi:10.1242/dmm.039115

(Fig. 4C,D). Sinusoidal rotations at frequencies between 0.2 and 1 Hz and 30°/s were performed, and the angular vestibulo-ocular reflex (aVOR) was quantified. At 4 h after TTK injection, the aVOR was significantly impaired but present in all mice. At all tested frequencies, the aVOR gain dropped to approximately 50% of the pre-lesion value: 32.9±6.0% for 0.2 Hz, 39.9±8.5% for 0.5 Hz and up to 50±10.6% for 1 Hz (Fig. 4E and Table 2). When the aVOR was tested again 24 h after lesion induction, we observed a significant recovery of the horizontal canal function normalised values: 66±7.3% for 0.2 Hz, 69±7.6% for 0.5 Hz and up to 83±9.3% for 1 Hz (raw values reported in Table 2). The recovery continued over the following days until full recovery was observed at all tested frequencies after 1 week (Fig. 4D). In the UVN group, the reduction in the aVOR was significantly more severe than that after TTK administration. By 24 h after lesion induction, the UVN gain remained decreased to 14±2.5%, 12±4.3% and 24±7.1% of the initial value for 0.2, 0.5 and 1 Hz, respectively (F_{41}=18.818, P=0.944; P=0.007; P=0.001; compared with the TTK-administered group, using three-way ANOVA for time, frequency and lesion type). After 3 weeks, the recovery of the aVOR gain remained incomplete in all UVN-lesioned mice, with a maximum recovery of approximately 45% of the initial value for all frequencies (Fig. 4D). Sham experiments were performed for both the TTK administration and UVN protocols (4 and 6 mice, respectively). Although the transtympanic sham injection did not trigger any vestibular symptoms or deficit, the UVN sham experiments (complete surgery including the opening of the bulla) led to a 33% immediate decrease in aVOR, which rapidly recovered over the following 2 days (data not shown). Overall, the comparison of the alteration of the aVOR in TTK-administered and UVN-lesioned mice showed differences in both the intensity of the initial symptoms and in the capacity for recovery, which was largely achieved after 1 week in the TTK-administered mice but remained incomplete after 3 weeks in the UVN-lesioned mice.

To assess otolithic function, the off-vertical axis rotation test was performed (Fig. 4E,F) as previously described (Beraneck and Idoux, 2012; Emptoz et al., 2017; Romand et al., 2013). Before lesion induction, normal MORs with clear compensatory eye movements were observed in all animals (Fig. 4E). After lesion induction, the MOR was analysed exclusively during rotation towards the non-lesioned side to prevent the confounding of spontaneous vestibular nystagmus and MORs. At 4 h after TTK injection, the MOR completely disappeared such that, in most instances, only the spontaneous nystagmus caused by the lesion was observed during the MOR test. During the following days, MORs improved but remained significantly impaired at 24 h, 48 h and 72 h (F_6=5.940, P=0.004; P=0.008; P=0.024). Finally, after 1 week the MOR returned to the normal range and was not significantly different from the pre-lesion response (F_6=5.940, P=0.991). This recovery differed from that observed in the UVN-lesioned mice. Although the initial symptoms were quite similar to those of TTK-administered mice, the MORs never recovered to normal levels, even by 3 weeks after lesion induction (F_6=35.398, P<0.001), and remained completely absent in 83% of the animals (Fig. 4F).

Deafferentation of primary vestibular synapses evokes transient alterations in posturo-locomotor functions

A recently described battery of behavioural tests (Cassel et al., 2018) was used to assess the functional consequences of TTK administration on posturo-locomotor function and general behaviour (Fig. 5). Adult mice of the same strain that underwent UVN were also evaluated using the same paradigm to compare the consequences of the unilateral transient loss and the permanent loss of vestibular input. TTK administration evoked a dramatic and immediate increase in vestibular deficit symptoms (head tilt, muscle dystonia, circling, bobbing and barrel rolling; mean score±s.e.m.) that peaked at 4 h following lesion induction (11.5±0.76, n=9; Fig. 5A). The symptoms of vestibular deficits then progressively diminished until complete recovery 1 week after the lesion induction. A statistically significant effect of TTK administration ($F_{2,24}$=89.67, P<0.001) and statistically significant differences between the TTK-administered and sham mice were observed up to 72 h after lesion induction (P<0.001). Alterations in the general behaviour (including vertical and horizontal exploration, body height and gait quality) followed similar kinetics (Fig. 5B). Statistically significant differences between the TTK-administered and sham mice were observed up to 48 h after lesion induction (P<0.001). The TTK-treated mice presented significant behavioural

Table 2. Recovery of canal- and otolith-dependent vestibulo-ocular reflexes following peripheral lesion

Frequency	Group	Before	24 h	48 h	72 h	1 week	2 weeks	3 weeks
aVOR gain								
0.2 Hz	TTK	0.25±0.03	**0.16±0.02**	**0.15±0.02**	**0.15±0.02**	0.19±0.02	0.18±0.02	0.22±0.02
	UVN	0.21±0.04	**0.05±0.01**	**0.04±0.01**	**0.05±0.01**	**0.08±0.02**	**0.06±0.02**	**0.08±0.02**
0.5 Hz	TTK	0.43±0.03	**0.29±0.03**	**0.31±0.05**	**0.35±0.04**	0.42±0.03	0.43±0.02	0.41±0.04
	UVN	0.41±0.05	**0.09±0.03**	**0.11±0.03**	**0.15±0.03**	**0.18±0.04**	**0.16±0.04**	**0.19±0.03**
1 Hz	TTK	0.49±0.04	**0.40±0.05**	0.40±0.04	0.40±0.03	0.50±0.04	0.49±0.04	0.55±0.04
	UVN	0.51±0.06	**0.16±0.04**	**0.15±0.02**	**0.20±0.04**	**0.25±0.05**	**0.30±0.05**	**0.31±0.04**
aVOR phase								
0.2 Hz	TTK	27.5±2.7	32.5±0.02	40.2±2.7	37.4±4.1	36.1±1.95	42.7±3.5	34.9±1.8
	UVN	22.3±3.2	50.6±12.6	30.5±16.5	43.7±10.7	32.5±8.0	8.9±20.8	12.9±29.1
0.5 Hz	TTK	11.1±2.2	18.9±2.2	20.8±2.7	25.9±4.9	16.7±1.3	17.7±1.1	21.8±5.6
	UVN	24.1±6.2	62.2±27.6	42.4±10.2	45.9±9	43.2±5.6	48.5±11.0	49.4±7.5
1 Hz	TTK	8.5±2.8	17.9±4.6	14.4±4.2	9.6±4.2	6.4.5±3.5	5.6±2.3	2.4±1.5
	UVN	4.9±2.5	14.7±18.6	23.9±7.5	12.2±13.4	36.2±7.7	32.8±4.2	25.4±5.6
MOR bias								
50°/s	TTK	0.15±0.03	**0.06±0.06**	**0.05±0.03**	**0.06±0.04**	0.11±0.07	0.12±0.06	0.14±0.05
	UVN	0.22±0.12	**0.04±0.03**	**0.02±0.02**	**0.02±0.01**	**0.02±0.01**	**0.02±0.01**	**0.04±0.03**

Quantification of the canal-dependent angular vestibulo-ocular reflex (aVOR) gain and of the otolith-dependent maculo-ocular reflex (MOR) bias are reported for the TTK (n=11) and UVN (n=6) mice. Following lesion, UVN values are all lower than TTK values. UVN recovery is slower and incomplete compared with TTK. Numbers are the raw values mean±s.e.m. Post-lesion values were compared with the before-lesion value using ANOVA model and post-hoc Tukey test, significant values of aVOR gain and MOR bias are represented in bold (P<0.05).

Disease Models & Mechanisms (2019) 12, dmm039115. doi:10.1242/dmm.039115

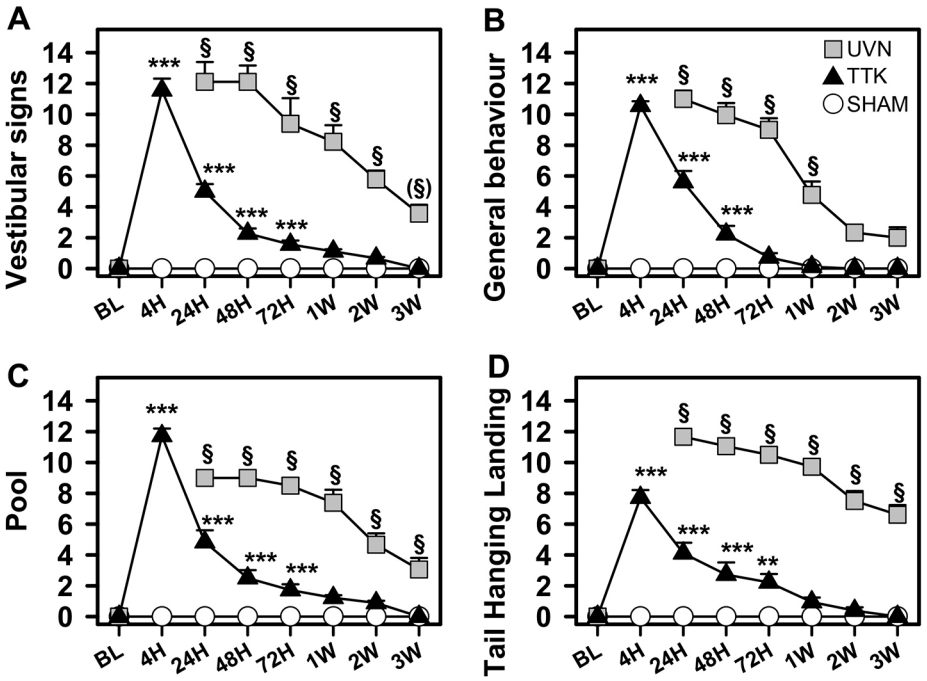

Fig. 5. Posturo-locomotor alterations and alterations of the general behaviour following TTK administration. Evolution of vestibular alteration over time in TTK-treated, UVN-operated and sham mice during the 2 min evaluation. (A) Vestibular signs and (B) general behaviour in the open field. (C) Swim deficit score in the pool. (D) Postural alterations during the tail-hanging landing paradigm. Results are expressed as mean±s.e.m. The sham mice are represented by open circles, the TTK-treated mice by dark triangles and the UVN-operated mice by grey squares (n=9 in each group). Repeated measures ANOVA followed by Bonferroni post-hoc analyses were used to observe TTK administration effects (i.e. TTK vs sham mice): **P<0.01; ***P<0.001. We performed a repeated measures ANOVA followed by Bonferroni post-hoc analyses to observe treatment effects (i.e. TTK vs UVN): $^{\S}P$<0.001, $^{(\S)}P$=0.06.

alterations ($F_{1,16}$=292.11, P<0.001) that recovered over time ($F_{7,112}$=123.17, P<0.001). The excitotoxic peripheral lesion also significantly impaired swimming ability. The swimming deficit score (see Materials and Methods section for details) transiently increased at 4 h (11.72±0.5, n=9; Fig. 5C) and then progressively decreased over the first week after lesion induction. Videos illustrating the swimming ability of the TTK-administered mice at 24 h and 2 weeks are provided (Movies 1 and 2). Statistically significant differences between the TTK-administered and sham mice were observed until 72 h after lesion induction (P<0.001). We found a global effect of TTK administration ($F_{1,16}$=164.75, P<0.001) on this parameter. In the tail hanging landing (THL) paradigm, we observed a transient effect of the lesion (Fig. 5D). THL scores peaked at 4 h (7.72±0.5; n=9) and then progressively decreased over the first week. Statistically significant differences between the TTK-administered and sham mice were observed until 72 h after lesion induction (P<0.001). ANOVA analyses revealed a significant effect of TTK treatment ($F_{1,16}$=73.58, P<0.001).

The UVN-lesioned mice also exhibited dramatic and immediate increases in posturo-locomotor function deficits and related behavioural changes (Fig. 5 grey squares). Compared with the TTK paradigm, the UVN protocol induced acute vestibular syndrome that was so severe that we could not perform behavioural testing at the 4 h time point, as the animals remained immobile, lying on their sides and sometimes barrel rolling. By 24 h after lesion induction, the mean vestibular deficit symptom score reached 12.11±1.27 (n=9). The recovery kinetics significantly differed from those observed in the TTK-administered mice. A reduction of 50% in the vestibular symptom deficit score was obtained 2 weeks after lesion induction, compared with 24 h after lesion induction in the TTK-administered mice (Fig. 5A). This score was still significantly different from that in the mice from the sham group 2 weeks after UVN induction (P<0.001). Similar results were obtained for swimming deficit scores (Fig. 5B), general behavioural deficits (Fig. 5C) and the syndrome reactivation in the THL paradigm (Fig. 5D). These results highlighted the difference in lesion severity and the difference between central compensation alone or central compensation plus peripheral repair.

Correlation between the state of hair cell afferentation and the symptoms of the acute vestibular syndrome

To better determine the temporal correlation between the tissue damage induced by TTK administration and its functional consequences, we established a correlation diagram for visualising the degree of synaptic damage within the two types of vestibular sensory epithelia, gaze stabilising alterations and posturo-locomotor deficits, in parallel (Fig. 6). For this purpose, we assumed that the percentage expression of CtBP2 in the utricle and the crista was representative of the percentage of intact synapses. Before excitotoxic lesion induction, 100% of the vestibular synapses within the selected observation fields in both the utricle and crista were intact. Under these conditions, both the aVOR and MOR gains were normal. No alterations in gait or balance were observed. Over the first hours following lesion induction, the maximum deafferentation of primary vestibular synapses (on the order of 67% in the utricle and 70% in the crista) was observed. The observed 60% and 82% reduction in the aVOR and MOR normalised gains (at 0.5 Hz) mirrored synaptic loss. Posturo-locomotor deficits peaked 4 h after lesion induction. Between 4 h and 24 h, before synaptic repair began, a massive restoration of aVOR gains and a marked reduction in vestibular deficit symptoms were achieved in the TTK-administered mouse model. During this period, functional recovery reached its maximal speed. By 24 h, both vestibulo-ocular and posturo-locomotor deficits recovered by half. Between 24 h and 1 week after lesion induction, the progressive regression of posturo-locomotor and vestibulo-ocular deficit symptoms continued, although the kinetics were different from those observed during the first 24 h. By 1 week after TTK administration, when the first changes in primary synapses were observed, the aVOR and MOR gains fully recovered. At this stage, the posturo-locomotor deficits and the resulting general behavioural alterations completely disappeared. In the UVN-lesioned mice, the aVOR also recovered, although this recovery remained incomplete

Disease Models & Mechanisms (2019) 12, dmm039115. doi:10.1242/dmm.039115

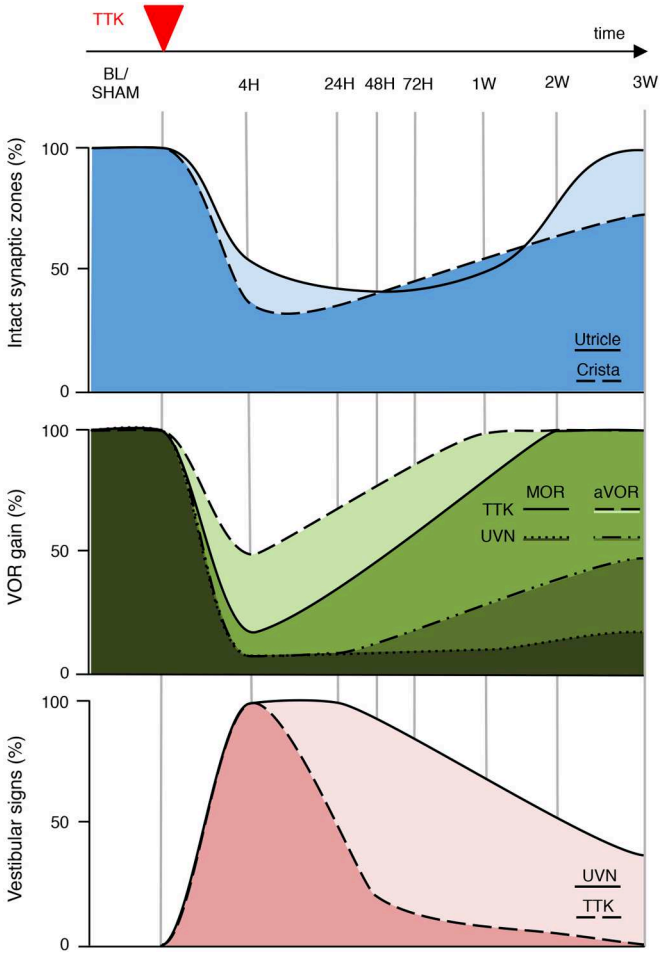

Fig. 6. Correlation grid between vestibular primary synapses afferentation state and signs of vestibular functional alterations. Upper traces: schematic representation of the percentage of intact synapses in the utricle (light blue) and crista (deep blue), drawn on the basis of CtBP2 expression in the sensory epithelia at each of the investigated time points (Fig. 3). Middle traces: schematic representation of the percentage of aVOR [dashed line (or light green) for TTK and dash-dotted line (or lighter dark green) for UVN] and MOR [full line (or green) for TTK and dotted line (or darkest green) for UVN] gains, drawn on the basis of the aVOR measurements shown in Fig. 4. Lower traces: schematic representation of the percentage of posture-locomotor alterations in the UVN (light pink) and TTK (dark pink) mice, drawn on the basis of the vestibular signs displayed in Fig. 5A.

(maximum recovery of 39% of the initial gain at 0.5 Hz). The MOR gain showed no recovery. Beyond 1 week after the lesion induction, the processes of synaptic repair were fully engaged in the TTK-administered mouse model. Both TEM and immunohistochemical analysis of CtBP2 and SHANK-1 expression at primary vestibular synapses indicated that synaptic repair was complete by 3 weeks after excitotoxic insult. Although the aVOR and posturo-locomotor deficits had already fully recovered in the TTK-administered mouse model, they remained only partially recovered at 3 weeks in the UVN-lesioned mice.

DISCUSSION

Excitotoxicity is a pathological process that induces neuronal alteration and destruction through the massive release of glutamate and its analogues (Olney, 1969). When glutamate is released in quantities exceeding glutamate transport capacity, the overactivation of glutamate receptors causes the massive entry of cations into cells expressing these membrane receptors. In synaptic terminals, this ion influx triggers both a cascade of cellular mechanisms leading to structural damage (such as cytoskeleton damage and DNA degradation) and a massive inflow of water that can cause swelling and subsequent synaptic uncoupling (Pujol and Puel, 1999). Many observations have suggested that such phenomena might be involved in various auditory and vestibular pathologies; however, there is still no reliable histopathological evidence of inner ear excitotoxic damage associated with functional impairments in humans. By contrast, the involvement of excitotoxicity in the destruction of the inner ear primary synapses under conditions of ischaemia (Puel et al., 1994), overstimulation (Spoendlin, 1971) or ototoxicity (Smith, 2000) has been confirmed in various animal models. We have previously demonstrated that the administration of the glutamate receptor agonist kainate to the middle ear of rodents causes excitotoxic lesions and that these lesions are prevented in the presence of specific AMPA-kainate receptor blockers (Brugeaud et al., 2007). Kainate, which is not recycled by the glutamate transporters expressed at vestibular synapses (Bonsacquet et al., 2006), exacerbates the excitotoxic response and facilitates the study of functional consequences.

This study was designed to document the time course of an excitotoxic lesion development in the peripheral vestibular system at the histological and molecular levels and to understand how the state of synaptic connectivity correlates with the functional assessment of acute and subacute vertigo-associated deficits. TEM confirmed that the delivery of kainic acid to the inner ear in our model causes characteristic signs of excitotoxic lesions, such as the swelling and retraction of nerve endings, similar to those previously reported in rat models (Brugeaud et al., 2007; Dyhrfjeld-Johnsen et al., 2013; Gaboyard-Niay et al., 2016).

We demonstrated that the distribution of CtBP2- and SHANK-1-staining matches the previously reported distribution of CtBP2- and Glu2A2/3-staining (50% of the mean distances between CtBP2- and GluA2-positive staining were within 1 µm, 70% were within 2 µm and 100% were within 4-5 µm) in the crista of young (younger than 21 days old) rats (Sadeghi et al., 2014). This observation confirms the lack of juxtaposition between afferent ribbons and postsynaptic glutamate receptors. This distribution pattern largely relies on the particular organisation of the postsynaptic region of the calyx terminal (Wersall, 1956; Lysakowski and Goldberg, 1997; Desai et al., 2005a,b; Moser et al., 2006; Sadeghi et al., 2014), in which the PSD is especially elongated and does not fully face the presynaptic ribbons. We also confirmed that TTK administration causes the selective deafferentation of vestibular hair cells. This deafferentation is determined, on the one hand, by a significant increase in the distances between the pre- and postsynaptic proteins and, on the other hand, by a reduction in protein expression. Whether this loss results from a downregulation of protein expression requires further molecular investigations. CtBP2 and SHANK-1 expression was reduced by up to 65% in both utricle and crista hair cells and in afferent terminals between 4 h and 48 h after excitotoxic lesion induction. A similar phenomenon has already been reported for CtBP2 and GluA2/3 at auditory synapses following overexposure to sound (Liberman and Liberman, 2015). The high propensity of primary vestibular neurons to restore synaptic contacts with hair cells has been previously reported *in vivo* in rat models of excitotoxic-type vestibular lesions (Brugeaud et al., 2007; Dyhrfjeld-Johnsen et al., 2013; Gaboyard-Niay et al., 2016) and in rat and mouse models of chronic ototoxic exposure (Sedó-Cabezón et al., 2015; Greguske et al., 2018), as well as *in vitro* in organotypic co-cultures of Scarpa's ganglia and vestibular sensory epithelia (Travo et al., 2012).

In the TTK mouse model, TEM examination revealed that an initial phase of damage reduction and the restoration of the contacts between hair cells and afferent nerve fibres takes place within 1 week of the excitotoxic insult. Nevertheless, the observation of fragmented calyx endings indicated that the repair process was still underway. Similar discontinuities in calyx endings have been observed in premature calyces in late developmental stages (Desmadryl and Sans, 1990) and in other models of calyx-ending damage and repair (Seoane et al., 2001; Sedó-Cabezón et al., 2015). Therefore, these calyx endings were probably in a late stage of regenerative repair. In a second phase of repair that lasts another 2 weeks, the progressive upregulation of CtBP2 and SHANK-1 and subsequent synaptic pairing also takes place. Although only electrophysiological investigations using single fibre recordings can confirm the functional restoration of primary synapse activity, histological observations demonstrated that primary vestibular synapses undergo spontaneous repair following selective deafferentation. A further examination of the expression kinetics of the glutamate receptor subunits is required to confirm that the reported changes in the expression of the SHANK-1 also apply to the glutamate receptors.

The parallel analysis of histological and functional changes that occur over the different phases of vestibular syndrome in the TTK mouse model produced interesting information regarding their correlation. For example, the proportional reduction in aVOR gains and synaptic loss in the first hours following excitotoxic lesion induction suggests that the aVOR gain reductions observed immediately after lesion induction are directly indicative of the severity of vestibular sensory epithelium deafferentation. Over the first 24 h, the massive restoration of the aVOR gains and the marked reduction in vestibular signs are independent of synaptic repair, which begins several days later. This functional recovery can therefore be attributed to the reactive compensation processes that takes place in the brainstem vestibular nuclei (Lacour and Tighilet, 2010; Sadeghi et al., 2010). It can be assumed that the preservation of part of the nerve fibres connected to vestibular sensors is sufficient to feed the vestibular nuclei with information from the damaged vestibule and quickly diminish the imbalance of electrical activity considered to be the neurophysiological substrate of vertigo syndrome (Curthoys and Halmagyi, 1995; Dieringer, 1995).

One can then query the functional relevance of the peripheral synaptic repair if functional recovery is fully achieved before synaptic repair starts. The different symptoms that constitute the acute vestibular syndrome compensate each other with their own kinetics. Some of them, such as the head tilt, are slower than others (Dyhrfjeld-Johnsen et al., 2013; Cassel et al., 2018). It cannot be excluded that this specific parameter depends, at least partially, on peripheral synaptic repair. It is likely that the ability to spontaneously reform functional synapses is preserved at adult stage, according to the concept that 'repair is better than compensation'. The feedback from peripheral sensory inputs, depending on the time it occurs, will possibly perturb the establishment of compensation mechanisms in the UVN-lesioned mice. We also anticipate that, during this phase, the progressive increase in peripheral inputs induces readjustments to the changes that occur in the earlier phases of repair.

The differences in the kinetics of gait and balance recovery between the TTK-administered and UVN-lesioned mice might result from central compensation processes that differ according to the type of peripheral lesion. This has been previously well demonstrated in different cat models of unilateral vestibular lesions (Lacour et al., 2009). The restoration of posturo-locomotor and oculomotor functions of cats subjected to UVN, was significantly delayed compared with that in groups subjected to the unilateral and transient pharmacological block of vestibular input or the selective destruction of the vestibular sensors. It has since been established that, upon UVN, profound rearrangements that affect local neuronal excitability, neurotransmitter and neurotrophin release, as well as local inflammatory responses (Lacour and Tighilet, 2010; Liberge et al., 2010; Dutheil et al., 2013, 2016), take place within the brainstem vestibular nuclei.

In patients with AUV, the segmental loss of isolated branches of the vestibular nerve peripheral to Scarpa's ganglion, with or without the degeneration of the associated sensory epithelium, has been reported (Schuknecht, 1993; Rauch, 2001). Although very scarce, such observations strongly support a causal link between the selective deafferentation of vestibular sensors and the occurrence of acute vestibular syndrome. Such patients display static and dynamic postural impairments, and alterations in canal- and otolith-dependent aVOR gains were also observed in the TTK mouse model (Hotson and Baloh, 1998). The spontaneous functional restoration of the injured vestibule has been demonstrated using different clinical assessments of the vestibular function, such as the caloric test, vestibular-evoked myogenic potential and, more recently, the video head impulse test. Over the weeks and months following the onset of pathology, significant functional recovery is observed in all semicircular canals (SCC), although to varying extents. This is well illustrated by a recent study of vestibular neuritis patients evaluated both during the acute phase and 2 months later (Büki et al., 2017); in this study, follow-up examinations reported 55% functional recovery in the horizontal canal and 38% in both the anterior and inferior canals. The precise mechanisms underlying the loss of vestibular endorgan function and its spontaneous functional recovery remain to be established. Given the paucity of histopathological observations confirming direct damage to vestibular nerve branches, however, an intralabyrinthine source is increasingly favoured (Uffer and Hegemann, 2016; Hegemann and Wenzel, 2017).

One question that remains is whether the reafferentation pattern of repaired synapses reproduces the preinjury pattern. One can, for example, imagine that orphan nerve fibres might simply reafferent the nearest neighbouring hair cells. This question is important because one can envisage that abnormal reafferentation (or at least reafferentation not completely corresponding to the initial pattern) might be a source of scrambled sensory inputs during movement. This type of situation could contribute to the chronic disabilities and the clinical deficits that often persist several years after AUV (Mandalà and Nuti, 2009; Strupp and Brandt, 2009). The demonstration that synaptic reafferentation might take several weeks to be established in mice suggests that, if this process is conserved in humans, a broad therapeutic window is available for pharmacological interventions. The identification of the molecular effectors and pathways involved in the repair of inner ear synapses should pave the way for the future development of therapeutic approaches aimed at protecting the peripheral synapses and stimulating their repair. Such studies would benefit all patients suffering the peripheral loss of synaptic connectivity.

MATERIALS AND METHODS

Animals

We used C57Bl6/J adult mice (2-3 months old) of both sexes (Charles River laboratories, L'Arbresle, France). All animals were kept in standard animal cages under conventional laboratory conditions (12 h/12 h light-dark cycle, temperature 22±2°C, humidity 55±5%) with *ad libitum* access to food and water. Behavioural experiments were conducted during the light phase. Experimental protocols and animal care were in compliance with the institutional guidelines (council directive 87/848, October 19 1987, Ministry of Agriculture and Forestry, Veterinary Department of Health

and Animal Protection) and international laws (directive 2010/63/UE609, 13 February 2013, European Community) and policies (personal authorisation #I-67 Université Louis Pasteur-F1-04 for R.C.). The procedures for behavioural experiments and aVOR recordings were approved by the Neuroscience Ethics Committee N°71 from the French National Committee on animal experimentation and by the ethical committee for animal research of the University Paris Descartes.

TTK administration

Unilateral TTK administration was performed on a total of 66 adult mice of both sexes. Under deep isoflurane anesthesia, a myringotomy was performed using a microneedle (30 gauge) and 20 µl of 25 mM kainate solution (Abcam ab120100 dissolved in NaCl 0.9%, pH 7.4) was infused into the middle ear using a Hamilton microliter syringe and a syringe pump. The anesthetised mice were then kept on their side (with lesion side facing up) for 30 min to optimise bathing of the round window with the kainate solution. For the sham condition, mice were administered NaCl 0.9% without kainate.

UVN

UVN was performed on a total of 15 adult mice of both sexes following the surgical procedure previously reported for the rat (Péricat et al., 2017). Animals were anaesthetised with a mixture of ketamine 1000 (Virbac; 100 mg/kg, i.p)/methedomidrine (Domitor® Orion Pharma; 0.2 mg/kg, i.p.). A tympanic bulla approach gave access to the vestibular nerve: cervical muscular planes were dissected leading to tympanic bulla, which was widely drilled to expose the stapedial artery and the promontory containing the cochlea. The cochlea was drilled exposing the cochlear nerve. The cochlear nerve meatus was enlarged with a needle leading to the vestibulocochlear nerve, which was sectioned, and the Scapa's ganglion aspirated. The wound was closed using a stapler. Before awakening the animal by intraperitoneal injection of Antisedan® (Orion-Pharma; 1 mg/kg), a solution of Ringer Lactate (Virbac; 10 ml/kg) was administered subcutaneously to reduce the dehydration resulting from the inability to drink normally owing to the lesion. Buprecare® (Axience; 0.005 mg/kg) was given as postsurgery analgesic. In another six sham mice, surgery was limited to the opening of the tympanic bulla.

Light microscopy and TEM

Light and TEM observations were performed as described (Greguske et al., 2018) in a total of nine adult mice of both sexes (three mice in each group): sham (NaCl-injected mice corresponding to the control group), 4 h following TTK administration and 1 week following TTK administration. The temporal bones were immersed in cold 2.5% glutaraldehyde in 0.1 M cacodylate buffer (pH 7.2) and the vestibular epithelia were dissected in a fume hood within 5 min of sacrifice. The specimens were fixed for 1 h in the same fixative, rinsed with buffer, post-fixed with 1% osmium tetroxide in cacodylate buffer for 1 h, rinsed and then stored at 4°C in 70% alcohol. Afterwards, the specimens were dehydrated with increasing concentrations of ethanol (up to 100%) and then embedded in Spurr resin. Semi-thin sections (1 µm) were stained with 1% Toluidine Blue and examined under a light microscope. Ultra-thin sections were stained with uranyl acetate and lead citrate and were observed with a JEOL 1010 TEM microscope at 75-80 kV.

Immunostaining of synaptic proteins

Immunolabelling experiments were performed using 45 adult mice of both sexes (6 mice at 4 h, 48 h, 72 h, 2 weeks and 3 weeks; 5 mice sham, 24 h and 1 week). Sham mice were NaCl-injected mice and correspond to the control group. The mice were deeply anaesthetised using intraperitoneal injection of pentobarbital (60 mg/kg). Their temporal bones were rapidly removed, and the vestibular epithelia were microdissected and fixed for 1 h at room temperature in 4% paraformaldehyde dissolved in PBS. The samples were stored at −20°C in a cryoprotectant solution (34.5% glycerol, 30% ethylene glycol, 20% PBS, 15.5% distilled water) until staining. The immunohistochemical analyses were performed on whole vestibular sensory epithelia (crista and utricle). Tissues were first incubated for a 15 min period in citrate sodium buffer (pH 6, 10 mM) at 95°C and then left for 90 min in PBS with 4% Triton X-100 and 5% donkey serum under slow agitation. The primary antibodies were incubated in 0.1% Triton X-100 and 1% donkey serum in PBS for 48 h at 4°C: mouse IgG1 anti-CtBP2, BD transduction #612044 (1/500); rabbit anti-SHANK1, Novusbio #NB300-167 (1/500); and goat anti-NKA α3, Santa Cruz #sc-16052 (1/750). We immunolabelled SHANK-1 rather than GluA2/3, because of the lack of reliability in our hands of anti-GluA2/3 antibodies in the vestibular tissues. After three washes, the secondary antibodies were incubated in 0.1% Triton X-100 in PBS overnight at 4°C: Alexa Fluor 488 donkey anti-rabbit IgG H&L (1/500) #ab150073; Alexa Fluor 568 donkey anti-mouse IgG H&L (1/500) #ab175472; Alexa Fluor 647 donkey anti-goat IgG H&L (1/500) #ab151031. A chromatin staining with DAPI was performed between the two final washes. The epithelia were oriented and mounted in Mowiol medium.

Acquisition of fluorescence images

Fluorescence images were acquired using a Zeiss (LSM 710 NLO) confocal microscope with a 63× Zeiss Plan Apochromat oil-immersion lens (NA 1.40) controlled with the Zen software (ZEN 2012 Black edition, Carl Zeiss Microscopy GmbH, Germany). We acquired *z*-stacks (20-50 optical sections) through the majority of preparations that we collected in 0.40 µm steps. The step size (optical section thickness) was determined by stepping at half the distance of the theoretical *z*-axis resolution. Images were acquired to a resolution of 1024×1024 pixels at subsaturating laser intensities for each channel.

Quantitative assessment of pre- and postsynaptic proteins

Quantitative analysis of CtBP2 (RIBEYE) and SHANK-1 spots was performed using IMARIS software (version 8.2.1) based on raw image stacks. We did not apply any deconvolution, filtering, gamma correction or resampling. We automatically detected the total number and relative location of CtBP2 and SHANK-1 puncta using the Spots function in the IMARIS 3D image visualisation. To evaluate the number of colocalisations/juxtapositions between CtBP2 and SHANK-1 proteins, an isosurface of each signal was created in independent colour channels (488 and 568 nm). Puncta volumes were then computed using IMARIS software functions that provide 3D rendering and visualisation of isosurfaces enveloping all pixel clusters. Puncta volumes were computed along the *x*, *y* and *z* coordinates of their centres. Automatically detected puncta were verified by eye in a rotary 3D reconstruction of the sample. Puncta that were not contained within or next to the hair cells were manually removed. The analysis software MatLab (The MathWorks, Natick, MA) was used to set the colocalisation distance threshold at 1 µm in vestibular end organ samples. We used a custom R software Script (R Foundation for Statistical Computing, Vienna, Austria) to calculate the distances between CtBP2 and SHANK-1 labels from the *x*, *y* and *z* coordinates.

Considering there were fewer CtBP2 than SHANK-1 spots, we assessed the distances from CtBP2 to SHANK-1 and vice versa (see Figs S3 and S4). Quantitative analyses were performed on observation fields of $4.5e^{-03}$ mm^2 (observation field in Fig. 3), which include about 75-100 hair cells in both utricles and crista for each of the five to six animals used per time point. In Fig. 3 and Table 1 the ribbon counts were normalised relative to the observation field. We could not estimate the volume of the observation fields, because the *z*-axis lengths differed in function of observed tissues.

Note that the calculated distances between CtBP2 and SHANK-1 immunolabelled spots do not necessarily reflect absolute distances, owing to deviations that probably result from the inherent limits of resolution imposed by immunofluorescence and confocal microscopy.

Video-oculography and vestibulo-ocular procedures

Video-oculography was performed to quantify vestibulo-ocular reflexes. A total of 27 C57Bl6/J mice of both sexes were subjected to either TTK, UVN or equivalent sham conditions. All surgical and pre-test procedures were similar to those previously described (Péricat et al., 2017). Briefly, mice were head-fixed in a custom-built Plexiglas tube secured on the superstructure of a vestibular stimulator. The aVOR were tested in complete dark (light intensity <0.02 lux). Eye movements were recorded using an infrared video system (ETL-200, ISCAN, Burlington MA). Eye and head position signals were sampled at 1 kHz, digitally recorded (CED power 1401 MkII) with the Spike 2 software and later exported into the

Matlab programming environment for off-line analysis (Matlab, The MathWorks). To maintain miosis throughout the experiment, 2% pilocarpine was applied 10 min before the start. Gaze stability was tested in the dark by recording spontaneous eye movements in the absence of any vestibular stimulation. Then, aVOR was tested during horizontal sinusoidal rotation of the turntable (0.2-1 Hz; peak velocity 30°/s). To specifically test otolithic function (MOR), the turntable was tilted by 17° and off-vertical axis rotation (OVAR) was performed (50°/s constant velocity; in clockwise and counter-clockwise direction). Analysis was performed off-line. Horizontal and vertical eye and head movement data were digitally low-pass-filtered (cut-off frequency 40 Hz), and position data were differentiated to obtain velocity traces. Segments of data with saccades were excluded from aVOR slow-phase analysis. Details of the analysis have been previously reported (Beraneck and Idoux, 2012; Carcaud et al., 2017).

Behavioural exploration

Behavioural evaluation of the posturo-locomotor function was performed in a group of 27 adult mice subjected to either TTK, UVN or sham conditions. We used three paradigms: the open field (OF), the tail-hanging landing (THL) and the swim test. For the OF and THL, a 30×30 cm square of Plexiglass fixed on a bottomless table was used. A camera was placed under the open field to monitor mouse behaviour from below. In the THL test, the mice were gently held by the tail and quickly moved vertically back and forth along a 50 cm long path. We used a Plexiglass box (length 34 cm, width 21 cm and height 20 cm) filled with water (maintained at 32°C to avoid hypothermia) as a pool for the swim test. Before surgery, a 5 day handling period was implemented to habituate the animals to manipulation (2 min per day for each mouse). We assessed mouse behaviour before surgery (base line, BL) and at the following time points thereafter: 4 h, 24 h, 48 h, 72 h, 1 week, 2 weeks and 3 weeks. The items were quantified in a scale from 0 (mice exhibited no deficits at all), to 3 (the highest degree of vestibular deficit). Briefly, in the OF, we recorded spontaneous animal behaviours over 2 min and quantified two sets of parameters: we first looked at items linked to specific vestibular deficit symptoms and scored behaviour relative to mouse global state (referred to as general behaviour). Signs of vestibular deficits included specific symptoms such as circling (stereotyped movement in circles around the hips of the animal), head tilt (inclination of the head in the roll plane), muscle dystonia (hypertonia on the lesioned side), barrel rolling (mice turning on themselves around their longitudinal axis) and head bobbing (abnormal intermittent flexion-extension of the neck in the pitch plane). General behaviour encompassed the quality of horizontal and vertical exploration, quality of locomotion and centre of gravity height. During the THL procedure we evaluated the quality of forelimb extension normally produced to reach the ground (i.e. quality of the landing) and the body axial rotation (twirl). We also measured the intensity of the syndrome reactivation after landing as the accentuation or the reappearance of vestibular deficit symptoms (circling, head tilt, muscle dystonia, bobbing) from 0 (no sign) to 3 (maximum expression/accentuation of vestibular deficit symptoms). The swimming abilities of the animals were then quantified for 30 s (cut-off time) by observing the quality of swimming (specific grid detailed in Cassel et al., 2018) and whether the mice were barrel rolling or not in the water. Once mice were removed from the water, we observed the intensity of syndrome reactivation and their grooming skills.

Statistics

Immunostaining counting and processing were analysed using one-way analysis of variance (ANOVA). When appropriate, the Dunnett multiple comparison test followed ANOVA. All data are reported as mean+s.e.m. Values of $P<0.05$ were considered significant.

For the aVOR and OVAR analyses, when considering the factor 'time', comparing values to the before-lesion values, significance was measured using a repeated measures ANOVA: two-way for aVOR values (time and frequency) and one-way for OVAR (time). When comparing values between UVN and TTK populations, significance was measured using a three-way (time, frequency and lesion type) or two-way (time and lesion type) ANOVA. Post-hoc comparisons were performed using the Tukey HSD test. All data are reported as mean±s.e.m. Values of $P<0.05$ were considered significant. We report the lack of statistically significant effects by the letters n.s.

For behavioural exploration, performances recorded across the different paradigms were analysed using one-between, one-within factor ANOVA, which considered the factors 'time' (time points 1-8; i.e. BL, 4 h, 24 h, 48 h, 72 h, 1 week, 2 weeks and 3 weeks) and 'treatment' (vehicle vs TTK) or (vehicle vs UNV). The ANOVA was followed by a Bonferroni multiple-comparisons test when appropriate. For all ANOVAs reported, violations of the sphericity assumption (homogeneity of covariance) were corrected using the Greenhouse-Geisser procedure; the corrected P-value along with the epsilon correction factor (ε) are reported. As ε was lower than 0.75 in all analyses, we used G-G corrected P-value for all data presented. Results are expressed as mean±s.e.m. Values of $P<0.05$ were considered significant. We report the lack of statistically significant effects by the letters n.s.

Acknowledgements

We acknowledge the PICSL imaging facility of the CIML (ImagImm), member of the national infrastructure France-BioImaging supported by the French National Research Agency (ANR-10-INBS-04) and, more precisely, M. Fallet for technical support. We are also grateful to A. Gharbi for technical assistance, Y. Autier, E. Belometti, E. Mansour and I. Scotto for their assistance in mouse production and animal care. The electron microscopy studies were performed at the Scientific and Technological Centers of the University of Barcelona (CCiT-UB). We thank J. M. Rebled, R. Rivera and A. Martínez Gené for technical assistance.

Competing interests

The authors declare no competing or financial interests.

Author contributions

Conceptualization: B.T., C.C.; Methodology: R.C., P.B., J.C., M.B., S.B., I.W., D.P., A.A., A.T., C.C.; Validation: R.C.; Investigation: R.C., P.B., J.C., F.S., M.B., A.L.G., A.B., V.B., B.P., S.B., I.W., D.P., A.A., A.T., J.L., C.C.; Data curation: R.C., P.B., J.C., F.S., M.B., A.L.G., A.B., V.B., B.P., S.B., I.W., D.P., A.A., A.T., J.L., C.C.; Writing - original draft: R.C., P.B., F.S., M.B., S.B., C.H., J.D.-J., J.L., B.T., C.C.; Writing - review & editing: R.C., P.B., F.S., M.B., S.B., C.H., J.D.-J., J.L., B.T., C.C.; Supervision: C.C.; Funding acquisition: C.C.

Funding

This work was supported by Centre National de la Recherche Scientifique (CNRS; UMR7260), Aix-Marseille Université, MINECO/FEDER (Fondo Europeo de Desarrollo Regional, EU; BFU2015-66109-R) and AGAUR (2017 SGR 621). R.C. and J.C. were recipients of a fellowship from Amidex (project A*MIDEX, ANR-11-IDEX-0001-02 from 2015 to 2017); P.B. was funded by a fellowship from Sensorion.

Supplementary information

Supplementary information available online at
http://dmm.biologists.org/lookup/doi/10.1242/dmm.039115.supplemental

References

Beraneck, M. and Idoux, E. (2012). Reconsidering the role of neuronal intrinsic properties and neuromodulation in vestibular homeostasis. *Front. Neurol.* **3**, 25. doi:10.3389/fneur.2012.00025

Bonsacquet, J., Brugeaud, A., Compan, V., Desmadryl, G. and Chabbert, C. (2006). AMPA type glutamate receptor mediates neurotransmission at turtle vestibular calyx synapse. *J. Physiol.* **576**, 63-71. doi:10.1113/jphysiol.2006.116467

Braude, J. P., Vijayakumar, S., Baumgarner, K., Laurine, R., Jones, T. A., Jones, S. M. and Pyott, S. J. (2015). Deletion of Shank1 has minimal effects on the molecular composition and function of glutamatergic afferent post synapses in the mouse inner ear. *Hear. Res.* **321**, 52-64. doi:10.1016/j.heares.2015.01.008

Brugeaud, A., Travo, C., Dememes, D., Lenoir, M., Llorens, J., Puel, J.-L. and Chabbert, C. (2007). Control of hair cell excitability by vestibular primary sensory neurons. *J. Neurosci.* **27**, 3503-3511. doi:10.1523/JNEUROSCI.5185-06.2007

Büki, B., Hanschek, M. and Jünger, H. (2017). Vestibular neuritis: Involvement and long-term recovery of individual semicircular canals. *Auris Nasus Larynx.* **44**, 288-293. doi:10.1016/j.anl.2016.07.020

Carcaud, J., de Barros, F. F., Idoux, E., Eugène, D., Reveret, L., Moore, L. E., Vidal, P. P. and Beraneck, M. (2017). Long-lasting visuo-vestibular mismatch in freely-behaving mouse reduces the vestibulo-ocular reflex and leads to neural changes in the direct vestibular pathway. *eNeuro* **4**, ENEURO.0290-16.2017. doi:10.1523/ENEURO.0290-16.2017

Cassel, R., Bordiga, P., Pericat, D., Hautefort, C., Tighilet, B. and Chabbert, C. (2018). New mouse model for inducing and evaluating unilateral vestibular deafferentation syndrome. *J. Neurosci. Meth.* **293**, 128-135. doi:10.1016/j.jneumeth.2017.09.002

Curthoys, I. S. and Halmagyi, G. M. (1995). Vestibular compensation: a review of the oculomotor, neural, and clinical consequences of unilateral vestibular loss. *J. Vestib. Res. Equilib. Orient.* **5**, 67-107. doi:10.1016/0957-4271(94)00026-X

Desai, S. S., Ali, H. and Lysakowski, A. (2005a). Comparative morphology of rodent vestibular periphery. II. Cristae Ampullares. *J. Neurophysiol.* **93**, 267-280. doi:10.1152/jn.00747.2003

Desai, S. S., Zeh, C. and Lysakowski, A. (2005b). Comparative morphology of rodent vestibular periphery. I. Saccular and Utricular Maculae. *J. Neurophysiol.* **93**, 251-266. doi:10.1152/jn.00746.2003

Desmadryl, G. and Sans, A. (1990). Afferent innervation patterns in crista ampullaris of the mouse during ontogenesis. *Brain Res. Dev. Brain Res.* **52**, 183-189. doi:10.1016/0165-3806(90)90234-P

Dieringer, N. (1995). 'Vestibular compensation': neural plasticity and its relations to functional recovery after labyrinthine lesions in frogs and other vertebrates. *Prog. Neurobiol.* **46**, 97-129. doi:10.1016/0301-0082(95)80009-W

Dutheil, S., Escoffier, G., Gharbi, A., Watabe, I. and Tighilet, B. (2013). GABAA receptor agonist and antagonist alter vestibular compensation and different steps of reactive neurogenesis in deafferented vestibular nuclei of adult cats. *J. Neurosci.* **33**, 15555-15566. doi:10.1523/JNEUROSCI.5691-12.2013

Dutheil, S., Watabe, I., Sadlaoud, K., Tonetto, A. and Tighilet, B. (2016). BDNF signaling promotes vestibular compensation by increasing neurogenesis and remodeling the expression of potassium-chloride cotransporter KCC2 and $GABA_A$ receptor in the vestibular nuclei. *J. Neurosci.* **36**, 6199-6212. doi:10.1523/JNEUROSCI.0945-16.2016

Dyhrfjeld-Johnsen, J., Gaboyard-Niay, S., Broussy, A., Saleur, A., Brugeaud, A. and Chabbert, C. (2013). Ondansetron reduces lasting vestibular deficits in a model of severe peripheral excitotoxic injury. *J. Vest. Res.* **3**, 177-186. doi:10.3233/VES-130483

Emptoz, A., Michel, V., Lelli, A., Akil, O., Boutet de Monvel, J., Lahlou, G., Meyer, A., Dupont, T., Nouaille, S., Ey, E. et al. (2017). Local gene therapy durably restores vestibular function in a mouse model of Usher syndrome type 1G. *Proc. Natl. Acad. Sci. USA* **114**, 9695-9700. doi:10.1073/pnas.1708894114

Foster, C. A. and Breeze, R. E. (2013). The Meniere attack: an ischemia/reperfusion disorder of inner ear sensory tissues. *Med. Hypoth.* **81**, 1108-1115. doi:10.1016/j.mehy.2013.10.015

Gaboyard-Niay, S., Travo, C., Saleur, A., Broussy, A., Brugeaud, A. and Chabbert, C. (2016). Correlation between afferent rearrangements and behavioral deficits after local excitotoxic insult in the mammalian vestibule: a rat model of vertigo symptoms. *Dis. Model. Mech.* **9**, 1181-1192. doi:10.1242/dmm.024521

Greguske, E. A., Carreres-Pons, M., Cutillas, B., Boadas-Vaello, P. and Llorens, J. (2018). Calyx junction dismantlement and synaptic uncoupling precede hair cell extrusion in the vestibular sensory epithelium during sub-chronic 3,3′-iminodipropionitrile ototoxicity in the mouse. *Arch. Toxicol.* **93**, 417-434. doi:10.1007/s00204-018-2339-0

Halmagyi, G., Weber, K. and Curthoys, I. (2010). Vestibular function after acute vestibular neuritis. *Restor. Neurol. Neurosci.* **1**, 37-46. doi:10.3233/RNN-2010-0533

Hegemann, S. C. A. and Wenzel, A. (2017). Diagnosis and treatment of vestibular neuritis/neuronitis or peripheral vestibulopathy (PVP)? Open questions and possible answers. *Otol. Neurotol.* **38**, 626-631. doi:10.1097/MAO.0000000000001396

Hotson, J. R. and Baloh, R. W. (1998). Acute vestibular syndrome. *N. Engl. J. Med.* **339**, 680-685. doi:10.1056/NEJM199809033391007

Huang, L.-C., Barclay, M., Lee, K., Peter, S., Housley, G. D., Thorne, P. R. and Montgomery, J. M. (2012). Synaptic profiles during neurite extension, refinement and retraction in the developing cochlea. *Neural Dev.* **7**, 38. doi:10.1186/1749-8104-7-38

Khimich, D., Nouvian, R., Pujol, R., Tom Dieck, S., Egner, A., Gundelfinger, E. D. and Moser, T. (2005). Hair cell synaptic ribbons are essential for synchronous auditory signalling. *Nature* **434**, 889-894. doi:10.1038/nature03418

Lacour, M. and Tighilet, B. (2010). Plastic events in the vestibular nuclei during vestibular compensation: the brain orchestration of a «deafferentation» code. *Restor. Neurol. Neurosci.* **28**, 19-35. doi:10.3233/RNN-2010-0509

Lacour, M., Dutheil, S., Tighilet, B., Lopez, C. and Borel, L. (2009). Tell me your vestibular deficit, and I'll tell you how you'll compensate. *Ann. N. Y. Acad. Sci.* **1164**, 268-278. doi:10.1111/j.1749-6632.2008.03731.x

Liberge, M., Manrique, C., Bernard-Demanze, L. and Lacour, M. (2010). Changes in TNFa, NFkB and MnSOD protein in the vestibular nuclei after unilateral vestibular deafferentation. *J. Inflam.* **7**, 91. doi:10.1186/1742-2094-7-91

Liberman, L. D. and Liberman, M. C. (2015). Dynamics of cochlear synaptopathy after acoustic overexposure. *J. Assoc. Res. Otolaryngol.* **16**, 205-219. doi:10.1007/s10162-015-0510-3

Liberman, M. C. and Kujawa, S. G. (2017). Cochlear synaptopathy in acquired sensorineural hearing loss: manifestations and mechanisms. *Hear. Res.* **349**, 138-147. doi:10.1016/j.heares.2017.01.003

Lysakowski, A. and Goldberg, J. M. (1997). A regional ultrastructural analysis of the cellular and synaptic architecture in the chinchilla cristae ampullares. *J. Comp. Neurol.* **389**, 419-443. doi:10.1002/(SICI)1096-9861(19971222)389:3<419::AID-CNE5>3.0.CO;2-3

Mandalà, M. and Nuti, D. (2009). Long-term follow-up of vestibular neuritis. *Ann. N. Y. Acad. Sci.* **1164**, 427-429. doi:10.1111/j.1749-6632.2008.03721.x

Moser, T., Brandt, A. and Lysakowski, A. (2006). Hair cell ribbon synapses. *Cell Tissue Res.* **326**, 347-359. doi:10.1007/s00441-006-0276-3

Olney, J. W. (1969). Brain lesions, obesity, and other disturbances in mice treated with monosodium glutamate. *Science* **164**, 719-721. doi:10.1126/science.164.3880.719

Péricat, D., Farina, A., Agavnian-Couquiaud, E., Chabbert, C. and Tighilet, B. (2017). Complete and irreversible unilateral vestibular loss: a novel rat model of vestibular pathology. *J. Neurosci. Meth.* **283**, 83-91. doi:10.1016/j.jneumeth.2017.04.001

Puel, J.-L., Pujol, R., Tribillac, F., Ladrech, S. and Eybalin, M. (1994). Excitatory amino acid antagonists protect cochlear auditory neurons from excitotoxicity. *J. Comp. Neurol.* **341**, 241-256. doi:10.1002/cne.903410209

Pujol, R. and Puel, J.-L. (1999). Excitotoxicity, synaptic repair, and functional recovery in the mammalian cochlea: a review of recent findings. *Ann. N. Y. Acad. Sci.* **884**, 249-254. doi:10.1111/j.1749-6632.1999.tb08646.x

Rauch, S. D. (2001). Vestibular histopathology of the human temporal bone: what can we learn? *Ann. N. Y. Acad. Sci.* **942**, 25-33. doi:10.1111/j.1749-6632.2001.tb03732.x

Richard, C. and Linthicum, F. H. (2012). Vestibular neuritis: the vertigo disappears, the histological traces remain. *Otol. Neurotol.* **33**, e59-e60. doi:10.1097/MAO.0b013e31824b7730

Romand, R., Krezel, W., Beraneck, M., Cammas, L., Fraulob, V., Messaddeq, N., Kessler, P., Hashino, E. and Dolle, P. (2013). Retinoic acid deficiency impairs the vestibular function. *J. Neurosci.* **33**, 5856-5866. doi:10.1523/JNEUROSCI.4618-12.2013

Ruttin, B. (1909). Zur differentialdiagnose der labyrinth-u. *Horenrverkrankugen Z Ohrenheilk* **57**, 327-331.

Sadeghi, S. G., Minor, L. B. and Cullen, K. E. (2010). Multimodal integration after unilateral labyrinthine lesion: single vestibular nuclei neuron responses and implications for postural compensation. *J. Neurophysiol.* **105**, 661-673. doi:10.1152/jn.00788.2010

Sadeghi, S. G., Pyott, S. J., Yu, Z. and Glowatzki, E. (2014). Glutamatergic signaling at the vestibular hair cell calyx synapse. *J. Neurosci.* **34**, 14536-14550. doi:10.1523/JNEUROSCI.0369-13.2014

Schuknecht, H. F. (1993). *Pathology of the Ear*, p. 273, 2nd edn. Philadelphia: Lea & Febiger.

Sedó-Cabezón, L., Jedynak, P., Boadas-Vaello, P. and Llorens, J. (2015). Transient alteration of the vestibular calyceal junction and synapse in response to chronic ototoxic insult in rats. *Dis. Model. Mech.* **8**, 1323-1337. doi:10.1242/dmm.021436

Seoane, A., Demêmes, D. and Llorens, J. (2001). Pathology of the rat vestibular sensory epithelia during subchronic 3,3'-iminodipropionitrile exposure: hair cells may not be the primary target of toxicity. *Acta Neuropathol.* **102**, 339-348.

Smith, P. F. (2000). Are vestibular hair cells excited to death by aminoglycoside antibiotics? *J. Vest. Res.* **10**, 1-5.

Spoendlin, H. (1971). Primary structural changes in the organ of Corti after acoustic overstimulation. *Acta Otolaryngol.* **71**, 166-176. doi:10.3109/00016487109125346

Strupp, M. and Brandt, T. (2009). Vestibular neuritis. *Semin. Neurol.* **29**, 509-519. doi:10.1055/s-0029-1241040

Strupp, M. and Magnusson, M. (2015). Acute unilateral vestibulopathy. *Neurol Clinics* **33**, 669-685. doi:10.1016/j.ncl.2015.04.012

Strupp, M., Zingler, V. C., Arbusow, V., Niklas, D., Maag, K. P., Dieterich, M., Bense, S., Theil, D., Jahn, K. and Brandt, T. (2004). Methylprednisolone, valacyclovir, or the combination for vestibular neuritis. *N. Engl. J. Med.* **351**, 354-361. doi:10.1056/NEJMoa033280

Travo, C., Gaboyard-Niay, S. and Chabbert, C. (2012). Plasticity of Scarpa's Ganglion neurons as a possible basis for functional restoration within vestibular endorgans. *Front. Neurol.* **3**, 91. doi:10.3389/fneur.2012.00091

Uffer, D. S. and Hegemann, S. C. A. (2016). About the pathophysiology of acute unilateral vestibular deficit - vestibular neuritis (VN) or peripheral vestibulopathy (PVP)? *J. Vestibular Res.* **26**, 311-317. doi:10.3233/VES-160581

Viana, L. M., O'Malley, J. T., Burgess, B. J., Jones, D. D., Oliveira, C. A. C. P., Santos, F., Merchant, S. N., Liberman, L. D. and Liberman, M. C. (2015). Cochlear neuropathy in human presbycusis: confocal analysis of hidden hearing loss in post-mortem tissue. *Hear. Res.* **327**, 78-88. doi:10.1016/j.heares.2015.04.014

Wersall, J. (1956). Studies on the structure and innervation of the sensory epithelium of the cristae ampullaris in the guinea pig. *Acta Otolaryngol. Suppl.* **126**, 1-85.

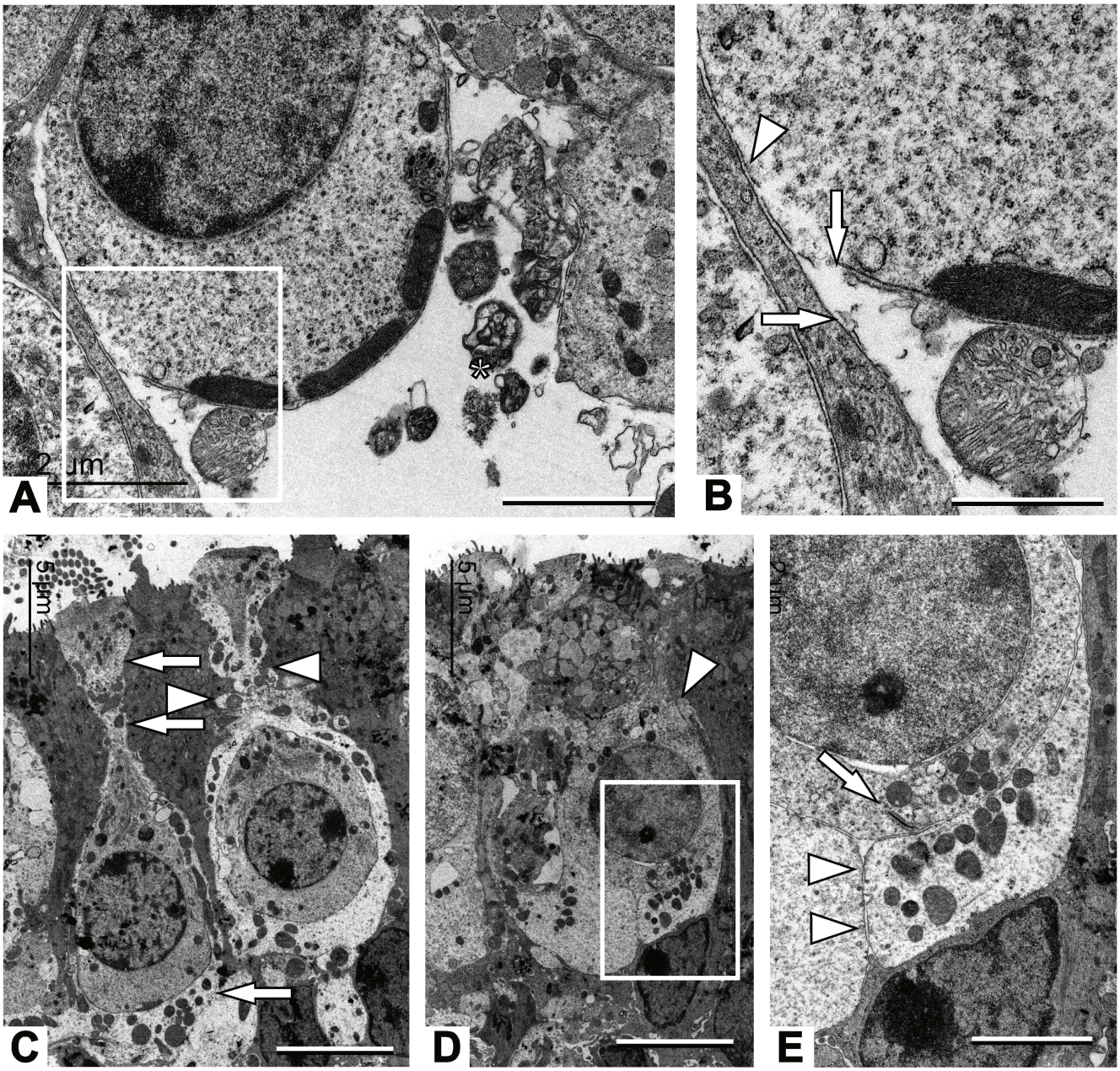

Figure S1: TEM observation of vestibular primary synapses in the mouse utricle following TTK. (**A and B**) Four hours following the TTK administration, a swollen calyx ending contacts a type I hair cell (A). The boxed area in A is shown at higher magnification in B. Disruptions in the hair cell and calyx membranes are clearly identifiable (arrows in B). Mitochondria display modified ultrastructure in the calyx afferent (* in A). (**C**) Two type I hair cells at one week after TTK. A calyx afferent displaying normal ultrastructure (arrows), encases the cell on the left. In contrast, the calyx ending surrounding the right cell shows a fragmented appearance in the neck region of the cell (arrowheads). (**D**) A type I hair cell with an incomplete and fragmented calyx. Note the upper end of the calyx, falling short of the position it should attain closer to the apical end of the cell. Note also the fragmented nature of the afferent in the

basal part of the cell (box). (**E**) This higher magnification of the area boxed shows the fragmented nature of the calyx ending (arrowheads). Nevertheless, a ribbon (arrow) is clearly observed in the pre-synaptic side. Sample: n = 3 in each group. Scale bars= 2 μm in A and E; 1 μm in B; and 5 μm in C and D.

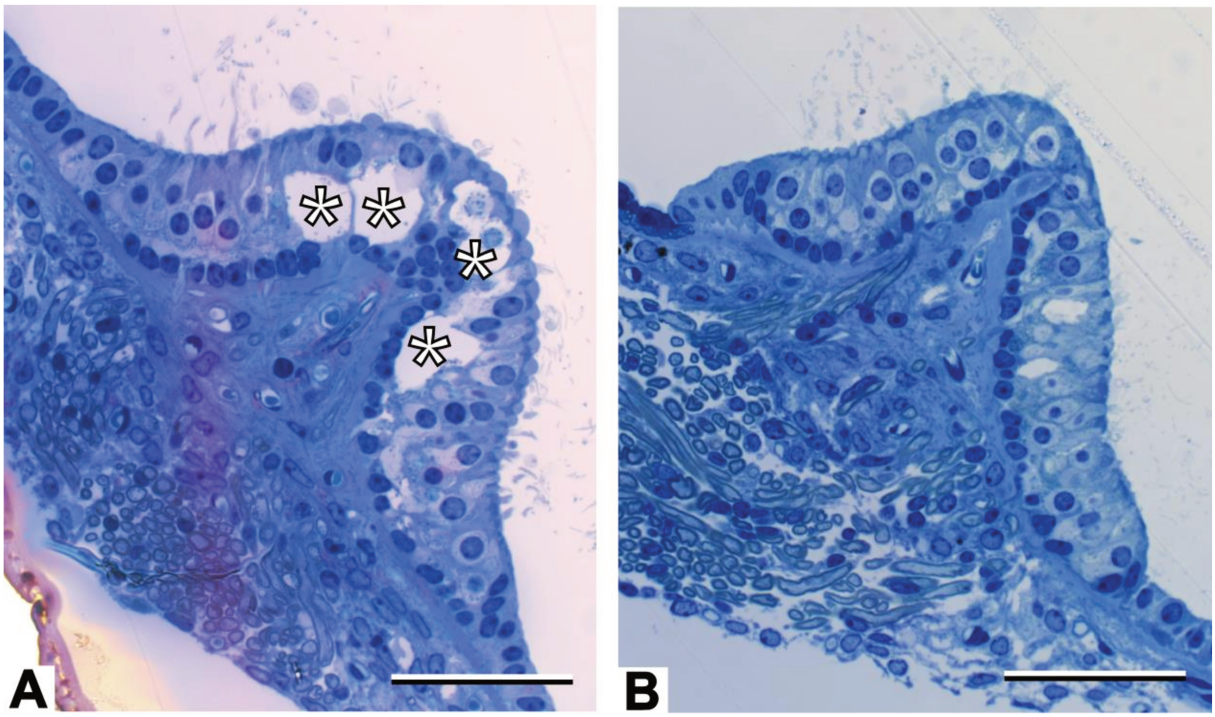

Figure S2: Light microscopy observation of vestibular crista following TTK. (**A**) At 4 h after TTK, large vacuoles are observed throughout the crista sensory cells layer. The swellings were often more visible in the central part of the crista (*). (**B**) A representative crista one week after TTK administration, showing control-like morphology. Sample: n = 3 in each group. Scale bars= 50 μm.

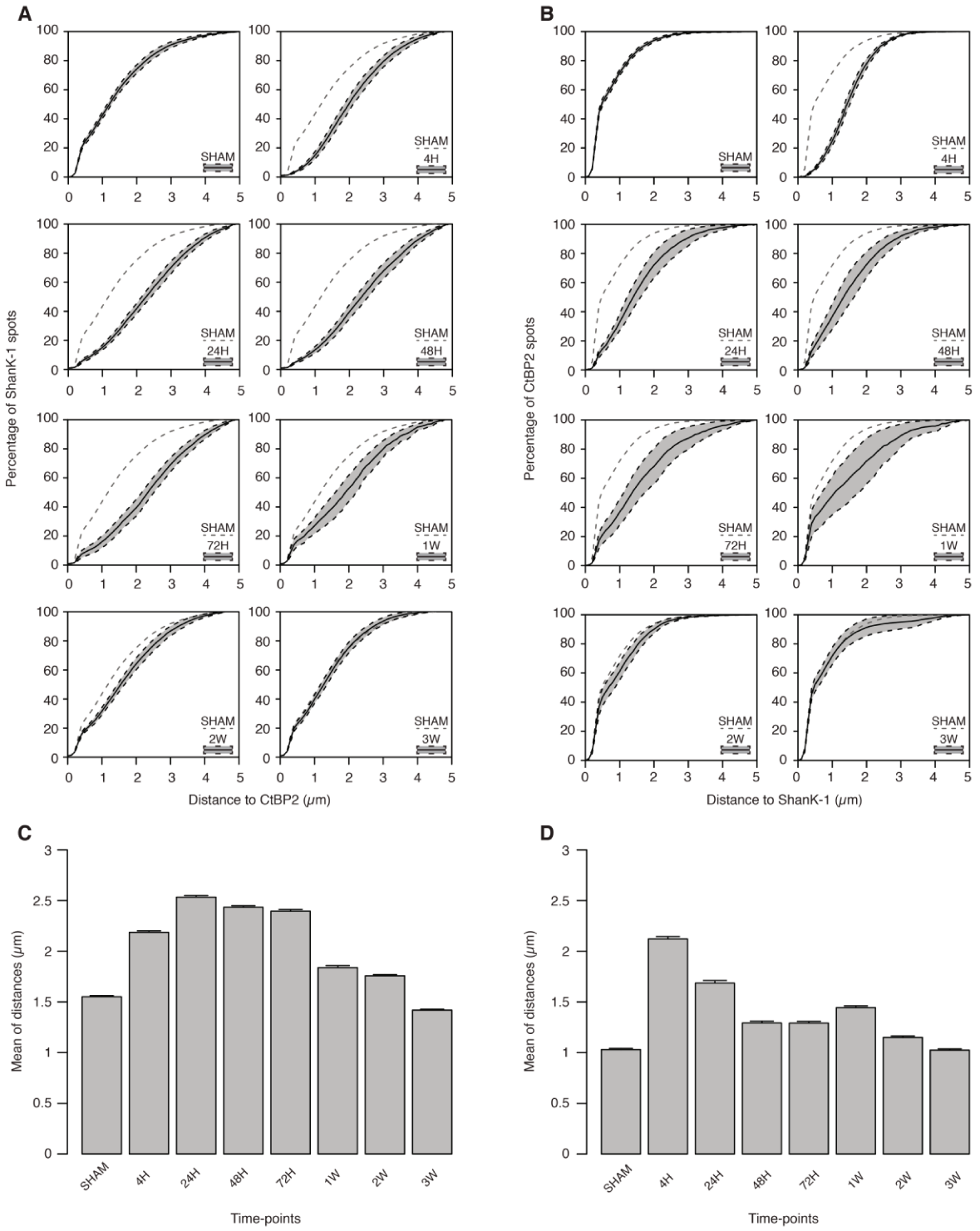

Figure S3: Time dependent variation of cumulative and mean distances between CtBP2 to SHANK-1 and vice versa following TTK administration in the crista. Variation of cumulative distances (**A and B**) and mean distances (**C and D**) at each selected time points. (n = 6) for 4h, 72h and 3W; (n = 5) for Sham, 24h, 48h, 1W and 2W. Results are expressed as mean ± SEM.

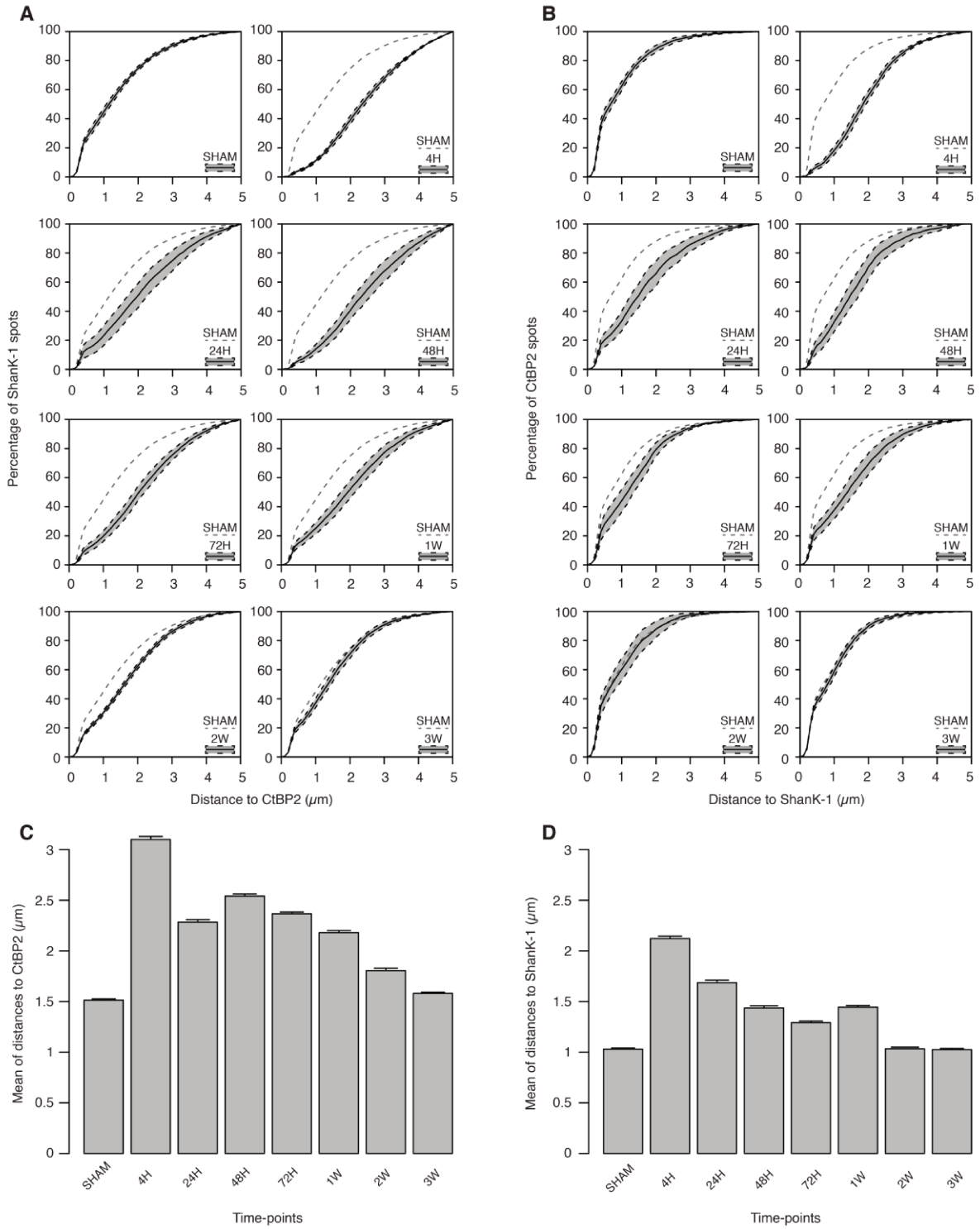

Figure S4: Time dependent variation of cumulative and mean distances between CtBP2 to SHANK-1 and vice versa following TTK administration in the utricle. Variation of cumulative distances (**A and B**) and mean distances (**C and D**) at each selected time points. (n = 6) for 48h, 72h and 2W; (n = 5) for Sham, 24h and 3W; (n = 4) for 4h and 1W. Results are expressed as mean ± SEM.

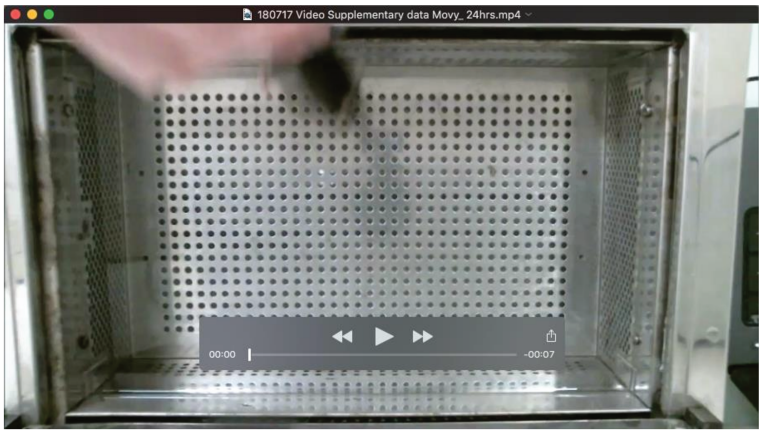

Movie 1: This video illustrates the loss of the swimming ability in a mouse at 24h after the TTK administration.

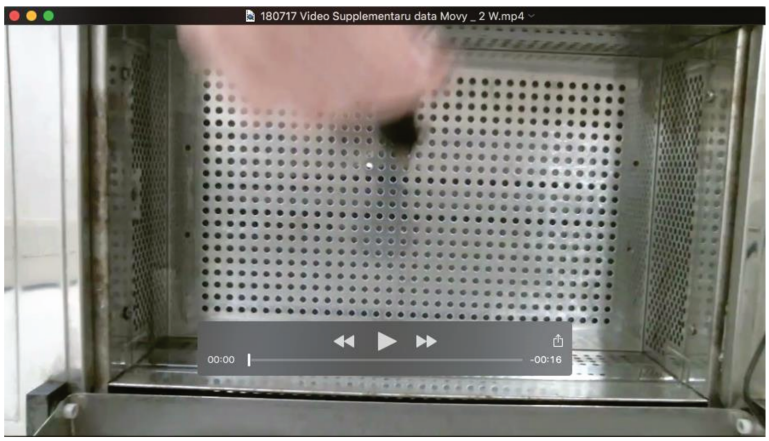

Movie 2. This video illustrates the recovery of the swimming ability in a mouse at 2 weeks after the TTK administration.

2.2.5. Conclusion

Nous avons montré la faisabilité d'un nouveau modèle murin de lésion neuroinflammatoire transitoire du nerf vestibulaire par atteinte synaptique. Cette lésion, obtenue par injection retro-tympanique d'un produit excitotoxique (kaïnate), permet une récupération rapide, en une semaine, de la fonction vestibulaire (normalisation du réflexe vestibulo-oculaire et disparition du comportement anormal locomoteur). Le mécanisme mis en évidence de réafférentation ouvre un nouveau champ de recherche thérapeutique, dont l'objectif serait de faciliter ou guider la récupération du côté lésionnel. Ce mécanisme est encore mal compris, notamment concernant la possibilité que la réafférentation se fasse de façon erronée (un neurone afférent donné se reconnectant à la mauvaise cellule ciliée), ce qui pourrait participer à la persistance de troubles vestibulaires à distance de lésion.

Lors de la récupération des souris TTK, les résultats de l'étude ne permettent pas de différencier la composante compensatoire (plasticité centrale avec les entrées contralatérales et résiduelles ipsilatérales) de la récupération de fonction ipsilatérale par réafférentation des neurones vestibulaires primaires. Poursuivre l'étude serait intéressant, car pourrait déboucher sur deux stratégies thérapeutiques complémentaires pour aider la réafférentation du côté lésionnel d'une part, et favoriser la compensation d'autre part.

2.3. Article 6 : Exploration fonctionnelle vestibulaire après lésion au 3.3' IDPN : étude du rôle des cellules ciliées de type 1

2.3.1. Contexte scientifique

Comme présenté dans l'introduction, l'épithélium vestibulaire et constitué de cellules de type I et type II. Les types I ont des synapses en calice et sont plutôt réparties au centre des organes vestibulaires ; alors que les type II ont des synapses en bouton et sont plutôt réparties en périphérie. Les neurones afférents sont également de deux types : phasiques adapté au codage de mouvements rapides de la tête, et répartis surtout sur les synapses des cellules de type I dans la région centrale des organes vestibulaires, et toniques adaptés au mouvements lents et répartis plutôt en périphérie préférentiellement sur les cellules de type II (Beraneck and Straka, 2011; Straka et al., 2009). Cependant, le lien entre l'organisation des cellules ciliées et des groupes de neurones et donc le rôle de chaque type de cellule ciliée dans la transmission des différentes composantes du mouvement ne sont pas démontrés. Aussi, le rôle fonctionnel de chaque type de cellule ciliée est mal connu.

Le 3.3' IDPN (3.3'-iminodipropionitrile) est un nitrile synthétique neurotoxique avec des effets ototoxiques et hépatotoxiques (Alwelaie et al., 2019; Greguske et al., 2019; Zeng et al., 2020). Au niveau vestibulaire, le 3.3'IDPN entraîne des lésions des cellules ciliées, principalement de type I. En fonction de la dose et de la durée d'exposition, le 3.3' IDPN entraine des lésions sur les synapses en calice : fragmentation et disjonction synaptique (lésions réversibles), fusion des stéréocils et extrusion cellulaire dans la zone péri-striolaire (lésions irréversibles). Au niveau moléculaire, une perte d'expression de marqueurs protéiques synaptiques des afférences neuronales et des cellules ciliées a lieu (Llorens and Demêmes, 1994). L'étude du comportement des animaux exposés montre une atteinte vestibulaire dont la gravité augmente avec la durée d'exposition et réversibles après l'arrêt de celle-ci (Greguske et al., 2019; Llorens et al., 1993). Aucune exploration fonctionnelle vestibulaire n'a été faite après administration de 3.3' IDPN.

2.3.2. Buts de l'étude

Pour mieux comprendre le rôle des deux types de cellules ciliées dans la fonction vestibulaire, nous proposons d'utiliser une substance ototoxique, la 3.3'IDPN, qui altère préférentiellement les cellules de type I. Nous corrélerons ensuite le degré de dommage cellulaire en microscopie (pourcentage de mort cellulaire et ratio cellules type I et type II) à la fonction vestibulaire (canalaire, otolithique et *velocity storage*).

2.3.3. Résumé en français

Un total de 43 souris a été réparti en 5 groupes avec une injection intrapéritonéale de différentes doses de 3.3'IDPN (16, 24, 32 ou 40 mmol/kg) ou de NaCl pour le groupe contrôle. Une exploration vestibulaire a été réalisée avant injection, puis à 14 et 21 jours après l'injection. Les souris avaient une fonction vestibulaire dose-dépendant, avec une destruction complète de l'ensemble de l'organe vestibulaire aux deux doses les plus élevée 32 et 40 mmol/kg. A 24 mmol/kg, la fonction vestibulaire était significativement moins bonne que les sham à l'ensemble des explorations sauf concernant le gain aVOR à la plus basse fréquence 0,2Hz. Enfin à 16mmol/kg, la fonction vestibulaire n'était significativement altérée que pour les stimulations sinusoïdales à très haute fréquence (1 et 2Hz). Les cellules de type I semblent coder surtout pour les mouvements de tête les plus rapides (fréquences élevées). Les fréquences basses ainsi que les réflexes otolithiques semblent atteintes aux concentrations plus élevées où le 3.3'IDPN pourrait avoir détruit plus largement les deux types de cellules ciliées.

2.3.4. Article original

Titre :

Vestibular function correlated to hair cell degeneration after 3.3'IDPN intraperitoneal injection in the mouse

Auteurs :

Travail d'encadrement du Master 2 de Cassandre DJIAN, en collaboration avec Jordi LLORENS (Cellular and Molecular Basis of Sensory Disorders Group, Université de Barcelone)

Etat d'avancement :

Article en préparation

Introduction:

Type I and type II hair cells constitute the sensory part of the vestibular epithelium and form respectively calyx and button synapses with the neuronal afferents. The vestibular epithelium transduces a mechanical signal, induced by the stimulation of hair cells by the movements of the endolymph, into an electrical signal transmitted by the afferent neuron to the homolateral vestibular nucleus.

Within the otolithic maculae and cristae ampullaris, the vestibular epithelium is organised very specifically: the central region of the cristae and the centriolar region of the maculae contain a majority of type I hair cells, whereas type II cells are predominant in the peripheral areas of the cristae and maculae. Type I and II cells are in equal proportion in intermediate zones [1].

Afferent neurons are classified as either phasic or tonic neurons. These neuronal afferent fibers are also organised according to a specific morphological and functional regionalisation [1, 2]. Phasic neurons are mostly located in the centre of otolith maculae and cristae ampullaris, and tonic neurons in the periphery. Each neuronal subgroup codes for different components of vestibular information: tonic neurons function as low-pass filters and their characteristics are favourable to low frequencies and head positions coding; phasic neurons function as band-pass filter and their characteristics are in favour of high frequency movements coding [3, 4]. Thus, there is a parallel organization between phasic neurons and type I hair cells on one hand, and tonic neurons and type II hair cells on the other. However, the link between the organisation of hair cells and sub-groups of neurons and thus the precise role of each type of hair cell for the transmission of different components of head movements has not been demonstrated.

The objective of this study is to target type I hair cells using an ototoxic substance, the 3.3'iodipropionitrile (3.3'IDPN), and to study the effect of this cellular loss on the vestibular function, by measuring the vestibulo-ocular reflex. 3.3' IDPN is a well described neurotoxic and vestibulotoxic substance [5, 6]. The effects of 3.3' IDPN on hair cells are known [7]: lesions are visible after a single injection of 3.3' IDPN, and are dose-dependent: lesions are observed preferentially on the calyx junctions of type I hair cells at low doses, while both types I and II are affected by higher doses [8, 9]. Intraperitoneal 3.3 ' IDPN injections lead to locomotor and postural abnormalities compatible with vestibular damage, the severity of which increases with the dose injected and duration of exposure [5].

These abnormalities may be observed after acute or chronic exposure to 3.3' IDPN [7, 8, 10]. However, quantitative alterations of the vestibulo-ocular reflex induced by 3.3' IDPN have never been studied.

Materials and Methods:

Ethics statement

Forty-five male and female C57/Bl6J mice aged 6 weeks were provided by Charles River. Animals were used in accordance with the European Communities Council Directive 2010/63/EU. All efforts were made to minimize suffering and reduce the number of animals included in the study. All procedures were approved by the ethical committee for animal research of the University of Paris (CEEA.34).

Groups

The mice were divided into 5 groups. Each mouse was weighed and given a single intraperitoneal injection of 3.3' IDPN at a dose of either 16; 24; 32 or 40 mmol/kg, or saline for sham mice. The vestibulo-ocular reflexes were studied immediately prior to exposure to 3.3'IDPN and again 14 and 21 days after injection.

Behavioural examination

Mouse behaviour was assessed before and after injection at day 14 and 21 according to 6 items: ability to swim (over a 30-second-long period), circling (stereotyped circulatory ambulation) , head bobbing or head tossing, retropulsion, air-righting reflex (ability to right themselves in the air during a fall), tail-lift reflex (forelimb extension toward the earth's center of gravity). All 6 items were quantified with a scale from 0 (normal behaviour, no deficit) to 4 (highest degree of abnormal behaviour), with a maximum deficit score of 24. The behavioural score used in this study is detailed in ***Table 1***.

Vestibular function exploration using video-oculography

In order to perform head restrained vestibular exploration, a head post was surgically implanted two days before vestibular exploration. Head implant surgery and peri-operative care has been described previously [11, 12]. Briefly, under gas anaesthesia (isofurane), a small custom-built head holder was cemented (C&B Metabond) to the skull just anterior to the lambda landmark (see França de Barros et al. 2019 for a video tutorial [13]).

Table 1: Vestibular behavioural score

SCORE	0	1	2	3	4
Swim	Normal	Head tilt	circling	Delayed drowning	Immediate drawning
Circling	Absence	No exploration	Intermittent	Very frequent	Permanent
Retropulsion	Absence	fréquent	Intermittent	Very frequent	Permanent
Head bobbing / tossing	Absence	Rare	Intermittent	Very frequent	Permanent
Air-righting reflex	Normal	Mildly unstable	Very unstable	No air-righting reflex	Spatial disorientation after the fall
Tail-lift reflex	Extension	Intermittent bending / curling	permanent bending	Intermittent agitation	Important agitation

Vestibular function was explored before IDPN injection; and after injection at day 14 and 21. As reported previously, [11, 12, 14, 15] all recordings were made in the dark using an infrared video system (ETL-200, ISCAN, Burlington MA), recording pupil and corneal reflection (CR) position.

Eye movements were recorded using non-invasive video-oculography [16]. The experimental set-up, apparatus and methods of data acquisition are similar to those previously described [12, 17, 18]. Briefly, mice were head-fixed at a ~30° nose-down position to align the horizontal canals in the yaw plane [19]. Animals were placed in a custom-built Plexiglas tube secured on the superstructure of a vestibular stimulator. The VOR tests were performed in a temperature-controlled room (21°C) with all sources of light turned off except for computer screens. The turntable was further surrounded with a closed box to isolate the animal from remaining light, with a final luminance inside the box <0.02 lux. Myosis was induced with 2% pilocarpine applied 10 minutes before experimentation. Recorded eye and head position signals were sampled at 1 kHz, digitally recorded (CED power1401 MkII) using Spike 2 software and later exported to the Matlab programming environment for off-line analysis (Matlab, The MathWorks).

Angular horizontal vestibulo-ocular reflex (aVOR) was tested during horizontal sinusoidal rotation of the turntable (at 0.2; 0.5; 1 and 1.5Hz; peak velocity 30°/s). Analysis was made on at least 10 cycles Two parameters were extracted from the recordings: the gain and the phase. The gain is the ratio between the amplitude of the eye (response) and head (stimulus) rotations. Since the animal is

head-fixed to the rotating table, head movements and table movements are identical. The phase is the temporal shift between the eye and table rotations, expressed as ratio of the sinusoidal cycle (2 pi). Details for gain and phase calculation are reported in Carcaud et al. 2017 [17]. Values with VAF (Variance-accounted-for) under 0.5 were discarded [11].

The eye movements evoked by a specific stimulation of the otoliths (maculo-ocular reflexes, MOR) were tested [20] using off-vertical axis rotation (OVAR) as previously described [12]. Briefly, the axis of rotation was tilted by 17° with respect to the vertical. Rotations were performed at constant speed (50°/s) for at least 10 rotations both in the clockwise (CW) and the counterclockwise (CCW) directions. Due to the inertial nature of the angular movement detection, a rotation at constant speed elicits a combined canalar and otolithic response at the beginning of the trace, however after a few seconds only the otolithic component remains [12, 21]. Since gravitational acceleration acts vertically, this stimulation is equivalent to a continuous rotation (at 0.14 Hz) around the mouse head of a 17° tilted constant linear acceleration stimulus (see figure 2B in Beraneck et al. 2012 [12]). For horizontal OVAR responses, quick-phases were identified and removed. During rotations, the velocity of horizontal slow phases is modulated (modulation, μ) around a constant bias (β). Both parameters (μ and β) were calculated from the sinusoidal fit of eye horizontal slow-phase velocity using the least-squares optimization of the equation:

- $$\boldsymbol{SP(t) = \beta + \mu \cdot \sin\ [2\pi \cdot f_0 \cdot (t + t_d)]}$$

where SP(t) is slow-phase velocity, β is the steady-state bias slow phase velocity, μ is the modulation of eye velocity, f_0 is the frequency of table rotation, t_d is the dynamic lag time (in msec) of the eye movement with respect to the head movement. The bias (Macuo-ocular reflex Bias; MOR_B) is reported here as the main index of otolithic response [12, 20]. Notably, MOR requires normal otolith function but also an efficient central velocity storage network.

Also, static vertical pupil position according to head tilt angle was measured first with the mouse maintained at a 0° horizontal position. The whole platform was then tilted into different roll positions, at 10°, 20°, 30° and 40° alternatively to the right and to the left. The platform was rotated manually and slowly to limit semi-circular canal stimulation. Measurements were made in a static position during at

least 15 seconds to identify the stable pupil position. The vertical eye angle was then calculated from the raw vertical CR and pupil position [22]. The $_{tilt}$MOR gain was calculated corresponding to the slope of a linear regression of both variables (vertical eye angle and head tilt degree).

Finally, angular velocity steps in a horizontal plane (hsteps) were performed at a speed of 50°/s in yaw plane. The horizontal slow phase velocity decay was fitted to an exponential curve ($f(x) = a*\exp(b*x)$) and the time constant τ was then calculated as $\tau=-1/b$. The time constant of the slow phase exponential velocity decay was calculated at start and stop of CW and CCW rotations to assess velocity storage. CCW-start and CW-stop, CCW-stop and CW-start, were combined to assess a bilateral function. VOR gain at the maximum slow phase velocity was also calculated.

Statistical analysis

Statistical analysis was made using XLstats (Addinsoft, New York, NY). All data are reported as mean and standard deviation. Outliers were identified using Grupps test and deleted. Repeated measures ANOVA was used, three-way to compare aVOR (lesion, time and frequency), two-way for ipsilateral and contralateral OVAR, angular velocity and static head-tilt stimulations and one-way for behaviour score. Tukey HSD test was used for post-hoc comparisons. $p < 0.05$ was considered significant.

Structural and immnunohistochemical analysis of the vestibular epithelium

The protocol is described in a previous study [7]. After the last vestibular tests, the mice were sacrificed in order to dissection the vestibular organs. Cristae ampullaris and maculae were collected for ultrastructural and immunohistochemical analysis. The first dissected ear from each animal was used for ultrastructural studies while the second was used for immunohistochemistry. The three cristae, the utricle, and the saccule were dissected using a binocular microscope under a fume hood. After dissection, the vestibular epithelia were fixed for 20min, rinsed with buffer, post-fixed with paraformaldehyde until further processing. Structural analysis: during scanning electron microscopy studies, each vestibular epithelium was assigned a pathology score according to a scale of 0–5, depending on the degree of alteration of the vestibular epithelium. During transmission electron microscopy studies, the distance between the centres of adjacent membranes at the contact between type I HCs (HCI) and the calyx afferent was measured. Immnuohistochemistry: mouse monoclonal anti-Caspr1 anti-GluA2 and anti-Ribeye/CtBP2 were used for identification of type I hair cells.

Results:

Animals

A total of 43 mice were included and divided into 5 groups according to the injected dose of IDPN: Sham (control group; NaCl injection; n = 8); 16 mmol/kg (n = 10); 24 mmol/kg (n = 9); 32 mmol/kg (n = 8) and 40 mmol/kg (n = 8). Two mice were excluded during the protocol (1 mouse died after xylocaine injection, 1 loss of headpost). The groups were sex-matched, and all mice were 6 weeks old at the beginning of the study.

Behavioural score

Results of the behavioural score are summarized in ***Table 2***. The severity of the behavioural impairment increased with the dose of IDPN received. For each group, behavioural scores at D14 were comparable to those at D21. Comparison of behavioural scores at different doses are reported in ***Table 3***.

Table 2: Behavioural score

Dose (mmol/kg)	Pre-injection	D14	D21
40	0	19±1.22	19±1.58
32	0	18±1.58	15.80±3.77
24	0	12±3.58	11±5.25
16	0	7.60±0.55	6.80±2.49
Sham	0	0.00±0.00	0.00±0.00

All values are represented as mean ± SD (standard deviation).

Table 3: Statistical significance when comparing behavioural scores at different doses

Behavioral score	D14	D21
40 vs Sham	***< 0.0001***	***< 0.0001***
32 vs Sham	***< 0.0001***	***< 0.0001***
24 vs Sham	***< 0.0001***	***< 0.0001***
16 vs Sham	***0.000***	***0.000***

Significant values are in bold

Table 4: Horizontal angular vestibulo-ocular reflex

Frequency	Dose (mmol/kg)	Pre-injection	D14	D21	*p* (D0-D21)	*p* (D14-D21)
			aVOR Gain			
0.2 Hz	40	0.24±0.09	0.01±0.01	0.02±0.02	***0.000***	*0.923*
	32	0.30±0.15	0.03±0.05	0.03±0.02	***< 0.0001***	*0.935*
	24	0.24±0.09	0.11±0.10	0.11±0.11	*0.049*	*0.917*
	16	0.25±0.15	0.2±0.14	0.20±0.12	*0.491*	*0.975*
	Sham	0.19±0.06	0.1 ±0.04	0.20±0.04	*0.876*	*0.436*
0.5 Hz	40	0.51±0.09	0.03±0.03	0.02±0.02	***< 0.0001***	*0.831*
	32	0.56±0.12	0.05±0.09	0.08±0.10	***< 0.0001***	*0.722*
	24	0.54±0.12	0.21±0.19	0.26±0.23	***< 0.0001***	*0.436*
	16	0.52±0.12	0.34±0.21	0.44±0.20	*0.256*	*0.103*
	Sham	0.39±0.13	0.42±0.05	0.46±0.09	*0.294*	*0.546*
0.8 Hz	40	0.63±0.13	0.02±0.01	0.03±0.03	***< 0.0001***	*0.894*
	32	0.59±0.12	0.08±0.13	0.06±0.07	***< 0.0001***	*0.929*
	24	0.55±0.07	0.27±0.25	0.33±0.27	***0.000***	*0.350*
	16	0.56±0.17	0.46±0.23	0.50±0.18	*0.350*	*0.493*
	Sham	0.50±0.15	0.51±0.11	0.58±0.13	*0.221*	*0.276*
1 Hz	40	0.67±0.11	0.02±0.01	0.02±0.02	***< 0.0001***	*0.984*
	32	0.67±0.12	0.08±0.13	0.09±0.13	***< 0.0001***	*0.908*
	24	0.69±0.08	0.32±0.25	0.34±0.29	***< 0.0001***	*0.691*
	16	0.62±0.13	0.52±0.26	0.53±0.17	*0.171*	*0.840*
	Sham	0.58±0.13	0.53±0.12	0.71±0.12	*0.052*	***0.005***
2 Hz	40	0.89±0.11	0.05±0.10	0.02±0.03	***< 0.0001***	*0.697*
	32	0.79±0.09	0.23±0.16	0.23±0.20	***< 0.0001***	*0.909*
	24	0.87±0.13	0.57±0.34	0.46±0.34	***< 0.0001***	*0.090*
	16	0.72±0.16	0.73±0.32	0.70±0.24	*0.697*	*0.674*
	Sham	0.76±0.16	0.72±0.20	0.99±0.33	***0.000***	***< 0.0001***
			aVOR phase			
0.2 Hz	24	28.31±10.23	25.16±13.96	31.36±12.18	*0.626*	*0.387*
	16	24.72±12.79	25.10±11	27.74±7.77	*0.929*	*0.953*
	Sham	35.6±8.14	37.83±10.69	37.42±5.85	*0.958*	*0.990*
0.5 Hz	24	15.28±6.23	18.76±13.86	27.75±21.74	*0.986*	*0.983*
	16	20.27±18.01	23.44±12.97	27.06±30.35	*0.841*	*0.966*
	Sham	31.45±25.14	25.25±18.10	23.04±12.73	*0.803*	*0.948*
0.8 Hz	24	1.95±5.33	16.94±20.29	21.84±22.47	*0.965*	*0.173*
	16	11.35±16.81	8.29±7.04	16.16±19.27	*0.887*	*0.918*
	Sham	7.38±8.74	6.84±7.59	7.63±7.25	0.994	0.981
1 Hz	24	-1.36±4.91	10.49±17.83	10.38±18.18	0.400	0.085
	16	-0.83±4.69	2.80±6.92	3.6 ±14.03	0.896	0.268
	Sham	3.33±8.46	0.05±7.98	-0.36±4.10	0.913	0.990
2 Hz	24	-25.52±5.26	-29.48±18.93	-18.31±7.43	0.188	0.896
	16	-23.62±4.64	-19.92±13.46	-20.66±5.46	0.930	0.963
	Sham	-24.03±3.65	-13.27±19.23	-23.22±5.80	0.981	0.238

All values are represented as mean ± SD (standard deviation). Phase is expressed in degrees. Statistically significant values are in bold. D0, D14 and D21 correspond to day before IDPN injection and 14 or 21 days after. *aVOR* angular vestibulo-ocular reflex

Table 5: $_{TILT}$MOR gain, $_{OVAR}$MOR bias, hSteps time constant (Tau) and maximum velocity gain

Dose (mmol/kg)	Pre-injection	D14	D21	*p* (D0-D21)	*p* (D14-D21)
			$_{TILT}$**MOR (gain)**		
40	0.63±0.04	0.05±0.10	0.03±0.04	***< 0.0001***	*0.671*
32	0.56±0.06	0.04±0.04	0.07±0.14	***< 0.0001***	*0.760*
24	0.57±0.14	0.18±0.21	0.25±0.20	***< 0.0001***	*0.208*
16	0.47±0.09	0.41±0.13	0.30±0.09	***0.003***	*0.064*
Sham	0.50±0.16	0.47±0.09	0.42±0.11	*0.143*	*0.387*
			$_{OVAR}$**MOR (bias)**		
40	0.11±0.06	0.01±0.02	0.00±0.00	***0.000***	*0.841*
32	0.10±0.04	0.1±0.01	0.01±0.01	***0.001***	*0.995*
24	0.09±0.03	0.01±0.02	0.05±0.06	*0.095*	*0.187*
16	0.12±0.13	0.06±0.06	0.09±0.05	*0.214*	*0.263*
Sham	0.07±0.05	0.07±0.03	0.11±0.03	*0.197*	*0.201*
			$_{HSTEPS}$**Time constant (Tau)**		
40	2.36±1.16	0.06±0.18	0.00±0.00	***< 0.0001***	*0.825*
32	1.75±0.72	0.13±0.22	0.00±0.00	***< 0.0001***	*0.667*
24	2.21±0.58	0.70±0.54	1.03±0.86	***< 0.0001***	*0.316*
16	1.88±0.64	1.06±0.72	1.65±0.71	*0.870*	*0.072*
Sham	1.52±0.54	1.72±0.57	1.66±0.41	*0.646*	*0.829*
			$_{HSTEPS}$**Max VOR gain**		
40	0.74±0.14	0.02±0.06	0.00±0.00	***< 0.0001***	*0.808*
32	0.71±0.07	0.08±0.15	0.00±0.00	***< 0.0001***	*0.368*
24	0.77±0.09	0.32±0.29	0.38±0.34	***< 0.0001***	*0.565*
16	0.67±0.14	0.41±0.13	0.63±0.31	*0.790*	*0.802*
Sham	0.64±0.15	0.47±0.09	0.71±0.16	*0.465*	*0.250*

All values are represented as mean ± SD (standard deviation). Significant values are in bold. D0, D14 and D21 correspond to day before IDPN injection and 14 or 21 days after. *MOR* maculo-ocular reflex. *OVAR* off-vertical axis rotation.

Vestibular function exploration using video-oculography

The results of aVOR gain, $_{OVAR}$MOR, $_{tilt}$MOR and hSteps time constant and maximal gain are reported in ***Table 3 and 4.*** Comparisons of canalo-ocular and maculo-ocular reflexes gains according to each dose and their statistical significance are summarized in ***Table 5***. These results are detailed below according to each test. Briefly, there was a dose-dependent effect of IDPN on aVOR gain, $_{OVAR}$MOR, $_{tilt}$MOR, hSteps maximal gain and time constant (***Figures 1 and 2***).

Concerning aVOR, at doses of 32 and 40 mmol/kg at D21, VOR gains were significantly decreased at all frequencies compared to the Sham group. At 24 mmol/kg, gains were significantly decreased at frequencies ≥ 0.5 Hz; at 16 mmol/kg, they were significantly decreased at 1 and 2 Hz only (***Table 3***). Comparing the gains before injection and at D21 post-injection showed that a dose ≥ 24 mmol/kg resulted in a significant decrease in the vestibulo-ocular reflex gain. At 16 mmol/kg, gains were not significantly changed by the injection. In the Sham group, gains were significantly increased at D21 compared to before injection. For all groups, there was no significant change between D14 and D21. VOR gains were not statistically different between male and female groups ($p = 0.307$).

Phase values for 32 and 40 mmol/kg groups were not included because their VAF was < 0.5. The results of Sham, 16 and 24 mmol/kg phases and their statistical significance are summarized in ***Table 3***. At 24 mmol/kg, there was a non-significant change in phase compared to the control group. During (hsteps) horizontal steps D21, at 24 mmol/kg and higher doses at D21, there was a significant decrease in the time constant and maximal gain of the per/post-rotatory nystagmus compared to the control group. At 16 mmol/kg, the time constant and maximum velocity gain were not significantly altered. Canalar (aVOR and hsteps) stimulations are reported in ***Figure 1***.

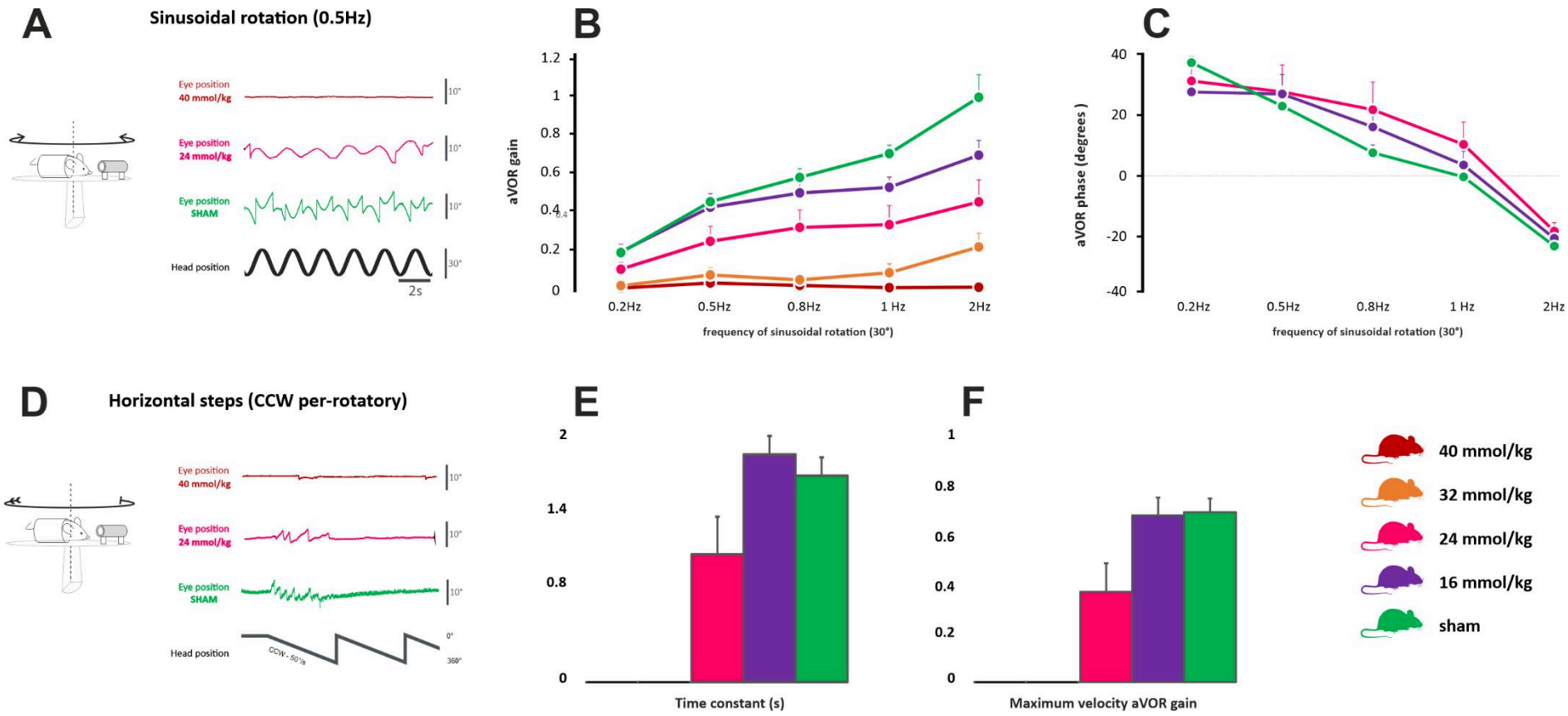

Figure 1: Semi-circular canal function.

The horizontal semi-circular canal (SCC) was tested. **A:** Horizontal sinusoidal rotation tested for aVOR. Traces show head position (corresponding to table position) and horizontal eye movement. The higher the dosage, the smaller the amplitude of the eye movement. **B:** aVOR gain for maximum 30°/s velocity according to frequency of stimulation. **C:** aVOR phase for maximum 30°/s velocity according to frequency of stimulation. **D:** Horizontal steps at 50°/s. Traces show head position and horizontal eye position, during per-rotatory nystagmus at the start of a CCW stimulation. The smaller number of nystagmus the more the mouse is impaired. **E:** Time constant for hsteps at 50°/s (mean of all four CW, CCW, per- and post-rotatory values). **F:** Peak velocity aVOR gain during hsteps at 50°/s (mean of all four CW, CCW, per- and post-rotatory values). *aVOR* angular vestibulo-ocular reflex *CW* Clockwise *CCW* Counter-clockwise *hsteps* horizontal steps.

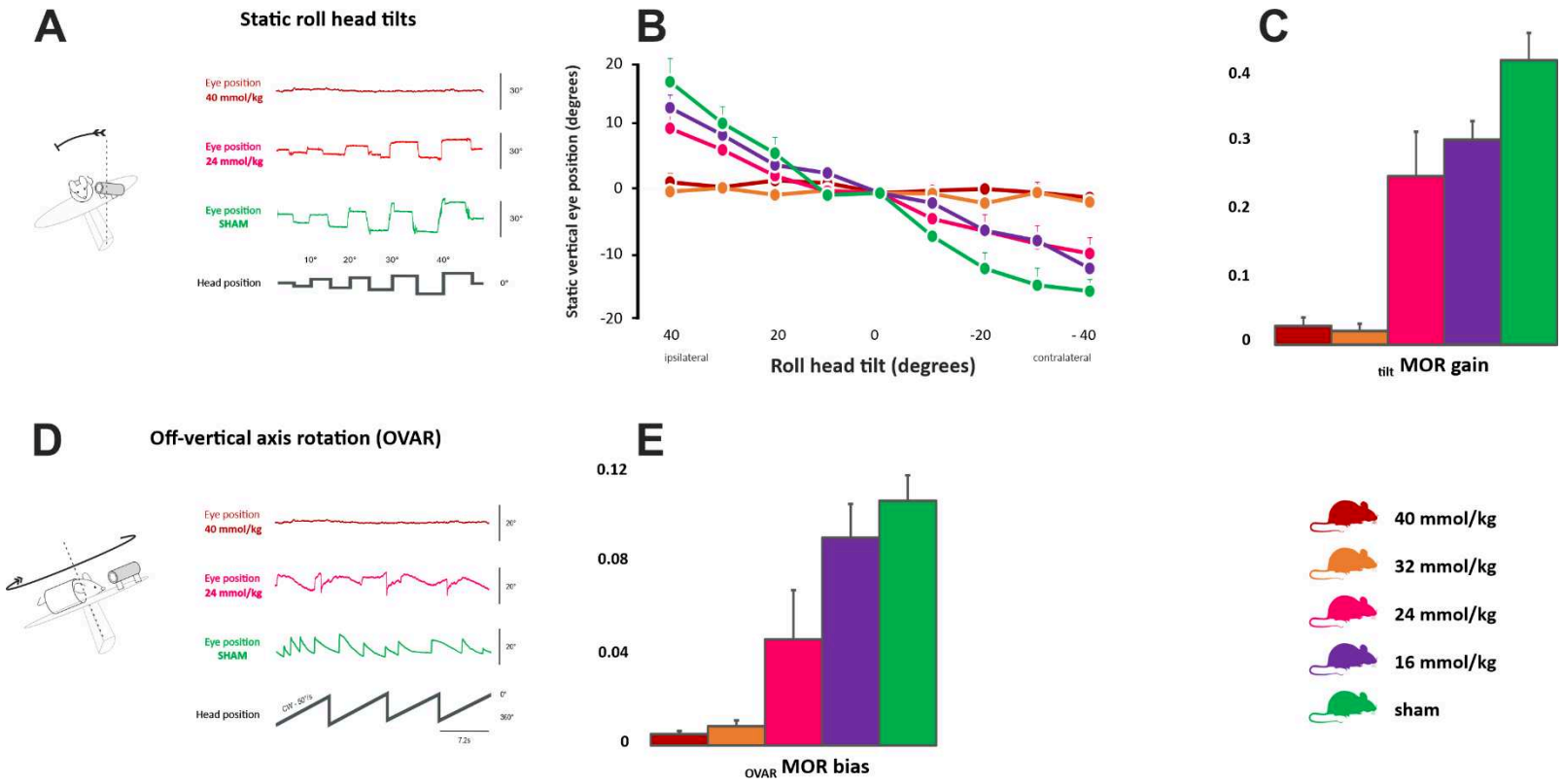

Figure 2: Otolithic system function.

A: Static roll head tilts to determine $_{tilt}$MOR corresponding to utricular function. Traces show head position (corresponding to table position) and vertical eye movement. 3.3'IDPN mice had slightly poorer gain to no gain at 40mm/kg. **B:** Vertical eye position in degrees according to static roll head tilt degree. The left eye pupil position was measured, tilts with positive degrees were towards the left side and with negative degrees towards the right side. **C:** $_{tilt}$MOR gain calculated from the slope in B. **D:** Off-vertical axis rotations at 50°/s. Traces show head position and horizontal eye position, during CW stimulation. All 3.3'IDPN mice were impaired, although not all had significantly different bias compared to sham. **E:** $_{OVAR}$MOR bias, mean value of CW and CCW rotations. *CW* Clockwise *CCW* Counter-clockwise *MOR* Maculo-ocular reflex *OVAR* Off-vertical axis rotation.

Concerning static roll head tilt, at D21, a significant decrease in $_{tilt}$MOR gain was observed starting from 24 mmol/kg (***Table 5***). During OVAR stimulation, at D21, a significant decrease in $_{OVAR}$MOR bias was observed from 24 mmol/kg (***Table 4***). MOR trends are reported in ***Figure 2***.

Table 6: Statistical significance when comparing different groups of IDPN doses

VOR	aVOR 0.2Hz		aVOR 0.5Hz		aVOR 0.8Hz		aVOR 1Hz		aVOR 2Hz		$_{tilt}$MOR	$_{OVAR}$MOR	$_{HSTEPS}$VOR	
Mesure	Gain	Phase	Gain	Phase	Gain	Phase	Gain	Phase	Gain	Phase	Gain	Bias	Tau	Max gain
16 vs Sham	*0.944*	*0.774*	*0.806*	*0.905*	*0.215*	*0.801*	***0.007***	*0.907*	***< 0.0001***	*0.940*	***0.037***	*0.536*	*0.561*	*0.884*
24 vs Sham	*0.185*	*0.450*	***0.002***	*0.804*	***< 0.0001***	*0.901*	***< 0.0001***	*0.417*	***< 0.0001***	*0.212*	***0.003***	***0.022***	***0.024***	***0.000***
32 vs Sham	***0.002***	-	***< 0.0001***	-	***< 0.0001***	-	***< 0.0001***	-	***< 0.0001***	-	***< 0.0001***	***0.000***	***< 0.0001***	***< 0.0001***
40 vs Sham	***0.005***	-	***< 0.0001***	-	***< 0.0001***	-	***< 0.0001***	-	***< 0.0001***	-	***< 0.0001***	***0.000***	***< 0.0001***	***< 0.0001***
24 vs 16	*0.163*	*0.639*	***0.004***	*0.714*	***0.006***	*0.706*	***0.003***	*0.487*	***0.000***	*0.241*	*0.335*	*0.09*	***0.05***	***0.000***
32 vs 16	***0.017***	-	***< 0.0001***	-	***< 0.0001***	-	***< 0.0001***	-	***< 0.0001***	-	***< 0.0001***	***0.002***	***< 0.0001***	***< 0.0001***
40 vs 16	***0.004***	-	***< 0.0001***	-	***< 0.0001***	-	***< 0.0001***	-	***< 0.0001***	-	***< 0.0001***	***0.001***	***< 0.0001***	***< 0.0001***
32 vs 24	*0.317*	-	***0.005***	-	***< 0.0001***	-	***< 0.0001***	-	***0.000***	-	***< 0.0001***	*0.146*	***0.001***	***< 0.0001***
40 vs 24	*0.131*	-	***0.000***	-	***< 0.0001***	-	***< 0.0001***	-	***< 0.0001***	-	***0.000***	***0.113***	***0.001***	***< 0.0001***
40 vs 32	*0.608*	-	*0.393*	-	*0.650*	-	*0.370*	-	***0.001***	-	*0.894*	*0.894*	*1.000*	*1.000*

Statistically significant values are in bold. aVOR values were compared using a three-way ANOVA and post-hoc Tukey test. Phase was not measurable for 32 and 40 mmol/kg. Tau, $_{tilt}$MOR and $_{OVAR}$MOR were each compared with a two-way ANOVA model, respectively. *aVOR* angular vestibular-ocular reflex *MOR* maculo-ocular reflex *OVAR* off-vertical axis rotation.

Optokinetic reflex

Optokinetic reflex was calculated and analysed at the 3.3'IDPN dose of 40 mmol/kg and found no change in optokinetic reflex gains at all frequencies compared to the sham group. This result demonstrates that the IDPN toxicity does not affect the eye maculae and that the VOR results are solely due to changes in the direct VOR pathway and not in the optokinetic pathway.

Discussion:

This study reports a dose-dependent effect of 3.3' IDPN on vestibular function, as shown by the vestibular behavioural score and quantitative analysis of the VOR. The highest doses of 3.3' IDPN (32 mmol/kg and 40 mmol/kg) induced an overall and almost complete impairment of the canalar and otolithic vestibulo-ocular reflexes. At intermediate doses, the results were contrasted, with canalar alteration starting from 16 mmol/kg upwards, and an alteration of otolithic function from 24 mmol/kg upwards (***Figure 3***).

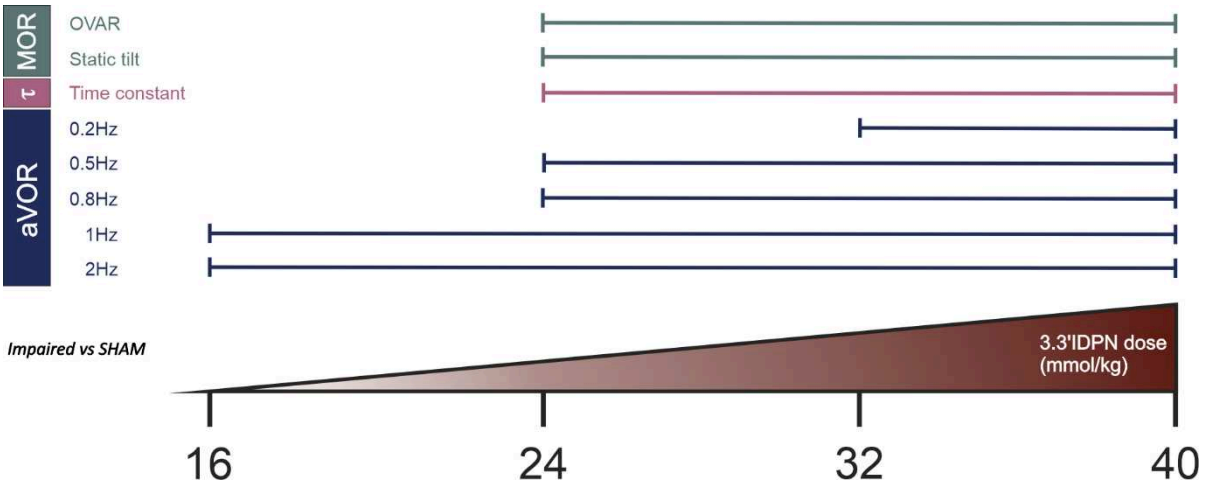

Figure 3: Vestibular function impairment according to 3.3'IDPN dose.
Vestibular function impairment is defined as a significantly different value to sham mice at day 21. *aVOR* angular vestibular-ocular reflex *MOR* maculo-ocular reflex *OVAR* off-vertical axis rotation.

Concerning aVOR, the gain was significantly diminished at 16 mmol/kg but only at high frequencies. Increasing the injected dose led to a progressive worsening of aVOR gains reaching the lower frequencies. At 24 mmol/kg, frequencies ≥ 0.5 Hz were altered, and at 32 mmol/kg, aVOR gains were diminished at all frequencies. According to our main hypothesis, type I hair cells are responsible for the coding of high-frequency movements, and IDPN at low doses would preferentially target type I hair cells. On the other hand, higher doses of IDPN would target both type I and type II, and therefore concern all frequency. Our results are thus compatible with the working hypothesis. the alteration of both low and high frequencies suggest a destruction of both type I and type II hair cells [9, 23, 24]. An increase in gain in the Sham group at D21 compared to prior to injection was also noticed. This result

could be an effect of habituation observed when repeating vestibular function exploration in mice [25], and confirms the necessity to compare the injected mice to shams at the same follow-up.

The analysis of the aVOR phases was possible only for the lower doses with a measurable gain and showed a non-significant abnormal phase advance in the higher frequencies. These results could be congruous with an impaired aVOR in the higher frequencies: in a physiological situation, a phase advance of the nystagmus is observed at the lowest frequencies, and a phase delay at the highest frequencies [26]. However, these phase results should be analysed with caution as they could also be explained by the very low gains at these frequencies and could in this case not be interpreted.

Starting from 24 mmol/kg upwards, there is a significant decrease in the time constant of the lateral canals, indicating impaired velocity storage. Velocity storage requires satisfactory canalar function as well as intact peripheral and central vestibular pathways [27, 28]. Decreased time constant is probably linked to the decreased aVOR gain which occurred at the same doses.

Two tests reflect otolithic function: static roll head tilt, which quantifies the static MOR mainly from a utricular stimulation; and OVAR, which studies otolithic function with the participation of semi-circular canals and central pathways [20]. During these two tests, MOR impairment appeared for doses ≥ 24 mmol/kg. At 16mmol/kg, there was no significant alteration of the MOR even though canalar function was already impaired, which could be explained by a different sensitivity of 3.3'IDPN for macular cells, rather than canalar hair cells. This difference may also be due to the fact that the otolithic system, which usually codes low frequency head movements or even static head positions, relies less on type I cells than the semi-circular canals which usually code for fast rotatory movements. This is especially true for $_{tilt}$MOR which is a static utricular stimulation.

Conclusion

The destruction of hair cells by 3.3' IDPN leads to dose-dependent quantitative changes in the canalo-ocular and maculo-ocular reflexes. The aVOR is altered at doses ≥ 16 mmol/kg, while the maculo-ocular reflex is impaired at higher doses ≥ 24 mmol/kg. In the aVOR, the responses are especially reduced in higher frequencies. These data are in agreement with the main hypothesis that type I hair cells would not play a major role in the coding of low frequency movements or static head positions. Increasing the injected dose also leads to a worse vestibular behavioural score which seems to correspond to the results of the VOR gains. These abnormalities are to be correlated with the cellular alterations found after microscopic analysis of the vestibular epithelium of injected mice, in order to clarify the role of type I hair cells in the coding of the vestibulo-ocular reflex.

References:

[1] A. Lysakowski et J. M. Goldberg, A regional ultrastructural analysis of the cellular and synaptic architecture in the chinchilla cristae ampullares, *J. Comp. Neurol.* **389**(3) (1997), 419-443.

[2] J. M. Goldberg, Afferent diversity and the organization of central vestibular pathways, *Exp. Brain Res.* **130**(3) (2000), 277-297.

[3] M. Beraneck et H. Straka, Vestibular signal processing by separate sets of neuronal filters, *J. Vestib. Res. Equilib. Orientat.* **21**(1) (2011), 5-19.

[4] H. Straka, F. M. Lambert, S. Pfanzelt, et M. Beraneck, Vestibulo-ocular signal transformation in frequency-tuned channels, *Ann. N. Y. Acad. Sci.* **1164** (2009), 37-44.

[5] Llorens J, The behavioral syndrome caused by 3,3'-iminodipropionitrile and related nitriles in the rat is associated with degeneration of the vestibular sensory hair cells., *Toxicol Appl Pharmacol 1993 Dec1232199-210.*

[6] H. A. Khan, A. S. Alhomida, et I. A. Arif, Neurovestibular toxicities of acrylonitrile and iminodipropionitrile in rats: a comparative evaluation of putative mechanisms and target sites, *Toxicol. Sci. Off. J. Soc. Toxicol.* **109**(1) (2009), 124-131.

[7] Greguske E, Calyx junction dismantlement and synaptic uncoupling precede hair cell extrusion in the vestibular sensory epithelium during sub-chronic 3,3'-iminodipropionitrile ototoxicity in the mouse, *Arch. Toxicol.* **93**(2) (2019), 417-434.

[8] Brent A, Effects of 3.3'-IDPN on hair cell numbers in cristae of CBA/CaJ and C57BL/6J mice, *JARO 19 483-491 2018.*

[9] S. Zeng, W. Ni, H. Jiang, D. You, J. Wang, X. Lu, *et al.*, Toxic Effects of 3,3'-Iminodipropionitrile on Vestibular System in Adult C57BL/6J Mice In Vivo, *Neural Plast.* **2020** (2020), 1823454.

[10] K. M. Crofton et J. Llorens, Evaluating the effects of acrylamide and 3,3'-iminopropionitrile (IDPN), using behavioral (functional observational battery and motor activity) and neuropathological end points, *Fundam. Appl. Toxicol. Off. J. Soc. Toxicol.* **19**(2) (1992), 315-316.

[11] M. Beraneck et K. E. Cullen, Activity of vestibular nuclei neurons during vestibular and optokinetic stimulation in the alert mouse, *J. Neurophysiol.* **98**(3) (2007), 1549-1565.

[12] M. Beraneck, M. Bojados, A. Le Seac'h, M. Jamon, et P. P. Vidal, Ontogeny of mouse vestibulo-ocular reflex following genetic or environmental alteration of gravity sensing, *PLoS One* **7**(7) (2012), e40414.

[13] F. França de Barros, J. Carcaud, et M. Beraneck, Long-term Sensory Conflict in Freely Behaving Mice, *J. Vis. Exp. JoVE* (144) (2019),.

[14] M. Beraneck et F. M. Lambert, Impaired perception of gravity leads to altered head direction signals: what can we learn from vestibular-deficient mice?, *J Neurophysiol* **102**(1) (2009), 12-4.

[15] M. Beraneck et E. Idoux, Reconsidering the Role of Neuronal Intrinsic Properties and Neuromodulation in Vestibular Homeostasis, *Front. Neurol.* **3** (2012),.

[16] J. S. Stahl, L. Averbuch-Heller, et R. J. Leigh, Acquired nystagmus, *Arch. Ophthalmol. Chic. Ill 1960* **118**(4) (2000), 544-549.

[17] J. Carcaud, F. França de Barros, E. Idoux, D. Eugène, L. Reveret, L. E. Moore, *et al.*, Long-Lasting Visuo-Vestibular Mismatch in Freely-Behaving Mice Reduces the Vestibulo-Ocular Reflex and Leads to Neural Changes in the Direct Vestibular Pathway, *eNeuro* **4**(1) (2017),.

[18] E. Idoux, M. Tagliabue, et M. Beraneck, No Gain No Pain: Relations Between Vestibulo-Ocular Reflexes and Motion Sickness in Mice, *Front. Neurol.* **9** (2018), 918.

[19] D. R. Calabrese et T. E. Hullar, Planar relationships of the semicircular canals in two strains of mice, *J. Assoc. Res. Otolaryngol. JARO* **7**(2) (2006), 151-159.

[20] B. J. M. Hess et N. Dieringer, Spatial Organization of the Maculo-Ocular Reflex of the Rat: Responses During Off-Vertical Axis Rotation, *Eur. J. Neurosci.* **2**(11) (1990), 909-919.

[21] R. Romand, W. Krezel, M. Beraneck, L. Cammas, V. Fraulob, N. Messaddeq, *et al.*, Retinoic acid deficiency impairs the vestibular function, *J Neurosci* **33**(13) (2013), 5856-66.

[22] B. S. Oommen et J. S. Stahl, Eye orientation during static tilts and its relationship to spontaneous head pitch in the laboratory mouse, *Brain Res.* **1193** (2008), 57-66.

[23] Seoane A, Relationship between insult intensity and mode of hair cell loss in the vestibular system of rats exposed to 3,3′-iminodipropionitrile., *J Comp Neurol 439385–399.*

[24] J. Llorens et D. Demêmes, Hair cell degeneration resulting from 3,3'-iminodipropionitrile toxicity in the rat vestibular epithelia, *Hear. Res.* **76**(1-2) (1994), 78-86.
[25] M. Iwashita, R. Kanai, K. Funabiki, K. Matsuda, et T. Hirano, Dynamic properties, interactions and adaptive modifications of vestibulo-ocular reflex and optokinetic response in mice, *Neurosci. Res.* **39**(3) (2001), 299-311.
[26] R. M. Peters, B. G. Rasman, J. T. Inglis, et J.-S. Blouin, Gain and phase of perceived virtual rotation evoked by electrical vestibular stimuli, *J. Neurophysiol.* **114**(1) (2015), 264-273.
[27] S. B. Yakushin, T. Raphan, et B. Cohen, Coding of Velocity Storage in the Vestibular Nuclei, *Front. Neurol.* **8** (2017), 386.
[28] G. P. Jacobson, D. L. McCaslin, S. Patel, K. Barin, et N. M. Ramadan, Functional and anatomical correlates of impaired velocity storage, *J. Am. Acad. Audiol.* **15**(4) (2004), 324-333.

2.3.5. Conclusion

La perte des cellules de type I semble, comme attendu, principalement retentir sur les mouvements rotatoires rapides de la tête, alors que les mouvements plus lents voire statiques de la tête détectés par le système otolithique sont moins dégradées sauf à des concentrations très importantes de 3.3'IDPN. La prochaine étape serait de corréler ces résultats fonctionnels à l'étude microscopique, pour quantifier précisément le taux de cellules de type I résiduelles versus type II résiduelles.

Partie 4 : Discussion générale

1. Discussion des résultats

Nous avons présenté dans ce travail six articles expérimentaux, s'intéressant à différents modèles murins mutants ou lésionnels, avec un retentissement sur différentes structures vestibulaires (la touffe ciliaire (articles 1 et 2), la cellule ciliée (articles 3 et 6), la synapse (articles 3 et 4) et le nerf vestibulaire (articles 4 et 5)) qui jouent un rôle décisif dans la transduction et la transmission des informations vestibulaires. Chacun de ces éléments peut théoriquement, en cas de dysfonctionnement, conduire à des anomalies dans le traitement du signal associé à des déficits fonctionnels spécifiques ou non. Au cours de cette thèse, j'ai ainsi cherché à déterminer dans quelle mesure des atteintes de ces structures moléculaires/cellulaires pouvaient se traduire par des anomalies de la stabilisation du regard. Le travail de thèse a également consisté à développer chez la souris des tests permettant de tester spécifiquement les réflexes canalaires, otolithiques, ou leurs différentes combinaisons, ainsi que des phénomènes caractéristiques du traitement vestibulaire. Ces articles sont détaillés dans le ***Tableau 4***.

Tableau 4: Vue d'ensemble du travail expérimental

Article	Modèle	Rôle	Collaboration	Lésion	Objectif
Clarine	Mutant	*Collaboration*	Institut de l'Audition | Institut Pasteur	Dégénérescence des touffes ciliaires & dysfonction synaptique	Rôles et interaction de clarine-1 et clarine-2
Celsr1	Mutant	1er auteur	UCLouvain Institute of NeuroScience; The University of Utah	Dépolarisation des touffes ciliaires	Rôle de la polarisation des cellules ciliées
Snap-25	Mutant	*Collaboration*	Institut de l'Audition | Institut Pasteur	Réduction de l'exocytose et dégénérescence des cellules ciliées	Rôle de snap-25
UVN/UL	Lésionnel	1er auteur	Aix Marseille université	Destruction unilatérale des organes vestibulaires ± ganglion de Scarpa	Description des lésions vestibulaires chirurgicales
TTK/UVN	Lésionnel	*Collaboration*	Aix Marseille université	Désafférentation des synapses des cellules ciliées	Nouveau modèle de lésion partielle et temporaire
3.3'IDPN	Lésionnel	Encadrement Master2	Institut de Neurociències, Universitat de Barcelona	Destruction préférentielle des cellules ciliées de type I	Rôle des cellules de type I

Au total, 165 souris ont été analysées pour produire ces différents résultats.

Les objectifs de la thèse étaient de valider sur le plan vestibulaire des modèles murins de pathologie cochléo-vestibulaire et mieux comprendre la physiologie vestibulaire.

Nous avons pu au cours de chacune des études de ce travail valider l'usage des modèles murins. Trois études en particulier correspondent à des modèles de pathologie humaine : l'étude clarine avec le modèle murin du syndrome de Usher type III, et les études TTK/UVN et UVN/UL qui correspondent respectivement à deux modèles de pathologie vestibulaire aigue, l'une légère et transitoire et l'autre profonde et définitive, pouvant correspondre à différents types de syndromes vestibulaires aigus en clinique (toutes classées sous le terme de névrite vestibulaire mais avec probablement différents mécanismes physiopathologiques sous-jacents).

L'étude celsr1 ne correspond pas à ce jour à une pathologie vestibulaire connue, mais la mutation étant décrite chez l'Homme dans le cadre de défauts de fermeture du tube neural, il serait intéressant d'explorer ces patients où une atteinte vestibulaire pourrait être méconnue. L'objectif principal de cette étude concernait avant tout de la physiologie vestibulaire et l'analyse de du codage de population et le rôle de la bonne orientation des touffes ciliaires dans ce codage.

Le fonctionnement de la touffe ciliaire a également été évalué dans l'étude clarine, pour mieux cerner le rôle des deux protéines clarine-1 et clarine-2 et surtout leur interaction et redondance. L'étude snap-25 s'intéressait au fonctionnement synaptique des cellules ciliées et a montré la dépendance de l'exocytose à la molécule snap-25. Enfin l'analyse de la compensation vestibulaire dans les deux travaux TTK/UVN et UVN/UL a rapporté deux mécanismes différents en fonction de la récupération de la fonction ipsilatérale à la lésion et a validé ces modèles pour de futures études sur le mécanisme de compensation vestibulaire.

1.1. Développement de nouveaux tests vestibulaires chez la souris

Nous avions, avant de débuter ce travail, deux tests de routine pour l'exploration du VOR chez la souris. Premièrement les rotations horizontales sinusoïdales, permettant de calculer l'aVOR à différentes fréquences pour évaluer la fonction canalaire, et l'OVAR pour calculer le biais MOR et évaluer la fonction otolithique (étude sur le kaïnate). Nous avons commencé à introduire et développer progressivement deux nouvelles explorations du VOR. Les *hsteps* en sens horaire et anti-horaire, permettant facilement de calculer i) la prépondérance directionnelle à partir des gains de pic de vitesse, et ii) la constante de temps. Aussi le test d'inclinaison latérale statique de la tête, qui est le test à notre connaissance le plus spécifique pour l'évaluation utriculaire (et donc globalement de la fonction otolithique), et de plus le seul test fonctionnel statistiquement corrélé à la nage (étude clarine). En revanche, le $_{OVAR}$MOR semble, avec l'expérience de ces différentes études, être d'avantage un marqueur d'intégrité du système vestibulaire périphérique et central, plutôt que spécifique du système otolithique. L'exploration d'un nombre important de souris normales C57BL/6, nous a permis de déterminer des normes pour ces différents tests, facilitant l'analyse et nous permettant d'acquérir une expertise unique dans l'exploration de la fonction vestibulaire chez la souris.

1.2. Lignées de souris et normes

Il est très importance de bien identifier les lignées de souris, car celles-ci peuvent influer sur les résultats expérimentaux (Enríquez, 2019). Pour l'exploration vestibulaire, où le contraste pupillaire est très important pour permettre une oculographie, la lignée C57BL/6 est privilégiée. A l'inverse, les lignées albinos (par exemple FVB/NJ) sont inutilisables pour l'exploration des VOR. Dans cette thèse la lignée majoritaire était C57BL/6, provenant de Janviers Labs ou Charles River. Certaines souris provenant de collaborations étaient de lignée majoritaire C57BL/6 avec quelques rétrocroisements avec des lignées 129 ou CD1. Nous avons colligé l'ensemble des résultats des souris normales (explorations contrôles ou pré-lésionnelles) des différentes études de cette thèse dans le ***Tableau 5***.

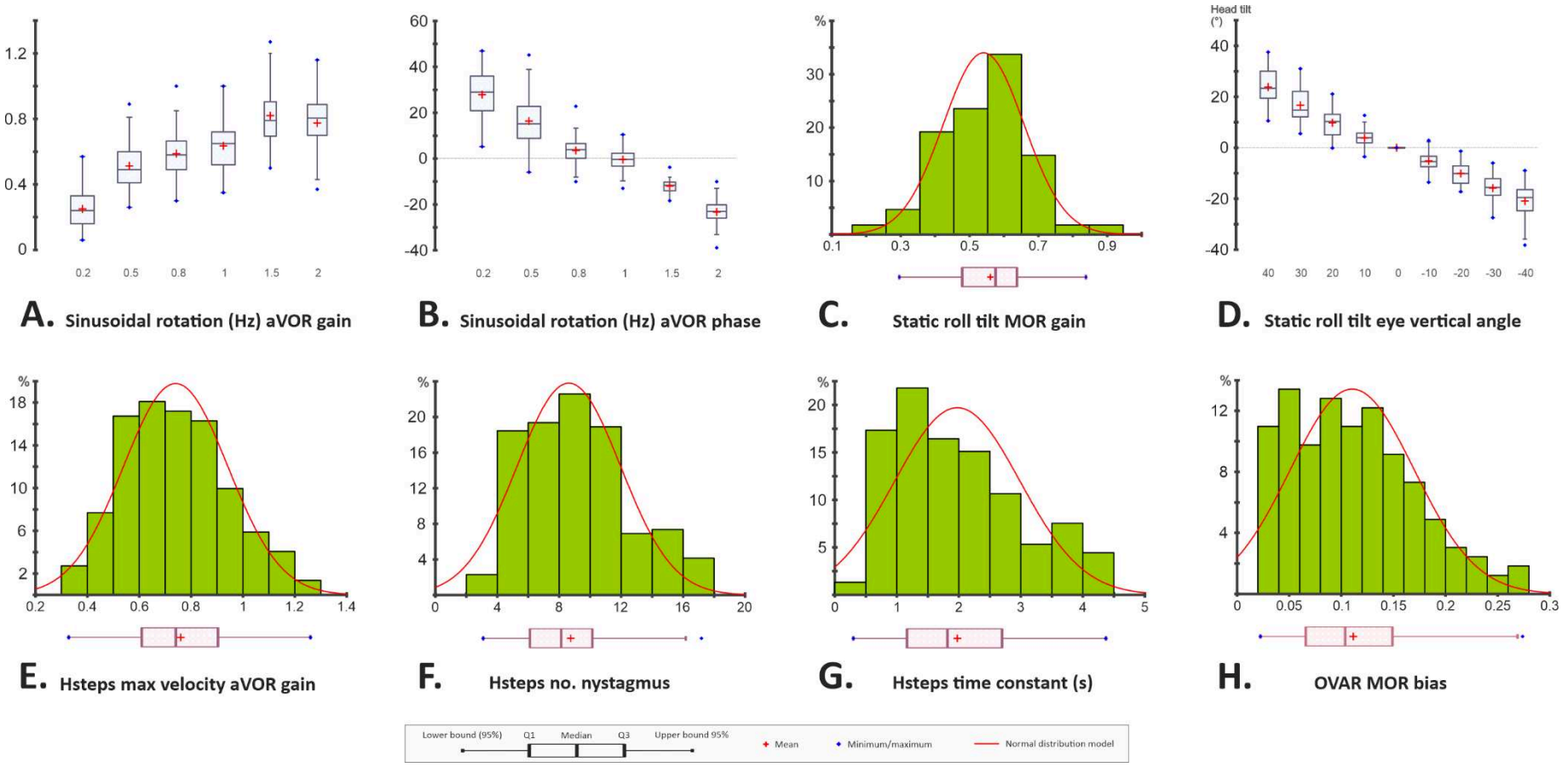

Figure 32 : Répartition des valeurs des explorations fonctionnelles vestibulaires de 91 souris C57B6 normales

A et B : *Gain et phase (degrés) des aVOR (rotation sinusoïdale à plusieurs fréquences et vitesse maximale 30°/s).* ***C et D :*** *Gain maculaire statique et valeurs brutes de position angulaire verticale oculaire en fonction du degré avec la tête inclinée de façon statique à gauche et à droite.* ***E, F et G :*** *différentes mesures réalisées lors du test hsteps, gain aVOR à vitesse maximale, nombre de nystagmus et constante de temps (les 4 valeurs pré- et per-rotatoires en rotation horaire et anti-horaire ont été prises en compte).* ***H :*** *les deux valeurs des deux stimulations horaires et anti-horaires ont été pris en compte.*

Tableau 5: Examen de souris normales (contrôles ou pré-lésionnels)

Article	Lignée de souris	Age (semaines)	Ratio M/F	Nombre de souris
Clarine	C57BL/6N	15 ± 1	10/0	10
Celsr1	129 ES (blastocyste B6 & rétrocroisement CD1)	15 ± 9	6/4	10
Snap-25	C57Bl/6N	19 ± 5	10/4	14
UVN/UL	C57BL/6N	-	-	-
TTK/UVN	C57BL/6J	8 ± 0	15/8	23
3.3'IDPN	C57BL/6J	6 ± 0	24/20	44

Pour des motifs éthiques de réutilisation de souris, les souris de l'étude UVN/UL provenaient des populations de souris *wild type* des études snap-25 et clarine. Les tests pré-lésionnels UVN/UL sont donc déjà comptabilisés dans ces études.

Les corrélations des valeurs ont été recherché avec les facteurs âge (en semaines), sexe et l'étude source dans le ***Tableau 6***. La répartition statistique des valeurs de chaque test concernant les souris de lignée C57BL/6 sont rapportées dans le ***Tableau 7*** et la ***Figure 32***.

Tableau 6: Analyse multivariée de facteurs de corrélation (significativité *p*)

	aVOR gain 1Hz	$_{tilt}$MOR gain	$_{OVAR}$MOR bias	Tau (s)
Corrélation à l'âge	*0.173*	*0.455*	*0.672*	*0.470*
Corrélation au sexe	*0.499*	*0.322*	*0.288*	*0.220*
Corrélation à l'étude	***< 0.001***	***0.004***	***0.001***	*0.152*

Les corrélations ont été calculées sur les 101 souris normales du Tableau 5, par un test multivarié ANCOVA.

Tableau 7: Valeurs théoriques fonctionnelles des 91 souris C57BL/6

	aVOR gain 1Hz	$_{tilt}$MOR gain	$_{OVAR}$MOR bias	Tau (s)
Nombre de valeurs	88	68	164	225
Moyenne ± écart-type	0.64 ± 0.13	0.54 ± 0.12	0.11 ± 0.06	1.98 ± 1.01
Médiane [Q1 ; Q3]	0.65 [0.52 ; 0.72]	0.56 [0.45 ; 0.63]	0.11 [0.06 ; 0.14]	1.82 [1.16 ; 2.70]

Les valeurs concernent uniquement les 91 souris lignée C57BL/6. Le nombre de valeurs varie en fonction du nombre de souris et du nombre de tests effectués par souris (pour tau par exemple, nous avons 4 valeurs par souris). La lignée 129 n'a pas été incluse à cause des différences de norme statistiquement significatives de l'étude celsr1 *versus* les autres.

1.2.1. Gestion des valeurs extrêmes

Avant l'interprétation des résultats, un test statistique de Grupps a été réalisé pour vérifier si des valeurs pouvaient être considérées comme extrêmes et exclues des analyses. Un certain nombre de facteurs (variabilité inter-individuelle d'une souris importante, stress inhabituel d'une souris lors de l'expérimentation, erreur humaine lors de l'expérimentation ou traitement des données) peuvent engendrer des valeurs extrêmes ou aberrantes, faussant les valeurs moyennes et analyses statistiques de petits groupes de souris (habituellement de l'ordre de 10 souris par groupe). Sur les 91 souris C57BL6, le pourcentage de valeurs exclues car statistiquement aberrantes est rapporté ci-après pour chaque test vestibulaire. Concernant la rotation sinusoïdale, 2% des gains VOR et 7% des phases ; 5% des $_{tilt}$MOR ; 10% des $_{OVAR}$MOR ; concernant les *hsteps*, 3% du nombre de nystagmus, 3% des constantes de temps et 1% des gains VOR à vitesse maximale. Il apparait donc que les valeurs de phase du VOR et de l'$_{OVAR}$MOR sont les moins fiables et reproductibles, l'interprétation de ces tests requière ainsi davantage de prudence.

1.2.2. Limites de l'utilisation des normes

Il est intéressant de noter l'étude pendant laquelle le test a été réalisé, influence la valeur pour quasiment l'ensemble des tests vestibulaires. Ce facteur est composite car il prend en compte la lignée (ou sous-lignée) de la souris d'une étude donnée, mais aussi l'expertise de l'examinateur au moment de la réalisation du test (facilité de manipulation de la souris, acquisition puis traitement des données). Il n'est pas possible avec ces données d'en tirer des conclusions plus précises (colinéarité importante en cas de multiplication des analyses statistiques). Ceci conforte la stratégie de toujours comparer des souris expérimentales à une population de contrôles similaires, soit à elles-mêmes en pré-lésionnel, soit à un groupe contrôle idéalement de la même portée. Par prudence il semble licite d'essayer d'avoir des souris du même âge et avec un ratio de sexe équilibré (même si cela ne doit pas limiter l'expérimentation). Enfin, il convient de réaliser l'ensemble des tests d'une même étude sur une fenêtre temporelle la plus courte possible pour limiter des phénomènes environnements, de stress

animal ou d'expertise de l'opérateur qui pourraient varier dans le temps et réduire al comparabilité des groupes.

Au total il ne semble pas souhaitable d'utiliser les normes calculées ici comme valeurs contrôles dans les études futures, mais plutôt comme une aide pendant l'expérimentation pour mieux cibler les valeurs aberrantes. Aussi, la variabilité que nous avons montrée sur des groupes de souris normales, implique qu'il faut être prudent sur les interprétations même statistiquement significatives, lors de petits échantillons ou de différences peu importantes.

1.2.3. Connaître le modèle C57BL/6 : sous-lignées et vieillissement

La lignée de souris C57BL/6 est la plus utilisée en recherche biomédicale dans le monde et a été développée en 1921, par C. Little, fondateur du laboratoire Jackson Laboratory. La sous-lignée C57BL/6J correspond à la lignée initiale, mais une autre sous-lignée fréquemment utilisée, la C57BL/6N existe depuis la création d'une nouvelle colonie de C57BL/6 en 1951. De nombreuses autres sous-lignées moins fréquemment utilisées dans les publications existent (une nouvelle sous-lignée de C57BL/6 est créée lorsqu'une colonie est isolée pendant plus de 20 générations). Cette distinction est très importante car de nombreux papiers ont montré des différences à la fois génétiques et phénotypiques entre les différentes sous-lignées (Bryant, 2011).

Concernant l'oreille interne, un phénotype commun aux sous-lignées 6J et 6N est la presbyacousie. De nombreuses études ont pris cette lignée comme modèle d'étude, rapportant une perte auditive commençant dans les fréquences aigues (32kHz) dès l'âge de 6 mois dans les deux sous-lignées 6N et 6J, et s'aggravant entre l'âge de 12 et 15 mois (Kane et al., 2012; Mianné et al., 2016; Zheng et al., 1999). Cette perte auditive est corrélée à un vieillissement de la cochlée et une perte des cellules ciliées externes et internes (Hequembourg and Liberman, 2001).

De façon parallèle à la presbyacousie, la presbyvestibulopathie est une atteinte nouvellement décrite chez l'Homme, définie par une diminution progressive et bilatérale du VOR (Agrawal et al., 2019). Si

aucune étude vestibulaire au long-terme n'a été réalisée sur les différentes sous-lignées de souris C57BL/6, une étude comportementale a montré une différence significative à un test d'équilibre (Rotarod test, qui évalue la durée pendant laquelle une souris est capable de rester sur un cylindre rotatoire sans tomber) avec une stabilité beaucoup plus importante de la sous-lignée C57BL/6J par rapport à la sous-lignée 6N (Matsuo et al., 2010). Cette différence serait à rechercher sur de larges populations avec des tests fonctionnels de VOR, avant de pouvoir affirmer une différence de fonction vestibulaire entre ces deux sous-lignées (il nous est notamment impossible de conclure sur ce point avec nos données). Deux études chez la sous-lignée C57BL/6J à l'âge de 6 mois ou plus n'ont pas retrouvé de presbyvestibulopathie fonctionnelle (pas de diminution du gain du VOR ni du potentiel évoqué vestibulaire) mais ont mis en évidence une dégénérescence histologique des organes vestibulaires liés à l'âge (Mock et al., 2016; Shiga et al., 2005).

Au total concernant la lignée C57BL/6, il serait préférable de ne pas réaliser d'exploration vestibulaire au-delà de 6 mois pour ne pas s'exposer à un risque théorique de presbyvestibulopathie. Par ailleurs nous insistons sur l'importance d'avoir un groupe contrôle de même âge mais aussi de même sous-lignée (l'idéal étant de même portée).

2. Perspectives

2.1. Mieux comprendre le fonctionnement vestibulaire

Nous l'avons vu, le modèle murin est intéressant car facile à produire et manipuler. Son utilisation pour l'étude du vestibule est également très pertinente, puisque le labyrinthe est une structure très bien conservée parmi les mammifères (Ekdale, 2013).

Les modèles murins mutés sont très intéressants car ils permettent de cibler précisément la fonction d'une molécule, mais aussi grâce à un transfert viral du gène ou bien grâce à des mécanismes d'activation ou inhibition du gène, d'étudier le rôle de la protéine lors de certaines fenêtres temporelles. Dans une perspective de thérapie génique chez l'Homme, ce dernier point est fondamental pour différencier les protéines qui participent à l'organogénèse de celles qui participent uniquement au fonctionnement cellulaire. En effet, même en cas de thérapie génique réussie, si celle-ci avait lieu après une organogénèse incomplète ou dans un contexte de dégénérescence de l'oreille interne, le bénéfice du traitement serait incertain.

Les modèles lésionnels unilatéraux sont très importants pour mieux comprendre les mécanismes de compensation vestibulaire et d'explorer différentes hypothèses comme la plasticité des organes vestibulaires périphériques, la repousse neuronales, la neurogénèse dans les noyaux vestibulaires, etc. Ils permettraient également de faire progresser les différentes hypothèses physiopathologiques des névrites vestibulaires (lésions synaptiques, ganglionnaires, etc.).

2.2. Retour vers l'Homme

Au-delà de la compréhension de la physiologie, l'objectif à moyen ou long-terme est une application chez l'Homme. Cependant beaucoup de progrès doivent être réalisés. La thérapie génique, pourtant séduisante, doit surmonter plusieurs difficultés avant d'être applicable chez l'Homme. En premier lieu, comme nous l'avons vu lors du chapitre sur l'embryogénèse, il existe un décalage important du stade de développement vestibulaire à la période péri-natale entre la souris et l'Homme. Ainsi si la majorité des thérapies géniques chez la souris sont actuellement administrées vers P2, ceci correspondrait chez l'Homme à injecter le traitement vers le 6è mois de vie fœtale. Aussi, même en cas de réussite de ces procédures, d'énormes progrès dans le diagnostic prénatal seraient nécessaire pour cibler les candidats à un traitement pendant l'organogénèse. Enfin, en ayant à l'esprit les débats intenses entourant l'implant cochléaire à ses débuts, de grands débats éthiques sur la normativité et l'eugénisme seraient nécessaires avant d'envisager cette technique chez l'Homme.

Concernant les modèles lésionnels, des débouchés plus rapides seraient envisageables. Des essais thérapeutiques pré-cliniques, sur les différents modèles lésionnels (désafférentation, lésion du ganglion de Scarpa, etc.) permettraient d'améliorer la prise en charge des pathologies vestibulaires aigues en facilitant la compensation vestibulaire, mais aussi des instabilités chroniques liées à une compensation vestibulaire incomplète.

3. Conclusion générale

L'étude du vestibule murin, grâce aux nouvelles technologies d'ingénierie génétique, ouvre un large champ de recherche sur la physiopathologie du vestibule permettant de progresser dans la compréhension de cet organe complexe. Ay cours de cette thèse nous avons analysé plusieurs types de dysfonctions vestibulaires et montré que à part quelques rares cas de figure (clarines double-KO, snap-25 ou 3.3'IDPN à fortes doses), il persistait toujours une fonction vestibulaire résiduelle. Ceci montre d'une part l'intérêt des explorations fonctionnelles, seul moyen de quantifier précisément des dysfonctions partielles, mais aussi la robustesse du système avec de nombreux mécanismes de compensation. Une question transversale à plusieurs de ces projets concerne donc la quantité d'information nécessaire et suffisante pour maintenir une fonction vestibulaire acceptable.

Encore méconnu d'une grande partie des cliniciens et chercheurs s'intéressant principalement à la cochlée, le vestibule a un rôle beaucoup plus large que celui réducteur qu'on lui prête habituellement, d'« organe de l'équilibre ». Indispensable pour la stabilisation du regard pendant les mouvements rapides de la tête, le vestibule joue par son cortex vestibulaire un véritable rôle de modulateur neurosensoriel. Le vestibule s'intègre dans un schéma corporel multisensoriel, de façon à ce que la représentation corporelle se construise et soit placée dans l'environnement. Philosophiquement, l'exploration du vestibule amène vers une approche holiste du corps humain, dépassant l'approche dualiste traditionnelle occidentale du corps et de l'esprit. Le vestibule influe sur notre perception du monde, mais aussi la perception de nous-même dans le monde et au monde. Ce véritable sixième sens, que pourtant nous ne ressentons pas directement, nous oriente, nous stabilise et nous construit.

Partie 5 : Bibliographie

Agrawal, Y., Van de Berg, R., Wuyts, F., Walther, L., Magnusson, M., Oh, E., Sharpe, M., Strupp, M., 2019. Presbyvestibulopathy: Diagnostic criteria Consensus document of the classification committee of the Bárány Society. J Vestib Res 29, 161–170. https://doi.org/10.3233/VES-190672

Ahmed, Z.M., Riazuddin, S., Riazuddin, S., Wilcox, E.R., 2003. The molecular genetics of Usher syndrome. Clin Genet 63, 431–444. https://doi.org/10.1034/j.1399-0004.2003.00109.x

Aitken, P., Zheng, Y., Smith, P.F., 2018. The modulation of hippocampal theta rhythm by the vestibular system. J. Neurophysiol. 119, 548–562. https://doi.org/10.1152/jn.00548.2017

Alagramam, K.N., Gopal, S.R., Geng, R., Chen, D.H.-C., Nemet, I., Lee, R., Tian, G., Miyagi, M., Malagu, K.F., Lock, C.J., Esmieu, W.R.K., Owens, A.P., Lindsay, N.A., Ouwehand, K., Albertus, F., Fischer, D.F., Bürli, R.W., MacLeod, A.M., Harte, W.E., Palczewski, K., Imanishi, Y., 2016. A small molecule mitigates hearing loss in a mouse model of Usher syndrome III. Nat. Chem. Biol. 12, 444–451. https://doi.org/10.1038/nchembio.2069

Albert, S., Blons, H., Jonard, L., Feldmann, D., Chauvin, P., Loundon, N., Sergent-Allaoui, A., Houang, M., Joannard, A., Schmerber, S., Delobel, B., Leman, J., Journel, H., Catros, H., Dollfus, H., Eliot, M.M., David, A., Calais, C., Drouin-Garraud, V., Obstoy, M.F., Tran Ba Huy, P., Lacombe, D., Duriez, F., Francannet, C., Bitoun, P., Petit, C., Garabedian, E.N., Couderc, R., Marlin, S., Denoyelle, F., 2006. SLC26A4 gene is frequently involved in nonsyndromic hearing impairment with enlarged vestibular aqueduct in Caucasian populations. Eur J Hum Genet 14, 773–9. https://doi.org/10.1038/sj.ejhg.5201611

Allache, R., De Marco, P., Merello, E., Capra, V., Kibar, Z., 2012. Role of the planar cell polarity gene CELSR1 in neural tube defects and caudal agenesis. Birth Defects Res. Part A Clin. Mol. Teratol. 94, 176–181. https://doi.org/10.1002/bdra.23002

Alwelaie, M.A., Al-Mutary, M.G., Siddiqi, N.J., Arafah, M.M., Alhomida, A.S., Khan, H.A., 2019. Time-Course Evaluation of Iminodipropionitrile-Induced Liver and Kidney Toxicities in Rats: A Biochemical, Molecular and Histopathological Study. Dose Response 17, 1559325819852233. https://doi.org/10.1177/1559325819852233

Angelaki, D.E., 2004. Eyes on target: what neurons must do for the vestibuloocular reflex during linear motion. J. Neurophysiol. 92, 20–35. https://doi.org/10.1152/jn.00047.2004

Angelaki, D.E., 1992. Two-dimensional coding of linear acceleration and the angular velocity sensitivity of the otolith system. Biol Cybern 67, 511–521. https://doi.org/10.1007/BF00198758

Angelaki, D.E., Cullen, K.E., 2008. Vestibular system: the many facets of a multimodal sense. Annu. Rev. Neurosci. 31, 125–150. https://doi.org/10.1146/annurev.neuro.31.060407.125555

Angelaki, D.E., Hess, B.J., 1996. Three-dimensional organization of otolith-ocular reflexes in rhesus monkeys. II. Inertial detection of angular velocity. J. Neurophysiol. 75, 2425–2440. https://doi.org/10.1152/jn.1996.75.6.2425

Angelaki, D.E., Hess, B.J., 1995. Lesion of the nodulus and ventral uvula abolish steady-state off-vertical axis otolith response. J. Neurophysiol. 73, 1716–1720. https://doi.org/10.1152/jn.1995.73.4.1716

Angelaki, D.E., Hess, B.J.M., 2005. Self-motion-induced eye movements: effects on visual acuity and navigation. Nat. Rev. Neurosci. 6, 966–976. https://doi.org/10.1038/nrn1804

Aranda-Moreno, C., Jáuregui-Renaud, K., Reyes-Espinosa, J., Andrade-Galicia, A., Bastida-Segura, A.E., González Carrazco, L.G., 2019. Stimulation of the Semicircular Canals or the Utricles by Clinical Tests Can Modify the Intensity of Phantom Limb Pain. Front Neurol 10, 117–117. https://doi.org/10.3389/fneur.2019.00117

Attyé, A., Eliezer, M., Boudiaf, N., Tropres, I., Chechin, D., Schmerber, S., Dumas, G., Krainik, A., 2017. MRI of endolymphatic hydrops in patients with Meniere's disease: a case-controlled study with a simplified classification based on saccular morphology. Eur Radiol 27, 3138–3146. https://doi.org/10.1007/s00330-016-4701-z

Ayar, D.A., Kumral, E., Celebisoy, N., 2020. Cognitive functions in acute unilateral vestibular loss. J. Neurol. https://doi.org/10.1007/s00415-020-09829-w

Azevedo, Y.J. de, Ledesma, A.L.L., Pereira, L.V., Oliveira, C.A., Bahmad Junior, F., 2019. Vestibular implant: does it really work? A systematic review. Braz J Otorhinolaryngol 85, 788–798. https://doi.org/10.1016/j.bjorl.2019.07.011

Bachmann, K., Sipos, K., Lavender, V., Hunter, L.L., 2018. Video Head Impulse Testing in a Pediatric Population: Normative Findings. J Am Acad Audiol 29, 417–426. https://doi.org/10.3766/JAAA.17076

Baker, R., Evinger, C., McCrea, R.A., 1981. Some thoughts about the three neurons in the vestibular ocular reflex. Ann. N. Y. Acad. Sci. 374, 171–188. https://doi.org/10.1111/j.1749-6632.1981.tb30869.x

Baloh, R.W., Sills, A.W., Honrubia, V., 1979. Impulsive and sinusoidal rotatory testing: a comparison with results of caloric testing. Laryngoscope 89, 646–654. https://doi.org/10.1288/00005537-197904000-00013

Bárány, R., 1906. Untersuchungen über den vom Vestibularapparat des Ohres reflektorisch ausgelösten rhythmischen Nystagmus und seine Begleiterscheinungen. Oscar Coblentz.

Baydan, M., Yigit, O., Aksoy, S., 2020. Does vestibular rehabilitation improve postural control of subjects with chronic subjective dizziness? PLoS ONE 15, e0238436. https://doi.org/10.1371/journal.pone.0238436

Benson, A.J., Bodin, M.A., 1966. Interaction of linear and angular accelerations on vestibular receptors in man. Aerosp Med 37, 144–154.

Beraneck, M., Bojados, M., Le Seac'h, A., Jamon, M., Vidal, P.P., 2012. Ontogeny of mouse vestibulo-ocular reflex following genetic or environmental alteration of gravity sensing. PloS one 7, e40414. https://doi.org/10.1371/journal.pone.0040414

Beraneck, M., Cullen, K.E., 2007. Activity of vestibular nuclei neurons during vestibular and optokinetic stimulation in the alert mouse. J. Neurophysiol. 98, 1549–1565. https://doi.org/10.1152/jn.00590.2007

Beraneck, M., Straka, H., 2011. Vestibular signal processing by separate sets of neuronal filters. J Vestib Res 21, 5–19. https://doi.org/10.3233/VES-2011-0396

Bigelow, R.T., Semenov, Y.R., du Lac, S., Hoffman, H.J., Agrawal, Y., 2016. Vestibular vertigo and comorbid cognitive and psychiatric impairment: the 2008 National Health Interview Survey. J. Neurol. Neurosurg. Psychiatry 87, 367–372. https://doi.org/10.1136/jnnp-2015-310319

Bigelow, R.T., Semenov, Y.R., Hoffman, H.J., Agrawal, Y., 2019. Association between vertigo, cognitive and psychiatric conditions in US children: 2012 National Health Interview Survey. International Journal of Pediatric Otorhinolaryngology 109802. https://doi.org/10.1016/j.ijporl.2019.109802

Bigelow, R.T., Semenov, Y.R., Trevino, C., Ferrucci, L., Resnick, S.M., Simonsick, E.M., Xue, Q.-L., Agrawal, Y., 2015. Association Between Visuospatial Ability and Vestibular Function in the Baltimore Longitudinal Study of Aging. J Am Geriatr Soc 63, 1837–1844. https://doi.org/10.1111/jgs.13609

Blouin, J., Bresciani, J.-P., Guillaud, E., Simoneau, M., 2015. Prediction in the Vestibular Control of Arm Movements. Multisens Res 28, 487–505. https://doi.org/10.1163/22134808-00002501

Bockisch, C.J., Haslwanter, T., 2001. Three-dimensional eye position during static roll and pitch in humans. Vision Res. 41, 2127–2137. https://doi.org/10.1016/s0042-6989(01)00094-3

Böhmer, A., Mast, F., 1999. Assessing otolith function by the subjective visual vertical. ANNALS-NEW YORK ACADEMY OF SCIENCES 871, 221–231. https://doi.org/10.1111/j.1749-6632.1999.tb09187.x

Borel, L., Lopez, C., Péruch, P., Lacour, M., 2008. Vestibular syndrome: a change in internal spatial representation. Neurophysiol Clin 38, 375–389. https://doi.org/10.1016/j.neucli.2008.09.002

Brandt, T., Dieterich, M., 2019. Thalamocortical network: a core structure for integrative multimodal vestibular functions. Curr. Opin. Neurol. 32, 154–164. https://doi.org/10.1097/WCO.0000000000000638

Brandt, T., Schautzer, F., Hamilton, D.A., Brüning, R., Markowitsch, H.J., Kalla, R., Darlington, C., Smith, P., Strupp, M., 2005. Vestibular loss causes hippocampal atrophy and impaired spatial memory in humans. Brain 128, 2732–2741. https://doi.org/10.1093/brain/awh617

Brandt, T., Strupp, M., Benson, J., 1999. You are better off running than walking with acute vestibulopathy. Lancet 354, 746. https://doi.org/10.1016/S0140-6736(99)03179-7

Braswell, J., Rine, R.M., 2006. Evidence that vestibular hypofunction affects reading acuity in children. Int. J. Pediatr. Otorhinolaryngol. 70, 1957–1965. https://doi.org/10.1016/j.ijporl.2006.07.013

Brodsky, M.C., Donahue, S.P., Vaphiades, M., Brandt, T., 2006. Skew deviation revisited. Surv Ophthalmol 51, 105–128. https://doi.org/10.1016/j.survophthal.2005.12.008

Bryant, C.D., 2011. The blessings and curses of C57BL/6 substrains in mouse genetic studies. Ann N Y Acad Sci 1245, 31–33. https://doi.org/10.1111/j.1749-6632.2011.06325.x

Büttner-Ennever, J.A., 1992. Patterns of connectivity in the vestibular nuclei. Ann. N. Y. Acad. Sci. 656, 363–378. https://doi.org/10.1111/j.1749-6632.1992.tb25222.x

Cahill, C.M., Murphy, K.C., 2004. Migraine and depersonalization disorder. Cephalalgia 24, 686–687. https://doi.org/10.1111/j.1468-2982.2004.00737.x

Cassel, R., Bordiga, P., Carcaud, J., Simon, F., Beraneck, M., Le Gall, A., Benoit, A., Bouet, V., Philoxene, B., Besnard, S., Watabe, I., Pericat, D., Hautefort, C., Assie, A., Tonetto, A., Dyhrfjeld-Johnsen, J., Llorens, J., Tighilet, B., Chabbert, C., 2019. Morphological and functional correlates of vestibular synaptic deafferentation and repair in a mouse model of acute onset vertigo. Dis Model Mech 12. https://doi.org/10.1242/dmm.039115

Cassel, R., Wiener-Vacher, S., El Ahmadi, A., Tighilet, B., Chabbert, C., 2018. Reduced Balance Restoration Capacities Following Unilateral Vestibular Insult in Elderly Mice. Front Neurol 9, 462. https://doi.org/10.3389/fneur.2018.00462

Catala, M., 2014. Embryologie de l'oreille interne. EMC - Oto-rhino-laryngologie 9, 1–10.

Chabbert, C., 2015. Anatomie et physiologie du vestibule. //www.em-premium.com/data/traites/or/20-58501/. https://doi.org/10.1016/S0246-0351(15)58501-2

Chandrakumar, M., Blakeman, A., Goltz, H.C., Sharpe, J.A., Wong, A.M.F., 2011. Static ocular counterroll reflex in skew deviation. Neurology 77, 638–644. https://doi.org/10.1212/WNL.0b013e3182299f71

Chays, A., Florant, A., Ulmer, E., 2009. Les vertiges. (DEPRECIATED).

Ciolek, P.J., Kang, E., Honaker, J.A., Woodson, E.A., Hopkins, B.S., Anne, S., 2018. Pediatric vestibular testing: Tolerability of test components in children. Int. J. Pediatr. Otorhinolaryngol. 113, 29–33. https://doi.org/10.1016/J.IJPORL.2018.07.009

Cohen, B., Henn, V., Raphan, T., Dennett, D., 1981. Velocity storage, nystagmus, and visual-vestibular interactions in humans. Ann. N. Y. Acad. Sci. 374, 421–433. https://doi.org/10.1111/j.1749-6632.1981.tb30888.x

Cohen, B., Maruta, J., Raphan, T., 2001. Orientation of the eyes to gravitoinertial acceleration. Ann. N. Y. Acad. Sci. 942, 241–258. https://doi.org/10.1111/j.1749-6632.2001.tb03750.x

Collewijn, H., Van der Steen, J., Ferman, L., Jansen, T.C., 1985. Human ocular counterroll: assessment of static and dynamic properties from electromagnetic scleral coil recordings. Exp Brain Res 59, 185–196. https://doi.org/10.1007/BF00237678

Cox, B.J., Swinson, R.P., 2002. Instrument to assess depersonalization-derealization in panic disorder. Depress Anxiety 15, 172–175. https://doi.org/10.1002/da.10051

Curthoys, I.S., Dlugaiczyk, J., 2020. Physiology, clinical evidence and diagnostic relevance of sound-induced and vibration-induced vestibular stimulation. Curr. Opin. Neurol. 33, 126–135. https://doi.org/10.1097/WCO.0000000000000770

Curthoys, I.S., Grant, J.W., 2015. How does high-frequency sound or vibration activate vestibular receptors? Exp Brain Res 233, 691–699. https://doi.org/10.1007/s00221-014-4192-6

Curtin, J.A., Quint, E., Tsipouri, V., Arkell, R.M., Cattanach, B., Copp, A.J., Henderson, D.J., Spurr, N., Stanier, P., Fisher, E.M., Nolan, P.M., Steel, K.P., Brown, S.D.M., Gray, I.C., Murdoch, J.N., 2003. Mutation of Celsr1 disrupts planar polarity of inner ear hair cells and causes severe neural tube defects in the mouse. Curr. Biol. 13, 1129–1133.

de Vargas Romero, M., Mota, H.B., Nóro, L.A., Valentins dos Santos Filha, V.A., 2020. Correlation between body balance exams and schoolchildren reading assessments. International Journal of Pediatric Otorhinolaryngology 137, 110230. https://doi.org/10.1016/j.ijporl.2020.110230

Deans, M.R., 2013. A balance of form and function: planar polarity and development of the vestibular maculae. Seminars in cell & developmental biology 24, 490–8. https://doi.org/10.1016/j.semcdb.2013.03.001

Dechesne, C.J., Sans, A., 1985. Development of vestibular receptor surfaces in human fetuses. Am J Otolaryngol 6, 378–387. https://doi.org/10.1016/s0196-0709(85)80016-8

Delmaghani, S., El-Amraoui, A., 2020. Inner Ear Gene Therapies Take Off: Current Promises and Future Challenges. J Clin Med 9. https://doi.org/10.3390/jcm9072309

Deroualle, D., Toupet, M., van Nechel, C., Duquesne, U., Hautefort, C., Lopez, C., 2017. Anchoring the Self to the Body in Bilateral Vestibular Failure. PLoS One 12, e0170488–e0170488. https://doi.org/10.1371/journal.pone.0170488

Dhondt, C., Dhooge, I., Maes, L., 2018. Vestibular assessment in the pediatric population. Laryngoscope. https://doi.org/10.1002/LARY.27255

Dieringer, N., Pantle, C., Reichenberger, I., Straka, H., 1996. The synaptic organization of the horizontal vestibulo-ocular reflex in the frog. Acta. Biol. Hung. 47, 61–72.

Dieterich, M., Brandt, T., 1993. Ocular torsion and tilt of subjective visual vertical are sensitive brainstem signs. Ann. Neurol. 33, 292–299. https://doi.org/10.1002/ana.410330311

Dietrich, H., Wuehr, M., 2019. Selective suppression of the vestibulo-ocular reflex during human locomotion. J. Neurol. 266, 101–107. https://doi.org/10.1007/s00415-019-09352-7

Dinculescu, A., Stupay, R.M., Deng, W.-T., Dyka, F.M., Min, S.-H., Boye, S.L., Chiodo, V.A., Abrahan, C.E., Zhu, P., Li, Q., Strettoi, E., Novelli, E., Nagel-Wolfrum, K., Wolfrum, U., Smith, W.C., Hauswirth, W.W., 2016. AAV-Mediated Clarin-1 Expression in the Mouse Retina: Implications for USH3A Gene Therapy. PLoS One 11, e0148874. https://doi.org/10.1371/journal.pone.0148874

DiZio, P., Lackner, J.R., 1990. Age differences in oculomotor responses to step changes in body velocity and visual surround velocity. J Gerontol 45, M89-94. https://doi.org/10.1093/geronj/45.3.m89

Dulon, D., Papal, S., Patni, P., Cortese, M., Vincent, P.F., Tertrais, M., Emptoz, A., Tlili, A., Bouleau, Y., Michel, V., Delmaghani, S., Aghaie, A., Pepermans, E., Alegria-Prevot, O., Akil, O., Lustig, L., Avan, P., Safieddine, S., Petit, C., El-Amraoui, A., 2018. Clarin-1 gene transfer rescues auditory synaptopathy in model of Usher syndrome. J. Clin. Invest. 128, 3382–3401. https://doi.org/10.1172/JCI94351

Dulubova, I., Khvotchev, M., Liu, S., Huryeva, I., Südhof, T.C., Rizo, J., 2007. Munc18-1 binds directly to the neuronal SNARE complex. PNAS 104, 2697–2702. https://doi.org/10.1073/pnas.0611318104

Dunbar, L.A., Patni, P., Aguilar, C., Mburu, P., Corns, L., Wells, H.R., Delmaghani, S., Parker, A., Johnson, S., Williams, D., Esapa, C.T., Simon, M.M., Chessum, L., Newton, S., Dorning, J., Jeyarajan, P., Morse, S., Lelli, A., Codner, G.F., Peineau, T., Gopal, S.R., Alagramam, K.N., Hertzano, R., Dulon, D., Wells, S., Williams, F.M., Petit, C., Dawson, S.J., Brown, S.D., Marcotti, W., El-Amraoui, A., Bowl, M.R., 2019. Clarin-2 is essential for hearing by maintaining stereocilia integrity and function. EMBO Mol Med 11, e10288. https://doi.org/10.15252/emmm.201910288

Duncan, J.S., Stoller, M.L., Francl, A.F., Tissir, F., Devenport, D., Deans, M.R., 2017. Celsr1 coordinates the planar polarity of vestibular hair cells during inner ear development. Developmental biology 423, 126–137. https://doi.org/10.1016/j.ydbio.2017.01.020

Dutheil, S., Brezun, J.M., Leonard, J., Lacour, M., Tighilet, B., 2009. Neurogenesis and astrogenesis contribution to recovery of vestibular functions in the adult cat following unilateral vestibular neurectomy: cellular and behavioral evidence. Neuroscience 164, 1444–1456. https://doi.org/10.1016/J.NEUROSCIENCE.2009.09.048

Ekdale, E.G., 2013. Comparative Anatomy of the Bony Labyrinth (Inner Ear) of Placental Mammals. PLoS ONE 8, e66624. https://doi.org/10.1371/journal.pone.0066624

Emptoz, A., Michel, V., Lelli, A., Akil, O., Boutet de Monvel, J., Lahlou, G., Meyer, A., Dupont, T., Nouaille, S., Ey, E., Franca de Barros, F., Beraneck, M., Dulon, D., Hardelin, J.P., Lustig, L., Avan, P., Petit, C., Safieddine, S., 2017. Local gene therapy durably restores vestibular function in a mouse model of Usher syndrome type 1G. Proceedings of the National Academy of Sciences of the United States of America 114, 9695–9700. https://doi.org/10.1073/pnas.1708894114

Enríquez, J.A., 2019. Mind your mouse strain. Nat Metab 1, 5–7. https://doi.org/10.1038/s42255-018-0018-3

Epema, A.H., Gerrits, N.M., Voogd, J., 1988. Commissural and intrinsic connections of the vestibular nuclei in the rabbit: a retrograde labeling study. Exp Brain Res 71, 129–146. https://doi.org/10.1007/BF00247528

Fabre-Adinolfi, D., Ceyte, H., Hoffmann, C.P., Frère, J., Parietti-Winkler, C., 2020. Postural disorders induced by cochlear implantation in normo-reflexic patients: A potential origin of a transient geocentric perception disorder. Gait Posture 81, 225–229. https://doi.org/10.1016/j.gaitpost.2020.08.106

Fernandez, C., Goldberg, J.M., 1971. Physiology of peripheral neurons innervating semicircular canals of the squirrel monkey. II. Response to sinusoidal stimulation and dynamics of peripheral vestibular system. J. Neurophysiol. 34, 661–675. https://doi.org/10.1152/jn.1971.34.4.661

Fife, T.D., Colebatch, J.G., Kerber, K.A., Brantberg, K., Strupp, M., Lee, H., Walker, M.F., Ashman, E., Fletcher, J., Callaghan, B., Gloss, D.S., 2017. Practice guideline: Cervical and ocular vestibular evoked myogenic potential testing: Report of the Guideline Development, Dissemination, and Implementation Subcommittee of the American Academy of Neurology. Neurology 89, 2288–2296. https://doi.org/10.1212/WNL.0000000000004690

Florival, G., Dudley, J., 1979. Structure, origine et affectivité: Quelques réflexions à propos de la. corporéité. Revue philosophique de Louvain 196–218. https://doi.org/10.3406/phlou.1979.6045

França de Barros, F., Carcaud, J., Beraneck, M., 2019. Long-term Sensory Conflict in Freely Behaving Mice. J Vis Exp. https://doi.org/10.3791/59135

Gacek, R.R., Schoonmaker, J.E., 1997. Morphologic changes in the vestibular nerves and nuclei after labyrinthectomy in the cat: a case for the neurotrophin hypothesis in vestibular compensation. Acta Otolaryngol. 117, 244–249. https://doi.org/10.3109/00016489709117780

Geller, S.F., Guerin, K.I., Visel, M., Pham, A., Lee, E.S., Dror, A.A., Avraham, K.B., Hayashi, T., Ray, C.A., Reh, T.A., Bermingham-McDonogh, O., Triffo, W.J., Bao, S., Isosomppi, J., Västinsalo, H., Sankila, E.-M., Flannery, J.G., 2009. CLRN1 is nonessential in the mouse retina but is required for cochlear hair cell development. PLoS Genet 5, e1000607. https://doi.org/10.1371/journal.pgen.1000607

Geng, R., Melki, S., Chen, D.H.-C., Tian, G., Furness, D.N., Oshima-Takago, T., Neef, J., Moser, T., Askew, C., Horwitz, G., Holt, J.R., Imanishi, Y., Alagramam, K.N., 2012. The mechanosensory structure of the hair cell requires clarin-1, a protein encoded by Usher syndrome III causative gene. J Neurosci 32, 9485–9498. https://doi.org/10.1523/JNEUROSCI.0311-12.2012

Geng, R., Omar, A., Gopal, S.R., Chen, D.H.-C., Stepanyan, R., Basch, M.L., Dinculescu, A., Furness, D.N., Saperstein, D., Hauswirth, W., Lustig, L.R., Alagramam, K.N., 2017. Modeling and Preventing Progressive Hearing Loss in Usher Syndrome III. Sci Rep 7, 13480. https://doi.org/10.1038/s41598-017-13620-9

Goebel, J.A., 2016. 2015 Equilibrium Committee Amendment to the 1995 AAO-HNS Guidelines for the Definition of Ménière's Disease. Otolaryngol Head Neck Surg 154, 403–404. https://doi.org/10.1177/0194599816628524

Goldberg, J.M., Cullen, K.E., 2011. Vestibular control of the head: possible functions of the vestibulocollic reflex. Exp Brain Res 210, 331–345. https://doi.org/10.1007/s00221-011-2611-5

Goldberg, J.M., Wilson, V.J., Angelaki, D.E., Cullen, K.E., Fukushima, K., Buttner-Ennever, J., 2012. The vestibular system: a sixth sense. Oxford University Press.

Gonzalez-Torres, M.A., Inchausti, L., Aristegui, M., Ibañez, B., Diez, L., Fernandez-Rivas, A., Bustamante, S., Haidar, K., Rodríguez-Zabaleta, M., Mingo, A., 2010. Depersonalization in patients with schizophrenia spectrum disorders, first-degree relatives and normal controls. Psychopathology 43, 141–149. https://doi.org/10.1159/000288635

Gorlin, R.J., Toriello, H.V., Cohen, M.M., 1995. Hereditary hearing loss and its syndromes. Oxford University Press, USA.

Goulème, N., Debue, M., Spruyt, K., Vanderveken, C., De Siati, R.D., Ortega-Solis, J., Petrossi, J., Wiener-Vacher, S., Bucci, M.P., Ionescu, E., Thai-Van, H., Deggouj, N., 2018. Changes of spatial and temporal characteristics of dynamic postural control in children with typical neurodevelopment with age: Results of a multicenter pediatric study. Int. J. Pediatr. Otorhinolaryngol. 113, 272–280. https://doi.org/10.1016/J.IJPORL.2018.08.005

Greene, N.D.E., Stanier, P., Copp, A.J., 2009. Genetics of human neural tube defects. Hum. Mol. Genet. 18, R113-129. https://doi.org/10.1093/hmg/ddp347

Greguske, E.A., Carreres-Pons, M., Cutillas, B., Boadas-Vaello, P., Llorens, J., 2019. Calyx junction dismantlement and synaptic uncoupling precede hair cell extrusion in the vestibular sensory epithelium during sub-chronic 3,3'-iminodipropionitrile ototoxicity in the mouse. Arch. Toxicol. 93, 417–434. https://doi.org/10.1007/s00204-018-2339-0

Gurvich, C., Maller, J.J., Lithgow, B., Haghgooie, S., Kulkarni, J., 2013. Vestibular insights into cognition and psychiatry. Brain Research 1537, 244–259. https://doi.org/10.1016/j.brainres.2013.08.058

György, B., Meijer, E.J., Ivanchenko, M.V., Tenneson, K., Emond, F., Hanlon, K.S., Indzhykulian, A.A., Volak, A., Karavitaki, K.D., Tamvakologos, P.I., 2019. Gene transfer with AAV9-PHP. B rescues hearing in a mouse model of usher syndrome 3A and transduces hair cells in a non-human primate. Molecular Therapy-Methods & Clinical Development 13, 1–13. https://doi.org/10.1016/j.omtm.2018.11.003

Hain, T.C., Cherchi, M., Perez-Fernandez, N., 2018. The Gain-Time Constant Product Quantifies Total Vestibular Output in Bilateral Vestibular Loss. Front Neurol 9. https://doi.org/10.3389/fneur.2018.00396

Halmagyi, G., Curthoys, I., Brandt, T., Dieterich, M., 1991. Ocular tilt reaction: clinical sign of vestibular lesion. Acta Oto-Laryngologica 111, 47–50. https://doi.org/10.3109/00016489109131342

Hamilton, S.S., Zhou, G., Brodsky, J.R., 2015. Video head impulse testing (VHIT) in the pediatric population. International journal of pediatric otorhinolaryngology 79, 1283–7. https://doi.org/10.1016/j.ijporl.2015.05.033

Han, B.I., Song, H.S., Kim, J.S., 2011. Vestibular Rehabilitation Therapy: Review of Indications, Mechanisms, and Key Exercises. J Clin Neurol 7, 184–196. https://doi.org/10.3988/jcn.2011.7.4.184

Hegemann, S.C.A., Wenzel, A., 2017. Diagnosis and Treatment of Vestibular Neuritis/Neuronitis or Peripheral Vestibulopathy (PVP)? Open Questions and Possible Answers. Otology & Neurotology 38, 626–631. https://doi.org/10.1097/MAO.0000000000001396

Hequembourg, S., Liberman, M.C., 2001. Spiral ligament pathology: a major aspect of age-related cochlear degeneration in C57BL/6 mice. J Assoc Res Otolaryngol 2, 118–129. https://doi.org/10.1007/s101620010075

Hess, B.J., Dieringer, N., 1991. Spatial organization of linear vestibuloocular reflexes of the rat: responses during horizontal and vertical linear acceleration. J. Neurophysiol. 66, 1805–1818. https://doi.org/10.1152/jn.1991.66.6.1805

Hess, B.J.M., Dieringer, N., 1990. Spatial Organization of the Maculo-Ocular Reflex of the Rat: Responses During Off-Vertical Axis Rotation. Eur. J. Neurosci. 2, 909–919.

Heydrich, L., Marillier, G., Evans, N., Seeck, M., Blanke, O., 2019. Depersonalization- and derealization-like phenomena of epileptic origin. Ann Clin Transl Neurol 6, 1739–1747. https://doi.org/10.1002/acn3.50870

Hitier, M., Besnard, S., Smith, P.F., 2014. Vestibular pathways involved in cognition. Front Integr Neurosci 8, 59. https://doi.org/10.3389/fnint.2014.00059

Hitier, M., Sato, G., Zhang, Y., Zheng, Y., Besnard, S., Smith, P.F., Curthoys, I.S., 2016. Anatomy and surgical approach of rat's vestibular sensors and nerves. Journal of neuroscience methods 270, 1–8. https://doi.org/10.1016/j.jneumeth.2016.05.013

Holstein, G.R., 2012. The Vestibular System, in: The Human Nervous System. Elsevier, pp. 1239–1269. https://doi.org/10.1016/B978-0-12-374236-0.10035-5

Horn, A.K.E., 2020. Neuroanatomy of Central Vestibular Connections, in: Reference Module in Neuroscience and Biobehavioral Psychology. Elsevier, p. B9780128093245240000. https://doi.org/10.1016/B978-0-12-809324-5.23911-4

Huterer, M., Cullen, K.E., 2002. Vestibuloocular reflex dynamics during high-frequency and high-acceleration rotations of the head on body in rhesus monkey. J. Neurophysiol. 88, 13–28. https://doi.org/10.1152/jn.2002.88.1.13

Imagawa, M., Isu, N., Sasaki, M., Endo, K., Ikegami, H., Uchino, Y., 1995. Axonal projections of utricular afferents to the vestibular nuclei and the abducens nucleus in cats. Neurosci. Lett. 186, 87–90. https://doi.org/10.1016/0304-3940(95)11288-8

Ito, J., Matsuoka, I., Sasa, M., Takaori, S., 1985. Commissural and ipsilateral internuclear connection of vestibular nuclear complex of the cat. Brain Res. 341, 73–81. https://doi.org/10.1016/0006-8993(85)91474-x

Iwashita, M., Kanai, R., Funabiki, K., Matsuda, K., Hirano, T., 2001. Dynamic properties, interactions and adaptive modifications of vestibulo-ocular reflex and optokinetic response in mice. Neurosci. Res. 39, 299–311. https://doi.org/10.1016/s0168-0102(00)00228-5

Janky, K.L., Rodriguez, A.I., 2018. Quantitative Vestibular Function Testing in the Pediatric Population. Semin Hear 39, 257–274. https://doi.org/10.1055/S-0038-1666817

Jáuregui-Renaud, K., Aranda-Moreno, C., Villaseñor-Moreno, J.C., Giráldez Fernández, M.E., Maldonado Cano, A.J., Gutierrez Castañeda, M.F., Figueroa-Padilla, I., Saucedo-Zainos, A.L., 2019. Derealization symptoms according to the subjective visual vertical during unilateral centrifugation in patients with type 2 diabetes mellitus. J Vestib Res 29, 111–120. https://doi.org/10.3233/VES-190652

Judge, P.D., Rodriguez, A.I., Barin, K., Janky, K.L., 2018. Impact of Target Distance, Target Size, and Visual Acuity on the Video Head Impulse Test. Otolaryngol Head Neck Surg 159, 739–742. https://doi.org/10.1177/0194599818779908

Kaliuzhna, M., Vibert, D., Grivaz, P., Blanke, O., 2015. Out-of-Body Experiences and Other Complex Dissociation Experiences in a Patient with Unilateral Peripheral Vestibular Damage and Deficient Multisensory Integration. Multisens Res 28, 613–635. https://doi.org/10.1163/22134808-00002506

Kane, K.L., Longo-Guess, C.M., Gagnon, L.H., Ding, D., Salvi, R.J., Johnson, K.R., 2012. Genetic background effects on age-related hearing loss associated with Cdh23 variants in mice. Hear Res 283, 80–88. https://doi.org/10.1016/j.heares.2011.11.007

Karnath, H.-O., Mölbert, S.C., Klaner, A.K., Tesch, J., Giel, K.E., Wong, H.Y., Mohler, B.J., 2019. Visual perception of one's own body under vestibular stimulation using biometric self-avatars in virtual reality. PLoS One 14, e0213944–e0213944. https://doi.org/10.1371/journal.pone.0213944

Kim, T.S., Lim, H.W., Yang, C.J., Kim, Y.H., Choi, W.R., Kim, Y.R., Park, J.W., Kang, B.C., Park, H.J., 2018. Changes of video head impulse test results in lateral semicircular canal plane by different peak head velocities in patients with vestibular neuritis. Acta Otolaryngol. 138, 785–789. https://doi.org/10.1080/00016489.2018.1481523

Kitahara, T., Sakagami, M., Ito, T., Shiozaki, T., Kitano, K., Yamashita, A., Ota, I., Wada, Y., Yamanaka, T., 2019. Ménière's disease with unremitting floating sensation is associated with canal paresis, gravity-sensitive dysfunction, mental illness, and bilaterality. Auris Nasus Larynx 46, 186–192. https://doi.org/10.1016/j.anl.2018.07.003

Kolev, O.I., Georgieva-Zhostova, S.O., Berthoz, A., 2014. Anxiety changes depersonalization and derealization symptoms in vestibular patients. Behavioural neurology 2014. https://doi.org/10.1155/2014/847054

Kretschmer, F., Tariq, M., Chatila, W., Wu, B., Badea, T.C., 2017. Comparison of optomotor and optokinetic reflexes in mice. J. Neurophysiol. 118, 300–316. https://doi.org/10.1152/jn.00055.2017

Kuhn, J.J., Lavender, V.H., Hunter, L.L., McGuire, S.E., Meinzen-Derr, J., Keith, R.W., Greinwald, J.H., 2018. Ocular Vestibular Evoked Myogenic Potentials: Normative Findings in Children. J Am Acad Audiol 29, 443–450. https://doi.org/10.3766/JAAA.17086

Kutz, D.F., Kolb, F.P., Glasauer, S., Straka, H., 2020. Somatosensory Influence on Platform-Induced Translational Vestibulo-Ocular Reflex in Vertical Direction in Humans. Front Neurol 11, 332. https://doi.org/10.3389/fneur.2020.00332

Lambert, F.M., Straka, H., 2012. The frog vestibular system as a model for lesion-induced plasticity: basic neural principles and implications for posture control. Front Neurol 3, 42. https://doi.org/10.3389/fneur.2012.00042

Lei, Y., Zhu, H., Yang, W., Ross, M.E., Shaw, G.M., Finnell, R.H., 2014. Identification of novel CELSR1 mutations in spina bifida. PLoS ONE 9, e92207. https://doi.org/10.1371/journal.pone.0092207

Lenggenhager, B., Lopez, C., 2015. Vestibular contributions to the sense of body, self, and others. Open MIND 23, 1–38.

Li, C.W., Hooper, R.E., Cousins, V.C., 1991. Sinusoidal harmonic acceleration testing in normal humans. Laryngoscope 101, 192–196. https://doi.org/10.1288/00005537-199102000-00016

Li, P., Ding, D., Gao, K., Salvi, R., 2015. Standardized surgical approaches to ear surgery in rats. Journal of Otology 10, 72–77. https://doi.org/10.1016/j.joto.2015.03.004

Lim, R., Drury, H.R., Camp, A.J., Tadros, M.A., Callister, R.J., Brichta, A.M., 2014. Preliminary characterization of voltage-activated whole-cell currents in developing human vestibular hair cells and calyx afferent terminals. J. Assoc. Res. Otolaryngol. 15, 755–766. https://doi.org/10.1007/s10162-014-0471-y

Llorens, J., Demêmes, D., 1994. Hair cell degeneration resulting from 3,3'-iminodipropionitrile toxicity in the rat vestibular epithelia. Hear. Res. 76, 78–86. https://doi.org/10.1016/0378-5955(94)90090-6

Llorens, J., Demêmes, D., Sans, A., 1993. The behavioral syndrome caused by 3,3'-iminodipropionitrile and related nitriles in the rat is associated with degeneration of the vestibular sensory hair cells. Toxicol. Appl. Pharmacol. 123, 199–210. https://doi.org/10.1006/taap.1993.1238

Lopez, C., Elzière, M., 2018. Out-of-body experience in vestibular disorders - A prospective study of 210 patients with dizziness. Cortex 104, 193–206. https://doi.org/10.1016/j.cortex.2017.05.026

Lopez-Escamez, J.A., Attyé, A., 2019. Systematic review of magnetic resonance imaging for diagnosis of Meniere disease. J Vestib Res 29, 121–129. https://doi.org/10.3233/VES-180646

Lysakowski, A., Goldberg, J.M., 1997. A regional ultrastructural analysis of the cellular and synaptic architecture in the chinchilla cristae ampullares. J. Comp. Neurol. 389, 419–443. https://doi.org/10.1002/(sici)1096-9861(19971222)389:3<419::aid-cne5>3.0.co;2-3

MacDougall, H.G., Weber, K.P., McGarvie, L.A., Halmagyi, G.M., Curthoys, I.S., 2009. The video head impulse test: diagnostic accuracy in peripheral vestibulopathy. Neurology 73, 1134–1141. https://doi.org/10.1212/WNL.0b013e3181bacf85

Mackrous, I., Carriot, J., Jamali, M., Cullen, K.E., 2019. Cerebellar Prediction of the Dynamic Sensory Consequences of Gravity. Curr. Biol. 29, 2698-2710.e4. https://doi.org/10.1016/j.cub.2019.07.006

Maes, L., De Kegel, A., Van Waelvelde, H., De Leenheer, E., Van Hoecke, H., Goderis, J., Dhooge, I., 2017. Comparison of the Motor Performance and Vestibular Function in Infants with a Congenital Cytomegalovirus Infection or a Connexin 26 Mutation: A Preliminary Study. Ear and hearing 38, e49–e56. https://doi.org/10.1097/aud.0000000000000364

Maes, L., De Kegel, A., Van Waelvelde, H., Dhooge, I., 2014. Rotatory and collic vestibular evoked myogenic potential testing in normal-hearing and hearing-impaired children. Ear Hear 35, e21-32. https://doi.org/10.1097/AUD.0b013e3182a6ca91

Martin, T., Mauvieux, B., Bulla, J., Quarck, G., Davenne, D., Denise, P., Philoxène, B., Besnard, S., 2015. Vestibular loss disrupts daily rhythm in rats. J. Appl. Physiol. 118, 310–318. https://doi.org/10.1152/japplphysiol.00811.2014

Matsuo, N., Takao, K., Nakanishi, K., Yamasaki, N., Tanda, K., Miyakawa, T., 2010. Behavioral profiles of three C57BL/6 substrains. Front. Behav. Neurosci. 4. https://doi.org/10.3389/fnbeh.2010.00029

McGarvie, L.A., MacDougall, H.G., Halmagyi, G.M., Burgess, A.M., Weber, K.P., Curthoys, I.S., 2015. The Video Head Impulse Test (vHIT) of Semicircular Canal Function - Age-Dependent Normative Values of VOR Gain in Healthy Subjects. Front Neurol 6, 154. https://doi.org/10.3389/fneur.2015.00154

Mejdoubi, M., Dedouit, F., Mokrane, F.-Z., Telmon, N., 2015. Semicircular canal angulation during fetal life: a computed tomography study of 54 human fetuses. Otol. Neurotol. 36, 701–704. https://doi.org/10.1097/MAO.0000000000000640

Merleau-Ponty, M., 1945. Phénoménologie de la perception.

Mianné, J., Chessum, L., Kumar, S., Aguilar, C., Codner, G., Hutchison, M., Parker, A., Mallon, A.-M., Wells, S., Simon, M.M., Teboul, L., Brown, S.D.M., Bowl, M.R., 2016. Correction of the auditory phenotype in C57BL/6N mice via CRISPR/Cas9-mediated homology directed repair. Genome Med 8, 16. https://doi.org/10.1186/s13073-016-0273-4

Migliaccio, A.A., Meierhofer, R., Della Santina, C.C., 2011. Characterization of the 3D angular vestibulo-ocular reflex in C57BL6 mice. Exp Brain Res 210, 489–501. https://doi.org/10.1007/s00221-010-2521-y

Mock, B.E., Vijayakumar, S., Pierce, J., Jones, T.A., Jones, S.M., 2016. Differential effects of Cdh23(753A) on auditory and vestibular functional aging in C57BL/6J mice. Neurobiol Aging 43, 13–22. https://doi.org/10.1016/j.neurobiolaging.2016.03.013

Moser, T., Beutner, D., 2000. Kinetics of exocytosis and endocytosis at the cochlear inner hair cell afferent synapse of the mouse. Proc. Natl. Acad. Sci. U.S.A. 97, 883–888. https://doi.org/10.1073/pnas.97.2.883

Nouvian, R., Neef, J., Bulankina, A.V., Reisinger, E., Pangršič, T., Frank, T., Sikorra, S., Brose, N., Binz, T., Moser, T., 2011. Exocytosis at the hair cell ribbon synapse apparently operates without neuronal SNARE proteins. Nat. Neurosci. 14, 411–413. https://doi.org/10.1038/nn.2774

Ohlemiller, K.K., Jones, S.M., Johnson, K.R., 2016. Application of Mouse Models to Research in Hearing and Balance. J Assoc Res Otolaryngol 17, 493–523. https://doi.org/10.1007/s10162-016-0589-1

Oommen, B.S., Stahl, J.S., 2008. Eye orientation during static tilts and its relationship to spontaneous head pitch in the laboratory mouse. Brain Res. 1193, 57–66. https://doi.org/10.1016/j.brainres.2007.11.053

Otero-Millan, J., Treviño, C., Winnick, A., Zee, D.S., Carey, J.P., Kheradmand, A., 2017. The video ocular counter-roll (vOCR): a clinical test to detect loss of otolith-ocular function. Acta Otolaryngol. 137, 593–597. https://doi.org/10.1080/00016489.2016.1269364

Papathanasiou, E.S., Straumann, D., 2019. Why and when to refer patients for vestibular evoked myogenic potentials: A critical review. Clin Neurophysiol 130, 1539–1556. https://doi.org/10.1016/j.clinph.2019.04.719

Parker, A., Chessum, L., Mburu, P., Sanderson, J., Bowl, M.R., 2016. Light and Electron Microscopy Methods for Examination of Cochlear Morphology in Mouse Models of Deafness. Curr Protoc Mouse Biol 6, 272–306. https://doi.org/10.1002/cpmo.10

Paul, E.R., Farmer, M., Kämpe, R., Cremers, H.R., Hamilton, J.P., 2019. Functional Connectivity Between Extrastriate Body Area and Default Mode Network Predicts Depersonalization Symptoms in Major Depression: Findings From an A Priori Specified Multinetwork Comparison. Biol Psychiatry Cogn Neurosci Neuroimaging 4, 627–635. https://doi.org/10.1016/j.bpsc.2019.03.007

Pender, D.J., 1992. Practical otology. JB Lippincott.

Péricat, D., Farina, A., Agavnian-Couquiaud, E., Chabbert, C., Tighilet, B., 2017. Complete and irreversible unilateral vestibular loss: A novel rat model of vestibular pathology. J. Neurosci. Methods 283, 83–91. https://doi.org/10.1016/J.JNEUMETH.2017.04.001

Peterson, B.W., Maunz, R.A., Fukushima, K., 1978. Properties of a new vestibulospinal projection, the caudal vestibulospinal tract. Exp Brain Res 32, 287–292. https://doi.org/10.1007/BF00239733

Pollack, S.M., Popratiloff, A., Peusner, K.D., 2004. Vestibular ganglionectomy and otolith nerve identification in the hatchling chicken. J. Neurosci. Methods 138, 149–155. https://doi.org/10.1016/j.jneumeth.2004.04.023

Pujol, R., Lavigne-Rebillard, M., 1995. Sensory and neural structures in the developing human cochlea. Int. J. Pediatr. Otorhinolaryngol. 32 Suppl, S177-182. https://doi.org/10.1016/0165-5876(94)01156-r

Raghu, V., Salvi, R., Sadeghi, S.G., 2019. Efferent Inputs Are Required for Normal Function of Vestibular Nerve Afferents. J. Neurosci. 39, 6922–6935. https://doi.org/10.1523/JNEUROSCI.0237-19.2019

Raphan, T., Matsuo, V., Cohen, B., 1979. Velocity storage in the vestibulo-ocular reflex arc (VOR). Exp Brain Res 35, 229–248. https://doi.org/10.1007/BF00236613

Rauch, S.D., 2001. Vestibular histopathology of the human temporal bone. What can we learn? Ann. N. Y. Acad. Sci. 942, 25–33. https://doi.org/10.1111/j.1749-6632.2001.tb03732.x

Ravni, A., Qu, Y., Goffinet, A.M., Tissir, F., 2009. Planar cell polarity cadherin Celsr1 regulates skin hair patterning in the mouse. J. Invest. Dermatol. 129, 2507–2509. https://doi.org/10.1038/jid.2009.84

Richard, C., Linthicum, F.H., 2012. Vestibular neuritis: the vertigo disappears, the histological traces remain. Otol. Neurotol. 33, e59-60. https://doi.org/10.1097/MAO.0b013e31824b7730

Rodriguez, A.I., Thomas, M.L.A., Janky, K.L., 2018. Air-Conducted Vestibular Evoked Myogenic Potential Testing in Children, Adolescents, and Young Adults: Thresholds, Frequency Tuning, and Effects of Sound Exposure. Ear Hear. https://doi.org/10.1097/AUD.0000000000000607

Ross, L.M., Helminski, J.O., 2016. Test-retest and Interrater Reliability of the Video Head Impulse Test in the Pediatric Population. Otology & neurotology : official publication of the American Otological Society, American Neurotology Society [and] European Academy of Otology and Neurotology 37, 558–63. https://doi.org/10.1097/mao.0000000000001040

Rubinstein, J.T., Ling, L., Nowack, A., Nie, K., Phillips, J.O., 2020. Results From a Second-Generation Vestibular Implant in Human Subjects: Diagnosis May Impact Electrical Sensitivity of Vestibular Afferents. Otol. Neurotol. 41, 68–77. https://doi.org/10.1097/MAO.0000000000002463

Safieddine, S., El-Amraoui, A., Petit, C., 2012. The auditory hair cell ribbon synapse: from assembly to function. Annu. Rev. Neurosci. 35, 509–528. https://doi.org/10.1146/annurev-neuro-061010-113705

Sakatani, T., Isa, T., 2004. PC-based high-speed video-oculography for measuring rapid eye movements in mice. Neurosci. Res. 49, 123–131. https://doi.org/10.1016/j.neures.2004.02.002

Schlax, J., Wiltink, J., Beutel, M.E., Münzel, T., Pfeiffer, N., Wild, P., Blettner, M., Ghaemi Kerahrodi, J., Michal, M., 2020. Symptoms of depersonalization/derealization are independent risk factors for the development or persistence of psychological distress in the general population: Results from the Gutenberg health study. J Affect Disord 273, 41–47. https://doi.org/10.1016/j.jad.2020.04.018

Schmid, D.A., Allum, J.H.J., Sleptsova, M., Welge-Lüssen, A., Schaefert, R., Meinlschmidt, G., Langewitz, W., 2020. Relation of anxiety and other psychometric measures, balance deficits, impaired quality of life, and perceived state of health to dizziness handicap inventory scores for patients with dizziness. Health Qual Life Outcomes 18, 204. https://doi.org/10.1186/s12955-020-01445-6

Schneider, A.D., Jamali, M., Carriot, J., Chacron, M.J., Cullen, K.E., 2015. The increased sensitivity of irregular peripheral canal and otolith vestibular afferents optimizes their encoding of natural stimuli. J. Neurosci. 35, 5522–5536. https://doi.org/10.1523/JNEUROSCI.3841-14.2015

Schönherr, A., May, C.A., 2016. Influence of Caloric Vestibular Stimulation on Body Experience in Healthy Humans. Front Integr Neurosci 10, 14–14. https://doi.org/10.3389/fnint.2016.00014

Schubert, M.C., Herdman, S.J., Tusa, R.J., 2002. Vertical dynamic visual acuity in normal subjects and patients with vestibular hypofunction. Otol. Neurotol. 23, 372–377. https://doi.org/10.1097/00129492-200205000-00025

Schubert, M.C., Minor, L.B., 2004. Vestibulo-ocular physiology underlying vestibular hypofunction. Phys Ther 84, 373–385.

Schuknecht, H.F., 1982. Behavior of the vestibular nerve following labyrinthectomy. Ann Otol Rhinol Laryngol Suppl 97, 16–32.

Semenov, Y.R., Bigelow, R.T., Xue, Q.-L., du Lac, S., Agrawal, Y., 2016. Association Between Vestibular and Cognitive Function in U.S. Adults: Data From the National Health and Nutrition Examination Survey. J. Gerontol. A Biol. Sci. Med. Sci. 71, 243–250. https://doi.org/10.1093/gerona/glv069

Shiga, A., Nakagawa, T., Nakayama, M., Endo, T., Iguchi, F., Kim, T.-S., Naito, Y., Ito, J., 2005. Aging effects on vestibulo-ocular responses in C57BL/6 mice: comparison with alteration in auditory function. Audiol Neurootol 10, 97–104. https://doi.org/10.1159/000083365

Shinoda, Y., Sugiuchi, Y., Izawa, Y., Hata, Y., 2006. Long descending motor tract axons and their control of neck and axial muscles. Prog. Brain Res. 151, 527–563. https://doi.org/10.1016/S0079-6123(05)51017-3

Shotwell, S.L., Jacobs, R., Hudspeth, A.J., 1981. Directional sensitivity of individual vertebrate hair cells to controlled deflection of their hair bundles. Ann. N. Y. Acad. Sci. 374, 1–10. https://doi.org/10.1111/j.1749-6632.1981.tb30854.x

Simon, F., Pericat, D., Djian, C., Fricker, D., Denoyelle, F., Beraneck, M., 2020. Surgical techniques and functional evaluation for vestibular lesions in the mouse: unilateral labyrinthectomy (UL) and unilateral vestibular neurectomy (UVN). J Neurol. https://doi.org/10.1007/s00415-020-09960-8

Smith, P.F., 2019. The Growing Evidence for the Importance of the Otoliths in Spatial Memory. Front Neural Circuits 13, 66. https://doi.org/10.3389/fncir.2019.00066

Smith, P.F., 2017. The vestibular system and cognition. Curr. Opin. Neurol. 30, 84–89. https://doi.org/10.1097/WCO.0000000000000403

Smith, P.F., Darlington, C.L., 2013. Personality changes in patients with vestibular dysfunction. Front Hum Neurosci 7, 678–678. https://doi.org/10.3389/fnhum.2013.00678

Smith, P.F., Zheng, Y., Horii, A., Darlington, C.L., 2005. Does vestibular damage cause cognitive dysfunction in humans? J Vestib Res 15, 1–9.

Spiegel, D., Lewis-Fernández, R., Lanius, R., Vermetten, E., Simeon, D., Friedman, M., 2013. Dissociative Disorders in DSM-5. Annual Review of Clinical Psychology 9, 299–326. https://doi.org/10.1146/annurev-clinpsy-050212-185531

Stahl, J.S., 2004. Eye movements of the murine P/Q calcium channel mutant rocker, and the impact of aging. J. Neurophysiol. 91, 2066–2078. https://doi.org/10.1152/jn.01068.2003

Stahl, J.S., Averbuch-Heller, L., Leigh, R.J., 2000. Acquired nystagmus. Arch. Ophthalmol. 118, 544–549. https://doi.org/10.1001/archopht.118.4.544

Starkov, D., Strupp, M., Pleshkov, M., Kingma, H., van de Berg, R., 2020. Diagnosing vestibular hypofunction: an update. J. Neurol. https://doi.org/10.1007/s00415-020-10139-4

Straka, H., Lambert, F.M., Pfanzelt, S., Beraneck, M., 2009. Vestibulo-ocular signal transformation in frequency-tuned channels. Ann. N. Y. Acad. Sci. 1164, 37–44. https://doi.org/10.1111/j.1749-6632.2008.03740.x

Tagliabue, M., Arnoux, L., McIntyre, J., 2013. Keep your head on straight: Facilitating sensori-motor transformations for eye–hand coordination. Neuroscience 248, 88–94. https://doi.org/10.1016/j.neuroscience.2013.05.051

Tagliabue, M., McIntyre, J., 2014. A modular theory of multisensory integration for motor control. Frontiers in computational neuroscience 8, 1. https://doi.org/10.3389/fncom.2014.00001

Tian, G., Lee, R., Ropelewski, P., Imanishi, Y., 2016. Impairment of Vision in a Mouse Model of Usher Syndrome Type III. Invest. Ophthalmol. Vis. Sci. 57, 866–875. https://doi.org/10.1167/iovs.15-16946

Tian, J., Shubayev, I., Demer, J.L., 2002. Dynamic visual acuity during passive and self-generated transient head rotation in normal and unilaterally vestibulopathic humans. Exp Brain Res 142, 486–495. https://doi.org/10.1007/s00221-001-0959-7

Toupet, M., Van Nechel, C., Hautefort, C., Heuschen, S., Duquesne, U., Cassoulet, A., Bozorg Grayeli, A., 2019. Influence of Visual and Vestibular Hypersensitivity on Derealization and Depersonalization in Chronic Dizziness. Front. Neurol. 10. https://doi.org/10.3389/fneur.2019.00069

Uchino, Y., Sasaki, M., Sato, H., Imagawa, M., Suwa, H., Isu, N., 1996. Utriculoocular reflex arc of the cat. Journal of Neurophysiology 76, 1896–1903. https://doi.org/10.1152/jn.1996.76.3.1896

Ulmer, E., Bernard-Demanze, L., Lacour, M., 2011. Statistical study of normal canal deficit variation range. Measurement using the Head Impulse Test video system. Eur Ann Otorhinolaryngol Head Neck Dis 128, 278–282. https://doi.org/10.1016/j.anorl.2011.05.005

Vignaux, G., Besnard, S., Denise, P., Elefteriou, F., 2015. The Vestibular System: A Newly Identified Regulator of Bone Homeostasis Acting Through the Sympathetic Nervous System. Curr Osteoporos Rep 13, 198–205. https://doi.org/10.1007/s11914-015-0271-2

Vignaux, G., Besnard, S., Ndong, J., Philoxène, B., Denise, P., Elefteriou, F., 2013. Bone remodeling is regulated by inner ear vestibular signals. J. Bone Miner. Res. 28, 2136–2144. https://doi.org/10.1002/jbmr.1940

Wangemann, P., Griffith, A.J., 2017. Mouse Models Reveal the Role of Pendrin in the Inner Ear, in: The Role of Pendrin in Health and Disease. Springer, pp. 7–22.

Washbourne, P., Thompson, P.M., Carta, M., Costa, E.T., Mathews, J.R., Lopez-Benditó, G., Molnár, Z., Becher, M.W., Valenzuela, C.F., Partridge, L.D., Wilson, M.C., 2002. Genetic ablation of the t-SNARE SNAP-25 distinguishes mechanisms of neuroexocytosis. Nat. Neurosci. 5, 19–26. https://doi.org/10.1038/nn783

Wei, M., Angelaki, D.E., 2006. Foveal visual strategy during self-motion is independent of spatial attention. J. Neurosci. 26, 564–572. https://doi.org/10.1523/JNEUROSCI.3986-05.2006

Wenzel, A., Hülse, R., Thunsdorff, C., Rotter, N., Curthoys, I., 2019. Reducing the number of impulses in video head impulse testing - It's the quality not the numbers. Int. J. Pediatr. Otorhinolaryngol. 125, 206–211. https://doi.org/10.1016/j.ijporl.2019.07.013

Wiener-Vacher, S.R., Hamilton, D.A., Wiener, S.I., 2013. Vestibular activity and cognitive development in children: perspectives. Front Integr Neurosci 7, 92. https://doi.org/10.3389/fnint.2013.00092

Wiener-Vacher, S.R., Obeid, R., Abou-Elew, M., 2012. Vestibular impairment after bacterial meningitis delays infant posturomotor development. J. Pediatr. 161, 246-251.e1. https://doi.org/10.1016/j.jpeds.2012.02.009

Wiener-Vacher, S.R., Quarez, J., Priol, A.L., 2018. Epidemiology of Vestibular Impairments in a Pediatric Population. Semin Hear 39, 229–242. https://doi.org/10.1055/S-0038-1666815

Wiener-Vacher, S.R., Wiener, S.I., 2017. Video Head Impulse Tests with a Remote Camera System: Normative Values of Semicircular Canal Vestibulo-Ocular Reflex Gain in Infants and Children. Frontiers in neurology 8, 434. https://doi.org/10.3389/fneur.2017.00434

Williams, P., Warwick, R., 1980. Gray's anatomy. 36th Edition.

Wolter, N.E., Gordon, K.A., Papsin, B.C., Cushing, S.L., 2015. Vestibular and Balance Impairment Contributes to Cochlear Implant Failure in Children. Otol. Neurotol. 36, 1029–1034. https://doi.org/10.1097/MAO.0000000000000751

Wong, A.M.F., 2015. New understanding on the contribution of the central otolithic system to eye movement and skew deviation. Eye (Lond) 29, 153–156. https://doi.org/10.1038/eye.2014.243

Wong, A.M.F., Sharpe, J.A., 2005. Cerebellar skew deviation and the torsional vestibuloocular reflex. Neurology 65, 412–419. https://doi.org/10.1212/01.wnl.0000171860.02355.61

Yakushin, S.B., Raphan, T., Cohen, B., 2017. Coding of Velocity Storage in the Vestibular Nuclei. Front Neurol 8. https://doi.org/10.3389/fneur.2017.00386

Yardley, L., Beech, S., Weinman, J., 2001. Influence of beliefs about the consequences of dizziness on handicap in people with dizziness, and the effect of therapy on beliefs. J Psychosom Res 50, 1–6. https://doi.org/10.1016/s0022-3999(00)00202-6

Yardley, L., Redfern, M.S., 2001. Psychological factors influencing recovery from balance disorders. J Anxiety Disord 15, 107–119. https://doi.org/10.1016/s0887-6185(00)00045-1

Yates, B.J., Miller, A.D., 1998. Physiological evidence that the vestibular system participates in autonomic and respiratory control. J Vestib Res 8, 17–25.

Zallocchi, M., Meehan, D.T., Delimont, D., Askew, C., Garige, S., Gratton, M.A., Rothermund-Franklin, C.A., Cosgrove, D., 2009. Localization and expression of clarin-1, the Clrn1 gene product, in auditory hair cells and photoreceptors. Hear Res 255, 109–120. https://doi.org/10.1016/j.heares.2009.06.006

Zeng, S., Ni, W., Jiang, H., You, D., Wang, J., Lu, X., Liu, L., Yu, H., Wu, J., Chen, F., Li, H., Wang, Y., Chen, Y., Li, W., 2020. Toxic Effects of 3,3'-Iminodipropionitrile on Vestibular System in Adult C57BL/6J Mice In Vivo. Neural Plast. 2020, 1823454. https://doi.org/10.1155/2020/1823454

Zhan, Y.-H., Luo, Q.-C., Zhang, X.-R., Xiao, N.-A., Lu, C.-X., Yue, C., Wang, N., Ma, Q.-L., 2016. CELSR1 Is a Positive Regulator of Endothelial Cell Migration and Angiogenesis. Biochemistry Mosc. 81, 591–599. https://doi.org/10.1134/S0006297916060055

Zheng, Q.Y., Johnson, K.R., Erway, L.C., 1999. Assessment of hearing in 80 inbred strains of mice by ABR threshold analyses. Hear Res 130, 94–107. https://doi.org/10.1016/s0378-5955(99)00003-9

Zingler, V.C., Kryvoshey, D., Schneider, E., Glasauer, S., Brandt, T., Strupp, M., 2006. A clinical test of otolith function: static ocular counterroll with passive head tilt. Neuroreport 17, 611–615. https://doi.org/10.1097/00001756-200604240-00011

Résumé

Les déficits vestibulaires chez l'enfant sont retrouvés dans environ un tiers des consultations pour troubles de l'équilibre et dans la moitié des consultations pré-implant cochléaire. Les complications peuvent être importantes avec au premier plan des troubles de l'équilibre et un retard à l'acquisition de la verticalité (position assise, marche), mais aussi un déficit de la stabilisation du regard, de l'orientation spatiale et de la construction du soi. Les modèles murins peuvent aider à mieux comprendre la physiologie vestibulaire, à identifier les acteurs moléculaires ou cellulaires de la physiopathologie vestibulaires, et aider à mettre en place des thérapeutiques innovantes telles que la thérapie génique. L'exploration fonctionnelle chez la souris permet grâce à la vidéonystagmographie, d'explorer différents réflexes vestibulo-oculaires canalaires et otolithiques. Nous avons dans ce travail exploré différents modèles murins, soit des modèles mutants (inactivation des gènes de la *clarine*, *snap-25* ou *celsr1*), soit des souris normales en induisant une lésion vestibulaire chirurgicale ou chimique par kaïnate (TTK) ou 3-3'-iminodipropanenitrile (IDPN). Les mutations du gène *CLARINE-1* sont responsables du syndrome cochléo-vestibulaire de Usher type III. Des modèles murins avec invalidation des gènes *clarine-1* et/ou *clarine-2* ont été développés pour mieux comprendre le rôle de ces molécules et étudier l'efficacité de la thérapie génique. Nous avons montré que la clarine-1 semble indispensable au bon fonctionnement vestibulaire (dysfonction en son absence malgré une présence de clarine-2), à l'inverse de la clarine-2. La molécule SNAP-25 est une protéine impliquée dans le mécanisme d'exocytose synaptique des cellules ciliées. Les souris *snap-25-KO* sans thérapie génique étaient incapable de nager et leurs explorations vestibulaires ont montré des déficits canalaire et otolithique complets. La fonction vestibulaire était entièrement restaurée après thérapie génique, ce qui semble montrer le caractère essentiel de la protéine snap25 dans le fonctionnement de la cellule ciliée vestibulaire mature. Enfin, la molécule CELSR1 est une protéine qui participe à la polarité cellulaire planaire et le modèle de souris *celsr1-KO* présente une désorganisation de la polarité des cellules ciliées vestibulaires chez la souris, surtout au niveau de la cupule. L'étude fonctionnelle a montré chez les souris mutantes une hypo-fonction canalaire d'environ 50% surtout sur les basses fréquences et otolithique d'environ 70%. La polarité ciliaire semble particulièrement critique pour le bon fonctionnement otolithique, ainsi que le recrutement d'un nombre suffisant de cellules ciliées avec des informations concordantes pour les mouvements rotatoires, surtout lors des mouvements lents. Le modèle de lésion vestibulaire le plus ancien pour étudier la compensation vestibulaire chez le rongeur est chirurgical. Une labyrinthectomie unilatérale (UL) est plus simple à réaliser avec moins de comorbidités qu'une neurectomie unilatérale du VIII (UVN), même si cette dernière technique est utile si une destruction du premier neurone vestibulaire est recherchée. La fonction vestibulaire résiduelle et la récupération fonctionnelle sont cependant comparables pendant le 1er mois de compensation. Un autre modèle de lésion chimique a été développé par injection trans-tympanique de TTK, qui permet de déclencher une désafférentation des cellules ciliées, avec un déficit fonctionnel transitoire et partiel par rapport à la neurectomie. Enfin une lésion chimique par injection péritonéale d'IDPN permet de détruire préférentiellement les cellules de type I. L'analyse fonctionnelle a montré une relation dose-dépendante, avec un déficit canalaire surtout sur les fréquences rapides et un déficit otolithique peu prononcé lors d'inclinaisons statiques de la tête. L'exploration des troubles fonctionnels vestibulaires de modèles murins de pathologies cochléo-vestibulaires est une étape décisive pour permettre d'une part une meilleure compréhension de la physiopathologie et d'autre part le développement de thérapies ciblées comme la thérapie génique.